The Role of Systemic Sclerosis Dermal Fibroblast-derived Exosomes in the Induction of Type I Interferon in Keratinocytes

Jessica Bryon

Submitted in accordance with the requirements for the degree of Doctor in Philosophy

The University of Leeds

School of Medicine and Health

January 2023

The candidate confirms that the work submitted is her own and that appropriate credit has been given where reference has been made to the work of others.

Acknowledgements

Firstly, I would like to thank my primary supervisor, Professor Francesco Del Galdo for the opportunity to undertake a PhD in his laboratory. I would also like to thank my co-supervisors; Professor Elton Zeqiraj and Dr Rebecca Ross for their guidance and advice, which helped me troubleshoot and develop as a researcher. Secondly, I would like to thank all my laboratory colleagues within the scleroderma team for all their emotional and technical support.

As part of this work, I would like to acknowledge a series of colleagues, whose expertise aided the development of work created within this thesis; Dr Leon Willis for his guidance with DLS, Francesca Chandler for help with microscopy and sample preparation for TEM and Zoe Wigston with her ‘tips and tricks’ to extract the cleanest of RNA, as well as aid the quantitative analysis of my Flow Cytometry datasets. In addition, I would like to thank Katja Koeppen for kindly performing bioinformatics analysis on the RNA sequencing data collected throughout this thesis.

Finally, I would like to thank my family and friends for their continued support and encouragement throughout my studies, especially my brother Daniel; who listened to countless rants and complaints about the struggles I faced. Lastly, a special thank you to my partner; Ioanna, without whom my final year would have been a complete emotional and physical disaster. Thank you for your love, patience and never ending support.

Abstract

Systemic sclerosis (SSc) is a devastating chronic autoimmune disease, which is typically characterised by dysregulated immune activation, inflammation, vasculopathy and the fibrosis of skin and internal organs. An elevated type I interferon (IFN) response has been observed in the blood and skin of SSc patients, before fibrosis onset, which correlates with disease activity and response to therapy. However, the exact role of type I IFN and its origination and amplification in early disease pathogenesis in the skin is unclear. Immunohistochemistry and RNA sequencing of skin biopsies has illustrated that upregulated IFN signalling occurs in the dermis and epidermis of the skin layer, however it is lost when cells are removed from the skin environment and cultured in-vitro. The current literature consensus is that SSc fibroblasts are targeted by activated immune cells, which promotes fibroblast activation and a pro-fibrotic drive. Here, we investigated the cell-cell communication between fibroblasts and keratinocytes in the skin layer to identify if fibroblasts can drive an interferon response in keratinocytes; in particularly through exosomes, which are small extracellular vesicles that act as key intercellular communicators, which have been previously implicated in many cancers and autoimmune diseases.

Healthy and SSc dermal fibroblasts released exosomes of similar quantities with indistinguishable biophysical properties, which were internalised by keratinocytes over a period of time, maximised at 48 hours. RNA sequencing analysis indicated that SSc fibroblast-derived exosomes induced type I IFN signalling in keratinocytes, after 48 hours compared to healthy exosomes. Concurrently, immunoblotting indicated that SSc exosomes induced increased phosphorylation

of STAT1 at 48 hours. Mechanistically, SSc fibroblast-derived exosomes required Tank Binding Kinase 1 (TBK1) and JAK-STAT to induce the expression of interferon stimulatory genes in keratinocytes. Further evaluation of JAK-STAT inhibition indicated that SSc exosomes induced STAT3 and pSTAT3 protein expression. RNA sequencing of healthy and SSc fibroblast exosome cargo indicated an array of differentially expressed transcripts, however there was no indication of a viable biological molecule capable of inducing an innate immune response.

Overall, this study demonstrated that SSc dermal fibroblast-derived exosomes can induce type I IFN signalling in keratinocytes, in a TBK1 and JAK-STAT dependent manner. However, no biological molecule was found to be responsible for the IFN activation in keratinocytes. Therefore, further evaluation of the mechanism and contents of SSc exosomes, which are responsible for induced type I IFN signalling in keratinocytes will aid the understanding behind immunopathogenesis in SSc, as well as provide a potential therapeutic target to alleviate the dysregulated IFN signalling observed in early disease.

Table of Contents

List of Figures

List of Tables

Abbreviations

7-AAD	7-Aminoactinomycin D
ACA	Anticentromere Antibodies
ADH1B	Alcohol Dehydrogenase 1B
AFF3	ALF Transcription Elongation Factor 3
AFTPH-DT	Aftiphilin Divergent Transcript
AKT	Serine/Threonine-protein Kinase
ALIX	Programmed Cell Death 6-interacting Protein
AMPK	Adenosine Monophosphate Deaminase-activated Protein Kinase
ANOVA	Analysis of Variance
ANXA2R-AS1	Annexin A2 Receptor-Antisense RNA 1
APS	Ammonium Persulfate
ARA	Anti-RNA Polymerase III Antibodies
ATA/Scl-70	Anti-Topoisomerase Antibodies
B2M	Beta-2 Microglobulin
BCA	Bicinchoninic Acid Assay
BCAT1	Branched Chain Amino Acid Transaminase 1
BSA	Bovine Serum Albumin
BST2	Tetherin
CACNG6	Calcium Voltage-Gated Channel Auxiliary Subunit Gamma 6
CAF	Cancer Associated Fibroblast
CARD	Caspase Activation and Recruitment Domains
CBP	Cyclic Adenosine Monophosphate Response Element Binding Protein
CCL2	C-C Motif Chemokine Ligand 2
cDNA	Complementary DNA
CENP	Centromere Protein
CFSE	Carboxyfluorescein Succinimidyl Ester
cGAMP	Cyclic Guanosine Monophosphate-Adenosine Monophosphate
cGAS	Cyclic GMP-AMP Synthase
CLEC2B	C-Type Lectin Domain Family 2 Member B
COL	Collagen Type
CTGF	Connective Tissue Growth Factor

CTR	Control
CTSA	Cathepsin A
CTSC	Cathepsin C
CXCL	C-X-C Motif Ligand
CYP	Cyclophosphamide
DAMPs	Damage-associated Molecular Patterns
DAPI	4',6-Diamidino-2-Phenylindole
DEGs	Differentially Expressed Genes
DLS	Dynamic Light Scatter
DMEM	Dulbecco's Modified Eagle Medium
DNA	Deoxyribonucleic Acid
DNTPS	Deoxynucleotide Triphosphates
dsDNA	Double Standed DNA
dsRNA	Double Standed RNA
dSSc	Diffuse Scleroderma
E-Cadherin	Epithelial Cadherin
ECM	Extracellular Matrix
EDTA	Ethylenediaminetetraacetic Acid
EFEMP1	Epidermal Growth Factor-Containing Fibulin Extracellular Matric Protein 1
ELISA	Enzyme-linked Immunosorbent Assay
EMT	Epithelial-Mesenchymal Transition
EPHA5	Ephrin Type-A Receptor 5
ER	Endoplasmic Reticulum
ERG	Erythroblast Transformation-specific Related Gene
ESCC	Esophageal Squamous Cell Carcinoma
ESCRT	Endosomal Sorting Complex Required for Transport
FACS	Fluorescence-activated Cell Sorting
FBLN2	Fibulin-2
FBS	Fetal Bovine Serum
FC	Flow Cytometry
FDR	False Discovery Rate
FITC	Fluorescein Isothiocyanate
FVC	Forced Vital Capacity
GAPDH	Glyceraldehyde-3-Phosphate Dehydrogenase
GAS	Gamma Interferon Activation Site

GBP1	Guanylate Binding Protein 1
GFP	Green Fluorescent Protein
GO	Gene Ontology
HaCats	Spontaneously Transformed Human Keratinocyte Cell Culture
HC	Healthy Control
HCN2	Hyperpolarization Activated Cyclic Nucleotide Gated Potassium and Sodium Channel 2
HOTTIP	HOXA Distal Transcript Antisense RNA
HPGD	15-Hydroxyprostaglandin Dehydrogenase
HPRT1	Hypoxanthine-guanine Phosphoribosyltransferase
HRNR	Hornerin
HSH2D	Hematopoietic SH2 Domain Containing
HSP70	Heat Shock Protein 70
HTERT	Human Telomerase Reverse Transcriptase
IFI44	Interferon Induced Protein 44
IFIH1	Interferon Induced With Helicase C Domain 1
IFIT1	Interferon Induced Protein with Tetratricopeptide Repeats 1
IFNAR	Interferon alpha/beta Receptor
IFU	Infectious Units
IKK	Ikappa B Kinase
IL6	Interleukin 6
ILD	Interstitial Lung Disease
IMID	Immune-mediated Inflammatory Diseases
IRAK	Interleukin -1 Receptor Associated Kinase
IRFs	Interferon Regulatory Factors
IRSE	Interferon-responsive Sequence Element
ISG15	Interferon Stimulated Gene 15
ISGF3	Interferon Stimulated Gene Factor 3
ISGs	Interferon Stimulated Genes
ISRE	Interferon-sensitive Response Element
JAK	Janus Kinase
K63	Lysine 63
kDa	Kilodalton
KEGG	Kyoto Encyclopedia of Genes and Genomes
LCMT2	Leucine Carboxyl Methyltransferase 2
LGP2	RIG-I-like Receptor

Lipo	Lipofectamine2000
lncRNA	Long non-coding RNA
LRP1	Low Density Lipoprotein Receptor-related Protein 1
lSSc	Limited Scleroderma
LTBP4	Latent Transforming Growth Factor Beta Binding Protein 4
MAVs	Mitochondrial Antiviral Signalling Protein
MDA5	Melanoma Differentiation-associated Protein 5
miR	Micro-RNA
MMF	Mycophenolate Mofetil
mRNA	Messenger RNA
mrSS	Modified Rodnan Skin Score
mt-DNA	Mitochondrial DNA
MVB	Multivesicular Bodies
MX1	MX Dynamin Like GTPase 1
MyD88	Myeloid Differentiation Primary Response 88
N-Cadherin	Neural Cadherin
ncRNA	non-coding RNA
NEAT1	Nuclear Paraspeckle Assembly Transcript 1
NFW	Nuclease Free Water
NF-κB	Nuclear Factor Kappa B
NS	Not Significant
NTA	Nanoparticle Tracking Analysis
OAS	2'-5'-Oligoadenylate Synthase
OKT3	Orthoclone
PBMC	Human Peripheral Blood Mononuclear Cells
PBS	Phosphate Buffered Saline
PCBP3	Poly-binding Protein 3
PCR	Polymerase Chain Reaction
pDCs	Plasmacytoid Dendritic Cells
PDI	Polydispersity Index
PEG	Polyethylene Glycol
PET	Polyethylene Terephthalate
PFA	Paraformaldehyde
PLA2G2A	Phospholipase A2 Group IIA
Poly-IC	Polyinosinic : Polycytidylic Acid
PPP1R36	Protein Phosphatase 1 Regulatory Subunit 36

PRDM15	PR/SET Domain 15
PRRs	Pattern Recognition Receptors
PRSS16	Serine Protease 16
qPCR	Quantitative Polymerase Chain Reaction
RA	Rheumatoid Arthritis
RIG-I	Retinoic Acid-inducible Gene I
RIP1	Receptor-interacting Serine/Threonine-protein 1
RIPA	Radioimmunoprecipitation Assay Buffer
RN7SL1	RNA Component Of Signal Recognition Particle 7SL1
RNA	Ribonucleic Acid
RPLP0	Ribosomal Protein Lateral Stalk Subunit P0
RPM	Revolutions Per Minute
rRNA	ribosomal RNA
RSAD2	Radical S-Adenosyl Methionine Domain Containing 2
RT	Room Temperature
RTP4	Receptor Transporter Protein 4
RT-qPCR	Real Time - Quantitative PCR
RTX	Rituximab
SC	Scleroderma Control
SECTM1	Secreted and Transmembrane 1
SEM	Scanning Electron Microscope
Ser	Serine
SFM	Serum Free Media
SH2	Src Homology 2
shRIG-I	Short Hairpin RIG-I
shRNA	Short Hairpin RNA
siRNA	Small Interfering RNA
SLE	Systemic Lupus Erythematosus
SLS	Scleroderma Lung Study
SMAD	Suppressor of Mothers against Decapentaplegic
SNP	Single Nucleotide Polymorphisms
SOCS	Suppressor of Cytokine Signalling
SRP	Signal Recognition Particle
SSc	Scleroderma
STAT	Signal Transducer and Activator of Transcription
STING	Stimulator of Interferon Genes

TAK1	TGFβ-activated Kinase I
TBK	Tank Binding Kinase
TBS	Tris Buffered Saline
TBS-T	Tris Buffered Saline - Tween
TEI	Total Exosome Isolation Reagent
TEM	Transmission Electron Microscopy
TEMED	Tetramethylethylenediamine
TGFβ	Transforming Growth Factor Beta
TIR	Toll-interleukin-1 Receptor
TLR	Toll Like Receptor
TMB	3,3',5,5'-Tetramethylbenzidine
TMPRSS11E	Transmembrane Serine Protease 11E
TNF	Tumour Necrosis Factor
TOF	Tofacitinib
TRAF	TNF Receptor-associated Factor
TRIF	TIR-domain-containing Adaptor-inducing Interferon β
TRIM25	Tripartite Motif Containing 25
TSG101	Tumour Susceptibility Gene 101
TYR	Tyrosine
TYR2	Tyrosine Kinase 2
UC	Ultracentrifugation
UF	Ultrafiltration
USP18	Ubiquitin Specific Peptidase 18
VEGF	Vascular Endothelial Growth Factor
VSIG1	Viral Intergration Site I
Wnt	Wingless-related Integration Site
ZG16B	Zymogen Granule Protein 16B
α-SMA	Alpha Smooth Muscle Actin
β-actin	Beta-Actin

1. Introduction

1.1. Systemic Sclerosis and the Interferon Signature

1.1.1. Systemic Sclerosis

Systemic Sclerosis (SSc), also known as Scleroderma, is a complex rare connective tissue disease, which affects approximately 17.6 per 100,000 people worldwide (Bairkdar et al., 2021). The aetiology of the disease is characterised by upregulated immune activation and inflammation, vasculopathy (weakened blood vessels and restricted blood flow), as well as the fibrosis of skin and organs through excessive deposits of collagen and other extracellular matrix (ECM) proteins. Although the cause of SSc is unknown; research suggests that patients have a genetic predisposition for the disease, where a secondary environmental stimulus can initiate inflammation, caused by vascular damage, which later results in fibrosis (Fett et al., 2013).

Scleroderma is mainly split into two major subsets: limited cutaneous (lcSSc) and systemic sclerosis/diffuse cutaneous scleroderma (dcSSc), which is dependent upon the extent of skin fibrosis (Varga et al, 2007). Limited cutaneous SSc is a form of scleroderma, which is typically led by vascular fibrosis and affects skin distal to the elbow and knee, as well as various other clinical features, such as: Calcinosis, Raynaud's phenomenon, Telangiectasia and Oesophageal Dysmotility. lcSSc commonly originates from isolated Raynaud's phenomenon, where lcSSc is typically diagnosed several years after the onset of Raynaud's (Del Galdo et al., 2020). Patients with diffuse scleroderma display skin involvement proximal to the elbow and knee, as well as an increased risk of

cardiac disease, lung fibrosis, renal failure, and mortality (Kim et al., 2008). The major differences between lcSSc and dcSSc are the speed of progression and type of organ damage (Del Galdo et al., 2020).

Skin thickening is a determinant of the clinical onset of SSc, which is commonly measured routinely to assess the extent, degree, and prevalence of skin thickness in scleroderma patients (Khanna et al., 2017). The Modified Rodnan Skin Score (mRSS) was developed in 1980's, where Rodnan compared skin scores, calculated by skin thickness of 17 areas scored 0-4, to the net weight of patient skin biopsies (Rodnan et al., 1979). The net weight of the SSc patient's skin biopsies correlated well with the skin score and reflected the pathology of SSc (Rodnan et al., 1979). Thus, the mRSS became a gold standard widely used clinical tool to measure skin thickening semi quantitatively in SSc. Currently, the mRSS is measured by assessing the skin thickness of 17 cutaneous areas and scoring these areas from 0 (normal) to 3 (severe), yielding a total score of 51 (Clements et al., 1993). Commonly, patients with early dcSSc have a heightened skin score, which declines over the disease continuum, and the peak skin score usually occurs between 12-18 months of skin involvement (Khanna et al., 2017, Dobrota et al., 2016). A heightened skin score is associated with an increased risk in mortality and organ involvement, whereas patients with a low skin score often have less major organ involvement and improvement of skin score leads to better outcomes and survival rate (Steen and Medsger., 2001, Dobrota et al., 2016).

The initiation and pathogenesis of scleroderma is poorly understood, however there are disease specific autoantibodies that are associated with scleroderma

and can be used clinically to diagnose and evaluate clinical outcomes of the disease. Anti-centromere (ACA), anti-topoisomerase I (ATA, Scl-70) and anti-RNA polymerase (ARA) autoantibodies are linked to SSc. Approximately 20-30% of SSc patients are ACA positive, typically lcSSc patients. Likewise, ACA positivity is associated with better prognosis, when compared to other SSc-associated antibodies (Ho and Reveille, 2003). ACAs can bind up to 1 to 6 centromere proteins (CENPA-F). CENPB binds to a 17-base region in α-satellite DNA and has an important role in centromere-specific nucleosome formation and the translational positioning of the nucleosome (Tanaka et al., 2005). Moreover, approximately 20% of scleroderma patients have Scl-70 antibodies, which are more commonly present in dcSSc patients (Ho and Reveille., 2003). Topoisomerases I is an enzyme which aids chromatic remodelling and prevents DNA supercoiling, by creating single and double stranded DNA breaks. It is also associated with 36 nuclear proteins, which are involved in RNA splicing (Champoux., 2001). Scl-70 autoantibodies correlate with a greater disease severity, where patients have more severe skin and lung fibrosis, as well as an increased risk of early mortality (Ho and Reveille., 2003).

The role of autoantibodies in the disease pathogenesis of scleroderma has been poorly understood. However, a recent paper by Paul et al., (2022) observed that damaged skin fibroblasts from SSc patients contained an array of centromere defects. Further, Paul et al., (2022) discovered that abnormal overexpression of CENPA in fibroblasts from skin lesions correlated with the expression of pro-fibrotic and pro-inflammatory markers. Immunofluorescence imaging illustrated cGAS accumulation around excess micronuclei in SSc fibroblasts, which resulted in an increase in phosphorylated IRF3 and secretion of IFNβ (Paul et al., 2022).

This paper highlights that centromere alterations, observed in SSc fibroblasts, are linked to clinical manifestations of innate immune activation and skin fibrosis.

There are no current cures for scleroderma, only therapeutics which can alleviate and mildly modify disease progression. Mycophenolate Mofetil (MMF) and Cyclophosphamide (CYP) are common established therapies for scleroderma. MMF is an immunosuppressant drug which inhibits purine nucleotide synthesis and is commonly used in SSc to treat disease associated lung fibrosis (Zamora et al., 2017). Approximately, 80% of scleroderma patients have some form of lung disease, where intestinal lung disease (ILD) is the most common form (Pellar and Pope., 2017). Further, Zamora et al., (2008) showed that MMF treatment led to stabilisation or improvement on lung function in 94% of patients after 12 months of treatment. Secondly, Baqir et al., (2017) observed that MMF treatment could stabilise lung and pulmonary hypotension over 2 years of treatment. Collectively, both studies showed that patients responded well to the treatment and little adverse effects were documented (Baqir et al., 2017, Zamora et al., 2008).

Cyclophosphamide (CYC) is an alkylating chemotherapy drug which depresses the immune response. Cyclophosphamide treatment has showed improvement in ILD and skin involvement in scleroderma (Pellar and Pope., 2017), however it is often used with caution, as treatment can result in severe side effects, such as bone marrow suppression, infection, infertility, and increased risk of cancer (Nannini et al., 2008). A scleroderma lung study (SLS), which was a double-blind randomised control trial of 126 patients that were treated with either CYC or MMF, illustrated that both drugs preserved lung function, measured by % Forced Vital Capcaity (FVC), as well as mild mRSS improvements. However, CYC-treated

patients displayed severe adverse effects, such as Anaemia and Leukopenia, whereas MMF was described as better tolerated with a lower toxicity profile (Tashkin et al., 2016).

Moreover, a recent randomised control study of 102 early diffuse scleroderma lung disease patients compared CYC with Rituximab (RTX), which is an anti-B cell monoclonal antibody, and observed that both CYC and RTX-treated patients had an increase %FVC and significant improvements in their mRSS scores. The trial illustrated that both CYC and RTX have similar efficiencies, however the RTX cohort displayed significantly fewer adverse effects (Sircar et al., 2018). Further, the SENSCIS trial was a phase 3 randomised placebo trial on 576 IL-D SSc patients that investigated Nintendanib, which is a well-established intracellular tyrosine kinase inhibitor already approved for idiopathic pulmonary fibrosis. Patients treated with Nintendanib showed a reduction of 44% in the rate of decline of FVC over 12 months, as well as mild gastrointestinal adverse effects, such as diarrhoea. Although no other clinical benefit of Nintendanib for other manifestations of SSc, it was approved by the US Food and Drug Administration in 2019 for treatment of SSc patients with IL-D (Distler et al., 2019, Denton et al., 2020).

Furthermore, IL-6 is a proinflammatory cytokine which has been associated with fibrosis in SSc. Two recent trials (faSScinate and focussed) have investigated the role of Tocilizumab, an anti-IL6 receptor antibody, in patients with SSc. The 24-week faSScinate study was a randomised double-blind placebo-controlled phased II trial on 87 patients. Tocilizumab treated patients displayed a reduction in the decline of FVC, as well as clinically relevant improvements in their skin

thickness, assessed by mRSS. However, treatment resulted in some adverse events, such as serious infections (Khanna et al., 2016). The focussed study was a randomised double blind placebo control trial on 210 patients. The phase III trial concluded that tocilizumab preserved lung function by preventing the rate of decline in early SSc-ILD patients, where infections were the most common adverse event (Khanna et al., 2021). Overall, the development of disease modifying drugs to reduce the onset of scleroderma has progressed rapidly in recent years, particularly in diffuse SSc patients with ILD.

1.1.2. Interferon Signature in SSc

Scleroderma is a progressive, heterogeneous immune-mediated inflammatory disease (IMID). The heterogeneity of the activation of type I interferon (IFN) signalling contributes towards treatment complications and the diversity of clinical phenotypes observed in SSc and other rheumatic diseases (Muskardin et al., 2018). Type I IFN, consisting predominantly of numerous IFNα subtypes and IFNβ, exert their effects by binding to the interferon type I receptor (IFNAR) and inducing the expression of interferon stimulated genes (ISGs). ISGs then promote antigen presentation, chemokine production, and the adaptive immune response by inducing antibody production. Chronic type I IFN responses are associated with autoimmune diseases, such as rheumatoid arthritis (RA), systemic lupus erythematosus (SLE) and scleroderma (Ivashkiv et al., 2014).

IFN inducible gene expression in blood cells or targeted tissues provides a measure of immune activation in IMIDs, known as an interferon signature (Skaug and Assassi., 2020). Approximately, 50% of SSc patients have a detectable IFN

signature in their whole blood or peripheral blood mononuclear cells (PBMC) (Brkic et al., 2016). Brkic et al., (2016) investigated the expression levels of 11 type I IFN-related genes and observed that early SSc patients, with no onset of clinical fibrosis, displayed the highest averaged IFN scores, as well as the highest prevalence of an IFN signature, when compared to all other SSc patients. This suggests that IFN upregulation is an early event in SSc pathogenesis before skin involvement.

Further, Assassi et al., (2010) generated a composite score of the expression of IFN-inducible genes from the serum of SSc patients (IFN score) and illustrated that anti-topoisomerase positive patients were positively associated with a high IFN score. In addition, there was no significant difference in IFN score when comparing limited and diffuse SSc patients. Likewise, Lui et al., (2013) observed increased IFN-inducible chemokines in the plasma and serum of SSc patients, compared to healthy control, which positively correlated with the severity of skin, lung, and skeletal muscle involvement in SSc patients (Liu et al., 2013).

In recent studies, single cell RNA sequencing of SSc patients with ILD have demonstrated that subpopulations of fibroblasts have upregulated genes associated with the inflammatory response (Valenzi et al., 2019). Valenzi et al., (2019) observed 3 subpopulations of fibroblasts in the lung; 2 majority populations and 1 minor population consisting of predominantly myofibroblasts. Gene ontology (GO) analysis indicated that one major fibroblast population displayed lower expression of collagen type proteins, however an increase in genes associated with the inflammatory response, when compared to the healthy population. In a more recent paper, Valenzi et al., (2021) observed by single cell

RNA sequencing that myeloid and lymphoid cell populations from SSc-ILD patients displayed upregulated genes associated with Type I IFN signalling and inflammation (Valenzi et al., 2021). These studies highlight that cellular populations within the lung contain an interferon signature.

Genome-wide gene expression profiling of SSc patient skin biopsies by DNA microarray showed that SSc patients skin gene expression profiled into four distinct groups; proliferative (dcSSc), inflammatory (dcSSc/lSSc), limited (lcSSc) and healthy-like (healthy, dcSSc and lcSSc). Likewise, patients within the proliferation group had an increase in proliferating cells in the epidermis, as well as patients within the inflammatory group displaying an increase in T cell infiltration in the dermis. Approximately, 177-genes were differentially expressed in dcSSc, which was associated with the severity of skin involvement, where 62 genes were upregulated and 115 downregulated (Milano et al., 2008). Further, Assassi et al., (2015), profiled the global gene expression of SSc patient's skin and identified 2,754 differentially expressed transcripts; where clustering analysis revealed that keratin and fibroinflammatory signatures were the most prominent transcriptomes. Additional pathway analysis of upregulated genes illustrated that type I IFNs, interferon regulator factors (IRFs), as well as the signal transducer and activator of transcription (STAT) family members, were the primary upregulated regulators of type I IFN signalling, where IRF7 was the most activated upstream transcription factor (Assassi et al., 2015).

Moreover, several genes with direct roles in IFN regulation (IRF4, IRF5, IRF7, IRF8 and STAT4) have scleroderma associated single nucleotide polymorphisms (SNPs) (Skaug and Assassi, 2020). Likewise, Assassi et al., (2010) showed that

a missense SNP mutation in IFNAR2 (rs7279064) was significantly associated with a high IFN score in scleroderma patients. This data indicates that polymorphisms could play an important role in dysregulated IFN signalling in SSc patients.

1.1.3. Type I Interferon Signalling and Scleroderma Pathogenesis

Together this data demonstrates that scleroderma patients have an excess of interferon signalling, present in their blood, lungs and skin. Collectively this could be due to polymorphisms in key IFN-regulatory genes (Skaug and Assassi, 2020), as well as cellular components, such as self-derived RNA and DNA, which could trigger pattern-recognition receptors and thus induce immune cell recruitment and infiltration and type I IFN secretion (Barrat et al., 2015). For instance, Lande et al., (2019) observed that CXCL4 organises DNA into an immune complex, which activates TLR9 to induce type I IFN signalling. Further, Kim et al., (2008) also illustrated that serum autoantibodies associated with diffuse scleroderma had IFNα-inducing properties. However, it is unknown how the presence of excess IFN establishes a pathological role in SSc. Azuma et al., (2005) demonstrated that treating bleomycin-induced fibroblasts with IFNβ attenuated fibrosis, through the inhibition of transforming growth factor β (TGFβ). Controversially, this study suggests that IFNβ could have an antifibrotic role in fibrosis, by the inhibition of TGFβ. However, there is a wealth of evidence which suggests that excess IFN has a pathological effect in SSc. For instance, a case report showed that a chronic hepatitis C patient receiving IFNα treatment

developed limited scleroderma with lung involvement (Solans et al., 2004). In addition, a randomised clinical trial of early SSc patients, who received subcutaneous injections of IFNα, displayed deterioration in lung function, increased vascular events and no significant changes in skin fibrosis were observed, when compared to the placebo group (Black et al., 1999). This trial illustrated that IFNα treatment was deleterious to scleroderma patients, and thus suggests that IFNα plays an aggravating role in SSc pathogenesis.

Moreover, Wu et al., (2019) showed that IRF7 gene and protein expression was upregulated in skin biopsies, as well as cultured fibroblasts and myofibroblasts in SSc patients. IRF7 is an essential regulator in type I IFN signalling. Upon phosphorylation, IRF7 translocates to the nucleus and binds to the IFN-stimulated response element (IRSE) promoter region, which leads to expression and secretion of type I IFN and other cytokines. Further, Wu et al., (2019) showed that IRF7 knockdown in bleomycin-induced mice attenuated skin and lung fibrosis, and knockdown of IRF7 in dermal fibroblasts prevented IFNα-induced profibrotic gene expression. Therefore, the observations support a link between type I IFN signalling and fibrosis.

Further, scleroderma patients were treated with an anti-IFNAR monoclonal antibody (Anifrolumab) in a phase I trial, which significantly reduced the IFN signature in the whole blood and skin of SSc patients within days of taking the drug (Goldberg et al., 2014). In addition, skin biopsies from patients taking Anifrolumab showed a reduction in TGFβ signalling (Guo et al., 2015). Overall, this literature illustrates a link between dysregulated IFN signalling observed in SSc patients and fibrosis, where inhibition of IFNAR by antibody therapy

alleviated fibrosis. However, further studies are required to elucidate the mechanism behind how excessive IFN contributes to fibrosis.

1.1.4. The Driving Force behind Excess Type I Interferon in Scleroderma

It is well documented in the literature that scleroderma patients have an IFN signature present in their blood, lungs and skin, however, a key clinical issue is to understand the upstream ligands, which are driving the dysregulated IFN signalling, and thus excess IFN (Valenzi et al., 2021, Skaug and Assassi., 2020). Plasmacytoid dendritic cells (pDCs) are immune cells which are activated through toll like receptor (TLR) 7 and 9 and release significantly more IFNα compared to other cells involved in the inflammatory response, thus have been implicated in the pathogenesis of multiple autoimmune diseases, such as SLE and SSc (Li et al., 2017). However, the importance of pDCs in the pathogenesis of SLE and SSc is not fully understood.

Kim et al., (2008) added serum from scleroderma patients, with anti-topoisomerase antibodies and nuclear extracts to healthy pDCs, which significantly induced IFNα when compared to serum from healthy and other auto-antibody groups. Likewise, the induction of IFNα was significantly higher in diffuse patients, compared to limited, and IFNα levels were positively correlated with lung fibrosis. They further observed that inhibition of a c-type lectin receptor, specific to pDCs, as well as FcγRII prevented the induction of IFNα by SSc serum, which implicates that SSc autoantibodies can induce a type I IFN signature. (Kim et al., 2008). Further, Duan et al. (2008) immunohistochemically stained SSc skin

biopsies for CD123, a common pDC marker, and showed an increased presence of pDCs when compared to control. Likewise, IFNα and IFNβ messenger RNA expression was observed in similar regions to pDCs in SSc skin (Duan et al., 2008). In addition, Ah Kioon et al., (2018), showed that chronically activated pDCs infiltrate the SSc skin layer and induce the secretion of IFNα and CXCL4.

Similarly, Ross et al., (2021) observed that TLR-activated healthy pDCs displayed similar gene expression signatures and enriched biological pathways, with inflammatory SSc skin subsets, as well as known dysregulated signalling cascades in SSc, such as JAK/STAT, NF-κB and angiogenesis. Further, they illustrated that human healthy pDCs induced IFN and a pro-fibrotic response in a bleomycin mouse model. This study supports the hypothesis that pDCs have a key role in immune-driven skin fibrosis.

Overall, the literature strongly supports the hypothesis that pDCs are involved in the pathogenesis of IMIDs, including SSc. However, most scientific studies, including the ones discussed in this thesis, are based on healthy human pDCs, which have been induced by immunostimulatory molecules to replicate their disease counterpart, rather than experiments based on their disease equivalent. Therefore, it is difficult to truly evaluate the importance of pDCs in scleroderma, without studying pDCs isolated from SSc patients. Further, the primary activator of pDCs, which leads to excessive release of IFN, has yet to be determined in scleroderma, which further challenges the theory that pDCs are central to immunopathogenesis observed in SSc.

Further, the activation of pattern recognition receptors (PRRs) has been implicated in SSc pathogenesis. For instance, TLR3 is an endosome-localised

receptor that is activated by double stranded RNA and was found to be upregulated in the dermis of SSc patient's skin biopsies, as well as in bleomycin-induced mice (Agarwal et al., 2011). Likewise, Agarwal et al., (2011) also showed that IFNα induced TLR3 expression, and thus IL-6 expression in dermal fibroblasts, which was augmented in scleroderma dermal fibroblasts. Poly-IC, a common TLR3 ligand, induced IFN and TGFβ response genes in dermal fibroblasts. Chronic stimulation of poly-IC in mice led to inflammation, dermal fibrosis, and skin remodelling (Farina et al., 2010). Moreover, Ah Kioon et al., (2018) showed that pDCs in scleroderma patients have increased expression of TLR8, which is an endosomal receptor that recognises single-stranded RNA. They observed that CXCL4 can potentiate IFN production in pDCs through TLR8. Further, depletion of pDCs reverted fibrosis in mice with established disease, and contrastingly TLR8 transgenic mice aggravated recruitment of pDCs to the skin (Ah Kioon et al., 2018). Further, Lövgren et al., (2004) observed that apoptotic cells released material, such as RNA and DNA, which induced IFNα in pDCs, that was dependent on purified IgG from SLE patient's serum. This work demonstrated a link between autoimmune disease-associated autoantibodies and dysregulated IFN signalling, where autoantibodies associate with endogenous self-nucleic acids and induced IFNα by activating pDCs. These observations highlight the potential role of self-nucleic acids and autoantibodies in PRR's in scleroderma.

Moreover, studies investigating the interferon signature in SLE describe the role of many different PRRs involved in the pathogenesis of the disease (Skaug and Assassi, 2020). Retinoic acid-inducible gene I (RIG-I) and Melanoma differentiation-associated protein 5 (MDA5) are cytosolic recognition receptors,

which recognise double-stranded RNA (dsRNA) and unleashes an innate immune response and the production of IFN. Binding of dsRNA leads to aggregation of mitochondrial antiviral-signalling protein (MAVS) to mediate the response. Shao et al., (2016), showed that one third of SLE patients had MAVs aggregation in their peripheral blood mononuclear cells (PBMCs) and the presence of MAVs aggregates positively correlated with type I IFN response in SLE patients. Furthermore, Kato et al., (2018) showed that SLE patient's serum contains heighted levels of double-stranded DNA which can induce IFN production in THP-1 cells. Knockdown of STING, an essential cytosolic double-stranded DNA (dsDNA) sensor, significantly reduced the ISG-inducing nature of the SLE patient's serum (Kato et al., 2018).

Currently, no upstream ligands have been identified in the blood or skin of scleroderma patients, which can bind and activate the pattern recognition receptors discussed above. Further, it is common knowledge that IFNα is predominantly released from pDCs, as well as IFNβ from numerous other cell types. However, upstream events which lead to pDC and immune activation in scleroderma patients is poorly understood. Thus, further work is required to understand the importance and contribution of PRR in SSc pathogenesis and the IFN signature.

1.1.5. Fibroblast Dysregulation in Scleroderma

In scleroderma pathogenesis, fibroblasts and myofibroblasts are key effectors in the development and progression of fibrosis (Gilbane et al., 2013). Cells infiltrating into the skin layer produce cytokines and growth factors, such as

TGFβ, which causes fibroblast recruitment and activation, which then promotes fibroblasts differentiation into myofibroblasts. Activated fibroblasts and myofibroblasts promote fibrosis, through vast and excessive collagen and fibronectin production. Likewise, activated fibroblasts secrete chemokines, IL6 and CCL2, which are key inflammatory markers in SSc (Leask, 2011, Agarwal et al., 2011, Gilbane et al., 2013).

It has been well documented that scleroderma patients have dysregulated TGF-β signalling in their fibroblasts and myofibroblasts, which results in fibrosis (Chakraborty et al., 2017, Pedroza et al., 2016, Pedroza et al., 2018). For instance, Sargent et al., (2010) showed that 59% of SSc skin biopsies showed a TGFβ response signature, compared to lcSSc and healthy, which was associated with severity of skin score and prevalence of lung disease. Kubo et al., (2002) demonstrated that SSc skin biopsies had upregulated expression in TGFβ stimulated genes. Likewise, immunohistochemically staining illustrated increased expression of TGFβ receptor in scleroderma dermal fibroblast skin sections (Kubo et al., 2002).

Moreover, genome wide profiling of scleroderma dermal fibroblasts showed that TGFβ signalling was associated with inflammatory and fibroproliferative signalling, where the inflammatory subset was strongly associated with activated innate immune signalling (Johnson et al., 2015). Likewise, interferon alpha signalling was strongly associated with early disease progression, compared to TGFβ, which was associated with disease severity and skin involvement (Johnson et al., 2015). This study highlights that inflammation, profibrotic and immune signalling pathways all interplay in scleroderma dermal fibroblasts, which

further implicates that innate immune activation has a key role in scleroderma pathogenesis. The relationship between inflammatory signalling and fibrosis was further investigated by Farina et al., (2010), who showed that poly IC, a TLR3 ligand, induced IFNα, TLR3 and TGFβ mRNA expression in SSc fibroblasts and chronic Poly IC exposure in mice induced dermal fibrosis in mice. Further, Agarwal et al., (2011) showed that pre-treating SSc dermal fibroblasts with IFNα, induced TLR3 expression and IL6; a pro-inflammatory cytokine implicated in fibrosis, and thus inducing their inflammatory potential. Although there is a lack of understanding in the way type I IFN contributes to scleroderma pathogenesis; these studies highlight an interplay between the innate immune response, type I IFN signalling and fibrosis, which leads to an increase in inflammatory potential and pro-fibrotic signalling in scleroderma dermal fibroblasts.

It is well understood that the dysregulation of dermal fibroblasts has a pivotal role in scleroderma pathogenesis by driving fibrosis (Gilbane et al., 2013). Whereas the role of fibroblasts in the abnormal immune response observed in scleroderma is not well understood. In addition, the role of keratinocytes, which are the predominant cell type in the epidermis, in scleroderma immunopathogenesis and fibrosis is also unknown. Fibroblasts are under the influence of a variety of cell types in the skin layer, which secrete growth factors essential to regulate fibroblast proliferation, activation and ECM deposition, specifically TGFβ, which is considered as a master contributor of fibrosis (Leask., 2011, Agarwal et al., 2011, Gilbane et al., 2013). A review by Russo et al., (2020) highlights that the cross-talk between fibroblasts and keratinocytes is highly heterogeneous and allows both cells to influence each other, which impacts the structure of the dermis and epidermis.

Recent work has highlighted that cross talk between dermal fibroblasts and epidermal keratinocytes was altered in scleroderma. For instance, McCoy et al., (2017) illustrated that SSc keratinocyte conditioned media can promote fibroblast activation and myofibroblasts differentiation, in a TGF-β independent mechanism. Further, Russo et al., (2021) stimulated fibroblasts with conditioned media from SSc epidermal cells, which induced the expression of pro-inflammatory cytokines (IL-6 and IL-8), as well as type-I collagen and fibronectin. Although McCoy et al., (2017) observed that SSc keratinocytes could induce a pro-fibrotic response in fibroblasts, they also observed that cultured SSc keratinocytes had repressed type I IFN regulated transcripts, compared to healthy keratinocytes. Whereas, it has been widely documented that SSc skin biopsies contain an upregulation of type I IFN-related gene and protein expression (Duan et al., 2008, Wu et al., 2019, Milano et al., 2008). Therefore, cell communication within the skin environment must maintain the type I IFN signature observed in keratinocytes, which is lost when cultured in-vitro. This suggests that cell-cell communication within the dermal layer could have an essential role in driving and maintaining immune-associated pathogenesis in scleroderma.

Khanna et al., (2022) investigated gene expression of skin cell populations in SSc patients treated with Tofacitinib. They observed that fibroblast and keratinocyte populations displayed a type I IFN signature, which was reduced by treatment with Tofacitinib. Further, genes in fibroblast populations were co-regulated by STAT1. Tofacitinib had minimal impact on T cells in the skin layer, and the most robust changes were observed in the inflammatory response observed in the basal layer of keratinocytes in the epidermis, where Tofacitinib decreased type I and II IFN expression.

Overall, the contribution of keratinocytes and the specific role of type I IFN in the epidermis to scleroderma pathogenesis is unclear. As fibroblasts are predominantly studied in SSc and they are commonly investigated as the 'target' cell. Thus, it is not well understood how fibroblasts can influence surrounding cells, such as keratinocytes in the skin environment. As discussed, fibroblasts and keratinocytes cross-talk within the skin, which is perturbed in scleroderma where communication between fibroblasts and keratinocytes can induce fibrosis. However, it is poorly understood how cell-cell communication across the skin layer can influence and contribute towards SSc pathogenesis and if it's key to the immune and/or fibrotic drive observed in early disease progression.

1.2. Cellular Pathways involved in Type I Interferon Signalling

The next section of this review will be a semi extensive literature review, somewhat beyond the focus of this thesis to assist with the context by explaining the complexity in the innate immune response cascade and mechanisms which regulate the type I interferon response.

1.2.1. Cyclic GMP-AMP Synthase (cGAS) – Stimulator of Interferon Genes (STING) (cGAS-STING)

Cyclic GMP-AMP Synthase (cGAS) – Stimulator of Interferon Genes (STING) (cGAS-STING) is a pattern recognition receptor complex, which can detect self/non-self dsDNA, and upon binding will trigger an innate immune response. Firstly, cGAS recognises double stranded DNA, which catalyses a reaction to create 2'3' cyclic GMP-AMP (cGAMP), which is an agonist of STING (Decout et

al., 2021). Upon recognition of cGAMP, STING is activated, which leads to dimerization, oligomerisation, and translocation from the endoplasmic reticulum (ER) through to the Golgi apparatus (Dobbs et al., 2015). STING acts as a docking protein and recruits TANK-binding kinase 1 (TBK1), which phosphorylates STING at serine 366, to create a STING-TBK1 complex (Gui et al., 2019). The STING-TBK1 complex recruits IRF3 and TBK1 phosphorylates IRF3, which leads to the dimerization and nuclear localisation of IRF3 (Liu et al., 2015). Phosphorylated IRF3 binds to the ISRE promoter region and induces gene expression of type I IFN, ISGs and proinflammatory cytokines (IL6 and IL12) (Wu et al., 2020).

In summary, cGAS-STING is an essential cytosolic DNA PRR, which induces antiviral activity through type I IFN signalling. However, STING can also modulate the activity of NF-κB signalling, both through the canonical and non-canonical pathways. For instance, STING activates the canonical NF-κB signalling pathway through TGF-β-activated kinase (TAK1) and IκκB, which leads to degradation of Iκκβ and thus NF-κB gene expression. TBK1 can also support canonical NF-κB signalling, however TBK1 isn't essential in NF-κB signalling (Balka et al., 2020). Likewise, cGAS-STING activation can also induce non-canonical NF-κB signalling by triggering p52-RELB nuclear translocation (Hou et al., 2018). Interestingly, non-canonical NF-κB signalling acts as a negative regulator of STING signalling by inhibiting type I IFN and canonical NF-Kb signalling (Hou et al., 2018, Decout et al., 2021).

Although, cGAS-STING is a cytosolic PRR, which is essential to protect against pathogens, it has also been recently discussed in literature that cGAS-STING can

be activated by self-DNA and mitochondrial DNA (mt-DNA). For instance, non-apoptotic cell death can lead to extracellular release of DNA, where Deng et al., (2014) illustrated that radiation treatment on tumour cells, led to cell stress, excessive DNA breaks and cell death. Surrounding dendritic cells then internalised the tumour cell DNA, which resulted in cGAS-STING activation and type I IFN signalling.

In addition, cellular stress prompts excessive cytosolic mitochondrial DNA, which is a prominent ligand for cGAS (Decout et al., 2021). Diseases which lead to damaged and dysfunctional mitochondria, such as Parkinson's, induce cytosolic mtDNA and thus STING activity (West et al., 2015). Likewise, proinflammatory cytokine and IFNα signalling can cause perturbed mitochondrial homeostasis, which further increases the efflux of mtDNA into the cytosol and thus creates a positive feedback cascade through cGAS-STING (West et al., 2015).

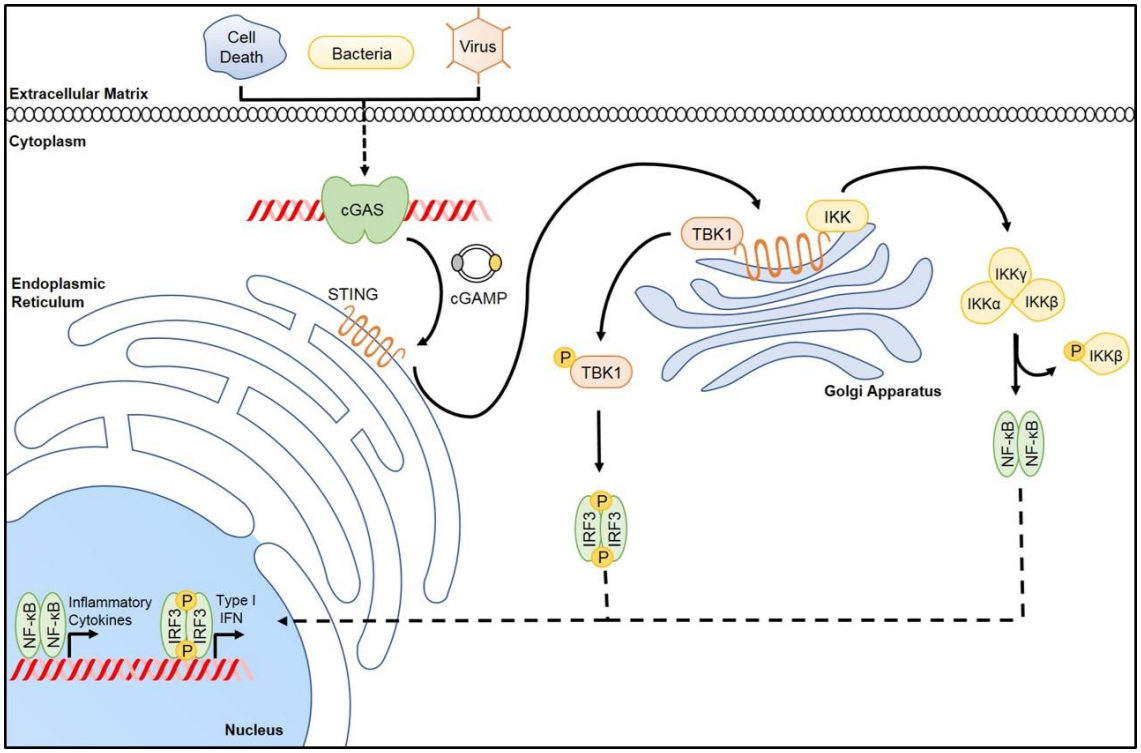

Figure 1.1 cGAS-STING Signalling Cascade

Schematic which illustrates the activation of cytosolic cyclic GMP-AMP synthase (cGAS) by double-stranded DNA (dsDNA). Double-stranded DNA is often released from dying cells or by pathogens, such as viruses and bacteria. Upon binding of dsDNA, cGAS dimerises and becomes enzymatically active to synthesis 2'3' cyclic GMP-AMP, which activates stimulator of interferon genes (STING) located on the endoplasmic reticulum (ER). STING is oligomerised and trafficked through the ER-Golgi network. Upon trafficking, STING recruits and activates Tank Binding Kinase 1 (TBK1), which promotes auto-phosphorylation of TBK1 and phosphorylation of STING Ser366, which recruits interferon regulatory factor 3 (IRF3). TBK1 phosphorylates IRF3, which leads to dimerization of IRF3 and nuclear localisation to induce gene expression of type I interferon and interferon-stimulated genes. STING activation also leads to the activation of canonical NF-κB and thus transcription of proinflammatory cytokines.

1.2.2. Retinoic acid-inducible gene (RIG-I)

Retinoic acid-inducible gene (RIG-I) (DDX58) is part of the RIG-I like helicase receptor family, which includes LGP2 and MDA5. The RIG-I receptor acts as a pattern recognition receptor for dsRNA, which when activated promotes a host cell immunological response (Boelens et al., 2014). RIG-I is composed of multiple domains, which are essential for activation and inhibition, such as two N-terminal caspase activation and recruitment domains (CARD), a DexH-box helicase

domain and a C-terminal domain (Li et al., 2014). When RIG-I is not primed with RNA, the N-terminal CARD domains restrict the ATP hydrolysis activity of the helicase domain, through steric hindrance and thus suppresses RIG-I activity (O'Neill and Bowie, 2011).

The C-terminal domain of RIG-I detects short uncapped 5'triphosphate single-stranded and double-stranded self/non-self RNA, which induces an ATP-dependent conformational change that exposes the central DexH-box helicase and N-terminal CARD domains (Cui et al., 2008, O'Neill and Bowie, 2011). Exposure of the N-terminal CARD domains, causes recruitment of an E3-ligase (TRIM25), which polyubiquitinates lysine 63 (K63) residues on the accessible N-terminal CARD domains, which results in recruitment and homophilic association with the mitochondrial antiviral signalling protein (MAVS) (Belgnaoui et al., 2011, O'Neill and Bowie, 2011).

MAVS becomes functionally active and forms a multimeric filament structure in which many adaptor proteins and kinases are recruited, such as TBK1 and IκB kinase-ε (IKKε). Activation of TANK-binding kinase and IKKε leads to phosphorylation, dimerization, and nuclear localisation of IRF3 and 7, which induces the expression of type I and II IFNs, ISGs and proinflammatory cytokines (Li et al., 2014). Simultaneously, activated MAVS can induce canonical NF-κB signalling through TAK1, and thus increase expression of pro-inflammatory

cytokines, via the IKKα/β/γ complex, by inducing degradation of IκB (Belgnaoui et al., 2011).

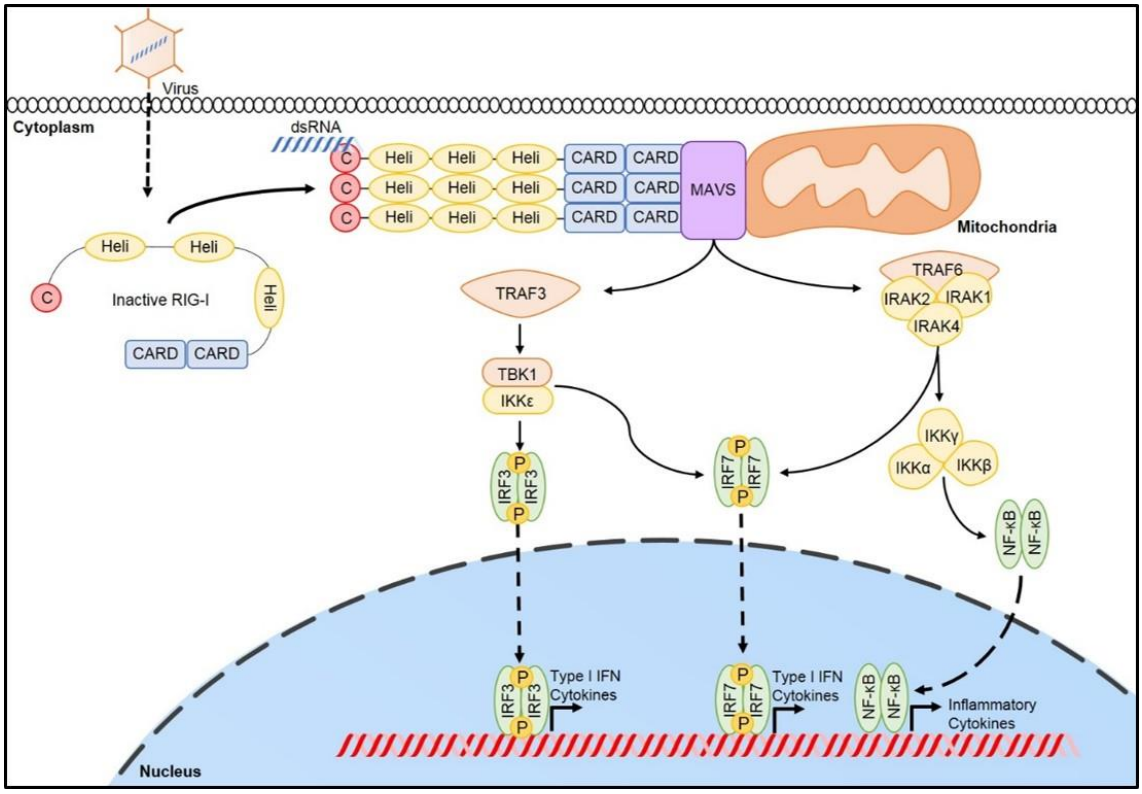

Figure 1.2 RIG-I Signalling Cascade

At resting state, RIG-I is kept inactive by its N-terminal CARD domains, which acts by blocking the helicase domain, through steric hinderance, which prevents ATP hydrolysis activity. RIG-I is activated by viral dsRNA, that leads to a conformational change, which aids oligomerisation of the CARD domains and interaction with MAVS, which is located on the mitochondria. This binding event leads to the recruitment of TRAF 3 and 6, and subsequently the IKKε/TBK1 and NF-κB signalling complex. The IKKε/TBK1 complex leads to the phosphorylation and dimerization of IRF3 and IRF7, which translocate into the nucleus and induces the transcription of type I IFN and interferon-stimulated genes. RIG-I and MAVS oligomerisation also lead to the activation of NF-κB and transcription of proinflammatory cytokines.

1.2.3. Toll-like Receptors (TLR)

Toll-like receptors are a family of pattern recognition receptors, which respond to an array of damage associated molecular patterns (DAMPs) (Gay et al., 2014). They act as type I transmembrane receptors that have an intracellular Toll/IL1 receptor domain (TIR), which is conserved for protein-protein interactions, a

transmembrane domain, as well as an extracellular leucine rich repeat domain (LRR), which is important for signal transduction and ligand recognition (Rock et al., 1998). There are 10 different TLR isoforms in humans, where TLR4 was first discovered and associated with the innate immune response (Medzhitov et al., 1997).

Moreover, TLR1, 2, 4, 5, 6 and 10 all exist on the cell membrane, whereas TLR 3, 7, 8 and 9 are intracellular and located in endosomes (Gay et al., 2014). Each TLR recognises different ligands, where intracellular TLRs recognise non-self-ligands: ssRNA (TLR7/8), dsRNA (TLR3) and DNA (TLR9) and cellular membrane TLRs response to pathogen-associated lipids and proteins, for instance; TLR4 recognises lipopolysaccharide that is commonly released from gram-negative bacteria (Murad, 2014). Upon ligand recognition, TLRs dimerise and activate two distinct signalling pathways: Myeloid differentiation primary response 88 (MyD88)-dependent and TIR-domain-containing adapter-inducing interferon-β (TRIF)-dependent pathways (Takeda and Akira, 2015, Behzadi et al., 2021).

The MyD88-dependent pathway is activated after ligand binding and TLR dimerization of every TLR, apart from TLR3, and this results in NF-κB gene expression. MyD88 forms a complex with IL1 receptor-associated-kinase (IRAK) 1, 2 and 4, which promotes IRAK complex dissociation and interaction with tumour necrosis factor receptor-associated factor 6 (TRAF6). TRAF6 activates TAK1, which phosphorylates IκκB, leading to degradation and thus nuclear translocation of NF-κB. Further, endosomal TLR stimulation promotes MyD88, IRAK1 and 4, as well as TRAF6 to form a complex and phosphorylate IRF7, which

induces type I IFN gene expression (Chang, 2010). Secondly, activation of TLR4 and TLR3 leads to TRIF-dependent signalling, where TRIF activates TBK1, which phosphorylates IRF3 and IRF7, resulting in type I IFN gene expression. Likewise, TRIF can also induce NF-κB signalling by the interaction with receptor interacting protein 1 (RIP1), which leads to polyubiquitination of RIP1. This subsequently induces the activation of TAK1, and thus NF-κB signalling and transcription of pro-inflammatory genes (Chang, 2010, Takeuchi and Akira, 2010, Behzadi et al., 2021).

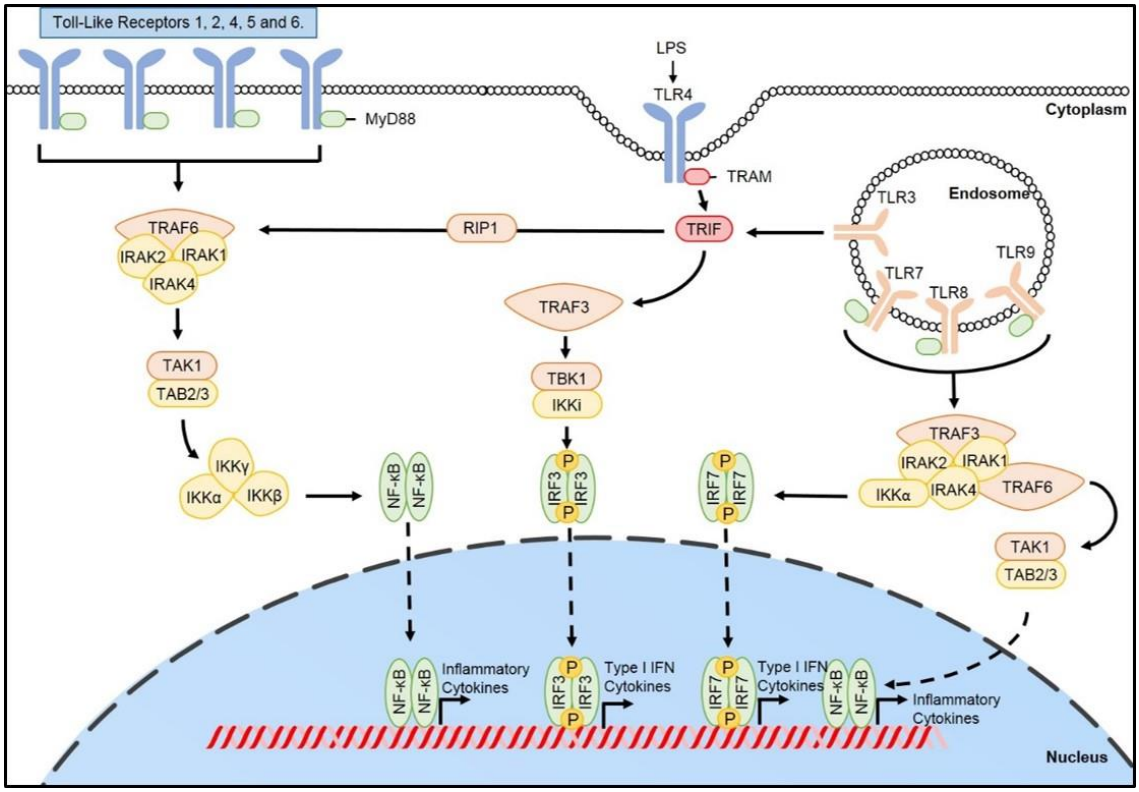

Figure 1.3 Toll-Like Receptor Signalling Cascade

Toll-like receptors 5 and 4, as well as heterodimers TLR2/3 and TLR2/6 are membrane specific receptors, which recognise pathogen associated molecular patterns (PAMPs) at the cell surface, whereas TLR3, 7, 8 and 9 are localised on the endosome and recognise self and pathogenic nucleic acids. Upon ligand binding, TLRs dimerise and engage with MyD88 or TRAM/TRIF domains. Although, TLR4 is localised on the plasma membrane; ligand binding leads to endocytosis, and thus ligand binding to TLR4 leads to primary MyD88 engagement, which is switched to TRIF upon endosome localisation. Binding of MyD88 leads to downstream recruitment of the IRAK1/2/4 and TRAF6 complex, which subsequently recruits and activates the TAK1 complex that activates NF-κB canonical signalling, and thus transcription of pro-inflammatory cytokines. TLR3 and TLR4 activation leads to TRIF recruitment of TRAF6 and TRAF3, where TRAF6 can recruit RIP1, which activates TAK1 and leads to NF-κB signalling. TRIF also promotes activation of TBK1 and IKKε, which leads to the phosphorylation and nuclear translocation of IRF3 and IRF7, which induces transcription of type I IFN and ISGs. Figure adapted from (Duan et al., 2022).

1.2.4. Interferon Regulatory Factors (IRFs)

The interferon regulatory family (IRF) transcription factors contain 9 family members (IRF1-9) and all share similar homology, specifically in their DNA binding domain, which binds to the ISRE and initiates type I IFN transcription in response to pathogens (Schoggins, 2019, Taniguchi et al., 2001). IRFs are

typically activated by kinases, which phosphorylate their transactivation domain that leads to either hetero or homo-dimerization, nuclear localisation, and translational activation, where IRFs can act as activators or repressors of transcription (Taniguchi et al., 2001).

Further, pattern recognition receptors; TLRs, cGAS-STING and RIG-I/MDA5 are the primary activators of the innate immune response, as they respond to pathogen associated molecules, which unleashes a signalling cascade that leads to phosphorylation of IRFs, and thus IFNα/β and cytokine expression (CXCL10, CXCL11, IFIT1 and others) (Cui et al., 2008, Panne et al., 2007). IRF3, 5, 7 and 8 act as positive regulators of PRRs, by inducing gene transcription through positive feedback (Honda et al., 2006). Whereas, IRF4 and IRF8 have important roles in myeloid cell development (Schoggins, 2019).

IRF3 and 7 resemble the strongest homology, compared to other IRFs, and act downstream of PRRs, discussed above. The basal gene expression level of IRF7 is low in most cell lines, compared to IRF3 which is ubiquitously expressed. Induction of IFN expression and signalling, leads to induced expression of IRF7, which drives a positive feedback loop through type I IFN signalling which increases IRF7 and type I IFN gene expression (Marié et al., 1998). Likewise, IRF3 is commonly phosphorylated by TBK1 and/or IKKε in two described regions; primarily IRF3 is phosphorylated between Ser396-Ser405, which removes the auto-inhibitory loop and facilitates the interaction with co-factor CBP (CREB-binding protein), which then enables secondary phosphorylation of Ser385/386, which promotes dimerization and full activation of IRF3 (Panne et al., 2007). Likewise, IRF7 is also activated by TBK and/or IKKε and can become a

homodimer or heterodimer with IRF3, which induces IFNα/β. Honda et al., (2005) showed that IRF7 deficient mice were more vulnerable to viral infection, and IRF7 was essential for IFNα/β gene expression. Further, Honda et al., (2005) illustrated that pDCs are entirely dependent on IRF7, for early and late phase IFN production, when activating TLR9 with single-stranded RNA.

Moreover, IRF5 and IRF8 are important transcription factors in the innate immune response, however they are cell specific. For instance, IRF5 is predominantly expressed in monocytes, macrophages, pDCs and B-cells. Likewise, IRF8 is only expressed in dendritic cells (Jefferies, 2019). Thus, these IRFs are out of scope of this thesis and literature review. Further, IRF9 directly affects type I IFN-driven gene expression, as it creates a complex with STATs, known as ISGF3, downstream of the interferon receptor, and aids dimerization, nuclear translocation and ISRE binding (Steen and Gamero, 2013). IRF9 facilitates binding of the ISGF3 complex to the promoter region of IRSE, through its DNA binding domain, as well as stabilisation of STAT1 (Steen and Gamero, 2013, Blaszczyk et al., 2015). Further, Majoros et al., (2016) recently described that in low level IFNβ environments; IRF9 can bind to unphosphorylated STAT1 and STAT2 and induce type I IFN-stimulated gene expression.

1.2.5. Type I Interferon Receptor

The Type I Interferon Receptor (IFNR) has an essential role in the immune response, by inducing interferon-stimulated genes, upon IFNα/β binding. The ISGs encode for proteins, which are essential for regulating immunity by their anti-viral and anti-proliferative qualities (De Weerd and Nguyen, 2012).

The Type I IFN receptor is made up of two heterogenic subunits: IFNAR1 and IFNAR2 (Darnell, 1994). These subunits interact with JAK1 and Tyrosine kinase 2 (Tyk2) (Darnell, 1994, Platanias, 2005). JAK and Tyk2 are essential for aiding cross tyrosine phosphorylation upon activation of the receptor, in which they create a docking platform for cytoplasmic proteins. Binding of interferon to the receptor induces a rearrangement and dimerization of the receptor, which results in a conformational change promoting tyrosine kinase autophosphorylation and activation of JAK and Tyk2. This produces docking sites on the cytoplasmic region of the receptor, which attracts signal transducers and activators of transcription (STATs) to the receptor (Platanias, 2005).

JAK1 has an important role in phosphorylating STAT1 at tyrosine 701 to promote homodimerization or heterodimerisation, with STAT1 or STAT2, respectively, via its Src homology 2 (SH2) domain in the N and C-terminal (Quelle et al., 1995). STAT1:STAT2 heterodimer requires IRF9 to create a transcription factor complex (ISGF3), which aids nuclear translocation, binding to interferon-stimulated regulatory element (IRSE) in the ISG promotor region and inducing ISG transcription (Majoros et al., 2016, Blaszczyk et al., 2015). STAT1 homodimers can enter the nucleus unaided and bind to the IFNγ activation sequence (GAS),

which is present in the ISG promotor region, inducing ISG transcription (De Weerd and Nguyen, 2012).

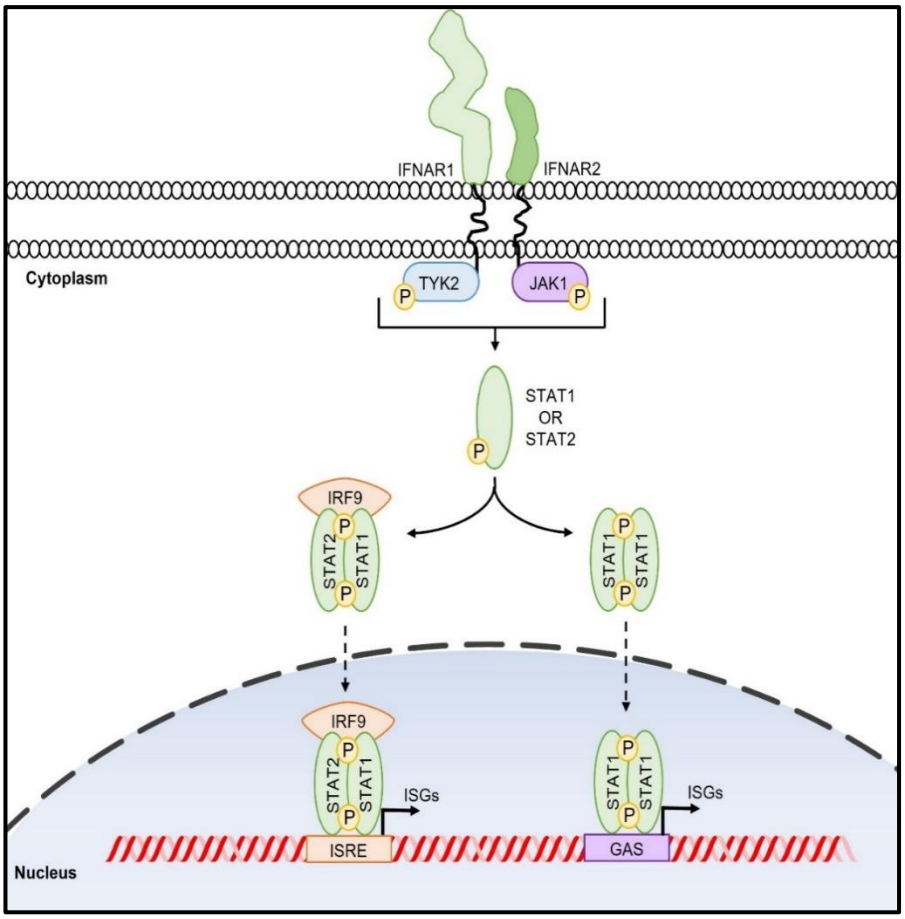

Figure 1.4 Type I Interferon Receptor Signalling.

The Type I IFN receptor is compose of two subunits, IFNAR1 which is associated with tyrosine kinase 2 (TYK2) and IFNAR2, which is associated with Janus activated kinase 1 (JAK1). The IFNAR complex is activated by the binding of type 1 IFN; which are comprised of 13 subtypes of IFNα, as well as IFNβ, IFNε and IFNω. Binding of type I IFN leads to cross-phosphorylation of JAK1 and TYK2, which subsequently triggers phosphorylation of STAT1 and STAT2. Phosphorylation of STATs leads to homodimerization of STAT1 and heterodimerisation of STAT1 and STAT2, as well as the recruitment of IRF9, which forms a complex with STAT1/STAT2 to aid nuclear localisation. These complexes translocate to the nucleus and induce the transcription of interferon-stimulated genes.

1.2.6. Interferon-Stimulated Genes

Type I Interferon is the largest subclass of interferon cytokines (IFNα, β, ε, κ and ω), which can induce the expression of 100's of interferon-stimulated genes (Schoggins, 2019, Schneider et al., 2014). ISGs can be divided into positive and negative regulators of IFN signalling, as well as antiviral effectors (Schneider et al., 2014). Janus Kinase 1/2 (JAK1/2) and non-receptor tyrosine-protein kinase 2 (TYR2) are 3 out of 4 members of the JAK family, which are ubiquitously expressed and act as ISGs, that can create a positive feedback loop and further enhance the IFN response (Schneider et al., 2014). The JAK family acts by binding and stabilising the IFNAR, which potentiates signalling through the receptor complex, and thus induces ISG signalling (Ragimbeau et al., 2003). Typically, ISGs are either expressed basally at low levels or are IFN-inducible. The main ISG regulators are IRF3, 7 and 9, as well as STAT1 and 2, as they are downstream of all PRR and the type I IFN receptor respectively (Mostafavi et al., 2016).

Moreover, Myxoma resistance protein 1 (MX1) is an interferon-induced GTP-binding protein, which acts as an antiviral effector, which prevents viral entry (Gao et al., 2010). Further, MX1 was one of the earliest identified antiviral effectors, where Horisberger et al., (1983) showed that MX1 gene expression was associated with suppression of the influenza A virus. In addition, some antiviral effectors can act as pattern-recognition receptors for DAMPS, for instance oligoadenylate synthetase (OAS) and interferon-induced protein with tetratricopeptide repeats 1 (IFIT1), which can recognise double-stranded and 5'triphosphate RNA respectively. OAS acts by catalysing the production of 2'-5'-linked oligoadenylate, which activates RNAse L to degrade cytosolic viral RNA

(Chakrabarti et al., 2011). Likewise, IFIT1 recognises and binds to 5'triphosphate RNA, which lacks 2'O-methylation, to create a complex, which then acts as a sensor to induce antiviral signalling (Vladimer et al., 2014).

Interferon-stimulated gene 15 (ISG15) is one of the most inducible ISGs, which can act as both a positive and negative regulator of type I IFN signalling. ISG15 acts as an ubiquitin-like protein, which can be covalently attached to target proteins by ISGylation (Zhao et al., 2013). There are many proteins which can control ISGylation, where ubiquitin specific peptidase 18 (USP18) is an important long-term de-sensitizer of type I IFN signalling, which removes ISG15 from proteins, were Ritchie et al., (2004) showed that knockdown of USP18 in mice, lead to hyper-sensitivity to type I IFN.

Further, ISG15 can induce type I IFN signalling by stabilising transcription factors, such as STAT1 and IRF3. For instance, ISG15 can prevent the polyubiquitination of IRF3 and stabilise the IRF3 dimeric complex, which leads to sustained transcription factor activity (Shi et al., 2010). Likewise, ISG15 can block STAT1 degradation by binding to STAT1 and restricting polyubiquitination of K48, thus preserving phosphorylation and activation of STAT1 (Ganesan et al., 2016). On the contrary, ISG15 can negatively regulate RIG-I signalling, where Kim et al., (2008) showed that ISG15 conjugated RIG-I reduced the level of IFN promoter activity.

Overall, interferon and ISGs are key activators and regulators of innate immune signalling. As discussed above, there is a high complexity between the interplay of pattern recognition receptor signalling pathways, which result in type I IFN activation. Developments of autoimmune diseases often occurs due to

perturbations between positive and negative feedback across the innate immune response cascade, where dysregulated ISG expression is an indicator for pathogenic disease (Skaug and Assassi, 2020, Duan et al., 2008, Kioon et al., 2018). As discussed above, over 50% of SSc patients have an IFN signature that is associated with disease pathogenesis and progression (Brkic et al., 2016, Liu et al., 2013). Although, literature consensus has described a strong association between type I IFN signalling and disease pathogenesis, the initiation of dysregulated IFN signalling is unknown. Due to the complexity of the innate immune response, described above, and lack of understanding behind disease initiation and development, it is essential to discover the biological components which are initiating IFN signalling in SSc patients.

1.3. Exosomes

Exosomes are nano-sized extracellular vesicles (30-150nm), which were first discovered in the 1970's from sheep reticulocytes and first assumed to be by-products of homeostasis and thus act by removing cellular waste (Johnstone et al., 1987). They can be found in most bodily fluids including urine, blood, saliva, breast milk and amniotic fluid, as well as in cell cultured medium from most cell types, such as platelets, neurones, epithelial and endothelial cells, dendritic cells, and lymphocytes (Théry et al., 2002). Exosomes act as biological cargo carriers, which transfer a range of biological materials, such as proteins, lipids, DNA, microRNA, mRNA and non-coding RNA and influence the behaviour of surrounding cells. Exosomes are released from the cell by exocytosis and can exert biological changes to corresponding cells via receptor-ligand interaction, internalisation (endocytosis) or vesicle membrane fusion (Gurung et al., 2021).

They act by regulating a range of physiological and pathological cellular processes through autocrine and paracrine signalling (Colletti et al., 2019).

The biogenesis of exosomes requires the endosomal sorting complex (ESCRT) pathway. Firstly, the plasma membrane invaginates and forms an endocytic vesicle, which later matures into a multivesicular body (MVB) and then into a late endosome, by acidification. The late endosome will either bind to the plasma membrane and release exosomes or bind to the lysosome and the contents become degraded (Figure 1.5) (Ibrahim and Marbán, 2016, Scita and Di Fiore, 2010). Tetraspanins (CD63, CD9 and CD81), heat shock proteins (HSP70), MVB biogenesis proteins (ALIX and TSG101), as well as membrane transporters and fusion proteins, are the most commonly identified proteins found in exosomes. Thus, several of these proteins are typically used as specific exosome markers, such as CD63, CD9 and CD81, as well as TSG101 and ALIX (Conde-Vancells et al., 2008).

Moreover, it was first reported in 2007 that exosomes contain RNA, mRNA and microRNA of over 1300 genes, and can be found in a range of different cell types, including human mast cells (Valadi et al., 2007). They further suggested that exosomes can ‘shuttle’ genetic material to other cells to influence their cellular behaviour. However, most of the RNA found in exosomes is often less than 200 nucleotides long and is degraded, although some full-length mRNAs might be present and could potentially influence protein production in recipient cells. Likewise, miRNAs are the most common sub-type of RNA, and exosome miRNAs have been associated with multiple disease pathogenesis and progression, such as in cancer and autoimmunity (Taylor and Gercel-Taylor., 2008, Yao et al.,

2021). In addition, disease-associated exosome miRNAs are an attractive non-invasive biomarker option as a clinical diagnostic (Lin et al., 2015), where Solé et al., (2019) observed a urinary exosome miRNA signature in lupus patients, which was associated with early renal fibrosis and disease progression.

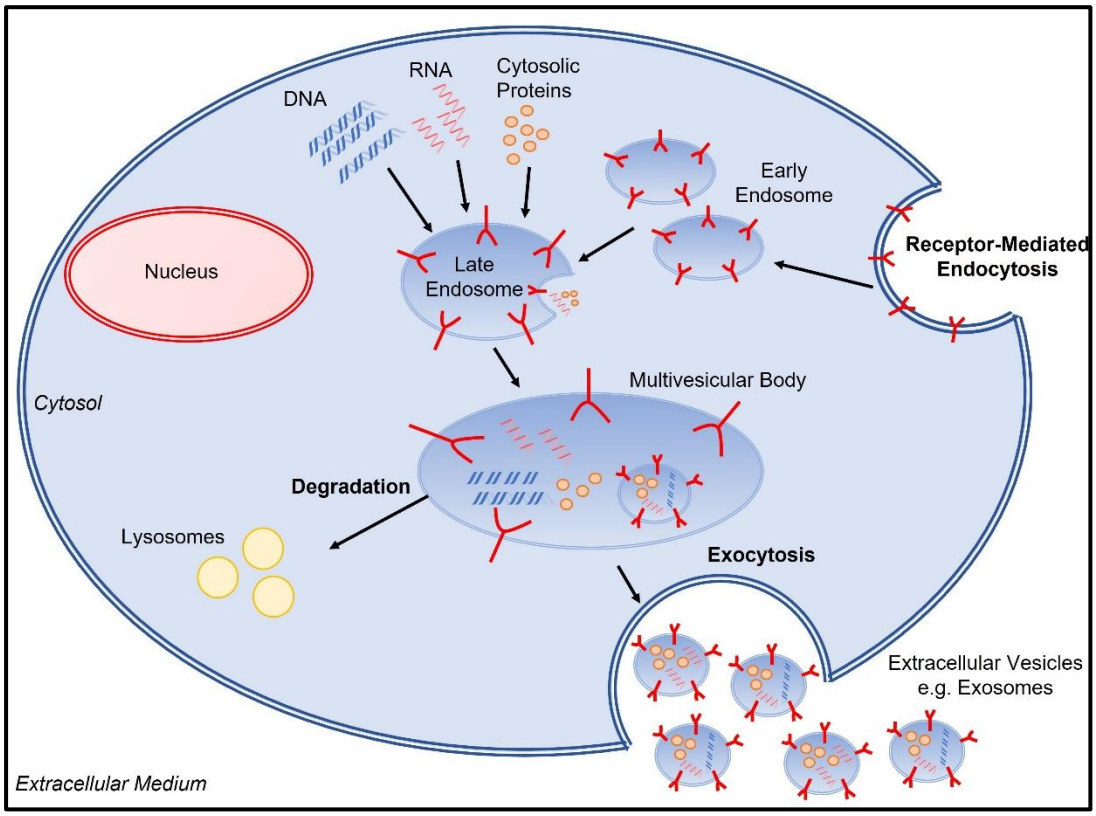

Figure 1.5 The Biogenesis of Exosomes.

Exosomes arise from the inward budding of the plasma membrane, typically by receptor-mediated endocytosis, which leads to the development of early endosomes. Early endosomes then mature into late endosomes and multivesicular bodies, which contain intraluminal vesicles, which sequester exosome cargoes, such as proteins, lipids, and other cytosolic components. The multivesicular body either fuses with the plasma membrane and releases exosomes by exocytosis into the extracellular space or follows the degradation pathway by direct fusion with the lysosome. Figure adapted from (Gurunathan et al., 2021).

1.3.1. The Role of Cancer-associated Fibroblast-derived Exosomes in Innate Immunity

Exosomes hold a pivotal role in the regulation of tumorigenesis and tumour progression, as well as the response to treatment, by acting as intercellular signalling vesicles within the tumour microenvironment (Li et al., 2021, Dai et al., 2020). Cancer-associated fibroblasts (CAF) are the predominant cell type in the tumour microenvironment of solid tumours, and CAF-derived exosomes can influence cancer cell behaviour by dysregulating signal pathways associated with proliferation, metabolism, and immune function (Yang et al., 2019). CAFs express specific markers, distinct from normal fibroblasts, which promote tumour invasion, proliferation, glycolysis, and the excessive release of pro-inflammatory markers (Li et al., 2021). CAFs and SSc fibroblasts share similar pathophysiology where both display abnormal signalling through NF-κB, IL-6/STAT3 and TGFβ/SMAD axis, as well as the overexpression of ECM-remodelling genes and α-SMA (Gilbane et al., 2013, Yang et al., 2019, Li et al., 2021).

Recently, Nabet., B et al (2017) showed that CAF-derived exosomes can induce growth and influence the response to radiation and chemotherapy in breast cancer, by initiating antiviral signalling. Firstly, breast cancer cells induced NOTCH-MYC signalling in CAFs, which led to an increase in signal recognition particle RNA (RN7SL1). Under basal conditions, RN7SL1 is often “capped” by RNA binding proteins (SRP9/14), however the increase in RN7SL1 led to altered stoichiometry in the ribonucleoprotein complex, and thus leading to an abundance of cytosolic uncapped RN7SL1, which was accumulated into exosomes. Uncapped RN7SL1 was transferred to breast cancer by exosomes,

and activated the RIG-I signalling cascade, which induced expression of ISGs; MX1, IFIT1, ISG15 and STAT1, as well as enhancing tumour growth, metastasis, and therapy resistance (Nabet et al., 2017, Boelens et al., 2014). Further, Cui., Y (2022) illustrated that CAF-derived exosomes can induce RIG-I and IFNβ mRNA and protein expression in esophageal squamous cell carcinoma (ESCC) cell lines, which induced cell proliferation, reduced cell apoptosis, and impacted the chemo-sensitivity of cisplatin. Although Cui., Y (2022) doesn't indicate a ligand responsible for RIG-I/IFNβ signalling, both papers highlight that exosomes from CAFs contain ligands, which can induce the antiviral signalling cascade in epithelial cells in the tumour-mediated environment to aid tumour progression and therapy resistance.

1.3.2. The Role of Exosomes in Autoimmune Rheumatology-related Diseases

Exosomes have been discussed to have numerous roles throughout the literature as immune response stimulators, biomarkers, and therapeutic agents. An accumulation of evidence has shown that exosomes play a central physiological and pathological role in autoimmune disease. For instance, rheumatoid arthritis is an autoimmune disease characterised by inflammation and chronic joint damage. Recent studies have illustrated that exosomes from RA patients can carry immunostimulatory molecules, which can trigger a patient's immune response and thus promote disease progression (Zhang et al., 2006, Yao et al., 2021). For example, Zhang et al. (2006) showed that synovial fibroblast-derived exosomes from patients with RA contained membrane bound TNF-α, which induced activation of NF-κB and AKT signalling in CD4+ T cells, activated by

OKT3, rendering them resistant to apoptosis, as well as prompting an inflammatory response. Thus, synovial fibroblast-derived exosomes could hold a pivotal role in T-cell mediated pathology of RA. Further, Yao et al., (2021) discovered that exosomes from synovial fibroblasts contain a long non-coding RNA (lncRNA), HOTTIP, which regulated the STAT3 signalling axis, by binding to miR-1908-5p, which is a negative regulator of STAT3, were elevated STAT3 signalling leads to chronic inflammation.

Exosomes have been shown to be important intracellular messengers in the progression of the inflammatory response in SLE and the abundance of serum exosomes from patients correlates with disease activity (Lee et al., 2016). Further, Lee et al., (2016) observed that SLE exosomes induced IFNα and pro-inflammatory cytokines; TNFα, IL-1β and IL-6, after 24 hours in PMBCs, which was alleviated when exosomes were disrupted by ultra-sonification. Likewise, immunofluorescent imaging showed CFSE-labelled SLE exosomes localised with TLR in PBMCs after 2hrs, and the inhibition of TLR4 prevented exosome induction of pro-inflammatory cytokines (Lee et al., 2016). This work suggests that exosomes can induce type I IFN and pro-inflammatory cytokines, via TLRs, however the biological molecule(s) within the exosomes were not characterised, and thus characterisation of DNA/RNA and proteins of SLE exosomes is essential in providing insight for a potential TLR ligand. Similarly, Salvi et al., (2018) illustrated that exosome from SLE patients' plasma activated IFNα in pDCs after 24 hours. Salvi et al., (2018) further investigated exosome contents and showed that synthetic microRNAs can activate pDCs through the TLR7 receptor.

Moreover, the apoptosis of endothelial cells is a key event in the pathogenesis of SSc and SLE. For instance, Rajagopalan et al. (2004) showed that young women with SLE have elevated levels of circulating apoptotic endothelial cells. Likewise, Maehara et al. (2020) observed an accumulation of apoptotic cells in SSc skin biopsies, where endothelial cells were the predominant targets for apoptosis by cytotoxic T cells. Further, RNA-Seq analysis of apoptotic endothelial cell-derived exosomes illustrated that these exosomes are enriched in non-ribosomal non-coding RNAs; such as long non-coding, protein coding, short non-coding, pseudogenes, rRNA, which can act as viral-like RNAs, which contain a 5'triphosphate motif, capable of activating pattern recognition receptors, such as RIG-I/MDA5 and TLR3, and thus unleashing an immunostimulatory response (Hardy et al., 2019).

1.3.3. The Role of Exosomes in Scleroderma

The role of exosomes in scleroderma pathogenesis and disease progression is still undetermined. However, Nakamura et al., (2016) illustrated that mRNA expression of key exosome markers (CD63 and CD9) was upregulated in the skin of scleroderma patients. Immunohistochemistry staining for CD63 indicated an accumulation in fibroblasts within the skin layer, where immunoblotting of SSc fibroblast lysates showed increased protein expression of CD63, CD9 and CD81, compared to healthy. Further, CD63 ELISA indicated that SSc fibroblasts released significantly more exosomes, than healthy fibroblasts, however no other exosome characterisation was performed. Cultured supernatant from SSc fibroblasts induced collagen type I alpha I chain (COL1A1) and collagen type I

alpha 2 chain (COL1A2) mRNA expression in healthy fibroblasts, which was reversed after exosome removal by filtration (Nakamura et al., 2016).

Exosomes can be isolated from cell supernatant, but also from bodily fluids such as serum, which is most predominantly studied in scleroderma and rheumatology research. Due to the complexity of SSc pathogenesis and the interplay between different tissues and cellular molecular pathways; serum exosomes are an attractive research option, as serum exosomes travel between multiple tissues and cell types all over the body, and thus could aid a more thorough understanding behind the characteristics of the complex multi-event, multi-organ pathology observed in SSc. In addition, investigating sera SSc exosomes could aid biomarker discovery. Guiducci et al., (2008) showed that dcSSc patients release more exosomes from T-cells, platelets, and endothelial cells, compared to healthy patients. Contrastingly, Nakamura et al., (2016) illustrated SSc patients released significantly less serum exosomes, compared to healthy, and hypothesised that vasculature involvement in SSc patients could disrupt the passage of exosomes to and from tissues and cells. Adversely, Wermuth et al. (2017) showed that SSc patients released more serum exosomes, compared to healthy patients. Subsequently, Wermuth et al., (2017) performed a miRNA array on serum exosomes from dcSSc, lcSSc and healthy patients, which showed the upregulation of 6 pro-fibrotic and the downregulation of 10 anti-fibrotic mRNAs. Interestingly, 8 of the 10 downregulated anti-fibrotic mRNAs were significantly different between lcSSc and dcSSc patients. Further, 4 of 6 pro-fibrotic miRNAs' (miR-17, miR-23b, miR-29a, let-7g) were increased by 5-fold in dcSSc patients. Similarly, 4 of 10 antifibrotic miRNAs (miR-125b, miR-140, miR-146b, let-7a) were downregulated by ~70-fold in dcSSc patients serum exosomes, compared

to healthy. Likewise, SSc serum exosomes induced gene expression of COL3A1, COL1A1, CTGF, TGFβ and α-SMA, as well as the protein expression of COL1A1 in fibroblasts after 72 hours (Wermuth et al., 2017). Similarly, Li et al., (2020) discovered that dcSSc neutrophil-derived exosomes contained 22 differentially expressed miRNA and 281 lncRNA, compared to healthy control. GO analysis indicated that miRNA and lncRNA targeted genes associated with IL-6, chemokine and IFN signalling, as well as Wnt, AMPK and NOTCH signalling pathways were upregulated. Interestingly, dcSSc-derived exosomes contained differentially expressed lncRNA involved in IFN production and signalling (Li et al., 2020).

To further understand the role of exosomes in pathogenesis within the skin layer, Bhandari et al., (2022) investigated the crosstalk between SSc dermal fibroblasts and macrophages. Firstly, Bhandari et al., (2022) showed that there were no significant difference in the size or concentration of exosomes from healthy and scleroderma fibroblasts. In addition, PKH-26-dye labelled healthy and SSc fibroblast exosomes were internalised into macrophages at 16 hours. Bhandari et al., (2022) demonstrated that scleroderma exosomes induced pro-inflammatory cytokines (IL6, IL10, VEGF and CCL2) and inflammatory mediators (IL-1α and TNF) in macrophages after 48 hours. Macrophages stimulated with SSc fibroblast-derived exosomes were then co-cultured with SSc fibroblasts, which induced mRNA expression of IL6, COL1A1/3 and fibronectin, when compared to healthy exosome-induced macrophages. Interestingly, SSc exosome-induced macrophages did not significantly induce gene expression of pro-inflammatory cytokines or ECM-related proteins in healthy fibroblasts (Bhandari et al., 2022). Thus, SSc exosome-induced macrophages could sustain

and prolong activation in SSc fibroblasts, however, were insufficient to initiate activation in healthy fibroblasts. Overall, this work suggests that cell-cell communication between SSc fibroblasts and macrophages, via exosomes, can prolong fibroblast activation in SSc, which results in chronic inflammation and fibrosis. However, SSc exosome-induced macrophages aren't sufficient to initiate SSc pathogenesis in healthy fibroblasts alone.

1.4. Summary

Conclusively, recent studies have highlighted the ability of exosomes to induce an immune response (Yao et al., 2021, Zhang et al., 2006, Lee et al., 2016, Salvi et al., 2018). Although there is evidence to show the involvement of exosomes in the autoinflammatory response, there is little knowledge and understanding behind the mechanism in which exosomes initiate and regulate the immune response and their role in autoimmune disease pathogenesis. Further, SSc patients display an elevated type I IFN signature in their blood, lungs and skin, which correlates with disease activity and therapy response (Valenzi et al., 2021, Skaug and Assassi., 2020). However, SSc keratinocytes removed from the skin layer and cultured in-vitro showed repressed IFN signalling, when compared to healthy keratinocytes (McCoy et al., 2017), which suggests that cell-cell communication within the SSc skin environment could induce and maintain type I IFN signalling in scleroderma.

The current literature highlights that SSc serum and dermal fibroblast exosomes could hold a pivotal role in the development of fibrosis, through fibroblast activation and pro-inflammatory cytokine induction respectively (Nakamura et al.,

2016, Bhandari et al., 2022). However, the role of SSc exosomes in immunopathogenesis observed in scleroderma is unknown. Interestingly, literature supports that SLE patient serum-derived exosomes are capable of inducing type I IFN in pDCs and PBMCs through TLRs (Salvi et al., 2018). Thus, they could play a role in elevating type I IFN, and contribute to the IFN signature observed in SLE patients.

Currently, little is understood about the contribution of keratinocytes to the immunopathogenesis, and the pro-fibrotic drive observed in scleroderma. However, recent work has highlighted that epidermal and dermal cells can influence each other, where cultured supernatant from SSc keratinocytes induced pro-fibrotic and pro-inflammatory markers in fibroblasts (McCoy et al., 2017, Russo et al., 2021). There were no further investigations into what biological materials within the supernatant was influencing the fibroblasts, and thus the response could be potentially driven by keratinocyte-derived extracellular vesicles. Considering, fibroblasts are key mediators of fibrosis in SSc, their influence on keratinocytes in the skin layer has been neglected in research. Further, keratinocytes removed from the skin layer and cultured in-vitro lost their IFN signature and thus must be influenced by cells within the skin environment (McCoy et al., 2017). Subsequently, further investigation into cell-cell communication between dermal fibroblasts and keratinocytes could unpick the contribution of the epidermis to the pathogenesis of dermal fibrosis and dysregulated IFN in SSc.

As discussed, SSc fibroblasts and CAFs share similar molecular and cellular features, and there is a wealth of literature which supports the role of CAF-derived

exosomes in inducing type I IFN signalling in epidermal cells in the tumour microenvironment, through pattern-recognition receptors, such as RIG-I (Nabet et al., 2017, Boelens et al., 2014, Cui., Y., 2022). Overall, little is understood about the origin of the IFN signature in SSc patients and recently exosomes have been implicated in the pathogenesis of many diseases, such as cancer and rheumatic autoimmune diseases. As SSc dermal fibroblast exosomes have already been shown to have a role in driving inflammation and fibrosis in the skin layer and there is a wealth of evidence supporting the role of CAF-derived exosomes inducing type I IFN in cancer, it is also highly probable that SSc dermal fibroblast exosomes could contribute towards driving and maintaining the interferon signature observed in SSc patients. Thus, we propose that exosomes from scleroderma dermal fibroblasts could re-introduce type I IFN signalling, and thus maintain the IFN signature in cultured keratinocytes.

1.5. Hypothesis

Exosomes from scleroderma fibroblasts induce a type I interferon response in keratinocytes.

1.6. Research Aim

Scleroderma is rare and uncurable autoimmune disease which affects vasculature and connective tissue. An upregulated immune response can be often observed in scleroderma patients, prior to skin thickening. The aim of this project is to investigate if exosomes from scleroderma fibroblasts contain biological materials, which can induce an immune response in recipient healthy

keratinocytes and the cellular signalling mechanistic behind this induction. Investigating the role in which scleroderma exosomes induce an initial interferon response in keratinocytes could aid the understanding behind a mechanism which initiates early disease pathogenesis and progression in the skin layer, and thus support the development for a therapeutic to target and prevent disease progression in scleroderma.

1.7. Objectives

- Isolate and characterise exosomes from healthy and scleroderma fibroblasts in cell culture supernatant.
- Investigate the role in which exosomes from scleroderma fibroblasts induce IFN-stimulated genes in human epidermal keratinocytes.
- Determine the mechanism in which exosomes induce an interferon response in human epidermal keratinocytes.
- Examine the differences in RNA contents of exosomes derived from healthy and scleroderma fibroblasts.

2. Materials and Method

2.1. Cell Culture

Full thickness skin biopsies were surgically obtained from the forearms of patients with scleroderma, satisfying the 2013 ACR/EULAR criteria for the classification of scleroderma. Three biopsies were taken from healthy controls. Written informed consent was obtained from all patients, and procedures were approved by NRES-011NE. Primary adult human dermal fibroblasts and keratinocytes were explanted from the biopsies (LeRoy et al., 2001) and immortalised using a human telomerase reverse transcriptase (hTERT) vector, which maintains cell immortality by the addition of TTAGGG repeats to the telomere end of the chromosome (Gillespie et al., 2018). Human immortalised epidermal keratinocytes (HaCats) were used as a keratinocyte cell-culture model. HaCats and dermal fibroblasts were maintained in Dulbecco's Modified Eagle Medium (DMEM) (Gibco™) and supplemented with 10% Fetal Bovine Serum (FBS) (Sigma Aldrich) and 100 U/mL Penicillin and 100 µg/mL Streptomycin (Sigma Aldrich). Scleroderma immortalised keratinocytes were cultured in Keratinocyte Growth Medium, with supplement mix containing $CaCl_2$ (PromoCell).

2.2. Experimental Setup

Fibroblasts were washed with Dulbecco's Phosphate Buffered Saline (PBS) (Sigma Aldrich) and treated with 1 mL of 1% Trypsin-EDTA (Sigma Aldrich). Upon cell detachment, the cells were resuspended in 4 mL of supplemented DMEM and split into a new T75 flask. HaCats were washed with PBS and incubated in 5 mL of 0.1% EDTA-PBS (Sigma Aldrich) for 10 minutes. The cells were then treated with 2 mL of 1% Trypsin-EDTA. Upon cell detachment the cells were

resuspended in 4 mL of supplemented DMEM and counted prior to seeding. 10 µL of cell suspension was added to a haemocytometer and cells were counted in each set of 16 squares, where cells occupying the top and right-hand boundary were excluded (Figure 1). Four sets of 16 squares were counted to create an average of cells per set and then total cells were calculated using the calculation below.

Cells were grown to 90% confluency prior to the start of the experiment. Cells were washed twice with PBS and serum-free media (SFM) was added to the cells. After 1 hour of starvation; 1% of exosomes was added for exosome stimulation experiments. A 5'-triphosphate hairpin was used as a positive control, which acts as a RIG-I agonist (InvivoGen). 10 ng/mL of RIG-I agonist was mixed with 1 µL of Lipofectamine™ 2000 (Invitrogen) in 100 µL of SFM and incubated at room temperature (RT) for 20 minutes before addition to the well. Small-molecule drug inhibitors (Table 11) were added to cells 1 hour before exosome / RIG-I agonist addition and paired with an equal volume Dimethyl Sulfoxide (DMSO) (Sigma Aldrich) as a control.

Calculation. Total cells in suspension.

$\frac{(X1 + X2 + X3 + X4)}{4}$ x 10^4 = cells/mL in suspension.

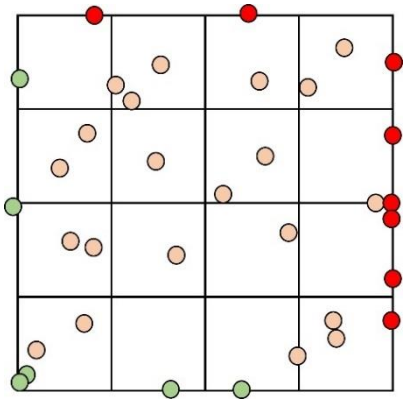

Figure 2. 1. Hemacytometer Schematic

A diagram of one set of 16 squares on a haemocytometer that is used for counting cells, where green and orange circles represent cells counted and red circles represent cells excluded from the counts.

2.3. Exosome Isolation

2.3.1. Ultracentrifugation

Fibroblast cell cultures used to isolate exosomes were grown to 90-100% confluency in DMEM, supplemented with 10% FBS and 100 U/mL penicillin and 100 µg/mL streptomycin. Prior to exosome isolation, the supernatant was removed and the cells were washed twice with PBS. DMEM, supplemented with 10% exosome-depleted FBS (Gibco™) was added to the fibroblasts and collected after 48-72hrs. Exosome-rich DMEM was centrifuged at 2000 x g for 30 minutes to remove cell debris. 5 mL of supernatant was added to Ultra-Clear™ centrifuge tubes (Beckman Coulter) and ultracentrifuged at 42,000 rpm for 2 hours at 4°C. The supernatant was carefully aspirated from the centrifuge tube and 50 µL of sterile PBS was used to resuspend the exosomes. Exosomes were stored at -80ºC.

2.3.2. Total Exosome Isolation Reagent

Fibroblasts were grown to isolate exosomes as discussed above. DMEM, supplemented with 10% exosome-depleted FBS (Gibco™) was added to cells and collected after 48-72hrs. The exosome-rich DMEM was centrifuged at 2,000 x g for 30 minutes to remove cell debris. 1 mL of supernatant was then aliquoted into 1.5 mL eppendorfs and 500 µL of Total Exosome Isolate Reagent (TEI) (Invitrogen) was added to each tube and vortexed. The eppendorfs were agitated at 4°C overnight and then further centrifuged at 10,000 x g for 1 hour at 4°C. The supernatant was removed, and exosomes were resuspended in 50 µL for 5 mL of supernatant.

2.3.3. Optimised Exosome Isolation

Fibroblast cell cultures were grown as discussed above. Exosomes were isolated from media collected after 48-72hr by ultracentrifugation and total exosome isolation reagent (Invitrogen). Exosome-rich media was centrifuged at 2000 x g for 30 minutes to remove cell debris. The supernatant was then ultracentrifuged at 42,000 rpm for 2 hours at 4°C. The top 4mL of supernatant was discarded, making sure to limit disruption to the bottom 1mL left in the centrifuge tubes. The final 1 mL of supernatant was then mixed with 500µL of total exosome isolation reagent and agitated at 4°C overnight. The sample was then further centrifuged at 10,000 x g for 1 hour at 4°C and the pellet was resuspended in 50µL of sterile PBS. Exosomes were aliquoted and stored at -80ºC prior to experiments.

2.4. Pierce™ BCA Protein Assay

A set of protein standards was prepared by diluting bovine serum albumin (BSA) in RIPA lysis buffer (Sigma Aldrich) to create a set of different concentrations,

discussed in Table 1. 5 µL of each standard and sample was loaded onto a 96-well flat-bottomed plate (Corning) in triplicate. A working reagent was created by mixing 50 parts of BCA reagent A with 1 part of BCA reagent B, sufficient to add 200 µL per well. 200 µL of working regent was added to each well and agitated on a plate shaker for 30 seconds at 150rpm. The plate was then covered with foil, to shield from light, and incubated for 30 minutes at 37ºC. The plate was cooled to room temperature and the absorbance of the plate was measured at a wavelength of 540nm.

The absorbance of the standards was plotted against concentration and a straight line was generated. The equation of the line ($y = mx + c$) was then used to work out the respective concentrations of each sample. Standards and samples were normalised against a blank well, which contained RIPA lysis buffer.

Table 1.The concentrations of the BCA standards.

Standards	Concentration µg / mL
1	2000
2	1500
3	1000
4	750
5	500
6	250
7	125
8	25
9	0

2.5. Immunoblotting

Cells were lysed with 150 µL of RIPA lysis buffer (Sigma Aldrich), containing cOmplete™ protease (Roche) and phosSTOP (Roche) inhibitor cocktails. Each well was scraped using Nunc™ cell scrapers (ThermoScientific™) and the lysates were collected in 1.5 mL eppendorfs and centrifuged at 13,000rpm for 15 minutes at 4ºC. The supernatant was collected, and protein concentration was determined using the Pierce™ BCA protein assay kit (ThermoScientific™), as discussed above. Protein lysates were diluted using RIPA lysis buffer to a final concentration of 20µg in a total volume of 20 µL. 8 µL of NuPAGE™ LDS Sample

Buffer (4x) (Invitrogen), containing β-mercaptoethanol (Sigma Aldrich), was added to each lysate and the samples were boiled at 105ºC for 10 minutes. For immunoblotting of exosome lysates, 20 µL of resuspended exosome pellets were boiled with 4 x LDS sample buffer for 10 minutes at 105°C.

A 10-12% polyacrylamide gel was produced using 4.8 mL of ddH_2O, 3.3 mL 30% Bis-acrylamide stock solution (Severn Biotech), 2.5 mL separating or resolving buffer (4x) (Alfa Aesar), 100 µL of 10% Ammonium persulfate (APS) (Sigma Aldrich) and 10 µL N, N, N', N' – Tetramethyl-ethylenediamine (TEMED) for the separating phase. A stacking phase was produced using 6.2 mL of ddH_2O, 1.3 mL acrylamide, 2.5 mL stacking buffer (4x) (Alfa Aesar), 100 µL APS and 10 µL of TEMED.

25 µL of sample was loaded into the wells of the polyacrylamide gel, along with 3 µL of the blue pre-stained protein standard molecular weight ladder (11-250 kDa) (New England BioLabs). The gel was run for 15 minutes at 120 volts during the stacking phase and 45 minutes at 150 volts for the resolving phase in 1 x 10 x Tris/Glycine/SDS Buffer (BioRad).

The proteins from the gel are transferred onto a nitrocellulose membrane by producing a transfer stack, as shown in Figure 2. The transfer stack is saturated in transfer buffer, which consists of; 700 mL ddH_2O, 200 mL Methanol and 100 mL Transfer blotting buffer (10x) pH 8.5 (Alfa Aesar). The transfer is typically run for 2 hours at 50 volts.

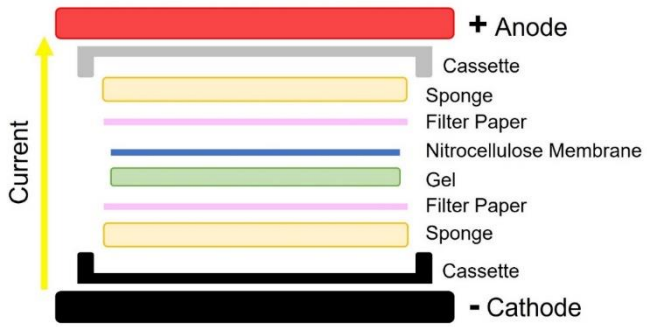

Figure 2. 2 Transfer Stack Schematic.

Prior to blocking, the membrane was stained using 0.1% Ponceau-S solution (G Biosciences), which is a red negative reversible stain that binds to proteins. The Ponceau-S stain was used to determine successful transfer of proteins, as well as the purity of exosome samples. The membrane was briefly washed with tris-buffered saline (TBS) (Alfa Aesar) and 0.1% Tween20 (Merck Life Scientific) until all red dye was eliminated. The nitrocellulose membrane was then blocked for 1 hour at room temperature in 5% skimmed milk (Merck Life Scientific) in TBS-T.

The membrane was then incubated overnight with the appropriate dilution of primary antibody in blocking buffer, discussed in Table 8, at 4ºC. After incubation, the membrane was washed 5 times for 5 minutes in TBS-T (0.1%). The membrane was then incubated at 1 in 15,000 of either rabbit or mouse IgG HRP-linked secondary antibodies (Cell Signalling) in 5% skimmed milk (TBS-T) at room temperature for 1 hour. The membrane was then washed 5 times for 5 minutes in TBS-T (0.1%). 1 mL of SuperSignal West Pico PLUS Chemiluminescent Substrate (ThermoScientific™) was added to each membrane, and they were protected from the light. Excess reagent was removed from the membrane and the membranes were imaged on the BioRad ChemiDoc™ MP Imaging System using the Auto Rapid Capture feature.

Image Lab 6.0.1 (BioRad) software was used to calculate the densitometry of each band on the western blots. The densitometry of a target protein was normalised to the densitometry of the house-keeping protein β-actin.

For re-use of membranes, the membrane will be stripped for 20 minutes in Restore™ Western Blot Stripper Buffer (ThermoScientific™) with agitation on a plate shaker, and then washed 3 times in TBS-T before being blocked for 1 hour in 5% milk (TBS-T).

2.6. CD63 Enzyme-Linked Immunosorbent Assay (ELISA)

Exosome abundance was measured using the ExoELISA-ULTRA CD63 enzyme-linked immunosorbent assay (ELISA) (System Biosciences). The ELISA plate is pre-coated with an anti-CD63 primary antibody, which recognises the tetraspanin CD63 on the exosome surface. The secondary antibody contains a horseradish peroxidase enzyme used for signal amplification. The colorimetric substrate 3,3',5,5'-Tetramethylbenzidine (TMB) is used for the assay read-out. The results are read on a spectrophotometer at a wavelength of 450nm.

25µl of suspended exosomes were diluted in 75µl of coating buffer, sufficient for duplicate wells. A protein standard and serial dilutions were prepared according to manufacturer's instructions (Table 2). 50µL of standards and samples were loaded onto the plate and the plate was incubated at 37°C for 1 hour.

After incubation, the plate was washed 3 times for 5 minutes with 1 x wash buffer. All residual liquid was removed by hard-tapping between each wash step. The primary antibody was diluted 1:100 in blocking buffer and 50µL was added to

each well. The plate was further incubated for 1 hour at room temperature on a micro-titer plate shaker. After incubation, the plate was washed 3 times for 5 minutes with 1 x wash buffer, with shaking. All residual liquid was removed by hard-tapping between each wash step. The secondary antibody was diluted 1:5000 in blocking buffer and 50µL was added to each well. The plate was further incubated for 1 hour at room temperature on a micro-titer plate shaker. The plate was then washed, and 50µL of TMB substrate was added to each well. The plate was incubated in the dark for 15 minutes at room temperature, with shaking. 50µL of stop buffer was added to each well and the plate was read at 450nm using the ThermoScientific Multiskan EX spectrometer.

Table 2. Number of exosomes in standards relating to dilution factor.

Exosome Abundance	Dilution Factor
$4.56x10^{10}$	1
$2.28x10^{10}$	1:2
$1.14x10^{10}$	1:4
$5.7x10^{9}$	1:8
$2.9x10^{9}$	1:16
$1.4x10^{9}$	1:32
$7x10^{8}$	1:64

A line of best fit was generated using the exosome dilutions discussed in Table 2 vs absorbance at 450nm. Samples and standards were normalised against a blank well, which contained 50µL of coating buffer. Exosome abundance was then calculated using the equation of the line of best fit; y = mx + c.

2.7. Transmission Electron Microscopy (TEM)

300 mesh carbon-coated copper grids (Agar Scientific) were glow discharged using the PELCO easiGlow™ (Ted Pella), for 30 seconds at 10 mA and 0.39 mBar pressure. 5µL of exosomes were then loaded onto the 300 mesh copper grids and left for 1 minute. The sample was removed with moist filter paper and immediately the copper grid was washed with 5µL of ddH_2O. The ddH_2O was removed using filter paper and 2% uranyl acetate was added to the grid for 1 minute. The stain was removed using fresh moist filter paper and the grid was washed 3 times with ddH_2O. The grids were left to dry for 15 minutes before being visualised on a FEI Tecnai TF20 microscope. Image J was later used to add a scale bar and quantify the size of the vesicles.

2.8. Dynamic Light Scattering (DLS)

Exosomes were diluted in sterile PBS to a concentration of 100nM. 300 µL of the samples were injected into a Wyatt miniDawnTreos® system (equipped with an additional DLS detector) and the data was analysed using ASTA 6.0.3® software. A 5 minute baseline measurement was obtained, using filtered (0.22 µm) PBS buffer, prior to sample injection. The sample was run for 10 minutes, where a three-minute window was used for final analysis. The flow cell was washed with 1mL of filtered (0.22 µm) 1M nitric acid and MilliQ-grade H_2O after each run. 2

mL of buffer was then run through the flow cell before baseline measurement and sample injection. The raw data was analysed using the ASTA 6.0.3® software to created correlation curves by methods of regularisation. The raw data was further analysed in OriginLab to create a histogram representing the intensity of signal vs hydrodynamic radius. Regularisation analysis yielded a distribution with two peaks, which were not baseline resolved. Therefore, a Gaussian was fit to each sub peak to yield true size distributions. Cumulant analysis was not performed as both peaks were not baseline resolved, and thus produced an incorrect polydispersity index (PDI).

2.9. Internalisation of fibroblast-derived exosomes in human epidermal keratinocytes

Exosomes were isolated from scleroderma and healthy fibroblast by ultracentrifugation and total exosome isolation buffer. The exosome pellet was re-suspended in 1 mL of sterile PBS and 5 µL of Vybrant™ DiO cell-labelling solution (Invitrogen). The exosomes were vortexed and then incubated in the dark at 37ºC for 1 hour. A 3 kDa Amicon Ultra 0.5 mL centrifugal filter (Millipore) was prewashed with 500 µL of sterile PBS and centrifuged at 14,000gx for 10 minutes. 500 µL of DiO-labelled exosomes were added to the filter and centrifuged for 15 minutes at 14,000gx, in two separate amounts. The filter was then washed 3 times with 500 µL of PBS for 15 minutes at 14,000gx. The filter was then removed and inverted into a new flow-through tube and centrifuged for 2 minutes at 1,000gx. The DiO-labelled exosomes were then diluted to 100 µL in PBS.

Simultaneously, HaCats were seeded into a 6-well plate containing a glass coverslip (22mm x 25mm x 0.4mm) into each well and allowed to grow to

approximately 70% in confluency. Serum-free DMEM was added to each well. After 1 hour of starvation, 1% of exosomes was added to each well. Exosomes were added at 3, 6, 10, 24 and 48 hours, over a time-course. At 0 hours, the DMEM was removed, and the cells were washed twice with PBS. The cells were then fixed for 15 minutes in 4% PFA and washed 3 times for 5 minutes. 12 µL of CellBrite® cytoplasmic membrane dye (Biotium) was added to 24 mL of PBS and vortexed. 2 mL of the PBS-membrane dye mixture was added to each well and incubated for 10 minutes in the dark. The dye was removed, and the plates were quickly washed twice with PBS and then three times for 5 minutes. The coverslip was then mounted onto a microscope slide (Thermo Scientific™) using aqueous fluoroshield mounting medium with DAPI (Abcam, ab104139) and left to dry overnight at room temperature in the dark.

The slides were then sealed with nail varnish and imaged on an inverted LMS700 confocal inverted scanning microscope. Images were taken with oil-immersion at 40x magnification at wavelengths of 405 (Blue/DAPI), 448 (Green/DiO) and 652nm (Far-Red/Cytoplasmic Dye). The images were processed in Image J and Zen 3.1 (blue edition) software.

2.10.RNA Lysis and Extraction

Supernatant from adherent cells was discarded and the cells were washed twice in ice cold PBS. 300µL of RNA lysis buffer was added directly onto the cells. The cells were then isolated and centrifuged at 16,000gx for 2 minutes, to remove debris. Prior to RNA extraction, surfaces and pipettes were cleaned with 70% ethanol and RNase AWAY spray (Thermo Scientific™). RNA was then extracted

and purified using the Quick-RNA™ Miniprep Kit (Zymo Research), according to the manufactures protocol. To summarise; the purification of RNA includes multiple centrifugation steps through a spin-column, paired with a DNAse I treatment. Purified RNA is then collected from the column using 50µL of nuclease-free water (Invitrogen).

The concentration and purity of RNA was measured by adding 2µL of each sample to a Nanodrop ND-1000 spectrophotometer (NanoDrop1000, (Thermo Scientific™). Nucleic acid concentration is quantified using a modified Beer-lambert equation, where DNA/RNA absorbs light at 260nm and a 340nm wavelength is used for baseline normalisation. A 260/280nm ratio of ~1.8-2.2 indicates pure DNA and RNA. A 260/230nm ratio of ~1.8-2.2 indicates no presence of phenol or chemical contaminants. RNA yields displaying optical density ratios between 1.8 and 2.2, were used for gene expression experiments discussed in this project.

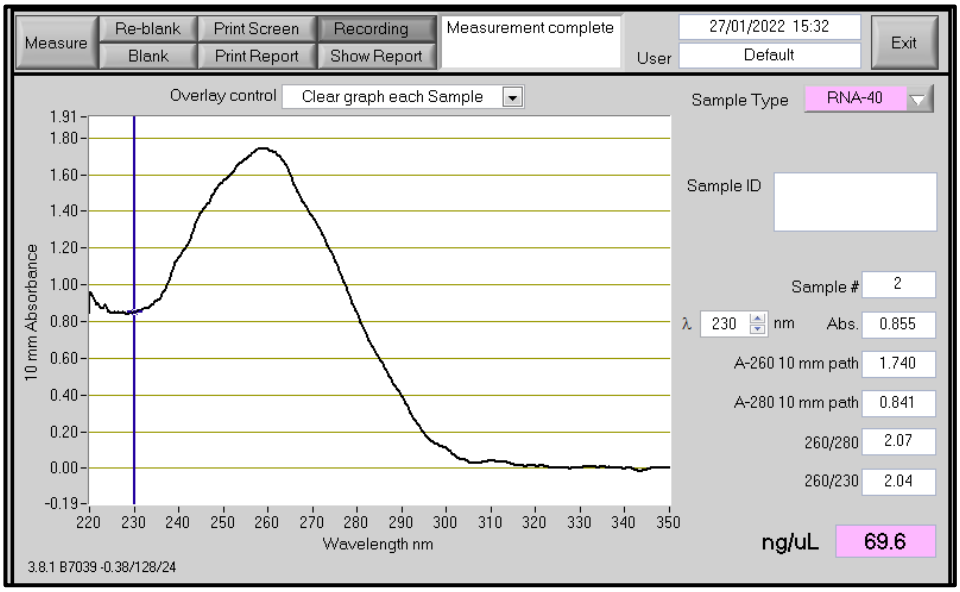

Figure 2.3. Nanodrop Absorbance Spectrum of an RNA sample.

An absorbance spectrum of an RNA sample which shows a good A260/260 and A260/230 ratio, with a concentration of 69.6 ng/µL, indicating that the sample is sufficient for further downstream analysis.

2.11.cDNA Synthesis

Complementary DNA (cDNA) is synthesised using the High Capacity cDNA Reverse Transcription Kit (Thermo Scientific™), according to manufactures instructions. 500ng of RNA from each sample was used in each synthesis reaction. The components required for the reaction are discussed below;

Table 3. cDNA Synthesis Master-mix.

Components	Volume / µL
10x RT Buffer	2
10x RT Random Primers	2
MultiScribe™ Reverse Transcriptase	0.8
25x dNTP Mix (100mM)	1
Total Volume	5.8

Total RNA and nuclease-free water (Invitrogen) was added to create a concentration of 500ng of RNA in a final volume of 20µL. The Applied Biosystems™ Veriti™ Thermal Cycler was used to complete the reaction and settings were as follows:

Table 4. Thermal Cycler Reaction Set-Up.

Settings	Step 1	Step 2	Step 3	Step 4
Temperature / °C	25	37	85	4
Time / Minutes	10	120	5	Hold

2.12. Quantitative Polymerase Chain Reaction (qPCR)

PowerUP™ SYBR™ Green Master Mix (Applied Biosystems™) was used to measure mRNA transcript levels. Each qPCR reaction was set up in a MicroAmp™ 384-well Reaction Plate (Applied Biosystems™) and ran on the QuantStudio™ 7 Flex Real-Time PCR System, 384-well. 1 µL of forward and reverse primer was added to 98 µL of nuclease-free water (NFW) to create a 1nM stock. A master-mix of Primers:SybrGreen was created in a 1:5 ratio. Where 1 µL of primer was added to each well with 5 µL of SybrGreen. cDNA, generated from 500ng of RNA, was diluted 2 in 3 with NFW and 1 µL of cDNA was added to each well. 3 µL of nuclease-free water was also added to each well to create a net volume of 10 µL per well. All reactions were performed in triplicate. The plates were sealed using a MicroAmp™ Optical adhesive film (Applied Biosystems™), centrifuged briefly and then ran on the program listed in Table 5.

Post run, the amplification curve and melt curve graphs were checked to ensure single peaks for each primer pair for the corresponding gene. Post-analysis was performed on excel to determine mRNA transcript gene expression using the efficiency-corrected ΔΔCt method.

Table 5. qRT-PCR Thermocycler Program

Stage	Temperature / °C	Cycles	Time / Seconds
1	95	1	120
2	95	40	15
	60		60
3	95	1	15
	60		60
	95		15

2.13.RT^2 Profiler PCR Array (384-well format) Type I Interferon Response

A genomic elimination mix was prepared with 400ng of RNA, 2 µL GE buffer and variable volumes of nuclease-free water to create a total volume of 10 µL. The genomic DNA elimination mixture was incubated at 42ºC for 5 minutes, and then immediately placed on ice for at least 1 minute. A reverse-transcript mix was prepared according to Table 6. 10 µL of genomic elimination mix was added to 10 µL of reverse-transcription mix and incubated at 42ºC for 15 minutes and then 95ºC for 5 minutes. Samples were placed immediately on ice after incubation. 91 µL of RNAse-free water was added to each reaction mixture and then a PCR mixture was created, following Table 7. 10 µL of PCR components mixture was added to the 384-well plate. Each 384-well plate contains 4 replicates of 96 primers that can be used to analyse 4 samples. Four covers of differing colour are used to aid pipetting of each sample into the plate. The 384-well plate is run

on an Applied Biosystems® QuantStudio™ 7 Real-Time PCR system (384-well) for the cycling conditions described in Table 8. Data was analysed using Qiagen RT^2 PCR Array data analysis tools found online at; https://dataanalysis2.qiagen.com/pcr. Gene expression was normalised to housekeeping genes RPLP0, HPRT1 and B2M.

Table 6. Reverse-Transcription Mix

Components	Volume / µL
5 x Buffer BC3	16
Control P2	4
RE3 Reverse Transcriptase Mix	8
RNase-free Water	12

Table 7. PCR mixture (384-well)

Components	Volume / µL
2x RT^2 SYBR® Green Master Mix	650
cDNA synthesis reaction Mix	102
RNase-free Water	548

Table 8. Cycling conditions for qPCR reaction

Cycles	Duration	Temperature	Comments
1	10 min	95ºC	HotStart DNA Taq Polymerase is activated by this heating step.
40	15 secs	95ºC	Perform fluorescence data collection.
40	1 min	60ºC	

2.14.Immunofluorescence

Glass coverslips (22mm x 25mm x 0.4mm) were placed into a 6 well plate (Thermo Scientific™) and washed with 100% ethanol (Fisher Scientific). The ethanol was removed, and the slides were further washed 3 times with sterile PBS. Human epidermal keratinocytes were seeded into each well at 250,000 cells per 2 mL of DMEM, supplemented with FBS and PenStrep. The cells were grown to approximately 80% confluency and then harvested. The DMEM was removed, and the cells were washed 3 times with PBS.

Cells were fixed by the addition of 1 mL of 4% paraformaldehyde (PFA) (Alfa Aesar) for 15 minutes. The PFA was removed and the coverslips were washed 3 times with PBS. 0.2% Triton X-100 (Sigma Aldrich) was added to permeabilise the cells for 15 minutes and then removed by washing 3 times with PBS. The coverslips were blocked for 10 minutes in 1% bovine serum albumin (BSA) (Sigma Aldrich) in PBS. Primary antibodies were made up in 1% BSA, to concentrations specified in Table 10, and centrifuged for 5 minutes at 10,000 x g to remove aggregates. 200 µL of primary antibody was pipetted directly on top of

each coverslip and then was sealed with parafilm (Sigma Aldrich). The coverslips were stored overnight at 4ºC.

After incubation, the parafilm was removed and the coverslips were washed 3 times with PBS. Secondary antibodies, discussed in Table 10, were diluted 1 in 300 in 1% BSA and centrifuged at 10,000 x g for 5 minutes. 200 µL of secondary antibody was pipetted onto each coverslip and sealed using parafilm. The coverslips were incubated at room temperature for 2 hours in the dark.

After incubation, the parafilm was removed and the cells were washed 3 times for 5 minutes in PBS. A droplet of ProLong Gold Antifade Mountant, with DAPI (Invitrogen), was added to each slide and the coverslip was lowered gently on top of the droplet with the cell-side facing down. The slides were allowed to dry over night at room temperature, shielded from the light. The next day the slides were sealed using clear nail varnish and imaged on the EVOS F1 digital inverted microscope (AMG) at 40x magnification and an inverted LMS700 confocal inverted scanning microscope. Images were taken with oil-immersion at 40x magnification.

2.15.shRNA Lentiviral Particle Transduction

HaCats were seeded into a 6-well plate and incubated until they reached 50% confluency. A kill curve was created by adding varying concentrations of puromycin (Invitrogen) to each well (8 – 1 µg/mL). The cells were checked every 24 hours and by day 6 all cells between 8 – 2 µg/mL had died. Therefore, 2 µg/mL of puromycin was used as the selection concentration.

For shRNA transduction; HaCats were plated into a 6-well plate to reach 50% confluency, 24 hours before viral infection. On the day of infection, 5 µg/mL of polybrene (Sigma-Aldrich) with supplemented DMEM (Gibco) was added to each well along with 1 x 10^6 infectious units of virus (IFU) (Santa Cruz) and then incubated overnight. After incubation, the media was removed and replaced with fresh DMEM without polybrene. After 8 hours, the cells were treated with 1% trypsin-EDTA and split into a T25 flask. Upon confluency, the cells were split into a T75 flask with selection media, containing DMEM and 2 µg/mL puromycin. Media was changed every 4 days and the cells reached confluency by day 10. The cells in the death control were dead by day 3. The shRIG-I knockdown was investigated by qPCR and protein analysis by immunoblotting.

2.16.Exosome RNA Extraction

Exosomes were isolated by ultracentrifugation and total exosome isolation and resuspended in 100 µL of PBS. Prior to RNA extraction, surfaces and pipettes were cleaned with 70% ethanol and RNase AWAY spray (Thermo Scientific™). RNA was then extracted and purified using the Total Exosome RNA & Protein Isolate Kit (Invitrogen), according to the manufacturers protocol. To summarise; 100 µL of PBS was added to exosome samples to total 200 µL and then 200 µL of 2x denaturing solution was added and the sample was incubated on ice for 5 minutes. 400 µL of acid-phenol:chloroform was added to each sample and then vortexed for 60 seconds, before centrifuging for 5 minutes at 16,000 x g. The centrifugation step separated the mixture into an aqueous (upper) and organic phase (lower). The aqueous upper layer was removed and mixed with 1.25 volume of 100% ethanol and then centrifuged through a filter column at 10,000 x

g for 30 seconds. The flow through was discarded and the column was washed with 700 µL of miRNA wash solution 1 and then twice with 500 µL of wash solution 2/3 by centrifugation at 10,000 x g for 30 seconds. The filter column was span for 2 minutes at 10,000 x g to remove any residual ethanol and then transferred into an RNAse-free Eppendorf. 50 µL of nuclease-free water, pre-heated to 95ºC, was added directly to the filter column and was centrifuged for 30 seconds at 10,000 x g. Concentration of RNA from exosomes couldn't be determined by Nanodrop, due to low concentrations and thus was sent for quality control at Novogene prior to RNA sequencing.

2.17.Transwell Assay

Fibroblasts were seeded onto 0.4-micron pore polyethylene terephthalate (PET) transmembranes (Corning). An equal number of HaCats were seeded into a separate cell-culture plate. Upon confluency, both cell lines were washed twice with PBS and combined, were equal volumes of serum-free media was added onto the HaCats and fibroblasts. After 48 hours, the DMEM was removed from the cells and the HaCats were harvested for RNA and protein. The fibroblasts were then fixed with 4% PFA, permeabilised with 0.2% triton and blocked for 10 minutes in 1% BSA. The membrane was then cut with a scalpel and the cell-side was mounted onto a glass slide using Prolong-Gold DAPI and sealed with a glass coverslip. The membranes were then imaged the next day on the EVOS fluorescent microscope at 405 nm.

2.18.RNASeq Library Preparation

RNA was isolated from exosomes and HaCats stimulated with exosomes, as described above, and was sent to Novogene for quality control and sequencing. Sample quality was investigated by nanodrop, agarose gel electrophoresis and Agilent 2100 for quantification, purity and RNA degradation/integrity. Poly-T-oligo-attached magnetic beads were used to purify messenger RNA (mRNA) from total RNA. The mRNA was then fragmented and then first strand cDNA was synthesised using reverse transcriptase and random hexamer primers. Upon completion, second strand cDNA synthesis was performed using dNTPs, RNase H and DNA polymerase I. Exonucleases were used to covert overhands into blunt ends and 3' ends of DNA fragments were adenylated. The cDNA fragments were then ligated and purified with an AMPure XP system. The library was quality controlled checked for library concentration and insert size. Quantified libraries were pooled and sequenced on the Illumina Novaseq platform and 150 bp paired-end reads were generated.

2.19.Sequencing Data Analysis

Quality control of fastq files was performed with FastQC version 0.11.9. Reads were aligned to the human reference genome version GRCh38.84 using STAR aligner version 2.5.2b. MultiQC version 1.11 was used to QC the alignment and generate an overall quality control report. Downstream analyses and visualizations were performed using R version 4.1.2. BAM alignment files generated by STAR were transformed into count tables using Rsubread version 2.8.1. The R package edgeR version 3.36.0 was used for differential gene expression analysis.

2.20. Flow Cytometry

2.20.1. Live/Dead Staining

Flow Cytometry was performed using a CytoFLEX S (Beckman Coulter). Analysis was performed using CytExpert (Beckman Coulter). For Live/Dead staining for HaCats and fibroblasts using 7AAD, 1 x 10^5 cells were resuspended in 1 mL of PBS and centrifuged at 400 x g for 5 minutes. The PBS was removed and the cells were resuspended in 300 µL of PBS. 5 µL of 7-Aminoactinomycin D (7-AAD) (BD Biosciences). Samples were run on a Beckman Coulter CytoFLEX S High Throughput (13 colour laser) flow cytometer.

Primarily, the cells were gated on their forward vs side scatter to obtain the gate P1 (Figure 4). Aggregates were then excluded from forward scatter by plotting forward area scatter against forward height scatter to yield gate P2. Dead cells were distinguished by gate P3 by plotting PC5-5A against forward scatter.

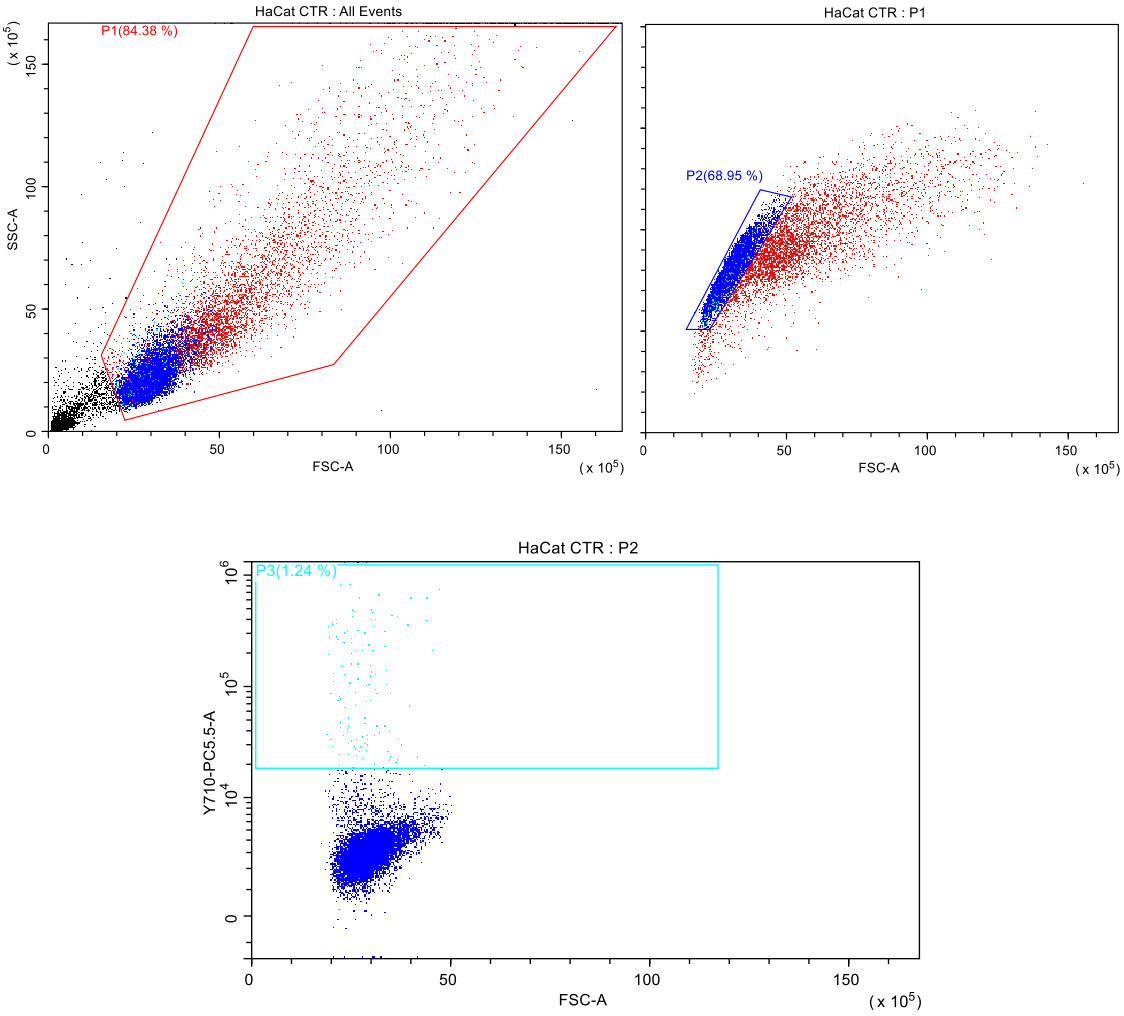

Figure 2.4. Gating strategy for live/dead staining using 7-AAD for HaCats.

2.20.2. Exosome Visualisation

Flow Cytometry was performed using a CytoFLEX S (Beckman Coulter). Analysis was performed using CytExpert (Beckman Coulter).

Samples were run on a Beckman Coulter CytoFLEX S High Throughput (13 colour laser) flow cytometer. Exosomes were isolated from healthy and scleroderma fibroblast supernatant as described in Methods 2.3.3. and stained with 5 uL of Vybrant™ DiO cell-labelling solution (Invitrogen). The exosomes were vortexed and then incubated in the dark at 37ºC for 1 hour. A 3 kDa Amicon

Ultra 0.5 mL centrifugal filter (Millipore) was prewashed with 500 µL of sterile PBS and centrifuged at 14,000gx for 10 minutes. 500 µL of DiO-labelled exosomes were added to the filter and centrifuged for 15 minutes at 14,000gx, in two separate amounts. The filter was then washed 3 times with 500 µL of PBS for 15 minutes at 14,000gx. The filter was then removed and inverted into a new flow-through tube and centrifuged for 2 minutes at 1,000gx. The DiO-labelled exosomes were then diluted to 300 µL in PBS. Exosomes stained with DiO-dye without filtration and DiO-dye in PBS +/- filtration were also diluted into 300 µL of PBS and investigated. 300 µL of PBS, which was used as the main buffer, as well as PBS mixed with 100 µL Megamix-Plus SSC (Biocytex) were investigated as background noise and to determine size regions on the flow, where Megamix-Plus SSC contains reference beads of varying parameters; 0.16 µM, 0.2 µM, 0.24 µM and 0.5 µM, which fluoresce in the FITC channel.

2.21.Statistical Analysis

Data was checked for Gaussian normality before statistical analysis by using normality tests; Anderson-Darling, D-Agostino, Shapiro-Wilk and Kolmogorov-Smirnov. Nonparametric data was analysed using Mann-Whitney U tests for unpaired samples. Parametric data was analysed using either an unpaired Student T Tests assuming equal variance or a Two-Way ANOVA with multiple comparison correction, using Tukey. Experimental data was presented as the mean ± standard error of the mean. A p-value < 0.5 was considered as statistically significant. Statisitcal analysis was performed using GraphPad Prism Software, Version 9.0 (San Diego, CA, USA).

Table 9. List of primers used for qPCR.

Gene	Forward Primer	Reverse Primer
IL-6	GGTACATCCTCGACGGCATCT	GTGCCTCTTTGCTGCTTTCAC
MX1	CGACACGAGTTCCACAAATG	AAGCCTGGCAGCTCTCTACC
CXCL10	TCCAGTCTCAGCACCATGAA	AGGTACTCCTTGAATGCCACT
CXCL11	TCCCCCATGTTCAAAAGAGGAC	ATATCTGCCACTTTCACTGCTTTTAC
OAS	CGGACCCTACAGGAAACTTG	GAAGCAGGAGGTCTCACCAG
IFIT1	GACTGGCAGAAGCCCAGACT	GCGGAAGGGATTTGAAAGCT
ISG15	GTGGACAAATGCGACGAACC	ATTTCCGGCCCTTGATCCTG
RIG-I	CACCTCAGTTGCTGATGAAGGC	GTCAGAAGGAAGCACTTGCTACC

STAT1	TTACTCCAGGCCAAAGGAAG	TTCAGCTGTGATGGCXGATAG
IFNβ	AAACTCATGAGCAGTCTGCA	AGGAGATCTTCAGTTTCGGAGG
GAPDH	ACCCACTCCTCCACCTTTGA	CTGTTGCTGTAGCCAAATTCGT
RIBO	GTAACCCGTTGAACCCCATT	CCATCCAATCGGTAGTAGCG
ACTIN	TGCCCTGAGGCACTCTTCCAG	CACACGGAGTACTTGCGCTC

Table 10. List of antibodies used for immunoblotting.

Antibodies	Dilution	Blocking Buffer	Applications	Source	Catalogue Number
RIG-I	1 in 500	5% Milk (TBS-T)	Western Blotting	Cell Signalling	3743S
STAT1	1 in 500	5% Milk (TBS-T)	Western Blotting	Cell Signalling	9172S
pSTAT1(Tyr701)	1 in 500	5% BSA (TBS-T)	Western Blotting	Cell Signalling	9167S
IRF3	1 in 500	5% Milk (TBS-T)	Western Blotting	Abcam	ab68481
pIRF3(S386)	1 in 500	5% BSA (TBS-T)	Western Blotting	Abcam	ab76493
STAT3	1 in 500 1 in 100	5% Milk (TBS-T) 1% BSA (TBS-T)	Western Blotting Immunofluorescence	Abcam	ab119352
pSTAT3(Tyr705)	1 in 500	5% BSA (TBS-T)	Western Blotting	Cell Signalling	9145S

pSTAT3(Ser727)	1 in 500	5% BSA (TBS-T)	Western Blotting	Abcam	ab32143
βactin	1 in 1000	5% Milk (TBS-T)	Western Blotting	Sigma (Merck)	A5441
STAT1	1 in 100	1% BSA (TBS-T)	Immunofluorescence	Cell Signalling	14994S
CD63	1 in 1000	5% Milk (TBS-T)	Western Blotting	Abcam	ab59479
TSG101	1 in 500	5% Milk (TBS-T)	Western Blotting	Abcam	ab125011
Histone H3	1 in 5000	5% Milk (TBS-T)	Western Blotting	Abcam	ab1791
α-SMA	1 in 2500	5% Milk (TBS-T)	Western Blotting	Abcam	ab7817
ISG15	1 in 1000	5% Milk (TBS-T)	Western Blotting	Protein Tech	15981
IKKαβ	1 in 1000	5% Milk (TBS-T)	Western Blotting	Cell Signalling	4814S

pIKKαβ (Ser32/36)	1 in 500	5% Milk (TBS-T)	Western Blotting	Cell Signalling	9246S

Table 11. List of small molecule drug inhibitors.

Compound	Solubility Reagent	Working Concentration (μM)	Biological Activity
GW4869	1mM/mL DMSO	5-20μM	Inhibits exosome biogenesis and release by inhibiting ceramide-mediated inward budding of multivesticular body (MVB) and release of exosomes from MVBs**.**
GSK8612	20 mM/mL DMSO	10μM	Binds to Tank-binding Kinase 1 (TBK-1) and prevents kinase activity by binding to ATP-binding pocket.
Tofacitinib	10 mM/mL DMSO	10μM	Inhibits Janus Kinase 1 (JAK1) and Janus Kinase 3 (JAK3), and thus prevents phosphorylation of STATs and interferes with JAK-STAT signalling cascade.

3. The Isolation and Characterisation of Exosomes from Healthy and Scleroderma Fibroblasts.

3.1. Introduction

Exosomes, as well as other types of membrane vesicles such as ectosomes, microparticles and apoptotic bodies, are released from many cell types and play an important role in intracellular communication (Gurunathan et al., 2019). Exosomes have been isolated from an array of bodily fluids including blood, semen, saliva, and urine. The isolation method of exosomes is critical for downstream application, as different methods have an array of positives and negatives (Thery et al., 2006), summarised in Table 12. Once exosomes are isolated, they can be analysed by several characterisation and validation methods developed for both research and clinical applications to investigate exosome quantity, cargo, and biophysical properties. These methods include transmission/scanning electron microscopy (TEM/SEM), flow cytometry (FC), nanoparticle tracking analysis (NTA), dynamic light scattering (DLS), immunoblotting, total protein quantification, enzyme-linked immunosorbent assay (ELISA) and fluorescence-activated cell sorting (FACS) (Gurunathan et al., 2019, Thery et al., 2006).

Moreover, exosomes act as biological carriers and therefore have a significant role in regulating many physiological and pathological processes in disease (Gurunathan et al., 2019). Numerous studies have suggested that exosomes can behave as biomarkers for prognosis and diagnosis of multiple diseases (Kalluri et al., 2020). The accessibility of exosomes and the lack of invasive procedures for isolation, means they hold promising potential as a biological diagnostic. Due

to their potential roles in health and disease, exosomes have become an attractive research area for clinical and pharmaceutical application.

As a result of clinical application and research interest, it is essential that the isolation method for exosomes is optimised to produce maximum purity, yield, and reproducibility between preparations. Although, ultracentrifugation (UC) and density centrifugation are considered the 'gold standard' for exosome isolation from bodily fluids and cell supernatant, there is no consensus on the best method for obtaining the optimal yield, purity, and quality of exosomes (Soares et al., 2018). The size similarity between extracellular vesicles and exosomes has been an obstacle in exosomes isolation (Iwai et al., 2016). In addition, bodily fluids and cell supernatant contains a multitude of contaminating proteins, such as albumin, which are often deposited when isolating exosomes (Soares et al., 2018).

Ultracentrifugation removes contaminating cellular debris and apoptotic bodies, which results in pure exosome preparations at a cost of reduced yield and problems with sample reproducibility (Iwai et al., 2016). Since UC is time-consuming and requires specific equipment, numerous companies have produced isolation kits, which are quick, easy and give reproducible exosome recovery rates (Gurunathan et al., 2019). Most commercially available kits for exosome isolation act by precipitating exosomes using hydrophilic polymers, such as polyethylene glycol (PEG), which lowers the solubility and thus pelleting of exosomes during low-speed centrifugation (Thery et al., 2006). Although, precipitation is an attractive method, as it is simple, time efficient and results in a good exosome yield; precipitation methods can lead to co-isolation of large proteins and contaminants (Soares et al., 2018). Overall, the methods of exosome isolation have different positives and negatives, thus it is essential that

the appropriate method is chosen based on the requirements of the isolated exosomes.

Table 12. The advantages and disadvantages of exosome isolation methods.

Methods	Advantages	Disadvantages
Ultracentrifugation (UC)	• "Gold Standard" Method • No additional reagents • Pure exosome yields • Large sample volume	• Requires specific equipment. • Time consuming. • Labour Intensive. • Potential to damage vesicles due to high speeds. • Low exosome yield. • Only suitable for large volumes.
Polymer-based Precipitation	• Quick and easy to follow protocols. • High yields of exosomes. • Good for RNASeq preparations. • Process numerous samples.	• High reagent cost. • Low volumes of samples. • Protein contamination. • Polymer contamination.
Ultrafiltration (UF)	• Process numerous samples. • Quick and easy. • High yields of exosomes. • No additional reagents.	• Protein contamination. • Vesicle Aggregation.
Size Exclusion Chromatography	• Pure exosome yields. • Most optimal in combination with UC/UF.	• Extracellular vesicle contamination. • Sample dilution, via pooling. • Time consuming.
Immunoaffinity Capture	• Simple and easy. • Good for mass spectrometry. • Extremely pure exosome yields. • Isolate specific exosome surface markers.	• High reagent cost. • Subset of vesicles isolated. • Low exosome yields. • Suitable for low volume.

3.2. Chapter Components

1. Examine the clinical heterogeneity of diffuse patients fibroblasts used in this study.
2. Optimise the isolation of exosomes from healthy and scleroderma dermal fibroblasts for downstream application.
3. Quantify and characterise the isolated dermal fibroblast exosomes.

3.3. Results

3.3.1. Scleroderma patient clinical data highlights the disease variability in the diffuse subclass of patient samples used in this study

Exosomes were isolated from 6 diffuse cutaneous SSc patients' dermal fibroblasts in this project. Below is a small review which highlights the heterogeneity of dcSSc patients used within this project.

The severity of scleroderma is commonly characterised by two sub-classes: localised (skin involvement) and diffuse (skin and organ involvement). Likewise, disease severity can vary between patients within the same subclass. The variability of disease progression, between patients with scleroderma, represents one of the key issues behind understanding the complexity of the disease.

Table 13 summaries clinical data which was collected from patients, prior to skin biopsy, whose fibroblasts were used in this thesis to culture and isolate exosomes from. All patients were characterised as diffuse scleroderma and had anti-topoisomerase antibodies (Scl70/ATAs), apart from patient S6, who had PmScl75-PmScl100 antibodies, which is a rare class of autoantibodies linked to diffuse scleroderma patients often in overlap with polymyositis (Ho and Reveille, 2003). All patients had mild lung involvement, apart from patient S2 who had severe lung fibrosis. Further, no information regarding autoantibodies or interferon (IFN) score was accessible for patient S2.

The IFN score was generated by an in-house Luminex-based multiplex assay which measures 4 IFN-inducible chemokines [chemokine pg/mL]. A logarithm is used to alter this into a combined score, where samples are deemed as a high

IFN score, when more than one standard deviation above the mean value of our measured healthy control population. All patients used in this study displayed high IFN scores, where patient S6 displayed the highest IFN score (6.40) and S4 the lowest (5.13) (Figure 3.1).

Moreover, the modified Rodnan skin score (mRSS) is a semi-quantitative measure of skin thickening, commonly used to measure disease progression in systemic sclerosis. The mRSS measures 17 cutaneous sites in the body and scores skin thickness between 0 (normal) to 3 (severe) to yield a total score between 0 and 51. Likewise, scores between 10 – 20 indicate moderate involvement and anything greater than 20 is classed as severe skin involvement. Patients S1 and S4 displayed moderate skin involvement, whereas patients S2 and S6 had severe skin involvement (Figure 3.1).

Further, phase microscopy of immortalised healthy fibroblasts illustrated a classic fibroblast morphology of long flat elongated spindle-shaped cells, which contained an oval shaped nucleus (Figure 3.1). Patient S1, who had a moderate skin score had fibroblasts which had a similar morphology to the healthy group. Patients S2 and S6, which had severe skin involvement, had populations of wider bodied spindle-like fibroblasts, as well as a population of myofibroblasts, where the cellular morphology appeared as web-like structures. Patient S6 had a higher population of myofibroblasts, which also compliments their skin involvement score (Figure 3.1). Furthermore, all fibroblast images were taken at a different confluency, as each fibroblast cell line has different growth rates. However each image is representative of the variance observed between different patients fibroblasts, regards of confluency.

Overall, patients diagnosed with diffuse scleroderma display a range of varying manifestations of the disease within the same subset, ranging from differing skin scores to organ involvement. Thus, the variations in the disease sub-set could lead to discrepancies in the molecular study of the disease, when using a small sample size.

Patient	Sex	Age	Antibodies	Disease Duration	mR Skin Score	IFN Score	Lung Fibrosis	Mycophenolate Mofetil (MMF)	Cyclophosphamide
S1	M	55	Scl70	60	10	5.50	Mild	1	1
S2	F	63	-	24	22	-	Severe	0	1
S3	F	39	Scl70	48	2	5.54	Mild	1	0
S4	F	52	Scl70	144	12	5.13	Mild	1	1
S5	M	62	Scl70	72	8	5.47	Mild	1	1
S6	F	52	PmScl75_PmScl100	48	32	6.40	Mild	1	1

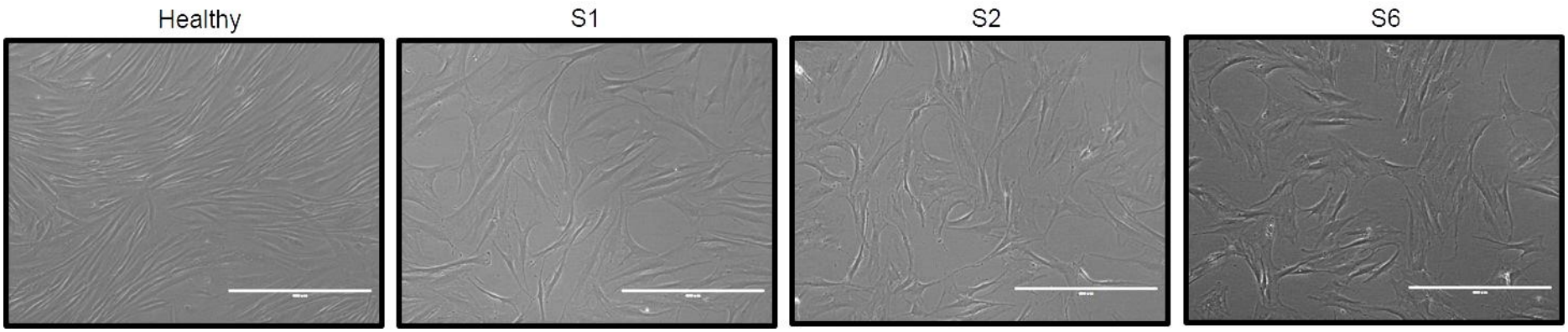

Figure 3.1. Clinical data of scleroderma patients who were used in this thesis, along with phase microscopy of Healthy and Scleroderma fibroblasts in culture.

Table 13. Clinical information from patients, taken by a clinician, prior to skin biopsy collection, which includes age, sex, disease prevalence, mRSS skin score, auto-antibodies, IFN score, prevalence of lung involvement/fibrosis and previous/current drug treatments to alleviate symptoms. Phase microscopy images of fibroblasts from scleroderma and healthy patients, post immortalisation, ranging between cell passages 8-12. Microscopy images taken on EVOS M5000 at 20x magnification. Images were adapted to panels using Image J software. White line indicates 400µM scale bar.

3.3.2. Method optimisation of exosome isolation

Three different isolation techniques were performed and investigated to optimise the method in which exosomes were isolated from cell supernatant from healthy and scleroderma dermal fibroblast (Figure 3.2).

Firstly, scleroderma fibroblasts were grown to 90% confluency and then treated with 10% exosome-depleted FBS-supplemented DMEM for 48-72 hours, and then exosomes were isolated from the supernatant. The supernatant was pooled, split evenly, and processed by UC, total exosome isolation reagent (TEI) and a combination of both methods (UC + TEI). Each exosome yield was then re-suspended in 50µL of filtered phosphate buffered saline (PBS).

To compare the efficiency of each method, total protein of each exosome preparation was quantified using the Pierce^{TM} BCA protein assay kit. Exosomes isolated by ultracentrifugation contained significantly less protein (0.39-fold, $p<0.05$), when compared to TEI. Combining UC and TEI reduced protein concentration by 0.51-fold (ns), compared to TEI (Figure 3.3.A).

Protein contamination was investigated by immunoblotting and staining for Ponceau S, which detects protein bands on the nitrocellulose membrane by

binding to positively charged amino groups within the protein. Equal volumes of exosomes were prepared for gel electrophoresis and immunoblotting. The samples were immobilized onto a nitrocellulose membrane and stained with Ponceau S solution (Figure 3.3.B). Banding patterns suggests similar characteristics amongst all samples, as well as serum protein contamination, were the predominant band at approximately 75 kDa suggests albumin contamination by the serum.

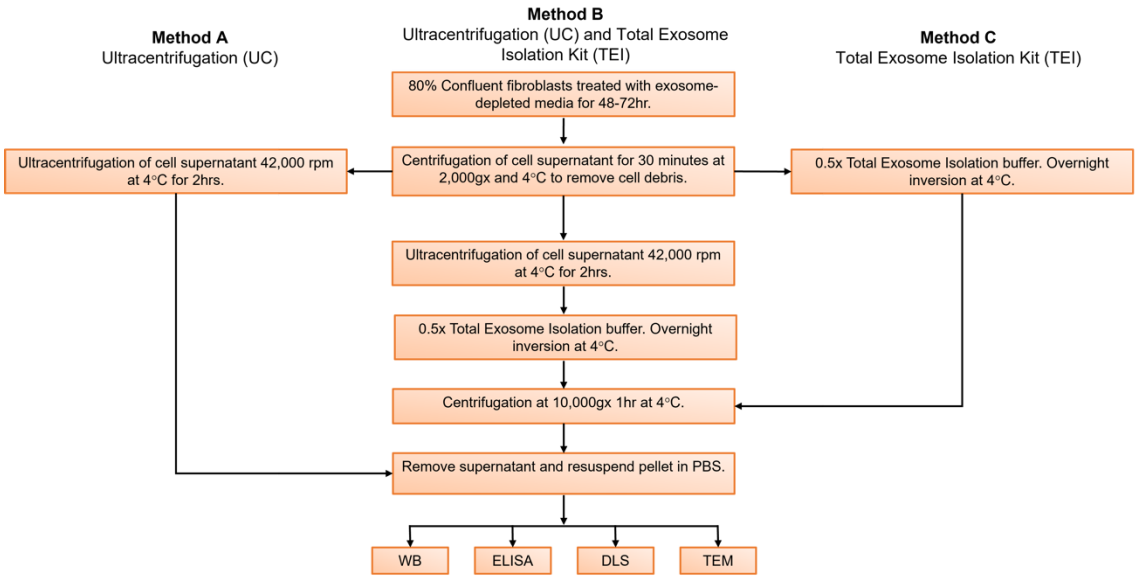

Figure 3.2. Flow chart of exosome isolation and characterisation.

A schematic to illustrate the experimental flow through of three different methods to isolate exosomes from fibroblast supernatant. Post isolation, the exosomes are characterized by western blot (WB), CD63 ELISA, Flow Cytometry, Dynamic light scattering (DLS) and Transmission electron microscopy (TEM).

To establish if protein concentration reflected true exosome yield; the nitrocellulose membrane was then probed against tumour susceptibility gene 101 (TSG101), which is an essential functional protein in exosome biogenesis, (Willms, Johansson et al. 2016). Ultracentrifuged exosomes contained 0.3-fold fold expression of TSG101, when compared to TEI-isolated exosomes. Exosomes isolated from TEI and UC+TEI methods displayed similar levels of TSG101 expression (Figure 3.3.C-D). In addition, Histone H3 was used as a negative control marker for cellular contamination, as a marker for nuclear material. Immunoblotting illustrates that TEI contains histone H3, when compared against UC and UC + TEI isolation methods (Figure 3.3.C).

Combining UC with TEI, requires removal of fractioned supernatant post ultracentrifugation (Figure 3.3.E). To investigate the loss of exosomes in the supernatant fraction; both supernatant and exosome fractions underwent TEI and immunoblotting against TSG101. The exosome fraction contained high levels of TSG101 expression, compared to the supernatant fraction, which illustrates that only low levels of exosomes are lost during fractioning (Figure 3.3.E).

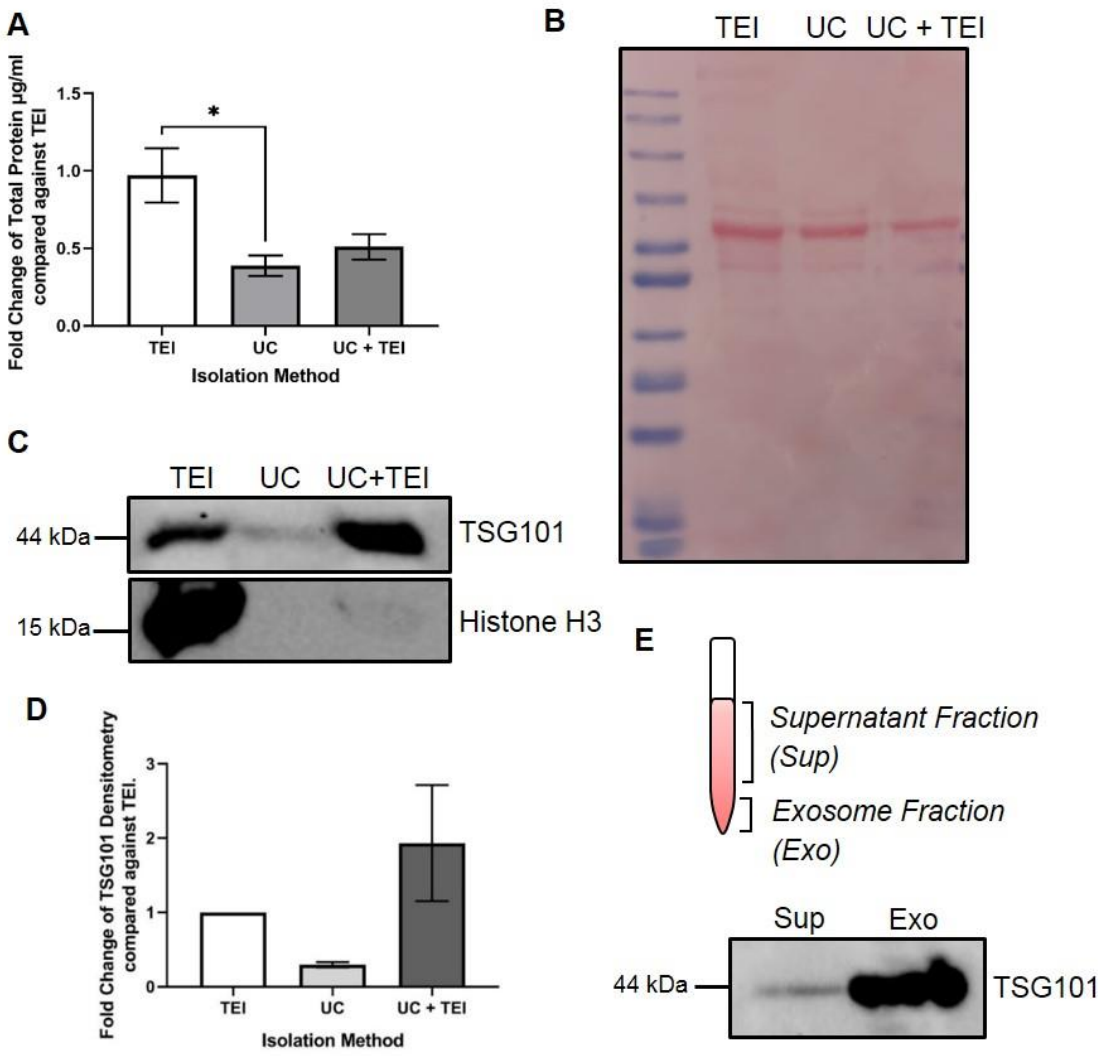

Figure 3.3. The optimisation of exosome isolation using the total exosome isolation reagent.

A) The protein quantification of exosome preparations, using the Pierce™ bicinchoninic acid (BCA) protein assay kit, from three varying isolation methods; total exosome isolation kit (TEI), ultracentrifugation (UC) as well as a combination of UC and the total exosome isolation kit (UC + TEI). B) 25 µL of LDS-treated sample were loaded onto a 10% SDS gel and underwent gel electrophoresis. The gel was transferred onto a nitrocellulose membrane and then stained with Ponceau S solution to detect purity of each sample. C) Immunoblotting of each exosome preparation for an antibody against TSG101 (n=3) and Histone H3 (n=1). D) A bar chart to show densitometry measurements of TSG101 western blot, calculated using Image J. E) Schematic to illustrate how ultracentrifuged supernatant is fractionated to isolate exosomes, as well as immunoblotting for TSG101 expression of supernatant and exosome fractions, post TEI. Statistical analysis was performed using a two-tailed equal variance student T-test (n=3) $p<0.05$*.

3.3.3. Healthy and Scleroderma fibroblasts release a similar quantity of exosomes, illustrated by CD63 ELISA and Immunoblotting

To investigate exosome quantification; exosomes were harvested from three healthy and six scleroderma fibroblasts via UC and total exosome isolation. Equal volumes of exosomes were prepared for gel electrophoresis and immunoblotting against TSG101 and CD63, which are common exosome markers (Gurunathan et al., 2019), as well as Histone H3 as a negative control (Figure 3.4.A). Densitometry analysis of the immunoblots showed no significant difference between TSG101 and CD63 protein expression in exosomes derived from healthy and scleroderma fibroblast (Figure 3.4.C). However, changes in protein expression varies across patients, which highlights that exosome characteristics could be patient specific (Figure 3.4.A). Immunoblots against Histone H3 indicates some partial contamination.

Moreover, CD9 and CD81 are also common exosome markers. Antibodies against CD9 (ab263019) and CD81 (ab109201) indicated no expression in healthy and fibroblast lysates and exosomes, when immunoblotting on a 15% gel (data not shown). Thus, due to repeatability, TSG101 and CD63 were chosen to illustrate successful exosome isolation. Prior to immunoblotting, the membrane was stained with Ponceau S stain to qualitatively assess the distribution and abundance of proteins between samples (Figure 1.4.B). Ponceau S staining illustrates similar protein profiles from exosomes isolated from healthy and scleroderma patients, as well as serum protein contamination, were the

predominant band at approximately 75 kDa suggests albumin contamination by the serum.

Immunoblotting of healthy and scleroderma fibroblasts (S1) lysates for antibodies against TSG101, CD63, Histone H3, α-smooth muscle actin (α-SMA), as well as β-actin as a loading control, were used as positive controls to illustrate parent cells express the protein markers (Figure 3.4.D). α-SMA protein expression was used as a positive control, to indicate the SSc phenotype of increased SMA.

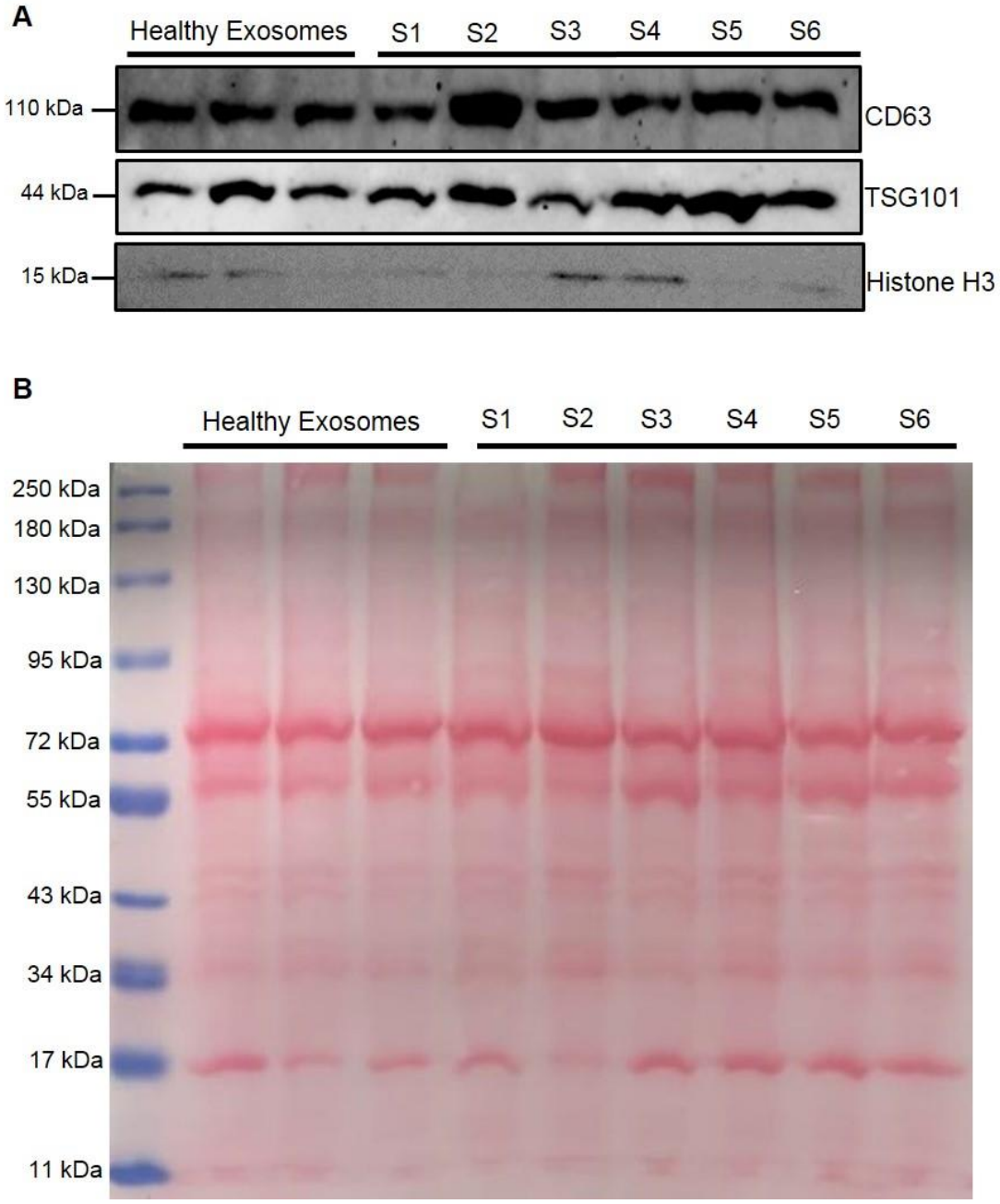

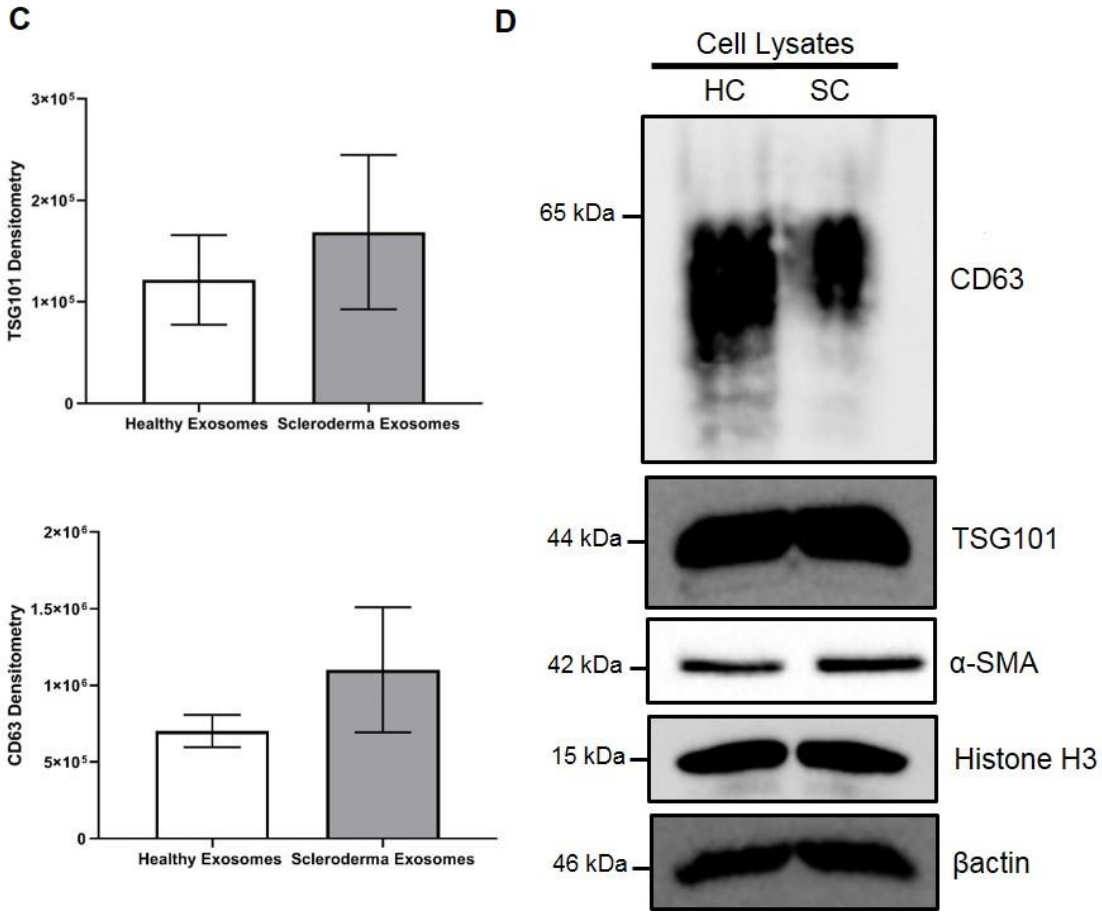

Figure 3.4. Characterisation of exosome preparations by western blot.

A) Immunoblotting of 25 µL LDS-treated exosome preparations from healthy (n=3) and scleroderma (n=6) cultured fibroblasts for antibodies against TSG101, CD63 and Histone H3. B) Ponceau S-stained nitrocellulose membrane of Figure 3.3.A. C) Quantification of the average relative intensity for each patient subgroup from CD63 and TSG101 western blots, determined using BioRad Image Lab software. D) 25 µL of LDS-treated healthy scleroderma fibroblast lysates were added to a 10% SDS-PAGE and underwent gel electrophoresis. Proteins were transferred onto a nitrocellulose membrane and probed for antibodies against TSG101, CD63, Histone H3, α-SMA and β-actin. The fibroblast lysates were harvested after exosome isolation (n=1) (HC = Healthy control, SC = Scleroderma control).

Despite immunoblotting illustrating sufficient exosome isolation through the observation of exosome markers; it is difficult to quantify the abundance of exosomes using densitometry measurements. The semi-quantitative data from immunoblotting provides a relative comparison of protein levels in exosomes, compared to an absolute measure of quantity. Therefore, a CD63 ELISA was used to calculate the quantity of exosomes, by comparing the expression of CD63 of known vesicle concentrations with relation to CD63 expression from each healthy and SSc exosome sample.

Preparations from 10 mL of supernatant from healthy fibroblasts yielded 7.95 x 10^9 exosomes (n=3), as well as scleroderma fibroblasts yielding 8.57 x 10^9 (n=6) (Figure 3.5.A). There was no significant difference in exosome concentration between groups, which reflects the semi-quantitative densitometry of the CD63 immunoblot (Figure 3.5.A-C). Sample S2 has the highest level of CD63 expression in the immunoblot, compared to all other samples and displayed 1.15 x 10^{10} vesicles expressing CD63 in the ELISA. Thus, immunoblotting and ELISA values positively correlated with each other to determine exosome quantity by investigating CD63 expression.

Moreover, total protein was calculated, via BCA protein assay, for each exosome preparation as an additional measure for exosome quantification. Healthy fibroblast exosome preparations contained 2208 µg/mL of protein (n=3), along with scleroderma fibroblasts exosome preparations which displayed a similar protein concentration 2541 µg/mL (n=5). There was no significant difference in protein concentration of healthy and scleroderma derived exosomes. Thus, healthy and scleroderma fibroblasts release a similar quantity of exosomes.

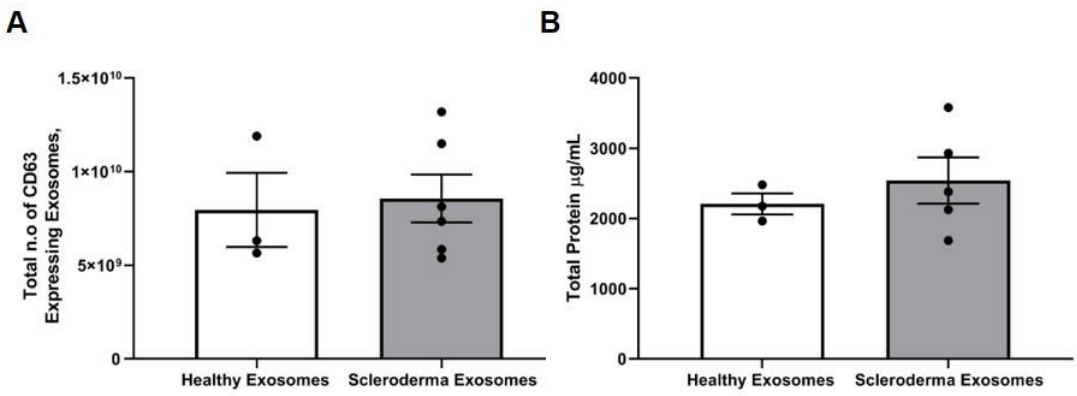

Figure 3.5. Quantification of exosomes by CD63 ELISA and PierceTM bicinchoninic acid (BCA) protein assay.

A) CD63 ELISA quantification of exosomes from healthy and scleroderma patient fibroblasts. This resembles the number of exosomes isolated from fibroblasts cultured in 10 mL of exosome-free DMEM. Each sample was pre-diluted in coating buffer and 50µL of each sample was loaded in duplicate. A standard curve was created, against known exosome standards, and exosome concentration was calculated after normalisation to the blank. B) A bar chart to illustrate the protein concentration of each exosome preparation, using the BCA assay.

3.3.4. No significant difference was observed in the size distribution of exosomes isolated from healthy and scleroderma fibroblasts

Various biophysical techniques are routinely used to characterise exosome size ranges; such methods include, nanoparticle tracking analysis (NTA), dynamic light scattering (DLS), flow cytometry and microscopy (Gurunathan et al., 2019). Due to sample volume and concentration, along with machine availability; DLS was chosen as a method to characterise exosomes, along with transmission electron microscopy (TEM) and flow cytometry (FC). TEM is a widely used technique to visualise the structure, morphology, and size of exosomes. Despite some concerns that staining of exosomes and the electron beam causes morphology and biological damage, TEM is a commonly used technique to

visualise exosomes in the literature and are described as small cup-shaped vesicles, when examined by TEM (Raposo and Stoorvogel et al., 2013).

Figure 3.6 is a representative selection of images, which reflects the vesicles observed. Negative staining of each preparation shows a typical intact exosome cup-shaped morphology. Observed exosomes displayed a size range between 30-50nM for both groups, calculated using Image J, which compliments the literatures characterisation of exosomes. Additionally, clumping and aggregation of exosomes can be seen throughout all samples which range between 100-500nM.

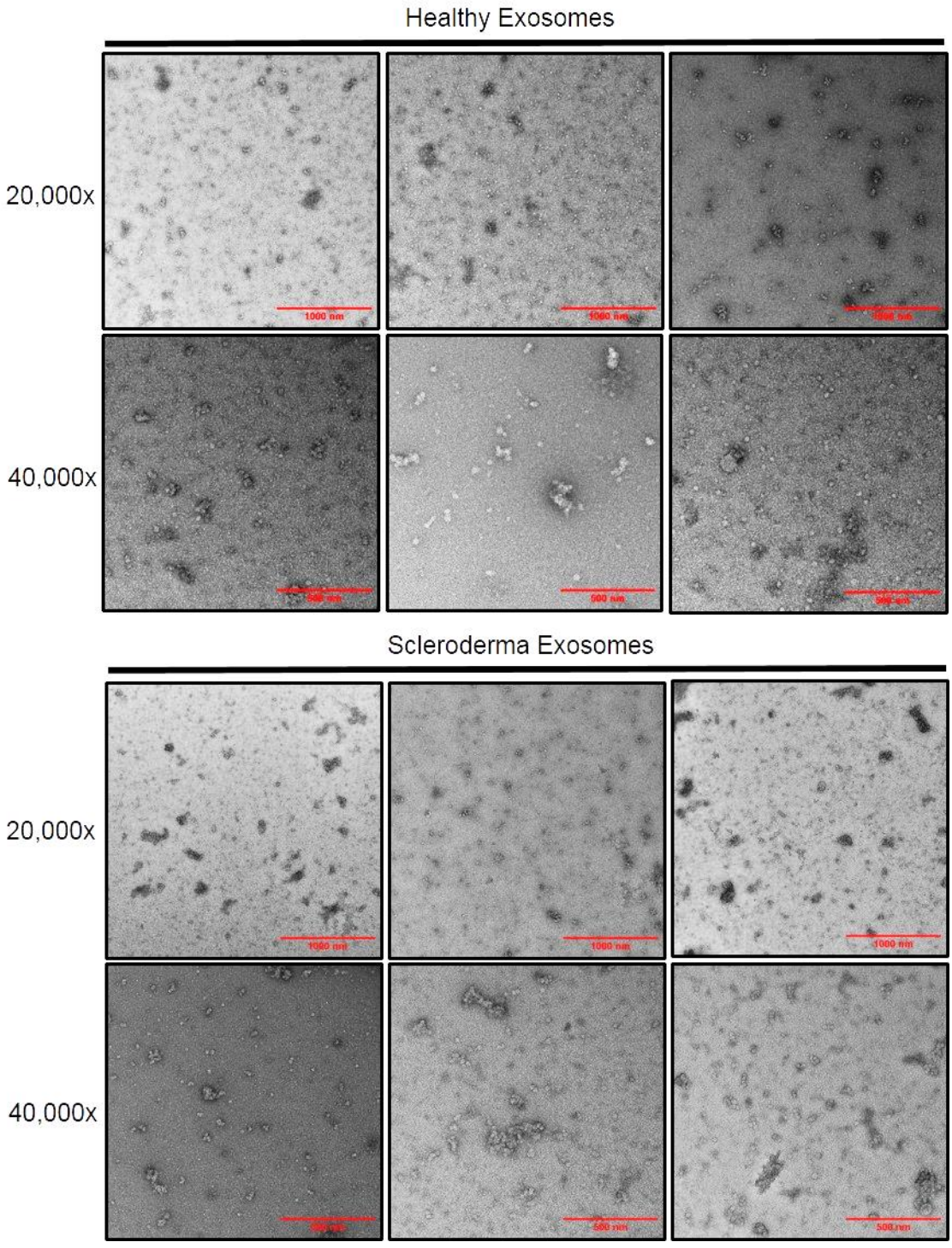

Figure 3.6. Visualisation of exosomes by negative stain transmission electron microscopy (TEM).

5 µL of exosomes from healthy and scleroderma fibroblasts were loaded onto 300nM copper mesh grids and stained with 1.5% uranyl acetate. One grid for each sample was prepared and five images were taken of each grid at different locations. Images were taken using the FEI Tecnai F20 microscope at 20,000 and 40,000x magnification. Images were further analysed in Image J, with the addition of a scale bar (red) for 1000nm at 20,000x magnification and 500nm at 40,000x magnification.

Dynamic light scattering was used to measure the size distribution and dispersity of healthy and scleroderma fibroblast-derived exosomes. Firstly, 3 scleroderma patient's exosomes were mixed to form a group, as well as 3 healthy patient exosomes. 300 µL of each group was injected into the Wyatt miniDawnTreos system, equip with DLS detector and data was analysed by Astra 6.0.3®. A correlation function graph was generated, based on scattered light fluctuations, in relation to time, as the samples were plunged into the DLS.

Correlation function curves generate information on the mean sample size, along with sample diversity, where a steeper lined correlation contains a more monodispersed sample (R^2 = 1). A single exponential decay function (red line) was fit to the correlation curve using the formula; $y = y_0 + Ae^{-x/\tau}$ (A = amplitude, y_0 = y axis offset, τ = time delay). Each sample generated a poor fit to the correlation curve, which indicates the presence of multiple species, within each sample. As exosomes differ in size (30-150nm), a smaller R^2 will be expected due to the diversity of biological samples. Healthy and scleroderma samples yielded fits of R^2 = 0.97 and R^2 =0.98 respectively (Figure 3.7.2A – 3A). Diluted total exosome isolation buffer was used to check for chemical contamination and yielded a fit of R^2 = 0.97, which also indicates some polydispersity (Figure 3.7.1A).

Regularisation analysis yielded a size distribution with numerous peaks for each sample, which were not baseline resolved, thus a Gaussian was fit to each sub peak (Figure 3.7. 1B-4B). The two primary peaks observed in both healthy and scleroderma exosome groups at 7.96±1.12 and 5.99±1.21 illustrate potential contaminants within the exosome suspension respectively, which were isolated using ultracentrifugation and TEI (Figure 3.7.2B - 3B). As well as potential protein

contamination; it was hypothesised that low levels of TEI solution could be precipitating with the exosomes. Where, Patel et al., (2019) showed that exosome preparations using TEI contained PEG, which interfered with mass spectrometry analysis of exosomes. Therefore, a TEI diluted sample was ran as a positive control. The TEI sample contained a single peak yielding the size distribution of 4.17±0.61 (Figure 3.7.1B). The peak observed in the TEI control illustrates that exosome samples contain small levels of TEI chemical contamination. In addition, the observable secondary peaks in the healthy (149.33±20nm) and scleroderma (212.47±36.65nm) exosome preparations represent the mean width of the extracellular vesicles present in each sample (Figure 3.7. 2B-4B). Collectively, investigating exosome biophysical properties by TEM and DLS, illustrates that healthy and scleroderma exosomes display similar characteristics.

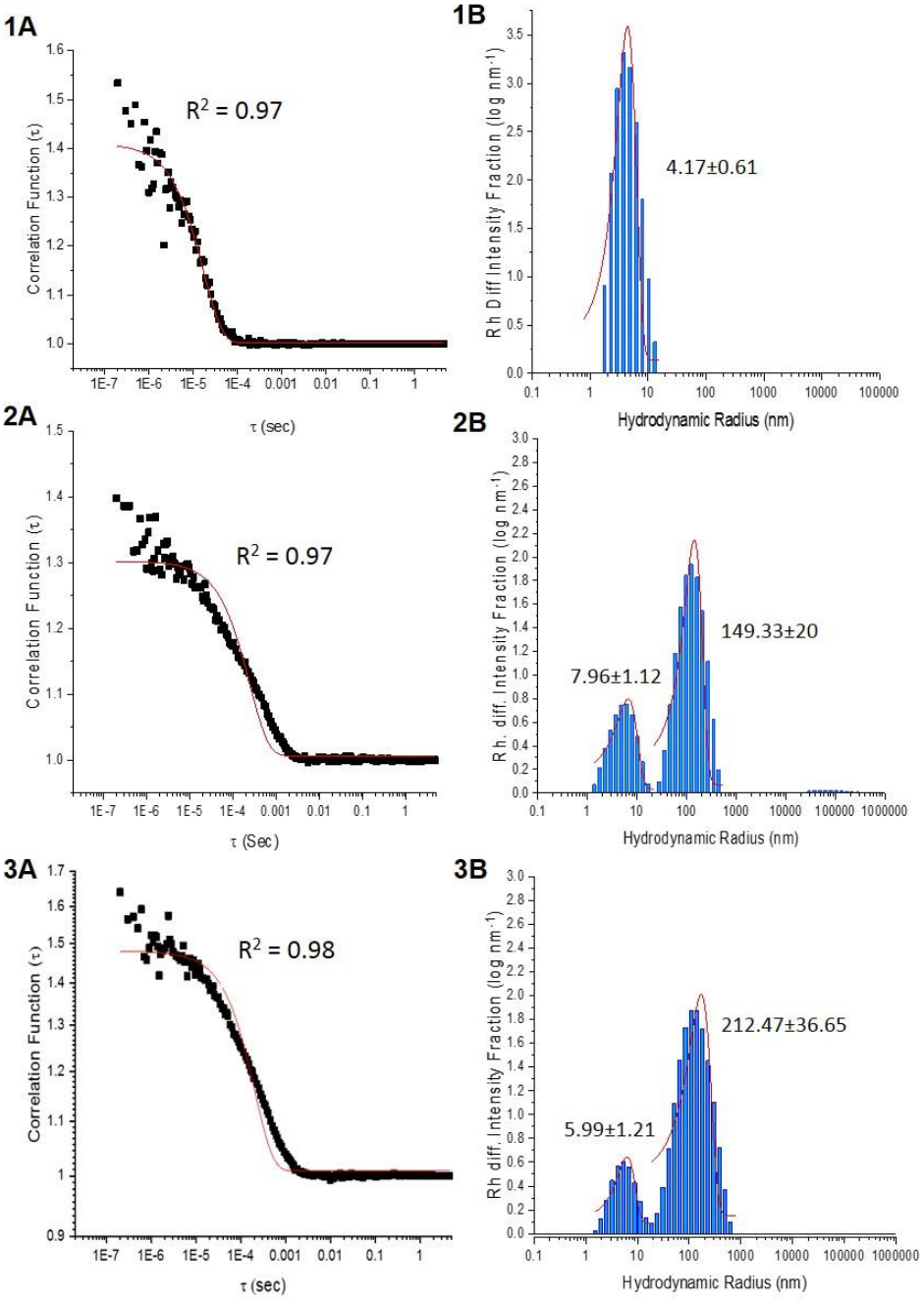

Figure 3.7. Dynamic Light Scattering (DLS) of exosome preparations from cultured healthy and scleroderma patient fibroblasts.

300 µL of a 100nM stock of exosomes and PBS was injected into a DLS system and the samples were run for 10 minutes. A three-minute window of peak activity was selected for final analysis. The raw data was analysed using ASTRA 6.0.3 software to create a correlation curve, where the correlation function (black boxes) was plotted against time for healthy (2A) and scleroderma (3A) exosomes. Diluted total exosome isolation (TEI) solution (1A) was used to determine chemical contamination. Data was further analysed by regularisation of each sample (1-3B), which generated a histogram illustrating intensity of signal and hydrodynamic radius. As the peaks weren't baseline resolved a Gaussian function (red line) was used to calculate the data spread of each peak. Healthy and scleroderma exosome groups contain a mixture of exosomes from three healthy and scleroderma patients respectively.

3.3.5. Staining exosomes with DiO-dye allows detection of small single vesicles by flow cytometry

Flow cytometry is an alternative method which investigates exosome characteristics and is highly popular in the literature due to equipment accessibility in research and clinical practises. Firstly, flow cytometry plots of PBS and Megamix-Plus SSC beads were analysed to gate for exosome size regions (30-150nm), were gating (red) in Figure 3.8.A, illustrates the region of 160nm beads. 10 µL of exosomes were added to PBS, which illustrated a population of events above PBS, similar to the 160 – 200 nm bead region, which was gated (purple). To distinguish their population, exosomes were further labelled using DiO-lipid dye, which fluoresces in the FITC channel. The addition of PBS mixed with DiO-dye highlighted debris in the FITC channel, which was gated (green). However, labelling exosomes with DiO-dye gave a distinct population of vesicles, which were gated (red/orange) (Figure 3.8.B), and totalled 5.04% of all events. Gating total exosome population illustrates that only 32.74% exosomes are stained with DiO-lipid dye and forward vs side scatter illustrates a large population, above the expected size region, which suggests potential aggregates in the sample, as well as overlay of the exosome sample with the debris (Figure 3.8.C).

Although staining of exosomes, allows ease of visualisation, dye debris could lead to overestimation of exosome population, as observed in histograms in Figure 3.8.B. Thus, a clean-up step was introduced to remove dye-excess by buffer-exchange. The addition of buffer-exchange reduced debris from 0.32% to 0.01% in PBS mixed with DiO, as well as 6.81% to 0.05% in DiO-stained

exosomes. Although filtration removed debris contamination, it also reduced exosome total events from 5.04% to 0.91% (Figure 3.9.A). Whereas the population of total exosomes stained with DiO-dye increased from 32.74% to 53.06% (Figure 3.9.B). Interestingly, forward and side scatter plots of filtered DiO-labelled exosomes illustrates distinctly different populations (Figure 3.9.B), than non-filtered (Figure 3.8.C), were the population of filtered DiO-exosomes is in the expected size region. Overall, we observed populations of exosomes stained and unstained in each preparation. The addition of filtration removed aggregation of vesicles and debris, however also lead to the reduction in exosome concentration. Thus, an increase concentration of exosomes is required when buffer exchanging to allow for the loss of exosomes when filtering. Likewise, flow cytometry analysis of exosomes yielded no quantitative measure to quantify the number of exosomes in each preparation, instead it illustrated the presence or absence of exosomes.

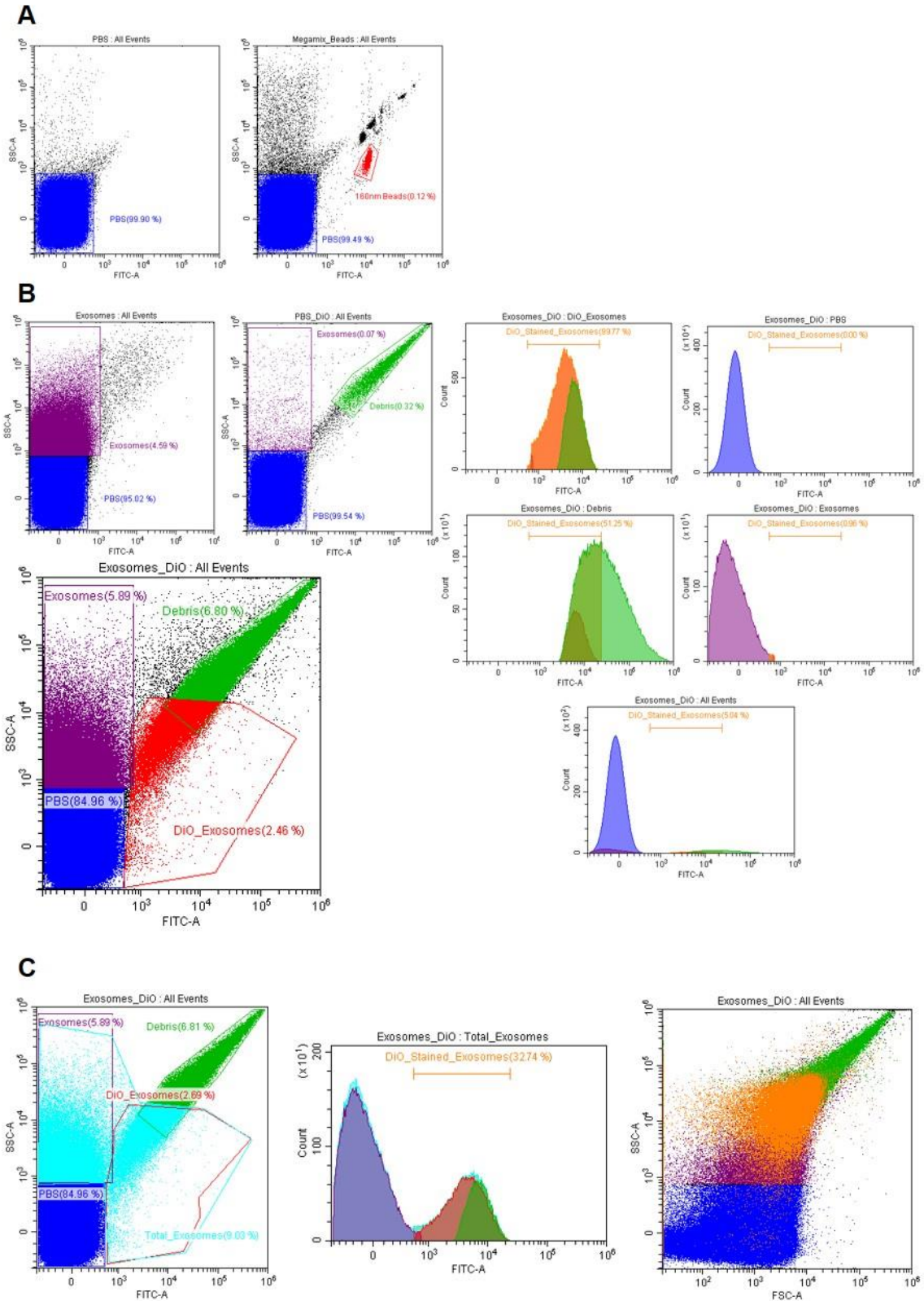
A
PBS : All Events
Megamix_Beads : All Events
SSC-A
FITC-A
PBS(99.90 %)
160nm Beads(0.12 %)
PBS(99.49 %)
B
Exosomes : All Events
PBS_DiO : All Events
Exosomes_DiO : DiO_Exosomes
Exosomes_DiO : PBS
Exosomes(4.59 %)
PBS(95.02 %)
Exosomes(0.07 %)
Debris(0.32 %)
PBS(99.54 %)
DiO_Stained_Exosomes(99.77 %)
DiO_Stained_Exosomes(0.00 %)
Count
Exosomes_DiO : Debris
Exosomes_DiO : Exosomes
DiO_Stained_Exosomes(51.25 %)
DiO_Stained_Exosomes(0.96 %)
Exosomes_DiO : All Events
Exosomes(5.89 %)
Debris(6.80 %)
PBS(84.96 %)
DiO_Exosomes(2.46 %)
DiO_Stained_Exosomes(5.04 %)
C
Exosomes_DiO : All Events
Exosomes(5.89 %)
Debris(6.81 %)
DiO_Exosomes(2.69 %)
PBS(84.96 %)
Total_Exosomes(9.03 %)
Exosomes_DiO : Total_Exosomes
DiO_Stained_Exosomes(32.74 %)
FSC-A

Figure 3.8. Flow cytometry of exosomes labelled with DiO-lipid dye illustrates an exosome population.

A) Flow cytometry analysis of PBS, which was used as the main buffer, as well as PBS mixed with 100 µL Megamix-Plus SSC. Megamix-Plus SSC contains reference beads of varying parameters; 0.16 µM, 0.2 µM, 0.24 µM and 0.5 µM, which fluoresce in the FITC channel. The 160 nM beads were gated and coloured red to illustrate the region, in which exosomes should be observed and PBS was gated and coloured blue. B) Plots which illustrate the visualisation of exosomes by lipid-dye staining (DiO), which fluoresces in the FITC channel. The left-hand panels shows side scatter vs FITC for samples which contains 10µL of unstained exosomes, as well as PBS mixed with 5 µL of DiO-dye respectively, were purple gating illustrates exosomes and green gating indicates DiO-dye debris. The lower left panel indicates side scatter vs FITC for samples which contain 10 µL exosomes stained with 5 µL of DiO-dye, were DiO-stained exosomes were preliminarily gated and coloured red. The right-hand panel contains histograms, which shows counts vs FITC for each gate. A secondary gate for total DiO-stained exosomes was created and coloured orange. C) Left hand plot shows side scatter vs FITC, which illustrates gating of total exosomes (light blue). Central histogram shows counts vs FITC for Total exosome gate, which includes gating of total DiO-stained exosomes (orange), indicated in B. Right hand plot illustrates forward vs side scatter for DiO-labelled exosomes, where total DiO-stained exosomes are indicated in orange, PBS (blue), unstained-exosomes (purple) and debris (green).

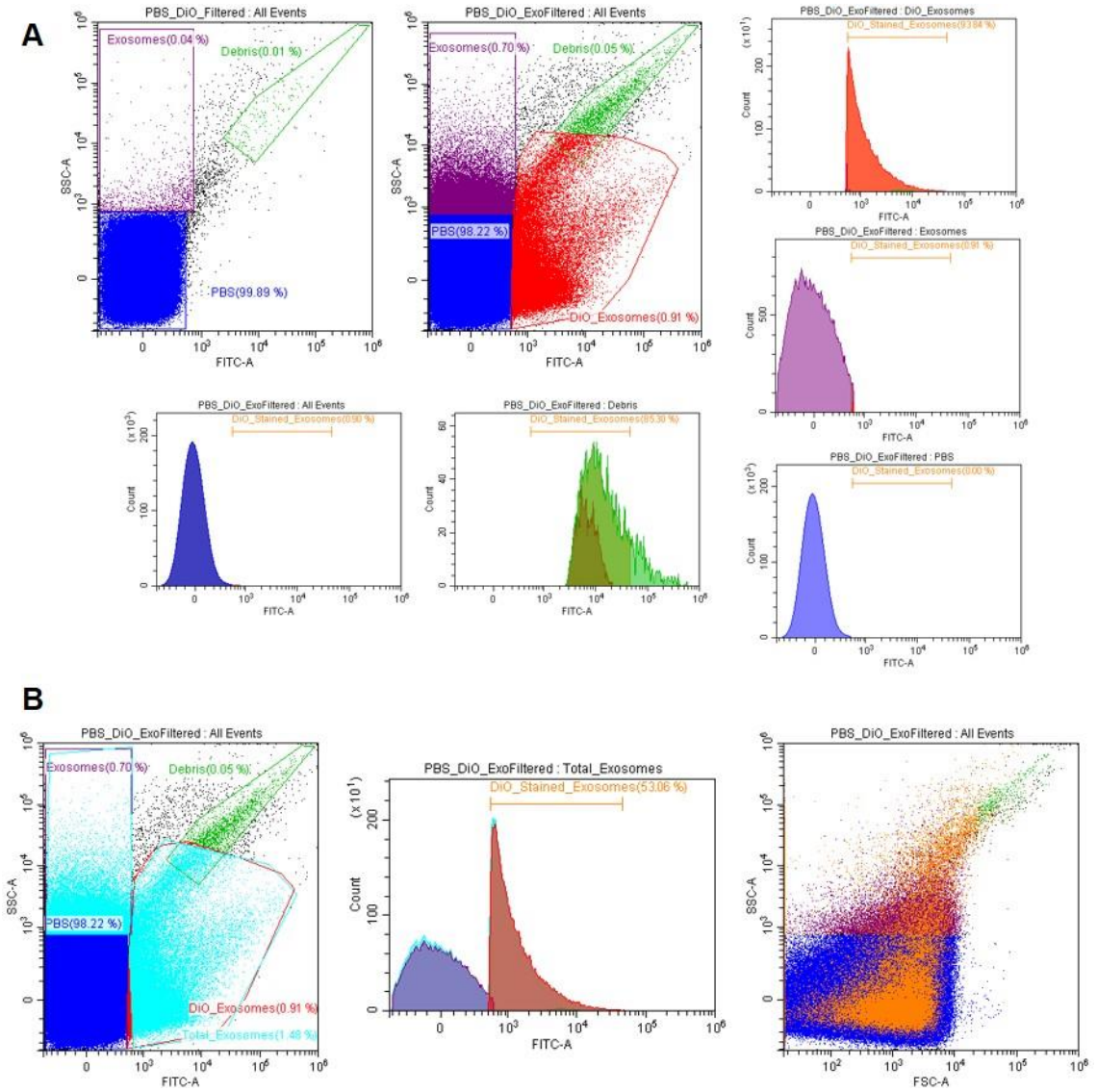

Figure 3.9. Buffer-Exchange of DiO-stained exosomes aids exosome identification by preventing debris contamination.

A) PBS which contained 5 µL Dio-dye (PBS_DiO_Filtered), as well as 10 µL exosomes-stained with 5 µL DiO dye (PBS_DiO_ExoFiltered), were buffer exchanged with PBS, using 3 kDa spin columns, as explained in Methods 2.22. The left-hand panel illustrates side scatter vs FITC for filtered DiO-PBS, which contains gating for PBS (blue), un-stained exosomes (purple) and debris (green), as gated in Figure 3.7.B. The middle panel indicates side scatter vs FITC for filtered DiO-stained exosomes, which contains gating for PBS (blue), un-stained exosomes (purple), DiO-exosomes (red) and debris (green), as gated in Figure 3.7.B. The other panels display histograms, which shows counts vs FITC for each gate. A secondary gate for total DiO-stained exosomes was created and coloured orange. B) Left hand plot of filtered DiO-stained exosomes, which shows side scatter vs FITC that illustrates gating of total exosomes (light blue). A central histogram showing counts vs FITC for total exosome gate, which includes gating of total DiO-stained exosomes (orange), indicated in 3.8.A. Right hand plot illustrates forward vs side scatter for filtered DiO-labelled exosomes, where total DiO-stained exosomes are indicated in orange, PBS (blue), unstained-exosomes (purple) and debris (green).

3.3.6. Healthy and scleroderma fibroblast exosomes are internalised at similar rates by human epidermal keratinocytes over a time-course, which peaks at 48 hours

To investigate the internalisation of fibroblast exosomes in cultured immortalised human epidermal keratinocytes (HaCats); exosomes were isolated from healthy and scleroderma dermal fibroblasts and labelled with a DiO-lipid dye and were added to HaCats over a time-course. Exosomes stained with DiO-lipid dye were buffer exchanged with sterile-PBS, to remove dye aggregates, as observed by flow cytometry (Figure 3.8.B-C).

The fluorescent microscopy images illustrate the presence of green spots in the cell, which accumulate and compartmentalise overtime (Figure 3.10.A). At 24 and 48hours, the exosome distribution becomes more localised around the nucleus, suggesting accumulation in the ER and Golgi for processing. Visualisation and quantification of green fluorescence, when normalised to DAPI, shows that exosomes significantly accumulate in HaCats after 48 hours ($p<0.05$). At 24 hours, SSc exosomes accumulated more inside HaCats, compared to healthy exosomes, however this normalised by 48 hours. Likewise, no significant difference in uptake of healthy and scleroderma exosomes in HaCats, over the time course, was observed (Figure 3.10.B).

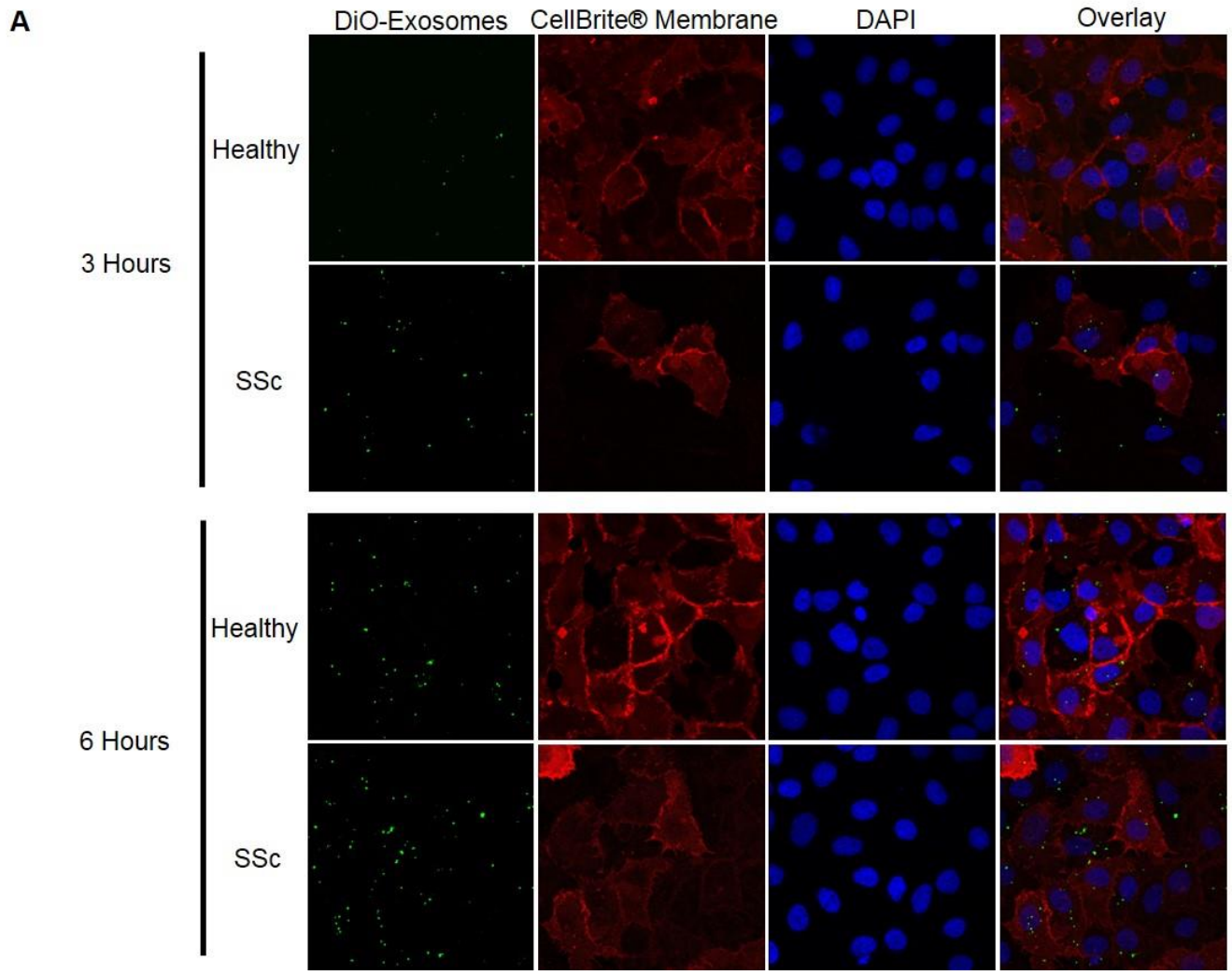
A
DiO-Exosomes
CellBrite® Membrane
DAPI
Overlay
3 Hours
Healthy
SSc
6 Hours
Healthy
SSc

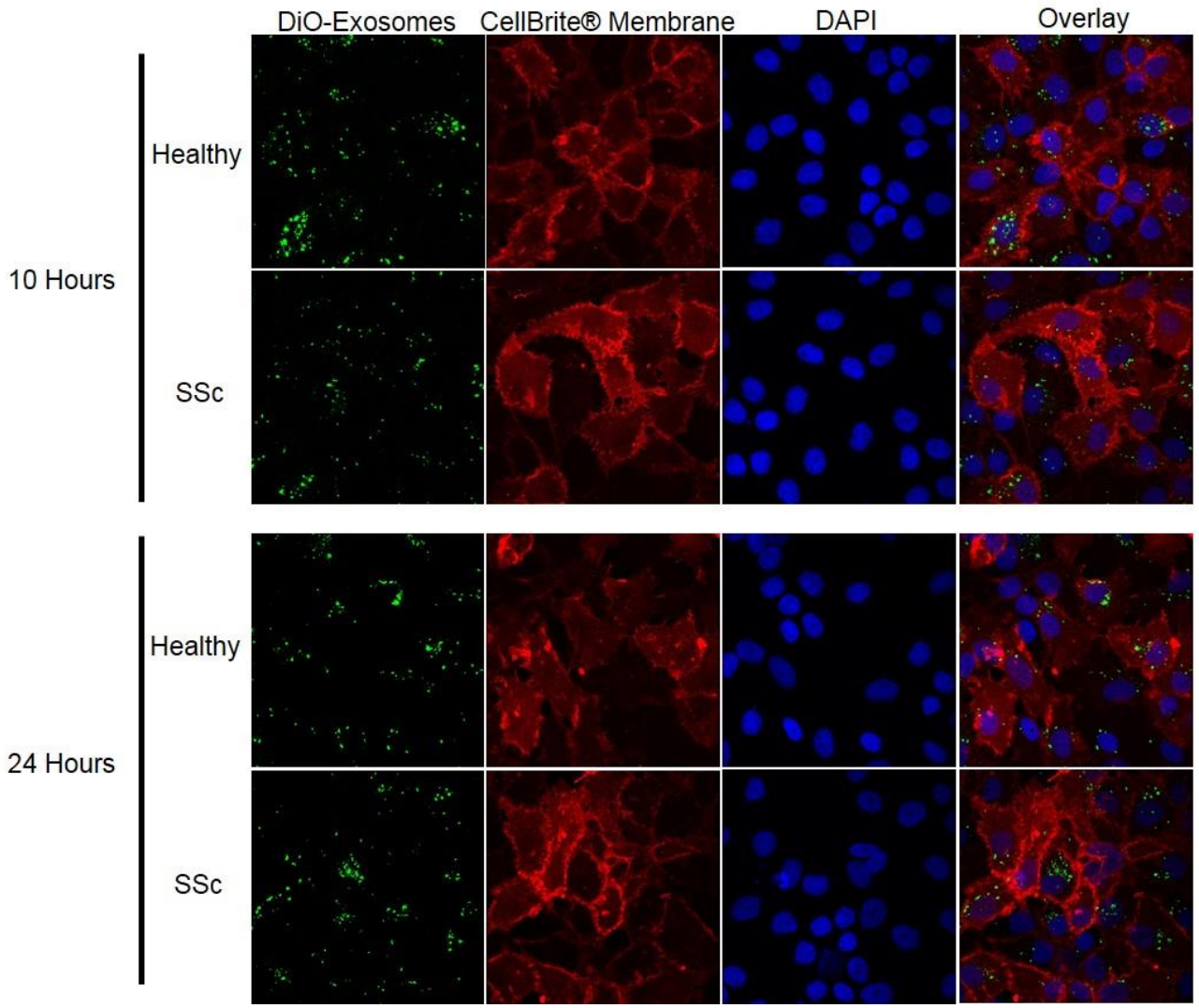
DiO-Exosomes
CellBrite® Membrane
DAPI
Overlay
10 Hours
Healthy
SSc
24 Hours
Healthy
SSc

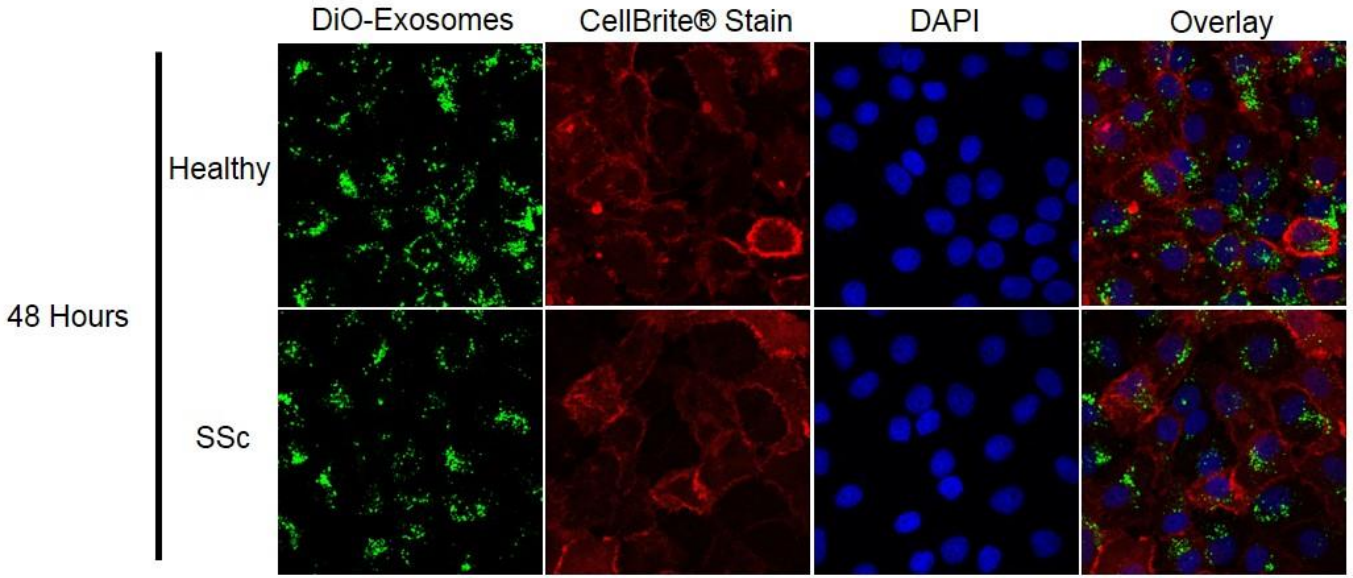
DiO-Exosomes
CellBrite® Stain
DAPI
Overlay
48 Hours
Healthy
SSc

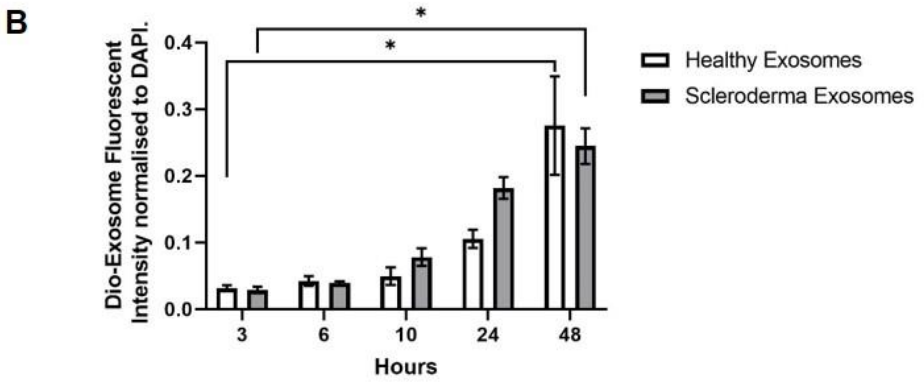
B
Dio-Exosome Fluorescent Intensity normalised to DAPI.
0.0
0.1
0.2
0.3
0.4
3
6
10
24
48
Hours
*
*
Healthy Exosomes
Scleroderma Exosomes

Figure 3.10. Internalisation of DiO-labelled healthy and scleroderma fibroblast exosomes into subcellular compartments of cultured HaCats over a time-course.

100 µL of exosomes were isolated from healthy and scleroderma fibroblasts and resuspended in 1 mL sterile PBS with 5 µL DiO-lipid dye. Excess dye was removed by buffer exchanged. 1% exosomes were added to HaCats at 3, 6, 10, 24 and 48 hours. A) Confocal fluorescent microscopy images illustrating DiO-labelled healthy and fibroblast exosomes (green wavelength) migrating into HaCats, stained with CellBrite® membrane dye (far-red wavelength) and DAPI (blue-wavelength), over a time period. An oil immersion inverted objective of 40x was used for image acquisition. Images were edited using Zeiss Zen and Image J. B) A Bar chart which illustrates the mean green, fluorescent intensity per image, normalised to DAPI intensity, per 3 images over a time-course (3, 6, 10, 24 and 48 hours). Data was checked for normal distribution and statistical analysis was performed by Kruskal-Wallis, Dunn's correction for multi-comparison. (Technical repeat, n=3). *$p<0.05$.

3.4. Discussion

As most experiments within this thesis require exosomes to stimulate cells, it is essential that exosome preparations are concentrated and display high levels of purity, thus it was essential to optimise exosome isolation from dermal fibroblasts. Differential ultracentrifugation is documented as the most popular technique for exosome isolation over the last 30 years, due to ease of use, little technical expertise, and scalable volume preparations. However, biological fluids contain multiple structures, similar to exosomes, such as apoptotic bodies, aggregated proteins, and micro-vesicles, which can also be precipitated during centrifugation, resulting in low purity exosome preparations. To overcome the limitations associated with ultracentrifugation-based methods, companies have produced polymer-based precipitation methods to isolate exosomes in a quick, inexpensive manner (Gurunathan et al., 2019). Although, polymer-based precipitation can isolate high yields of exosomes, the general literature consensus highlights that these methods co-isolate contaminating proteins (Patel et al., 2019, Yang et al., 2020).

Patel et al., (2019) compared ultracentrifugation and TEI for the efficiency of isolating exosomes from cultured pancreatic cancer cell supernatant. Further, TEI preparations contained significantly >2-fold more total protein, when compared UC. In addition, TEI exosome preparations displayed less CD9 expression when compared to UC (Patel et al., 2019). Our experiments illustrated that UC-preparations had 0.39-fold less total protein ($p<0.05$), as well as 0.3-fold less expression of TSG101, when compared to TEI-preparations. Our data doesn't follow the consensus that TEI preparations contain less TSG101 expression, and thus less exosomes. However, these results could differ as Patel et al., (2019) used 25µg of total protein when immunoblotting, compared to our experiment, which used 25 µL of each sample. Thus, the lack of expression observed could be due to total protein measurements not representing exosome concentration.

Moreover, an ultracentrifugation step prior to TEI reduced protein concentration, which indicates a reduction in protein contamination. Further, combining ultracentrifugation with precipitation resulted in an increased recovery of exosomes, as illustrated by TSG101 expression in Figure 3.3.D. This additional step overcomes low yield problems associated with ultracentrifugation. Thus, a combination of ultracentrifugation and polymer-based precipitation was used to isolate a high concentration of exosomes, with minimal protein contamination.

The secondary aim of this chapter was to quantify and characterise fibroblast-derived exosomes from healthy and scleroderma patients, using a range of conventional methods. Immunoblotting showed no significant differences in CD63 and TSG101 expression from healthy and scleroderma fibroblast-derived exosomes. However, expression of TSG101 and CD63 differed between patients

from both groups. As discussed, scleroderma patients (S1-S6) display a range of clinical features, which suggests differing disease severity across the group, where patients with severe skin score had large populations of myofibroblasts in their cultured fibroblasts. Thus, the pathological differences observed between scleroderma patients could resemble the differences in exosome marker expression. Nevertheless, Newman L et al., (2021) showed that fasting healthy patients significantly increased expression of exosome marker CD9. Likewise, diurnal sample collection highlighted significant changes in CD81 expression. Further, Kowal J et al., (2016) illustrated that exosomes released from the same cell vary in molecular composition. Thus, the molecular composition of vesicles may change due to an amplitude of factors, such as cell-to-cell variability, time of collection, rather than patient disease heterogeneity.

Total protein and CD63 ELISA quantification also indicated no significant differences between healthy and scleroderma fibroblast-derived exosomes, which compliments a recent publication, which also illustrated no significant difference in size, concentration, and exosome marker expression of scleroderma dermal fibroblast-derived exosomes, compared to healthy (Bhandari R et al., 2022). In contrast, Nakamura K et al., (2016) illustrated SSc fibroblasts released more exosomes, via CD63 ELISA, however, did not evaluate the purity or any other characteristics of exosomes, such as size, and thus expression of CD63 could originate from other types of extracellular vesicles (Conde-Vancells et al., 2008).

Determination of the biophysical properties of exosomes is as essential as quantification, to ensure correct biological characterisation. Dynamic light

scattering and transmission electron microscopy were used to determined size distribution and dispersity of each sample, along with visual characterisation. Further, nanoparticle tracking analysis (NTA) is one of the most popular techniques in the literature, as it can quantifies exosomes, as well as measure size distribution. NTA detects particles between a 10 nm to 2 µm range, when compared against DLS which measures between 1 nm to 6 µm. Therefore, NTA will miss any contaminating protein, chemicals or apoptotic bodies and potential aggregates. In addition, a major disadvantage to NTA analysis is sample preparation and dilution factors, which are critical for true sample representation. NTA also requires a minimum detection level of 1×10^8 exosomes per mL (Soares 2018). As previously discussed, exosomes isolated using the TEI method are somewhat impure, and each exosome harvest produces approximately 8×10^9 particles in 100µL. Thus, optimisation for nanoparticle tracking analysis will be time consuming and require a significant amount of material. As DLS only required a small concentration of exosomes (100nM), thus it was chosen to measure the size distribution of particles within each group.

Biophysical characterisation of healthy and SSc fibroblast-derived exosomes indicated that exosomes from both groups displayed exosomes with a cup-like morphology, which ranged in size between 30-100nm. TEM analysis of exosome preparations indicated exosome aggregates in both healthy and SSc preparations. Since, exosome aggregates were observed in both preparations it is likely that exosome isolation induced aggregation, where Linares et al., (2015) illustrated that high speed centrifugation induced the formation of extracellular vesicles aggregates. Moreover, DLS analysis showed that healthy and SSc exosome preparations were highly heterogeneous and exosomes ranged

between 150-220nm in size, which depicts larger vesicles, when compared to TEM analysis. Discrepancies observed could be due to TEM and DLS measuring different properties, for instance TEM represents a 2D characterisation using electron density of a selection of particles, whereas DLS measures the physical size of a 3D shape across the full sample. Secondly, DLS is sensitive to large particles and thus scatter can be disproportionate, and intensity can favour larger particles (Stetefeld J et al., 2016). Likewise, TEM analysis does indicate exosome aggregates in both healthy and SSc samples, which ranges between 100-500nm, that could be corresponding to the size distribution observed by DLS analysis.

Flow cytometry (FC) was an additional method employed to investigate exosome characteristics as approximately 75% of clinical exosome samples are analysed using FC (Lacroix R et al., 2010). FC is a high-throughput and multi-comparison technique which measures the physical and chemical characteristics of a population, by light scatter. The smallest polymer-based beads detected by FC, are approximately 200nm in size. Extracellular vesicles have a 10-fold lower refractive index than polymer beads, which suggests vesicles must be > 500nm to be detectable by conventional FC. Likewise, approximately 80% of extracellular vesicles are < 500nm in size, were exosomes range between 30-150nm (Mastoridis S et al., 2018, van der Pol E et al., 2012). To overcome these hurdles, we used an array of polymer-based beads to gate the sizing region for exosomes (160nm, 200nm, 240nm) (Figure 3.7.A), as well as fluorescently labelling exosomes using DiO-dye, which fluoresces in the FITC channel.

Flow cytometry analysis indicated a total exosome population and a DiO-labelled exosome population. DiO-labelled exosomes overlapped with FITC-positive

debris, which confounded the analysis and quantification of DiO-labelled exosomes. To remove FITC-positive debris, DiO-labelled exosomes were buffer exchanged into PBS. Although buffer exchange removed FITC-positive debris, it also reduced the number of total exosomes and DiO-labelled exosomes. Interestingly, forward vs side scatter of buffer exchanged, and non-exchanged DiO-labelled exosomes illustrated different exosome populations, where non-buffer exchanged exosomes appeared larger, and thus potentially aggregated; whereas buffer exchanged DiO-labelled exosomes appear in the expected size region. This suggests that buffer exchange removes exosomes, and exosome aggregates, as well as debris, and thus more concentrated exosome stocks will be required when buffer exchanging exosome preparations to make up for loss.

Overall, buffer exchanged DiO-labelled exosomes display characteristics previously observed by DLS and TEM, where they are populated primarily below the 150nm region, with a population of large events corresponding to aggregates, which were observed by TEM. However, due to size detection limits and background contamination, conventional flow cytometry analysis of exosomes yields little quantitative data, and only allows visualisation of vesicles.

Moreover, although FC is a commonly used method in the literature to characterise exosomes, we illustrated that it is insufficient to estimate concentration, size, as well as any biophysical properties, and thus only indicates absence or presence of vesicles. Further, Van der Pol et al., (2012) illustrated that FC measurements of vesicles can be skewed by “swarm detection”, which describes the quantification of multiple vesicles as one singular event, and this can lead to underestimated exosome concentrations by ~1000 fold. Whereas,

many other conventional methods, such as TEM, ELISA and DLS, as described, can successfully and accurately quantify, and characterise exosomes when used collectively. Recently, to overcome size-detection limitations and background detection; high-sensitive flow cytometers have been developed to allow detection of stained exosomes (Mastoridis S et al., 2018), however these FCs aren't routinely used in research and clinical environments, and thus removes the attractiveness of equipment accessibility.

Furthermore, buffer exchange of DiO-labelled exosomes was implemented as a method to visualise exosome internalisation; as it was shown to remove non-specific debris, which fluoresces in the FITC/GFP channel. Exosomes can be internalised by recipient cells via direct interaction with surface receptors, fusing with the plasma membrane or most commonly through endocytosis. The process of exosome endocytosis can occur by; clathrin-mediated or lipid raft endocytosis, as well as phagocytosis, where the intracellular fate of exosomes is through the endosomal pathway (Gurung S et al., 2021). We investigated exosomes internalisation by HaCats over a time-course of 3-48 hours. Accumulation of exosomes was observed around the nucleus, potentially in the endoplasmic reticulum and Golgi network, which was most prominent at 48 hours. This suggests that most exosomes were taken up through endocytosis and processed through the endosomal sorting pathway, due to their location around the nucleus and lack of GFP fluorescence observed in the extracellular membrane. However, HaCats weren't stained with an ER or Golgi marker to illustrate location of accumulation, and thus exosome sorting through the endosomal sorting pathway can only be hypothesised.

Conclusively, healthy and scleroderma fibroblasts release exosomes of similar quantities with analogous biophysical properties, that are internalised into recipient keratinocytes on a similar timescale at equal abundances. Thus, a cellular response to the treatment of scleroderma fibroblast-derived exosomes would be due to vesicle contents, compared to biophysical properties.

4. Investigating the Role of Scleroderma Fibroblast-derived Exosomes in the Induction of Type 1 Interferon Response in HaCats.

4.1. Introduction

The initiation and the role of dysregulated type I IFN signalling in scleroderma pathogenesis is unclear. Upregulated ISG expression has been observed in the blood and skin of SSc patients (Brkic et al., 2016, Assassi et al., 2010), where genome wide analysis of skin biopsies identified an upregulation of type I IFN, IRFs and STAT family members (Assassi et al., 2015). There is clear evidence that an IFN signature is observed in the skin and blood of SSc patients, prior to skin fibrosis (Brkic et al., 2016), and type I IFNα signalling in SSc dermal fibroblasts was strongly associated with early disease progression (Johnson et al., 2015). Further analysis highlighted an interplay between inflammation, type I IFN signalling and fibrosis in SSc dermal fibroblasts (Johnson et al 2015). Although it has been demonstrated that fibroblasts are key contributors to fibrosis (Gilbane et al., 2013), it is unknown how type I IFN signalling is initiated and exacerbated in the skin layer, and the role in which fibroblasts contribute towards the immune-driven pathogenesis in SSc.

Further, scleroderma dermal fibroblasts share similar molecular and cellular features with CAFs, such as dysregulated signalling through TGFβ/SMAD axis and the overexpression of ECM-remodelling genes (Gilbane et al., 2013, Yang et al., 2019, Li et al., 2021). Recent literature has highlighted that CAFs release exosomes, which can activate pattern-recognition receptors and induce type I IFN signalling to aid metastasis, tumour progression and therapy resistance in breast cancer, ESCC and epithelial cells (Nabet et al., 2017, Boelens et al., 2014,

Cui Y et al., 2022). In addition, SSc dermal fibroblast exosomes has recently been shown to induce pro-inflammatory cytokines and inflammatory mediators in macrophages, which then sustain the stimulation of active SSc fibroblasts (Bhandari et al., 2022). Thus, we aim to investigate the role of SSc dermal fibroblast-derived exosomes in the initiation and dysregulation of the type I IFN signalling pathway in healthy keratinocytes.

4.2. Results

4.2.1. RNA Sequencing of immortalised human keratinocytes (HaCats) stimulated with scleroderma fibroblast-derived exosomes shows upregulation of IFN-related pathways

To investigate the role of scleroderma-fibroblast exosomes in the pathogenesis of scleroderma and their effect on recipient keratinocytes, serum-starved HaCats were stimulated with 1% healthy fibroblast-derived exosomes (n=3 donors) and 1% scleroderma fibroblast-derived exosomes (n=5) for 48 hours and RNA was harvested for RNA sequencing. HaCats were stimulated for 48 hours as IF internalisation experiments indicated that maximum exosome uptake occurred at 48 hours (Figure 3.10 A-B).

HaCats treated with SSc exosomes had 212 significantly differentially expressed genes (DEGs) to HaCats treated with healthy exosomes. Using a cut-off of 1.2 fold to control, 94 DEGs were upregulated and 45 downregulated. Due to low biological repeats and high biological variability between samples the false discovery rate (FDR) was high, and thus comparisons were made by p-value. Generation of a heat map allowed the visualisation of gene expression profiles

across patients for each DEG (Figure 4.7.A), where distinct regions of expression differences can be observed between healthy and SSc exosome stimulated HaCats. All DEGs were then plotted as a volcano plot where log2(fold change) is on the x-axis, -log10(p-value) is the y axis and the significantly expressed genes are labelled red (Figure 4.1.B). In addition, the top 10 most significantly expressed genes were labelled on the volcano plot (Figure 4.1.B). The top 25 most DEGs are summarised as a bar chart (Figure 4.1.C), where reactome analysis indicated that 15 out of the 25 genes (60%) were associated with the immune system and 11 (73%) of those genes related to interferon signalling and cytokine signalling in the immune system. Appendix Table 16 indicates the key role of each gene listed in Figure 4.1.C.

Equivalently, gene ontology (GO) analysis of the DEGs illustrated a subset of significantly enriched genes associated with interferon signalling, such as ‘Response to Type 1 Interferon GO:0034340’, ‘Response to Virus GO:0009615’ and ‘Response to Chemokine GO:1990868’ (Figure 4.1.D). Intriguingly, GO analysis showed downregulated genes associated with the downregulation of endoplasmic reticulum protein homeostasis, such as ‘Response to ER Stress’ and ‘Response to Incorrect Protein’. Interestingly, Kyoto Encyclopaedia of Genes and Genomes (KEGG) showed significant upregulated pathways associated with fatty acid metabolism, as well as antigen processing and presenting and staphylococcus infection in SSc exosome-treated HaCats, compared to healthy exosomes (Figure 4.1.E). Moreover, 60 of the 94 significantly upregulated DEGs were associated with ‘Cytokine Signalling in Immune System’. Similarly, 47 of 94

were associated with IFN signalling, and 32 of 94 with IFNα/β signalling (Reactome).

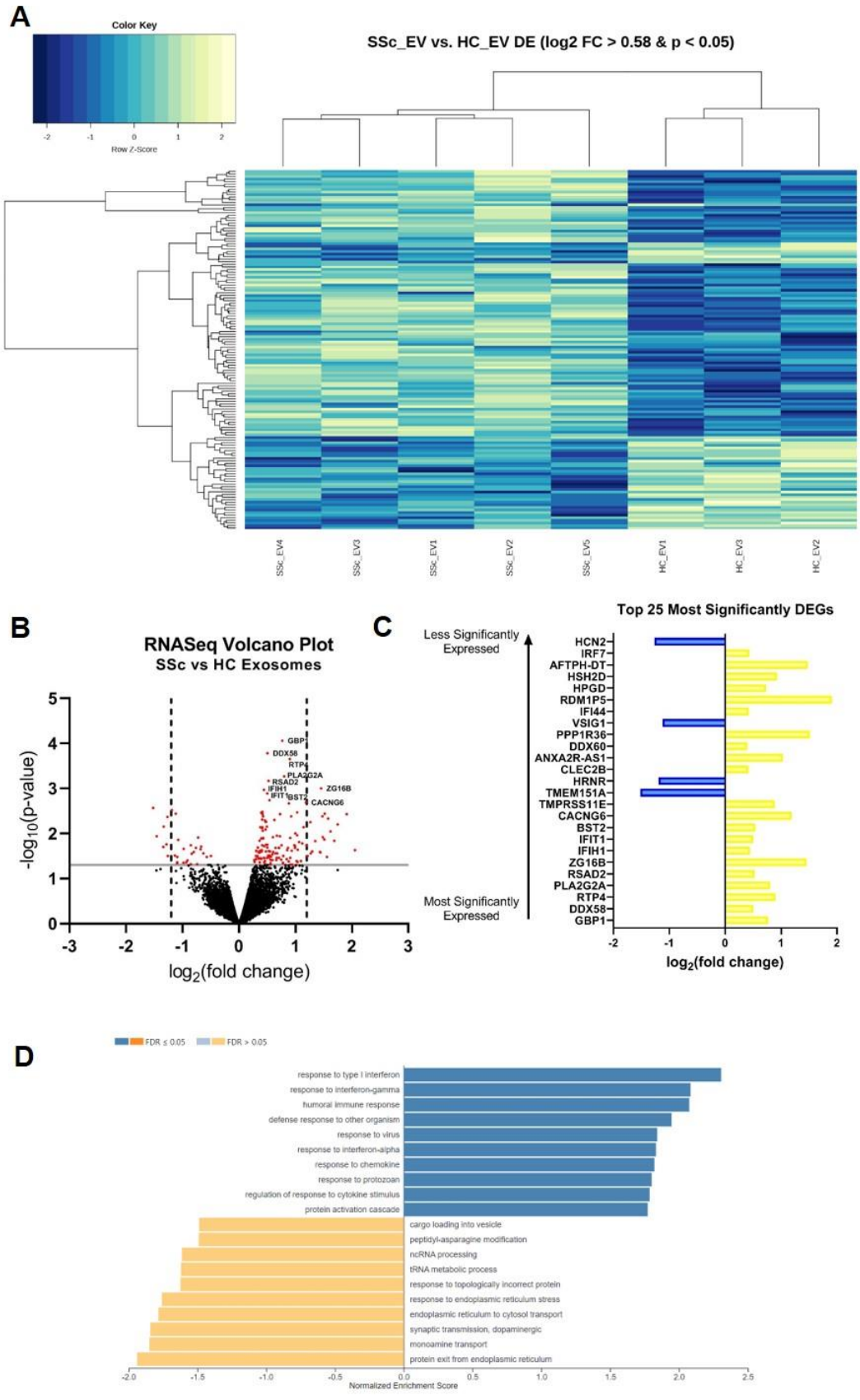

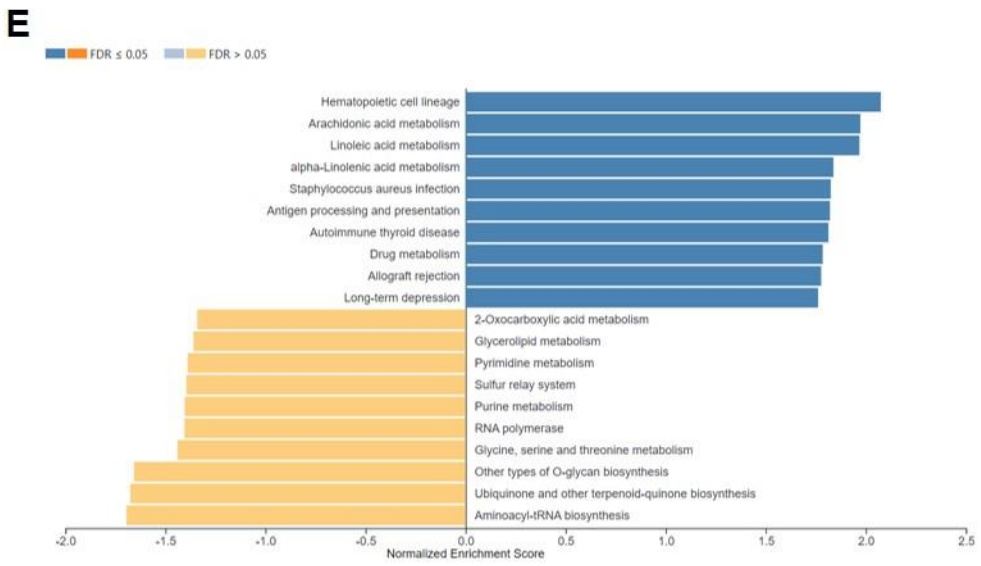

Figure 4.1. RNA Sequencing of HaCats stimulated with scleroderma fibroblast-derived exosomes shows upregulation of IFN-related pathways.

A) Heat map which shows differential expression of significantly expressed genes which are greater than 1.2-fold, between healthy and scleroderma fibroblast-derived exosomes. The heat map illustrates significantly ($p<0.05$) differentially expressed genes (DEGs) and the colour scale represents log2(FC); where low expression is blue and high expression is yellow. FC = Fold Change. SSc_EV = scleroderma exosomes. HC_EV = healthy exosomes. B) Volcano plot which illustrates log2(fold change) against -log10(p-value) for each DEG in HaCats stimulated with scleroderma fibroblast-derived exosomes, when compared against healthy exosomes. Grey line = p-value<0.05. Red = significant DEGs. C) A bar chart which shows the top 25 most significantly differentially expressed genes, as log2(FC) of DEGs, which are significantly (p-value<0.05) upregulated (yellow) and downregulated (blue) in HaCats treated with scleroderma fibroblast exosomes, compared to healthy. D) Gene ontology (GO) enrichment analysis of DEGs from HaCats treated with scleroderma exosomes, compared to healthy. E) Kyto encyclopaedia of genes and genomes (KEGG) analysis of upregulated biological pathways associated with DEGs, in HaCats treated with scleroderma exosomes. Blue and orange = false discovery rate (FDR)<0.05. Grey and yellow FDR>0.05.

4.2.2. Type I IFN-inducible gene super array validates the induction of ISG expression by scleroderma exosomes

To further validate and gain a more thorough understanding of the RNA sequencing data, which suggests that SSc exosomes can induce interferon signalling in HaCats, a RT^2 profiler PCR array for type-1-interferon-related genes was used to screen up to 79 IFN-related genes. HaCats were starved in serum-free DMEM and treated with 1% exosomes, derived from healthy (n=3) and scleroderma fibroblasts (n=3), for 48 hours. RNA was extracted and then prepared for cDNA synthesis and quantitative PCR with reverse transcriptase (RT-qPCR) using the RT^2 profiler PCR array.

IFN array analysis indicated that SSc exosomes significantly induced 16 interferon-related genes by more than 1.5-fold (Figure 4.2.A), when compared to healthy fibroblast exosomes, where the significantly expressed genes are illustrated in Figure 4.2.B. Further, ISG15, MX1 and OAS1 are the top three most significantly upregulated genes, when compared to healthy exosomes (Figure 4.2.B). SSc exosomes induced an additional 22 genes, where 10 genes were upregulated by more than 2-fold (NS), which are shown as a bar chart in Figure 4.2.C. Moreover, 7 genes were also downregulated, however these results were also not significantly different between scleroderma and healthy exosome treatments.

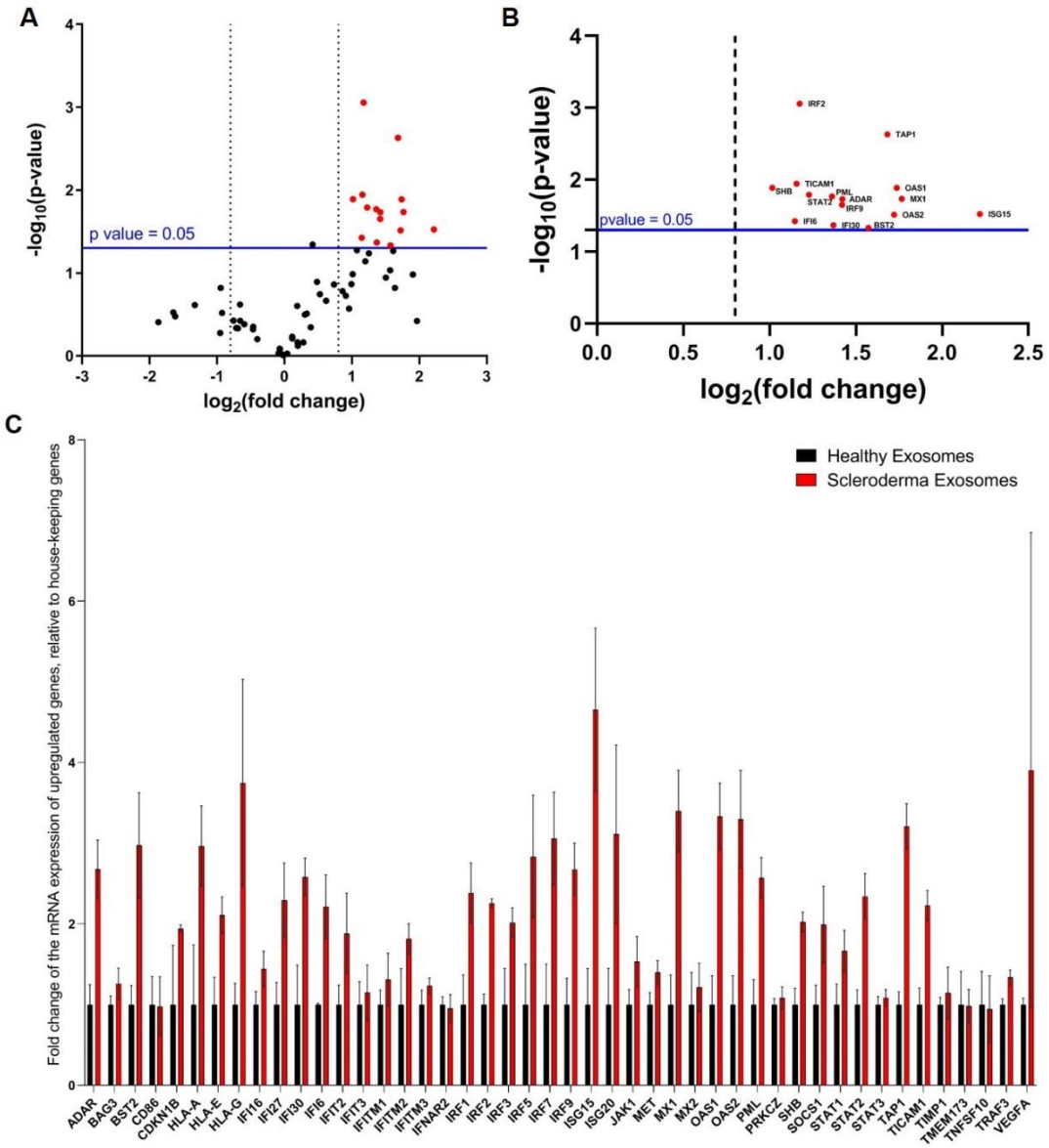

Figure 4.2. Screening of interferon-stimulated genes, by a type-1 Interferon RT2 profiler PCR array, in human epidermal keratinocytes (HaCats) after treatment with fibroblast-derived exosomes from healthy and scleroderma patients.

A) Volcano plot which shows the fold change of gene expression of interferon-type-1-stimulated genes relative to HaCats stimulated with healthy exosomes. B) A 'blown-up' version of the volcano plot in Figure 4.2.A, illustrating the names of the genes significantly upregulated in SSc exosome treated HaCats, compared to healthy. C) Bar chart which represents all interferon-type-1 related genes that were increased by more than 1.2-fold in scleroderma exosome treated HaCats, compared to healthy control. Data is presented as mean ± s.e.m. from three biological repeats. P values were calculated using a two-tailed student t-test assuming equal variance on triplicate $2^{-\Delta Ct}$ values for each gene in both scleroderma and healthy control conditions.

Independent ISG expression profiles from HaCats stimulated with scleroderma fibroblast-derived exosomes highlights variability across patients.

As scleroderma is a complex heterogeneous disease and the SSc patients within our cohort displayed a range of disease severity, such as mild/severe skin scores, high IFN scores and early/late disease progression (Figure 3.1.A), we investigated the ISG expression profiles of each individual SSc patient-derived exosomes (n=6), when added to HaCats after 48 hours. Scleroderma fibroblast-derived exosomes significantly induced gene expression of MX1 (1.57-fold), CXCL10 (2.05-fold), CXCL11 (2.32-fold) and OAS (1.26-fold) ($p<0.05$), compared to healthy fibroblast exosomes. Likewise, scleroderma exosomes induced gene expression in IFIT1 and ISG15 by 1.30 and 1.17-fold respectively, however, was deemed not significant (Figure 4.3.A).

The transcript mRNA gene expression data presented in Graph A is re-represented in Graph B to show individual gene expression levels of each patient's exosomes, for each gene (Figure 4.3.B). Patient S5 has the lowest induced mean ISG score of 1.29-fold, whereas patient S6 has the highest average fold increase of 2.01, when compared to healthy control. Both CXCL10 and CXCL11 were upregulated in patients S1-S4 and S6, while gene expression of IFIT1 and ISG15 was comparable to the healthy patient exosomes. The upregulation of ISGs was observed in all HaCats treated with SSc fibroblast exosomes. Similarly, ISG scores from SSc patient serum was also upregulated, as discussed in Figure 3.1, Table 13. This illustrates that all patients displayed an interferon signature in both their blood serum and dermal fibroblasts isolated from skin biopsies.

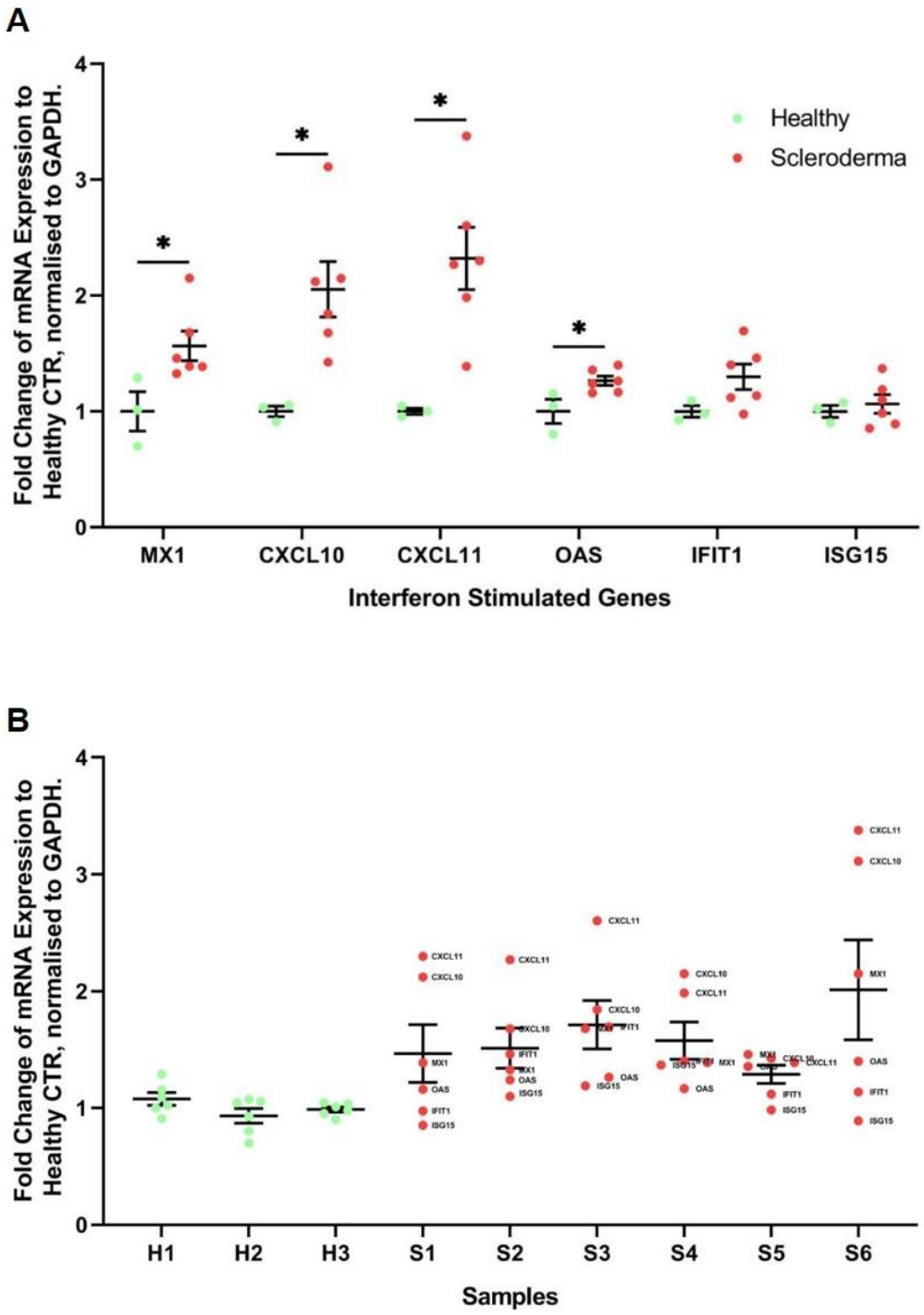

Figure 4.3. Independent ISG expression profiles from HaCats stimulated with scleroderma fibroblast-derived exosomes highlights variability across patients.

A) Fold change of mRNA transcript expression of MX1, CXCL10, CXCL11, OAS, IFIT1 and ISG15, normalised to GAPDH, of serum-starved HaCats treated with scleroderma and healthy fibroblast-derived exosomes after 48 hours. *p<0.05. Statistical analysis = Two-tailed Student T-Test, assuming equal variance. Data is presented as mean ± s.e.m. from biological repeats. Healthy exosomes = 3. Scleroderma exosomes = 6. B) Fold change mRNA transcript expression of each gene for each patient, normalised to overall healthy mRNA transcript expression for each gene (n=3). *Graph B uses data from Graph A to show individual patient expression levels.*

4.2.3. Treatment of scleroderma exosomes over a time-course, induces interferon-stimulated gene expression and phosphorylation of STAT1, after 48 hours

To evaluate the time in which SSc exosomes first induce IFN signalling in HaCats; 1% of healthy (n=3) and SSc (n=3) fibroblast-derived exosomes were added to serum-starved HaCats over a time-course of 6, 10, 24 and 48 hours, and the expression of ISGs was analysed. To further investigate the role in which exosomes induce ISGs in HaCats; the protein expression of type-I IFN-related proteins was evaluated over the time course.

The fold change of HaCats treated with SSc exosomes showed no significant difference in gene expression at 6, 10 and 24 hours, compared to healthy exosomes, when normalised to basal expression. Further, SSc exosomes significantly induced transcript expression of MX1 (1.31-fold, $p<0.05$), CXCL10 (1.43-fold, $p<0.01$) and CXCL11 (1.46-fold, $p<0.01$), after 48 hours. OAS and IFIT1 gene expression was also heightened in HaCats treated with scleroderma fibroblast-derived exosomes by 1.42 and 1.37 respectively, after 48 hours; however, was not significant (Figure 4.4.A). Interestingly, ISG15 expression increased in both healthy and SSc exosome treated HaCats at 48 hours, compared to the rest of the time course. Additionally, the induction of ISGs by SSc exosomes at 48 hours was significantly greater than when SSc exosomes were added to HaCats at 6 hours (MX1 ($p<0.01$), CXCL10 ($p<0.01$), IFIT1 ($p<0.05$) and ISG15 ($p<0.0001$), 10 hours (MX1 ($p<0.001$), CXCL10 ($p<0.0001$), CXCL11 ($p<0.01$), OAS ($p<0.01$), IFIT1 ($p<0.05$) and ISG15 ($p<0.0001$)) and 24 hours (MX1 ($P<0.01$), CXCL10 ($P<0.05$), OAS ($P<0.05$) and ISG15 ($P<0.0001$))

hours, and thus SSc exosomes induced ISGs in HaCats at 48 hours (Figure 4.4.A). This data is consistent with the immunofluorescent imaging, which illustrated the accumulation of internalised exosomes in the HaCats at 48 hours (Figure 3.10).

Further, immunoblotting for proteins associated with interferon signalling illustrated that HaCats treated with scleroderma exosomes displayed significantly increased expression of phosphorylated STAT1 at 48 hours ($p<0.05$), which was significantly induced when compared to treatment after 10 hours ($p<0.05$) (Figure 4.4.B-C). Likewise, no observable changes in protein expression were found in RIG-I, phospho-IRF3, as well as total protein levels of IRF3 and STAT1 in HaCats treated with healthy or scleroderma fibroblast exosomes.

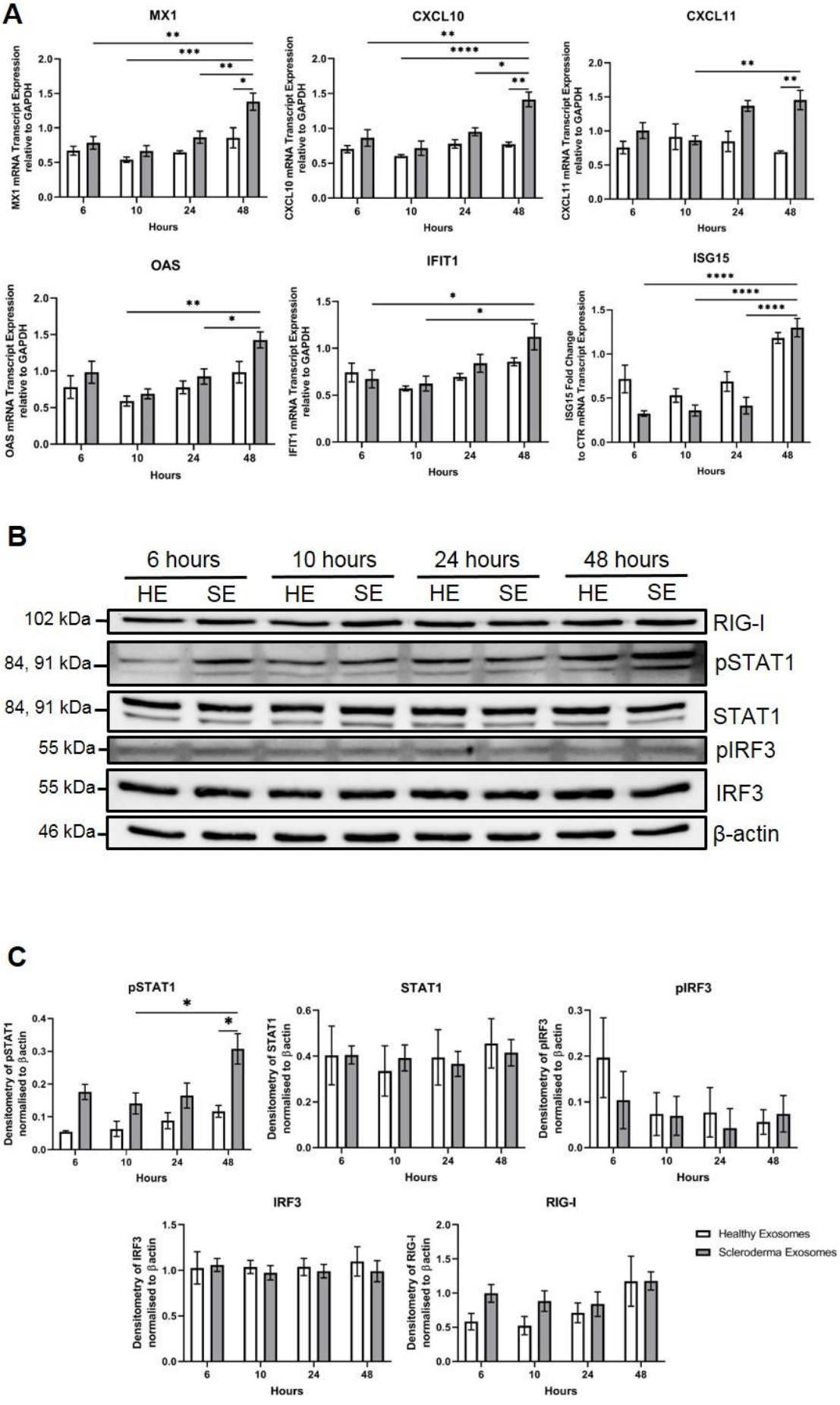
A
MX1
CXCL10
CXCL11
OAS
IFIT1
ISG15
MX1 mRNA Transcript Expression relative to GAPDH
CXCL10 mRNA Transcript Expression relative to GAPDH
CXCL11 mRNA Transcript Expression relative to GAPDH
OAS mRNA Transcript Expression relative to GAPDH
IFIT1 mRNA Transcript Expression relative to GAPDH
ISG15 Fold Change to CTR mRNA Transcript Expression
Hours
B
6 hours
10 hours
24 hours
48 hours
HE
SE
102 kDa
RIG-I
84, 91 kDa
pSTAT1
84, 91 kDa
STAT1
55 kDa
pIRF3
55 kDa
IRF3
46 kDa
β-actin
C
pSTAT1
STAT1
pIRF3
IRF3
RIG-I
Densitometry of pSTAT1 normalised to βactin
Densitometry of STAT1 normalised to βactin
Densitometry of pIRF3 normalised to βactin
Densitometry of IRF3 normalised to βactin
Densitometry of RIG-I normalised to βactin
Hours
Healthy Exosomes
Scleroderma Exosomes

Figure 4.4. Scleroderma fibroblast-derived exosomes induced the expression of Interferon-stimulated genes (ISGs), along with the phosphorylation of STAT1, in human epidermal keratinocytes (HaCats), when compared to healthy exosomes.

A) mRNA transcript expression of MX1, CXCL10, CXCL11, OAS, IFIT1 and ISG15, normalised to basal gene expression, in HaCats treated with exosomes isolated from healthy and scleroderma fibroblasts along a time-course of 6, 10, 24 and 48 hours. *p<0.05, **p<0.01, ***p<0.001, ****P<0.0001. Data was checked for normality and statistically analysed using a Two-way multiple comparison ANOVA, normalised by Tukey. Data represents means ± SE. Healthy Exosomes (n=3, 48hr n=6), Scleroderma Exosomes (n=6). B) Representative images of western blots against the antibodies; RIG-I, pSTAT1 (Tyr701), STAT1, pIRF3 (Ser386), IRF3 and β-actin. C) Quantification of (B) by densitometry and normalised to β-actin levels. Data represents means ± SE from three independent experiments: Data was checked for normality and statistically analysed using a Two-way multiple comparison ANOVA, normalised by Tukey. Healthy exosomes (n=3) and scleroderma exosomes (n=3). HE = healthy exosomes, SE = scleroderma exosomes.

As described previously, breast cancer exosomes induced ISGs through the activation of pattern recognition receptor (RIG-I) (Nabet et al., 2017, Boelens et al., 2014, Cui Y et al., 2022). Thus, 10 ng/mL of 5' triphosphate double stranded RNA (RIG-I Agonist) (InvivoGen) mixed with Lipofectamine™ 2000 was used as a positive control (n=2), as well as to investigate similarities between the mechanism of action of the exosomes, compared to the RIG-I agonist. HaCats treated with RIG-I agonist displayed increased expression in all ISGs listed in Figure 4.5.A, where expression peaks between 6 and 10 hours and then starts to decline at 24 and 48 hours. Immunoblotting showed significant upregulation in protein expression of pSTAT1 at 6 ($p<0.0001$) and 10 hours ($p<0.0001$), as well as pIRF3 at 6 ($p<0.05$) and 10 hours ($p<0.05$), which both significantly decreased by 48 hours ($p<0.001$ and $p<0.01$ respectively), compared to basal expression (Figure 4.5.B-C). RIG-I protein expression levels significantly increased after RIG-I agonist stimulation overtime from 6 to 24 ($p<0.002$) and 48 hours ($p>0.01$). Further, RIG-I agonist significantly induced RIG-I protein expression at 10 hours ($p<0.05$) and peaked between 24 ($p<0.0001$) and 48 hours ($p<0.0001$). Likewise, STAT1 protein expression opposed pSTAT1 levels by significantly increasing at

24 ($p<0.05$) and 48 hours (ns) (Figure 4.5.B-C). IRF3 protein levels maintained consistent throughout the time-course, regardless of treatment.

Lipofectamine was used alongside the RIG-I agonist as a further control, as lipofectamine is required for transfection of the RIG-I agonist into the cell. Likewise, lipofectamine treatments displayed similar expression profiles to basal level gene and protein expression (Figure 4.5.A-C).

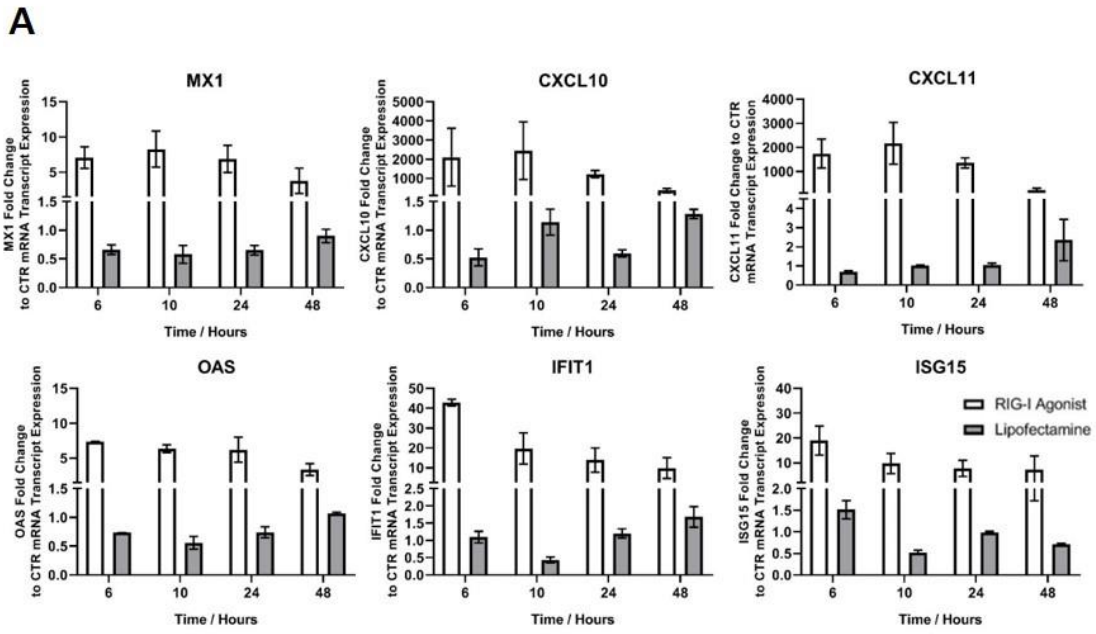

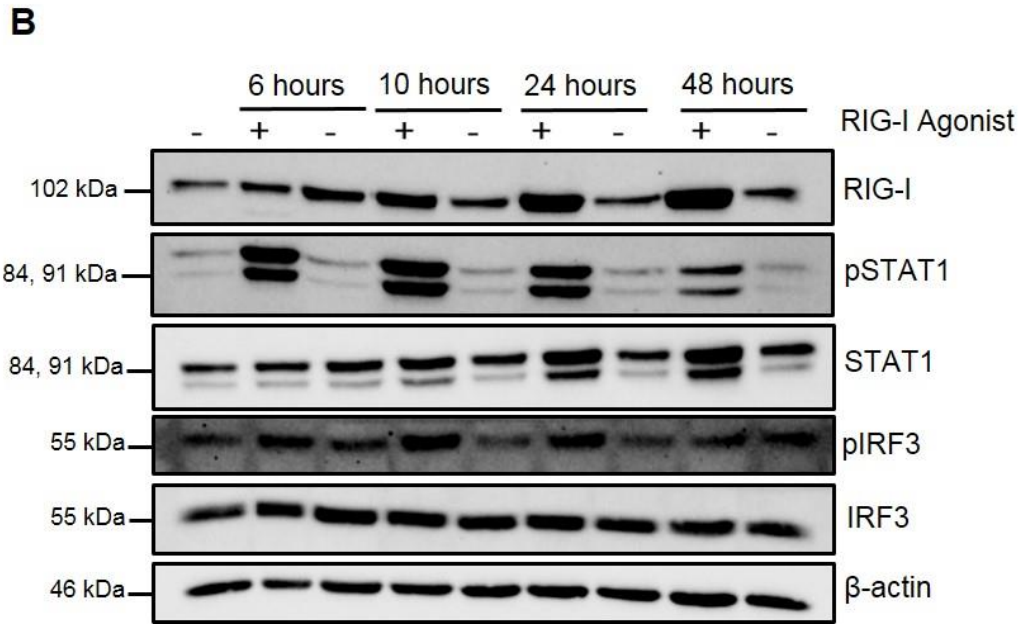

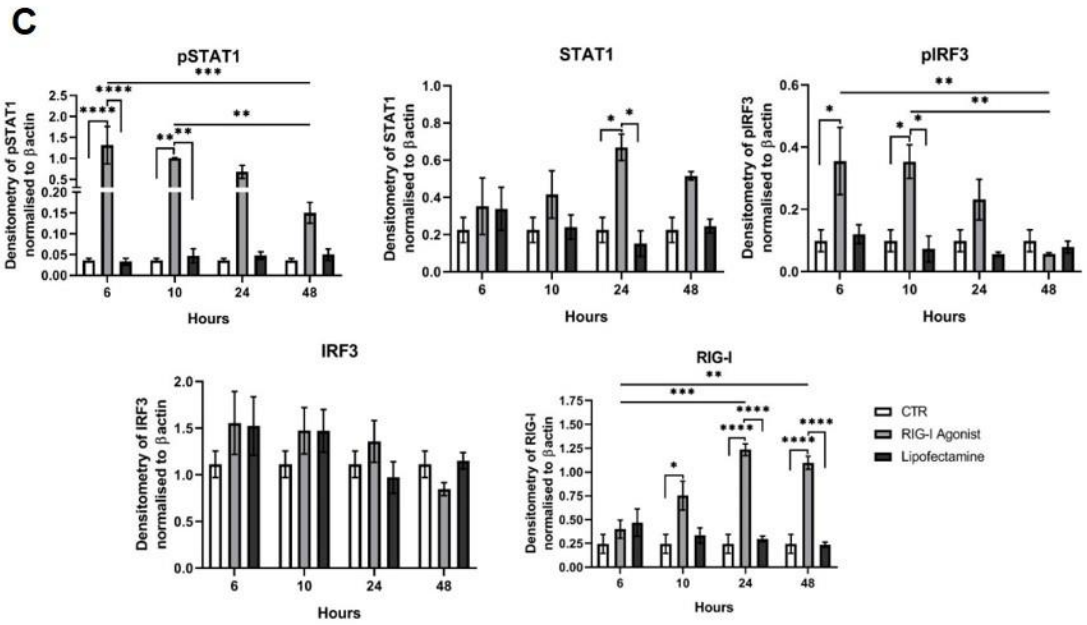

Figure 4.5. RIG-I agonist (5'triphosphate short-hairpin) significantly increased the expression of Interferon-stimulated genes (ISGs) and interferon-related proteins in human epidermal keratinocytes (HaCats), after 6 hours.

A) mRNA transcript expression of MX1, CXCL10, CXCL11, OAS, IFIT1 and ISG15, normalised to basal gene expression, in HaCats treated 10 ng/mL of RIG-I agonist and lipofectamine2000 along a time-course of 6, 10, 24 and 48 hours (n=2). B) Representative images of western blots against the antibodies; RIG-I, pSTAT1 (Tyr701), STAT1, pIRF3 (Ser386), IRF3 and β-actin for HaCats treated with 10 ng/mL of RIG-I agonist and lipofectamine2000 along a time-course of 6, 10, 24 and 48 hours (n=3), were CTR was treated with SFM and harvested after 48 hours. C) Quantification of (B) by densitometry and normalised to β-actin levels. Data represents means ± SE from three independent experiments: Data was checked for normality and statistically analysed using a Two-way multiple comparison ANOVA, normalised by Tukey. *P<0.05. **P<0.01. ***P<0.001. ****P<0.0001.

4.2.4. Autologous stimulation of Scleroderma fibroblast exosomes on Scleroderma Immortalized Keratinocytes illustrated mixed responses for pSTAT1 and ISG induction

As previously shown, scleroderma fibroblast-derived exosomes induce interferon stimulated genes and the phosphorylation of STAT1 in HaCats, after 48 hours of treatment. Indeed, HaCats are a common immortalised keratinocyte cell line,

widely used in scientific research to model keratinocytes present in the skin. However, to gain a more accurate in-vitro skin model, healthy primary keratinocytes were used to replace HaCats. Starvation of healthy primary keratinocytes, required for exosome stimulation experiments, led to cell death (data not shown). Likewise, immortalisation of primary healthy keratinocytes with human telomerase reverse transcriptase (hTERT), to create a more robust and reliable cell line to be used for starving experiments, wasn't achieved, due to an inability to become retrovirally transduced. Therefore, immortalised scleroderma keratinocytes (Patient 2, Figure 3.1.A) were used.

Scleroderma keratinocytes were grown to confluency and starved in keratinocyte media, supplemented with calcium chloride, for 1 hour before the addition of 1% exosomes. Following treatment with scleroderma exosomes, RIG-I protein expression was induced by 1.7-fold ($p<0.05$), in scleroderma keratinocytes compared to healthy exosomes (Figure 4.6.B). Although, all 3-donor scleroderma exosomes did induce phosphorylation of STAT1 by 1.64-fold, which can be observed in Figure 4.6.A, it was deemed insignificant when compared to healthy exosomes, as healthy donor 3 also induced pSTAT1. Total protein expression of STAT1 and IRF3 remained constant between healthy and scleroderma exosome treatments. In addition, scleroderma keratinocytes showed no basal expression of pIRF3, which wasn't induced by either healthy or scleroderma exosomes. Autologous fibroblast exosomes (Red box) and keratinocytes showed no observable differences at protein expression level, when comparing against scleroderma exosomes (Figure 4.6.A-B).

Furthermore, treatment of scleroderma exosomes on scleroderma keratinocytes showed no significant difference in interferon-related gene expression, when

compared to healthy exosomes (Figure 4.6.C). Although significance wasn't observed, scleroderma keratinocytes displayed increased gene expression of some ISGs: MX1 (1.37-fold), IFIT1 (2.24-fold) and RIG-I (1.39-fold), when treated with scleroderma exosomes compared to healthy exosomes.

Overall, scleroderma immortalised keratinocytes responded differently to scleroderma-fibroblast exosomes, compared to scleroderma exosome treated HaCats, and thus, HaCats were continued to be used as a healthy keratinocyte cell model.

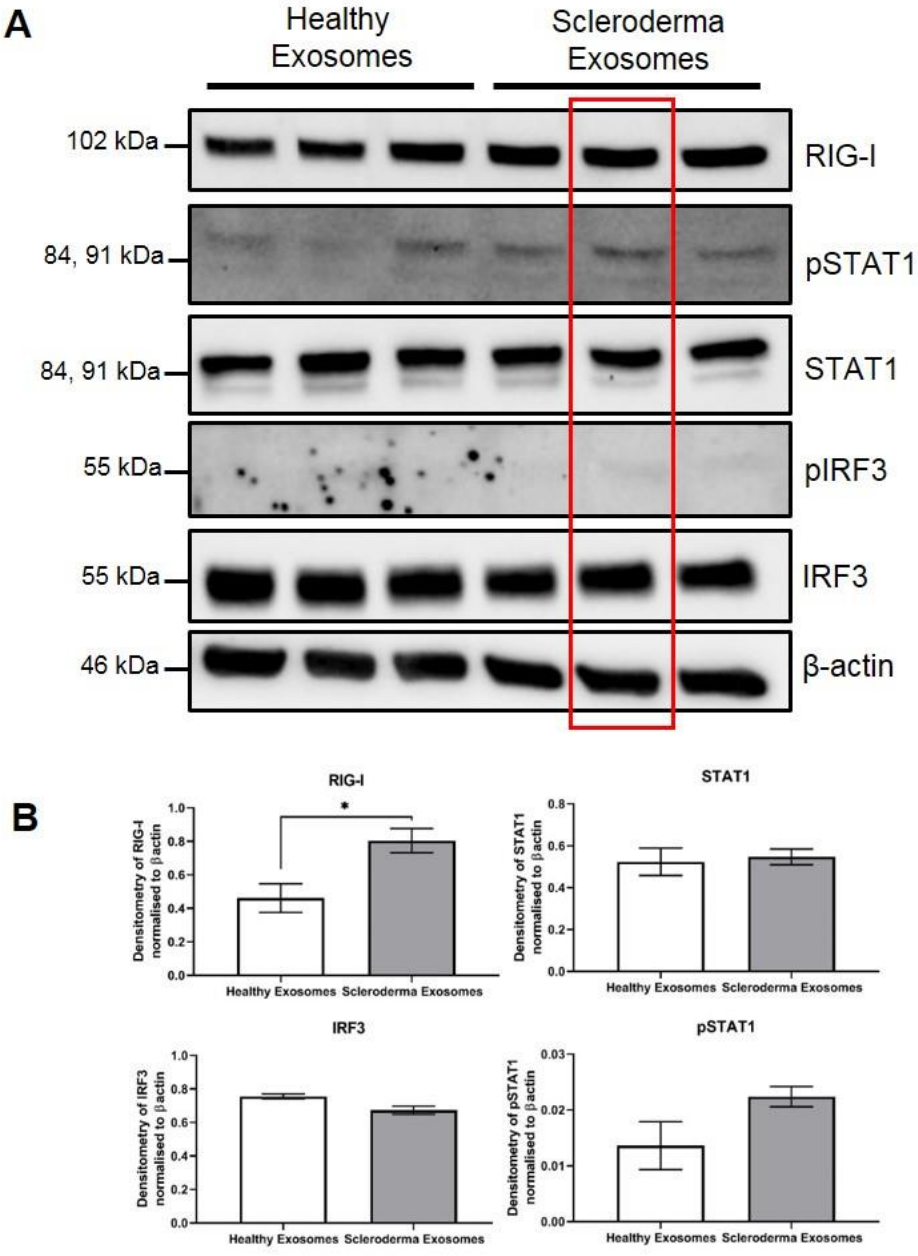

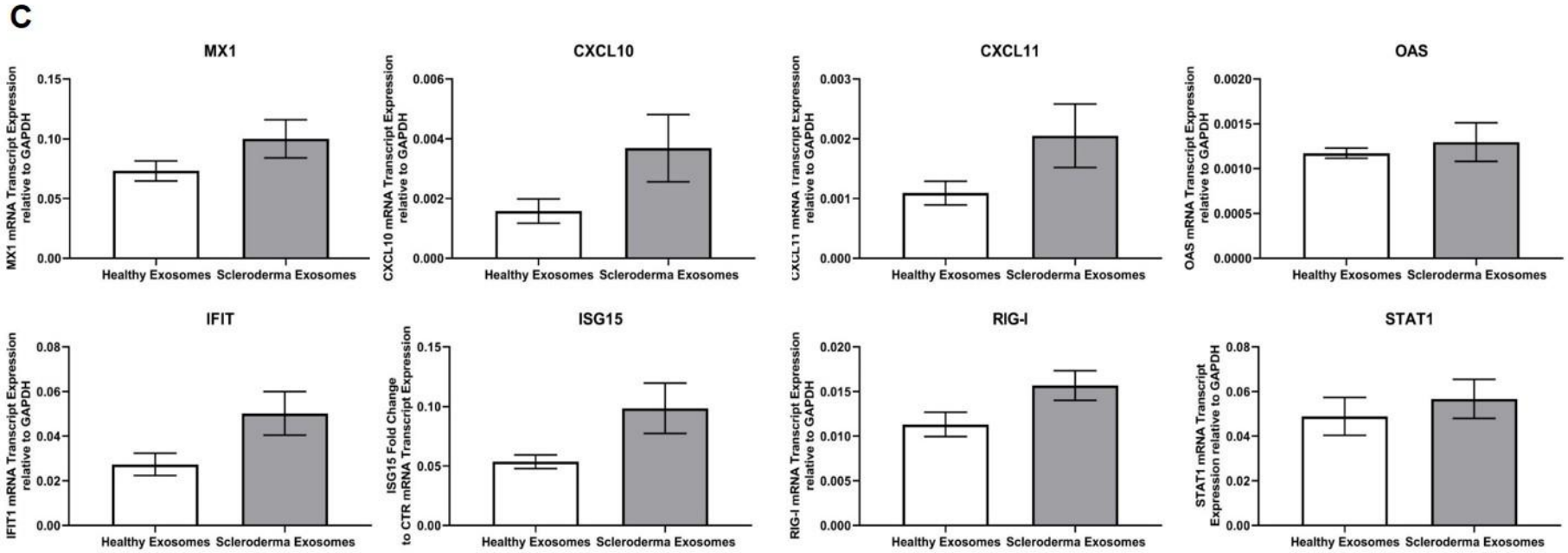

Figure 4.6. Autologous stimulation of Scleroderma fibroblast exosomes on Scleroderma Immortalized Keratinocytes illustrated mixed responses for pSTAT1 and ISG induction.

Immortalised scleroderma keratinocytes were starved with keratinocyte grown media, supplemented with calcium chloride, and stimulated with healthy and scleroderma fibroblast-derived exosomes for 48 hours. A) Western blots against the antibodies; RIG-I, pSTAT1 (Tyr701), STAT1, pIRF3 (Ser386), IRF3 and β-actin, for scleroderma keratinocytes treated with healthy (n=3) and scleroderma exosomes (n=3). Red box indicates scleroderma fibroblast-derived exosomes autologous to scleroderma keratinocyte cell line. B) Quantification of (A) by densitometry and normalised to β-actin levels. C) mRNA transcript expression of MX1, CXCL10, CXCL11, OAS, IFIT1, ISG15, RIG-I and STAT1, normalised to housekeeping gene GAPDH. Healthy Exosomes n=3, Scleroderma exosomes n=5. Data represents means ± SE from three independent experiments. Statistics analysis using a two-tailed unpaired Mann-whitney Test.

4.2.5. Co-culture of Scleroderma fibroblasts with HaCats significantly induces ISGs, as well as protein expression of pIRF3 and pSTAT1 in HaCats

Cells communicate in-vivo through predominantly autocrine, endocrine and paracrine signalling. Although, exosomes act as key intercellular communication vehicles; cells secrete numerous proteins, which can also actively interact with recipient cells and influence their behaviour. Thus, to analyse the overall function of exosomes in the cross talk between fibroblasts and keratinocytes in a more accurate in-vitro model, scleroderma fibroblasts were co-cultured with HaCats to investigate the role of cellular communication and cross talk between the two cell types. Firstly, scleroderma and healthy immortalised fibroblasts were equally seeded onto a 0.4 μM PET membrane and co-cultured with HaCats in serum-free DMEM for 48 hours. Fibroblast nuclei was stained with DAPI, and imaged by confocal microscopy, to ensure cell seeding was equal and thus differences in signalling observed was due to cell type, rather than cell number (Figure 4.7.A).

Immunoblotting for type 1 interferon-related proteins in the HaCats showed that scleroderma fibroblasts significantly induced pSTAT1 (2.50-fold, $p<0.05$) and pIRF3 (2.07-fold, $p<0.05$) (Figure 4.7.C). Expression of RIG-I was induced by scleroderma fibroblasts by 1.70-fold (NS). STAT1 and IRF3 protein expression was consistent in HaCats co-cultured with healthy and scleroderma fibroblasts (Figure 4.7.B-C). Likewise, total ISG15 protein expression was the same in HaCats for both conditions (Figure 4.7.C). However, when investigating the conjugates of ISG15, there is observably more interactions in HaCats with scleroderma fibroblast co-cultures, compared to healthy (Figure 4.7.B).

mRNA transcript expression further showed an induction of interferon signalling by a significant increase in CXCL10 (1.59-fold, $p<0.05$), CXCL11 (1.68-fold, $p<0.05$), IL6 (1.67-fold, $p<0.05$) and interferon β (1.42-fold, $p<0.01$), when compared to healthy fibroblasts (Figure 4.7.D). In addition, scleroderma fibroblast co-cultured HaCats showed an increase in gene expression for other ISGs, such as MX1 (1.27-fold, NS), OAS (1.28-fold, NS), IFIT (1.36-fold, NS), ISG15 (1.38-fold, NS), RIG-I (1.28-fold, NS) and STAT1 (1.26-fold, NS), when compared to healthy control.

Moreover, as a significant increase in mRNA transcript expression of IL6 was observed; we investigated the potential role of the NF-κB pathway by immunoblotting for phosphorylated Ikkαβ and total Ikkαβ. Immunoblotting of pIkkαβ and Ikkαβ showed no significant change between HaCats co-cultured with healthy or scleroderma fibroblasts (Figure 4.7.B-C). Therefore, the increase in IL-6 gene expression is likely to be independent of the NF-κB pathway.

Overall, co-culturing scleroderma fibroblasts with HaCats elicits a similar response to adding scleroderma fibroblast-derived exosomes to HaCats, where both methods induced phosphorylation of STAT1 and ISG induction. However, the induction of IL-6 and IFNβ gene expression hasn't been observed by RT-qPCR, IFN array or RNA Sequencing of HaCats treated scleroderma exosomes. In addition, phosphorylation of IRF3, the key transcription factor for IFNβ, also significantly increased in co-culture with scleroderma fibroblasts, compared to no changes observed at exosome level. Therefore, to understand the importance of exosomes in the induction of type 1 interferon of HaCats, we need to investigate the importance of other cellular communication from scleroderma fibroblasts by inhibiting exosome production and release.

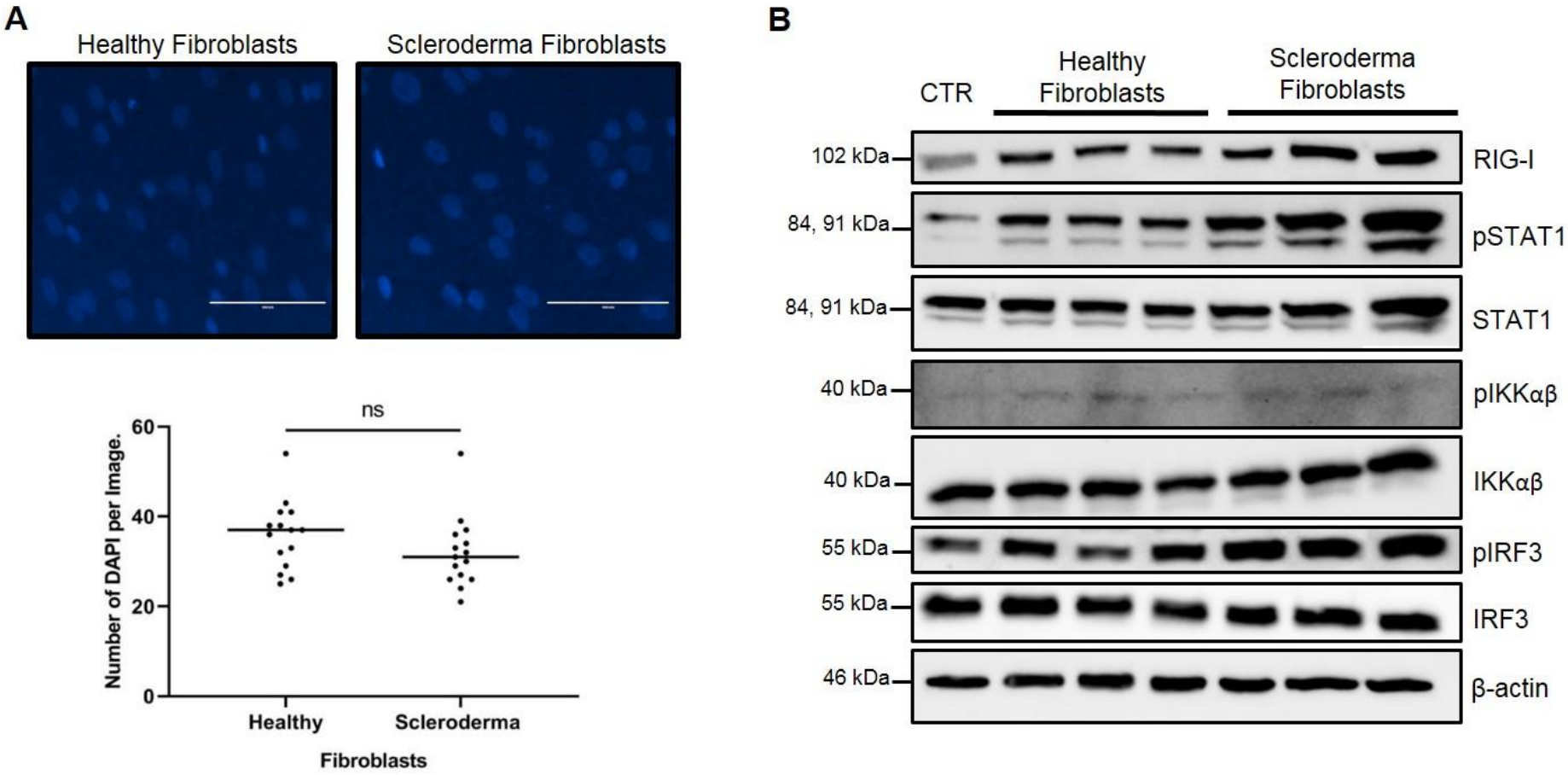
A
Healthy Fibroblasts
Scleroderma Fibroblasts
ns
Number of DAPI per Image.
60
40
20
0
Healthy
Scleroderma
Fibroblasts
B
CTR
Healthy Fibroblasts
Scleroderma Fibroblasts
102 kDa
RIG-I
84, 91 kDa
pSTAT1
84, 91 kDa
STAT1
40 kDa
pIKKαβ
40 kDa
IKKαβ
55 kDa
pIRF3
55 kDa
IRF3
46 kDa
β-actin

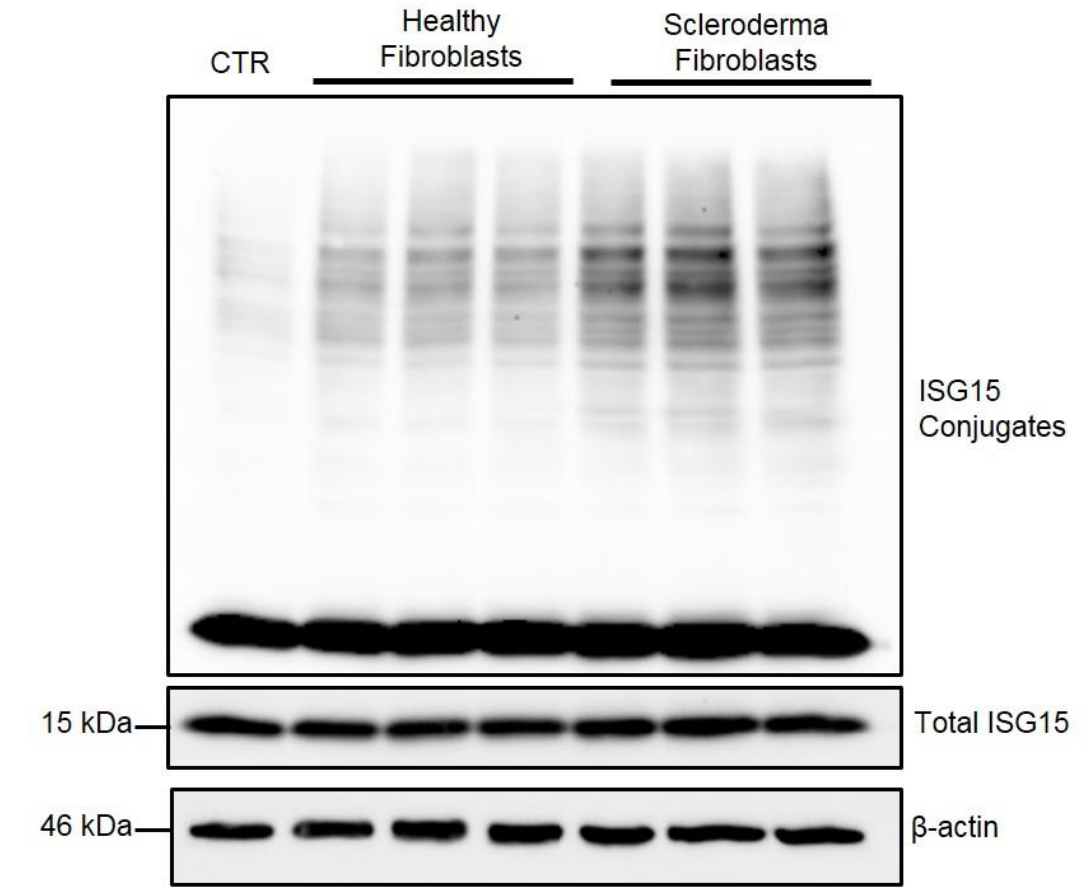
CTR
Healthy Fibroblasts
Scleroderma Fibroblasts
ISG15 Conjugates
15 kDa
Total ISG15
46 kDa
β-actin

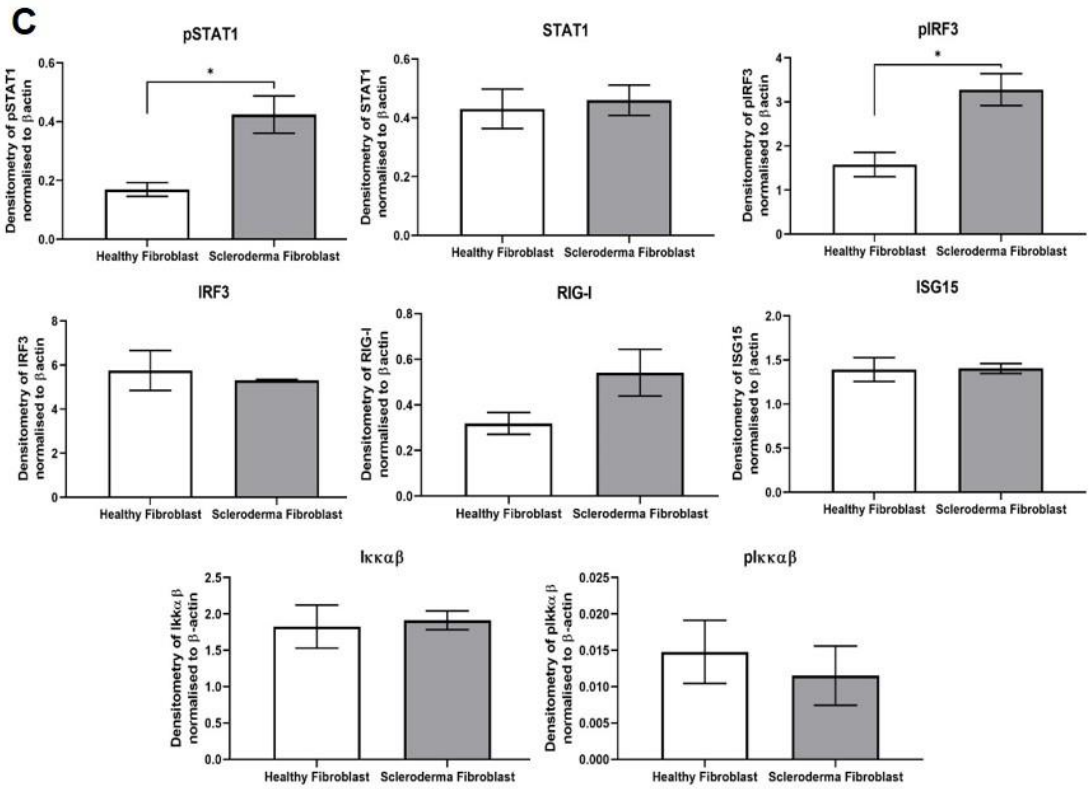
C
pSTAT1
STAT1
pIRF3
IRF3
RIG-I
ISG15
IκκαβIκκαβ
pIκκαβ
Densitometry of pSTAT1 normalised to βactin
Densitometry of STAT1 normalised to βactin
Densitometry of pIRF3 normalised to βactin
Densitometry of IRF3 normalised to βactin
Densitometry of RIG-I normalised to βactin
Densitometry of ISG15 normalised to βactin
Densitometry of Ikkαβ normalised to β-actin
Densitometry of pIkkαβ normalised to β-actin
Healthy Fibroblast
Scleroderma Fibroblast
*

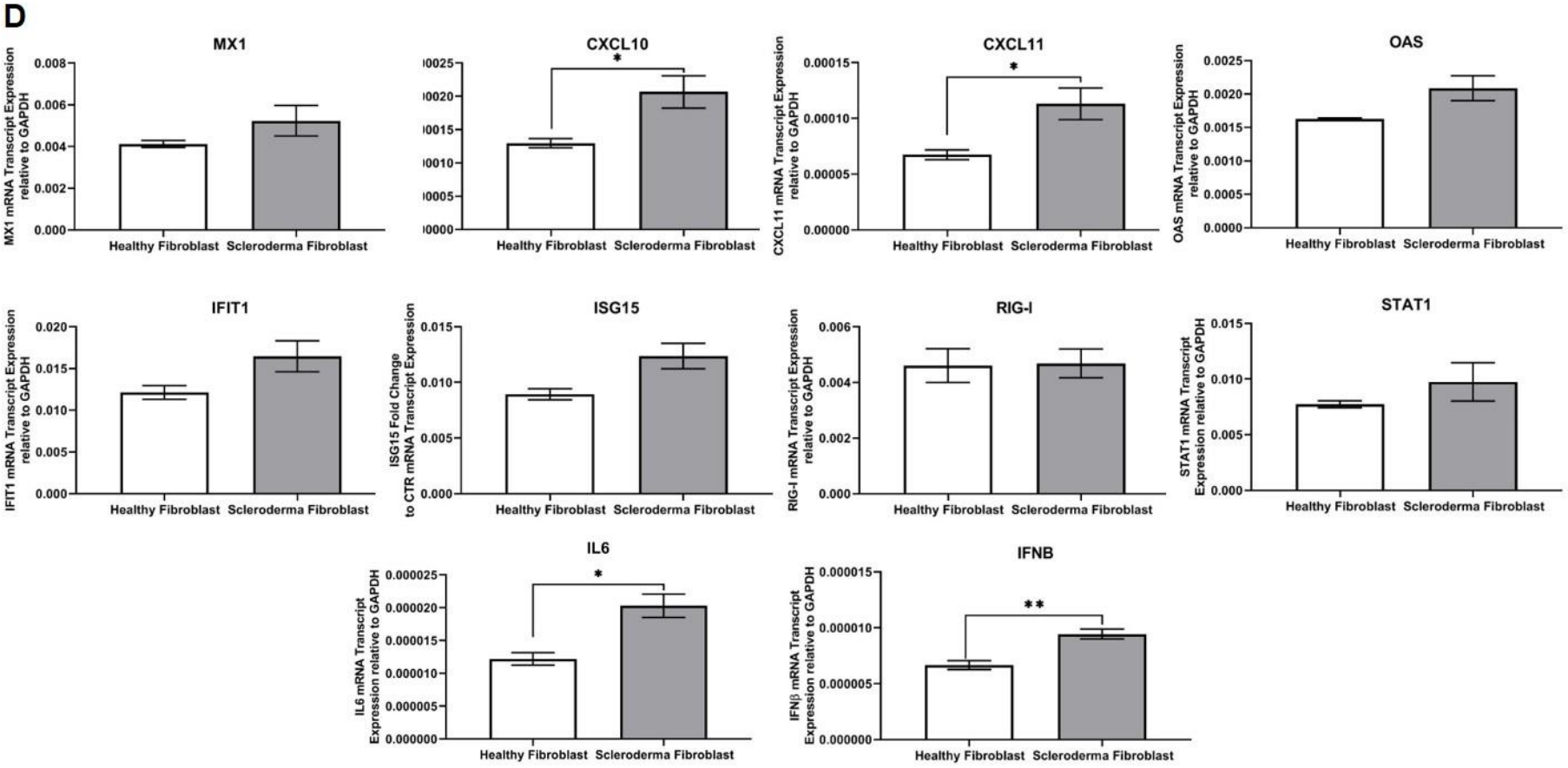
D
MX1
MX1 mRNA Transcript Expression relative to GAPDH
0.008
0.006
0.004
0.002
0.000
Healthy Fibroblast
Scleroderma Fibroblast
CXCL10
*
Healthy Fibroblast
Scleroderma Fibroblast
CXCL11
CXCL11 mRNA Transcript Expression relative to GAPDH
0.00015
0.00010
0.00005
0.00000
*
Healthy Fibroblast
Scleroderma Fibroblast
OAS
OAS mRNA Transcript Expression relative to GAPDH
0.0025
0.0020
0.0015
0.0010
0.0005
0.0000
Healthy Fibroblast
Scleroderma Fibroblast
IFIT1
IFIT1 mRNA Transcript Expression relative to GAPDH
0.020
0.015
0.010
0.005
0.000
Healthy Fibroblast
Scleroderma Fibroblast
ISG15
ISG15 Fold Change to CTR mRNA Transcript Expression
0.015
0.010
0.005
0.000
Healthy Fibroblast
Scleroderma Fibroblast
RIG-I
RIG-I mRNA Transcript Expression relative to GAPDH
0.006
0.004
0.002
0.000
Healthy Fibroblast
Scleroderma Fibroblast
STAT1
STAT1 mRNA Transcript Expression relative to GAPDH
0.015
0.010
0.005
0.000
Healthy Fibroblast
Scleroderma Fibroblast
IL6
IL6 mRNA Transcript Expression relative to GAPDH
0.000025
0.000020
0.000015
0.000010
0.000005
0.000000
*
Healthy Fibroblast
Scleroderma Fibroblast
IFNB
IFNβ mRNA Transcript Expression relative to GAPDH
0.000015
0.000010
0.000005
0.000000
**
Healthy Fibroblast
Scleroderma Fibroblast

Figure 4.7. Scleroderma fibroblasts in co-culture with HaCats induce an interferon response.

Healthy (n=3) and Scleroderma (n=3) fibroblasts were co-cultured in a 0.4 µM low protein binding PET membrane cell culture inserts with HaCats for 48 hours in serum-free conditions. A) Fluorescent microscope images of the nuclei of healthy and scleroderma fibroblasts post co-culture. Nuclei was stained using prolong gold DAPI. Images taken on EVOS M5000 at 40x magnification. 5 images were taken of each biological replicate: one image at each corner and a central image. Data was statistically analysed using a two-tailed unpaired Mann Whitney T-test assuming equal variance. Scatter graph illustrates number of nuclei per image, Black line illustrates sample mean. ns = not significant. B) Representative images of western blots against the antibodies; RIG-I, pSTAT1 (Tyr701), STAT1, Iκκαβ, pIκκαβ pIRF3 (Ser386), IRF3, ISG15 and β-actin. ISG15 expression shown by total protein (Exposure = 20 seconds) and ISG15-protein interactions (Exposure = 90 seconds). C) Quantification of (B) by densitometry and normalised to β-actin levels. D) mRNA transcript expression of interferon-related genes, normalised to GAPDH and ribosomal protein as a house-keeping gene. Data represents means ± SE from three biological repeats. Statistical analysis using a two-tailed student t-test, assuming equal variance. *p<0.05. **p<0.01.

4.2.6. Small molecule exosome inhibitor (GW4869) does not inhibit exosome secretion in fibroblasts and HaCats

GW4869 is a non-competitive sphingomyelinase inhibitor, which is widely used to inhibit exosome release and biogenesis. GW4869 acts by inhibiting the release of mature exosomes from multivesicular bodies (MVBs), by preventing ceramide-mediated inward budding of the MVB. Kobina et al., (2015) inhibited exosome induced proinflammatory cytokine production in macrophages, using 10µM and 20µM of GW4869. Thus, fibroblasts were treated with 10 and 20 µM GW4869 for 48 hours and exosomes were isolated by ultracentrifugation and precipitation. Interestingly, treatment of 20µM GW4869 lead to global cell death, compared to Kobina et al., (2015) who showed no changes to cell viability (Figure 4.8.A). Likewise, immunoblotting against TSG101, a common exosome marker, showed a 10-fold increase in protein expression of exosomes isolated from GW4869-treated fibroblasts (Figure 4.8.A).

To investigate further, the experiment was repeated using HaCats and fibroblasts treated with 5 and 10µM of GW4869 to explore if a reduced concentration would inhibit exosome production and reduce cell death. Treatments of 5 and 10µM GW4869 showed increased expression of TSG101, in exosomes isolated from HaCats and fibroblasts, were 5µM showed the greatest induction for both cell types (Figure 4.8.B). TSG101 protein expression in HaCats and fibroblast lysates treated with GW4869, was unchanged compared to control (Figure 4.8.C). Further, trypan blue and 7-AAD staining (Figure 4.8.D) was used to assess cell viability, post GW4869 treatment. Both trypan blue and 7-AAD staining showed induced toxicity in cells as GW4869 concentration increased, where 7-AAD staining showed that 10µM GW4869 treated fibroblasts displayed 89.50% cell viability (Figure 4.8.D-E).

Collectively, this data indicates that GW4869 does not inhibit exosome production in HaCats and fibroblasts over a 48-hour period and subsequently, GW4869 induced cellular toxicity at increased concentrations, where 20µM lead to global cell death in fibroblasts after 48 hours.

A

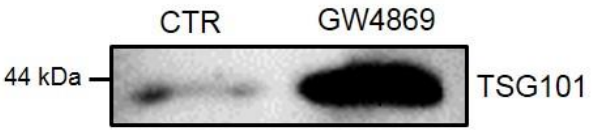

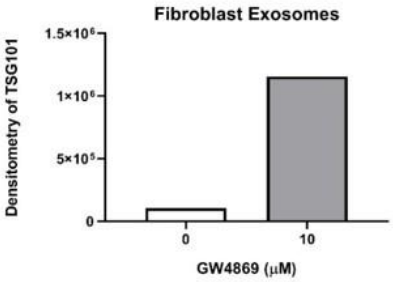

Sample	CTR	GW4869 (10μM)	GW4869 (20μM)
Viable Cells	5.07×10^5	4.43×10^5	0
Trypan Blue Stained	1.25×10^4	5.5×10^4	N/A
% Cell Viable	97.59%	88.96%	0%

B

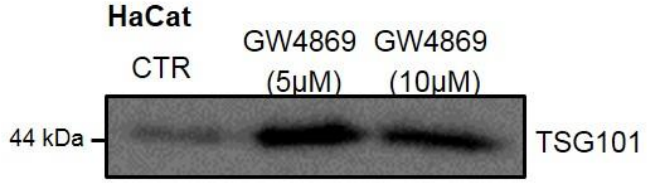

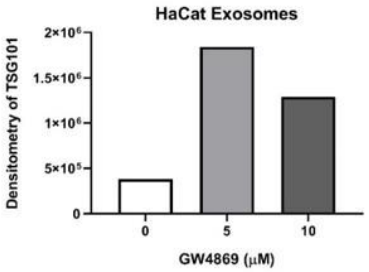

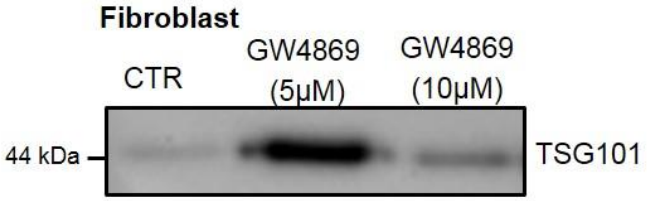

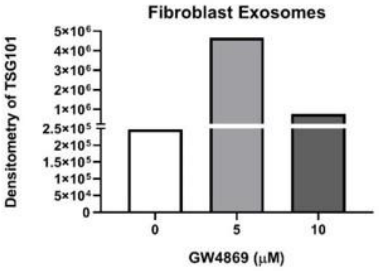

C

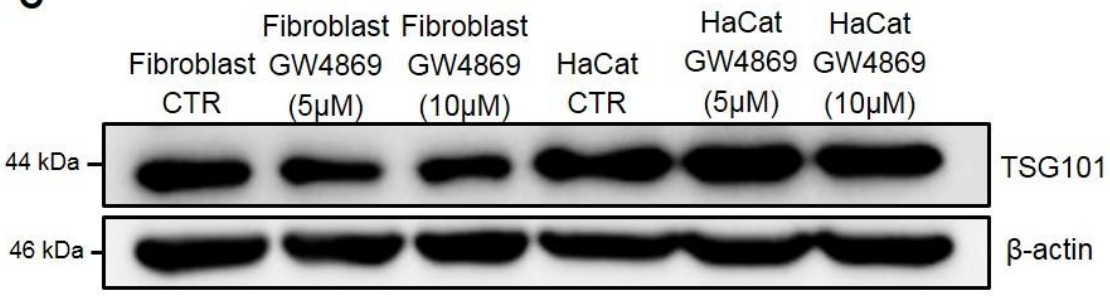

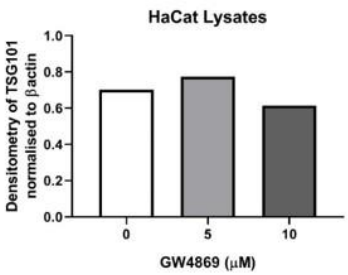

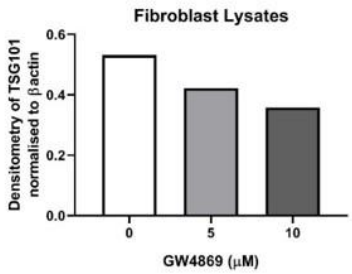

D

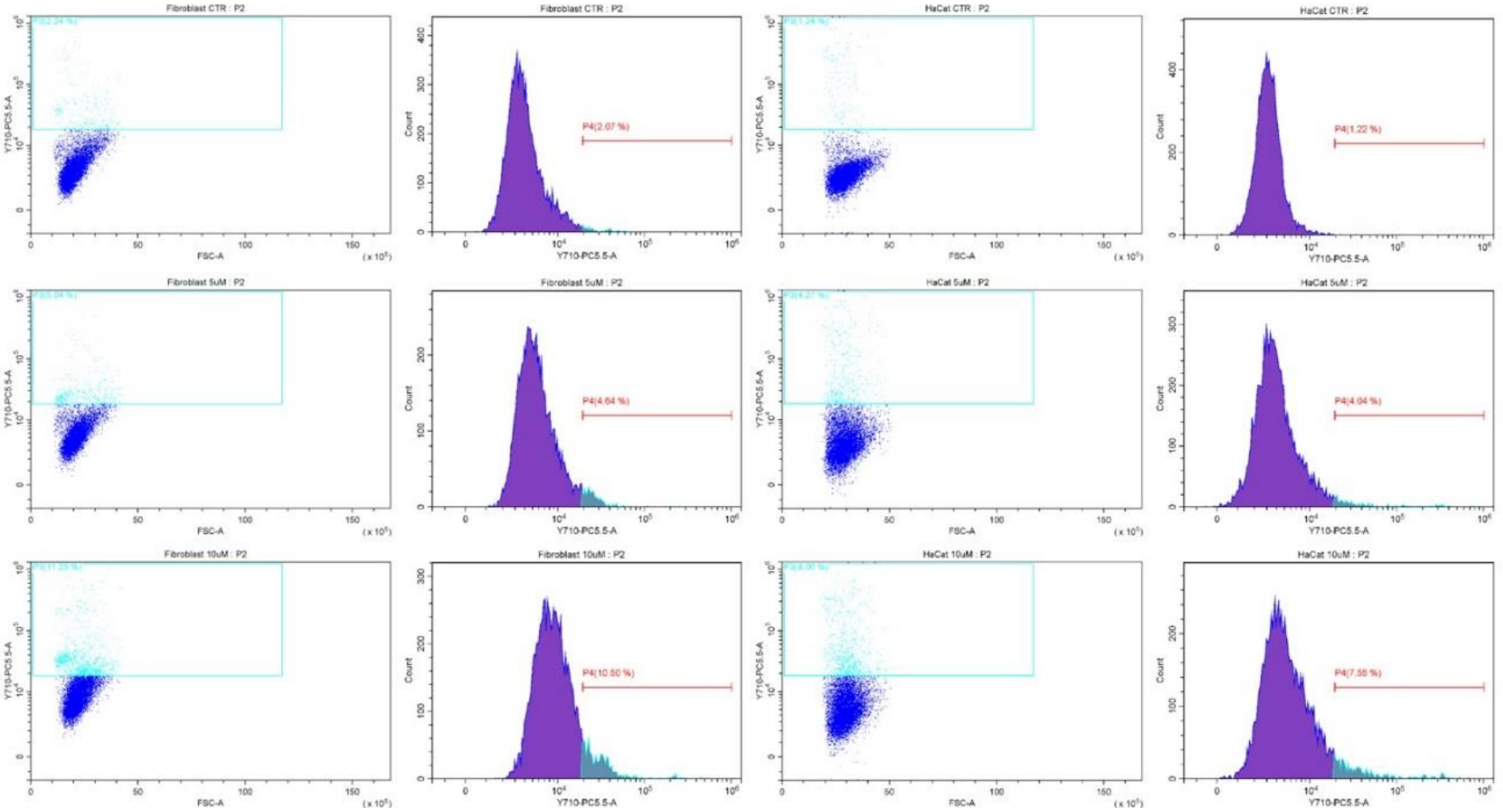
Fibroblast CTR : P2
Fibroblast CTR : P2
P4(2.07 %)
HaCat CTR : P2
HaCat CTR : P2
P4(1.22 %)
Fibroblast 5uM : P2
Fibroblast 5uM : P2
P4(4.64 %)
HaCat 5uM : P2
HaCat 5uM : P2
P4(4.04 %)
Fibroblast 10uM : P2
Fibroblast 10uM : P2
P4(10.50 %)
HaCat 10uM : P2
HaCat 10uM : P2
P4(7.55 %)
Y710-PC5.5-A
FSC-A
Count

Table 14. %Cell Viability using Trypan Blue.

Sample	Fibroblast CTR	Fibroblast GW4869 (5µM)	Fibroblast GW4869 (10µM)	HaCat CTR	HaCat GW4869 (5µM)	HaCat GW4869 (10µM)
Viable Cells	9.4×10^5	1.85×10^5	1.34×10^6	8.25×10^5	1.73×10^6	1.69×10^6
Trypan Blue Stained	0	3.70×10^3	4.02×10^4	5.79×10^4	1.04×10^5	1.35×10^5
% Cell Viable	100%	98%	97%	93%	94%	92%

Table 15. %Cell Viability using 7-AAD stained cells by Flow Cytometry.

Sample	Fibroblast CTR	Fibroblast GW4869 (5µM)	Fibroblast GW4869 (10µM)	HaCat CTR	HaCat GW4869 (5µM)	HaCat GW4869 (10µM)
% 7-AAD Stained	2.07%	4.64%	10.50%	1.22%	4.04%	7.55%
% Cell Viable	97.93%	95.36%	89.50%	98.78%	95.96%	92.45%

Figure 4.8. Treatment of HaCats and fibroblasts with exosome inhibitor (GW4869) for 48 hours induces exosome production from both cell types.

Healthy fibroblasts were treated with 10µM and 20µM of GW4869, to inhibit exosome release, in exosome-depleted FBS supplemented DMEM for 48 hours. GW4869 was solubilised in DMSO at 1mM and thus the control (CTR) was supplemented with 2% DMSO. After 48 hours, exosomes were extracted from the cultured DMEM by ultracentrifugation and precipitation. A) An immunoblot against TSG101 for exosomes isolated from fibroblasts treated +/- 10µM GW4869, as well as densitometry analysis. Quantification of cell viability was measured using tryphan blue staining (n=1). B) Immunoblotting of HaCats and fibroblast isolated exosomes after cells stimulated with 5 and 10µM GW4869, against TSG101. CTR contains 1% DMSO. Densitometry analysis is displayed alongside the blots (n=1). C) Immunoblots and densitometry analysis of healthy fibroblasts and HaCat lysates after treatment with 5 and 10µM GW4869, against TSG101 and β-actin, which was used as a loading control (n=1). Flow cytometry analysis of fibroblasts and HaCats treated with 5 and 10 µM of GW4869 and a 1% DMSO supplemented control, stained with 7-AAD. The left-hand panel depicts fibroblasts and the right HaCats. Events were plotted with Y710-PC5.5-A (Fluorescent laser which detects 7-AAD) on the y-axis, against forward scatter (x-axis). Gating (Light Blue – P3) was established from a pre-gated single cell population of unstained control for both cell types. Two tables which summarise different methods of determining cell viability; firstly, cells stained with tryphan blue and manually counted and secondly, cells stained with 7-AAD and measured by flow cytometry. All experiments were conducted on one healthy fibroblast and one HaCat cell line.

4.2.7. Removal of exosomes from scleroderma fibroblast-cultured serum-free supernatant, via ultracentrifugation, does not reduce pSTAT1 and ISG induction

As GW4689 did not successfully inhibit exosome release from fibroblasts and HaCats after 48 hours of treatment, exosomes were removed from fibroblast cultured supernatant via ultracentrifugation, depicted as a schematic in Figure 4.9.A. Ultracentrifuged (UC) scleroderma DMEM significantly induced pSTAT1 ($p<0.05$) by 2.4-fold, compared to UC healthy DMEM (Figure 4.9.B-C). In addition, non-centrifuged (non-UC) scleroderma DMEM induced pSTAT1 by 2.47-fold, however, wasn't found to be significant. Likewise, there was no change in protein expression of RIG-I, IRF3, STAT1 and pIRF3 for UC or non-UC healthy and SSc fibroblast cultured media.

Moreover, non-UC scleroderma fibroblast media induced interferon-stimulated genes; MX1 (2.39-fold, $p<0.05$), CXCL10 (11.50-fold, $p<0.05$), CXCL11 (1.23, NS), OAS (2.09-fold, $p<0.05$), IFIT1 (1.58-fold, NS), ISG15 (3.49-fold, $p<0.001$), RIG-I (1.97-fold, $p<0.01$), STAT1 (1.91-fold, NS), IFNβ (1.35-fold, NS) and IL6 (4.16-fold, $p<0.05$), compared to non-UC healthy fibroblasts, after 48 hours. Interesting, UC scleroderma fibroblast media also induced interferon-stimulated genes; MX1 (2.21-fold, $p<0.05$), CXCL10 (9.84-fold, $p<0.05$), CXCL11 (1.32, NS), OAS (1.98-fold, $p<0.05$), IFIT1 (1.91-fold, $p<0.05$), ISG15 (3.24-fold, $p<0.05$), RIG-I (1.94-fold, $p<0.001$), STAT1 (1.74-fold, $p<0.05$), IFNβ (1.77-fold, NS) and IL6 (2.88-fold, $p<0.01$), compared to UC healthy fibroblasts, after 48 hours. In addition, there is no significant decrease of gene expression of any induced ISG when comparing non-centrifuged scleroderma media with ultracentrifuged scleroderma media.

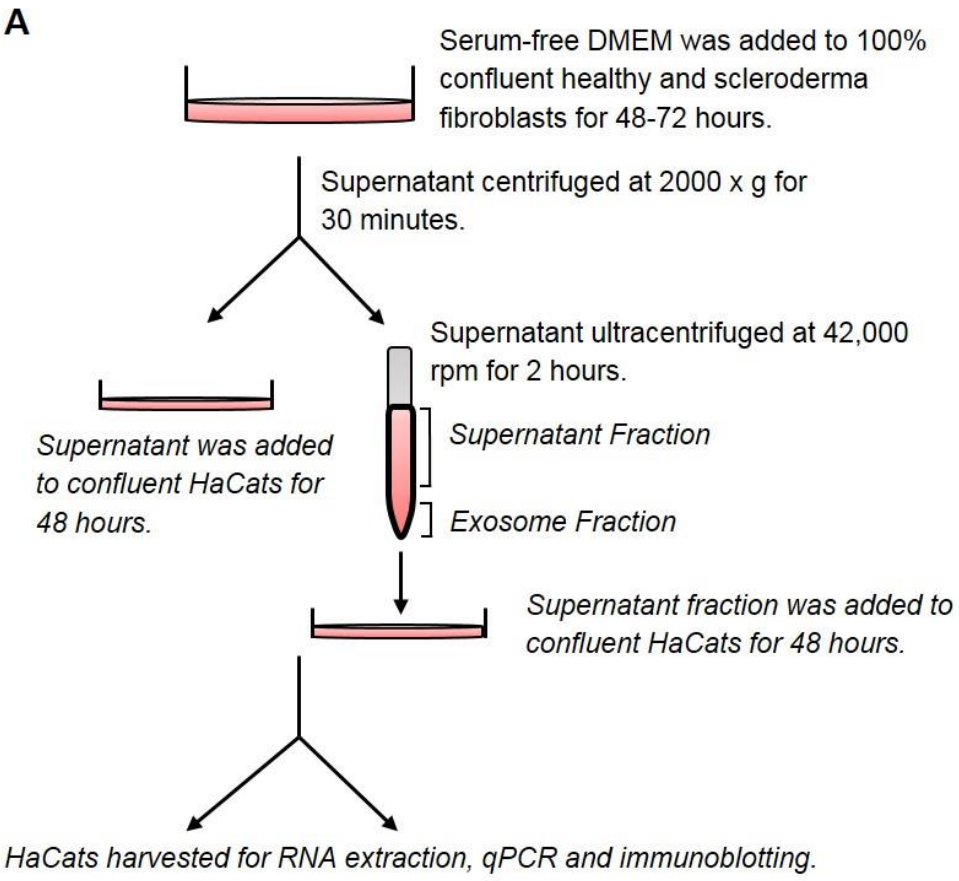

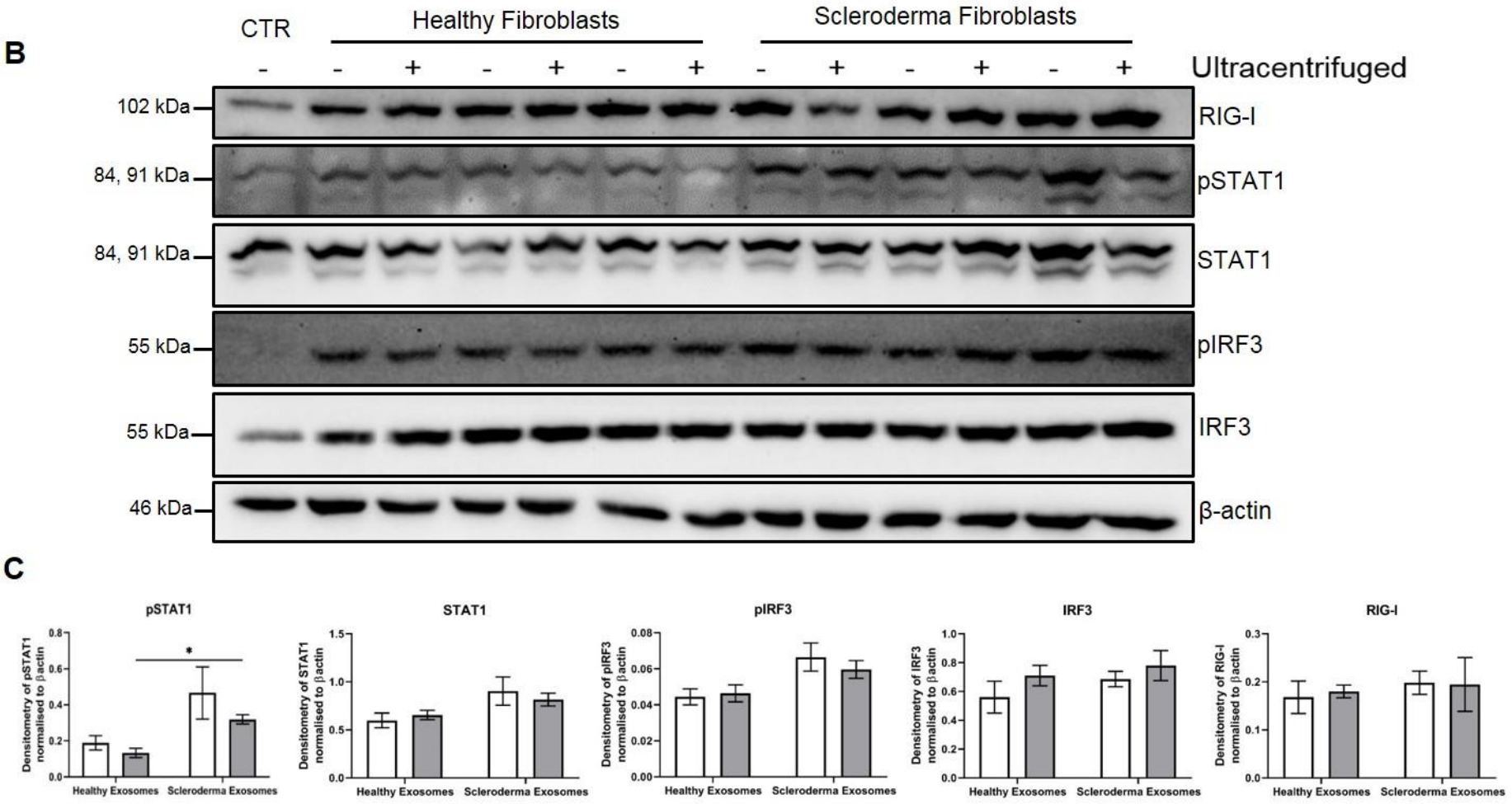
B
CTR
Healthy Fibroblasts
Scleroderma Fibroblasts
- - + - + - + - + - + - + Ultracentrifuged
102 kDa
RIG-I
84, 91 kDa
pSTAT1
84, 91 kDa
STAT1
55 kDa
pIRF3
55 kDa
IRF3
46 kDa
β-actin
C
pSTAT1
Densitometry of pSTAT1 normalised to βactin
*
Healthy Exosomes
Scleroderma Exosomes
STAT1
Densitometry of STAT1 normalised to βactin
pIRF3
Densitometry of pIRF3 normalised to βactin
IRF3
Densitometry of IRF3 normalised to βactin
RIG-I
Densitometry of RIG-I normalised to βactin

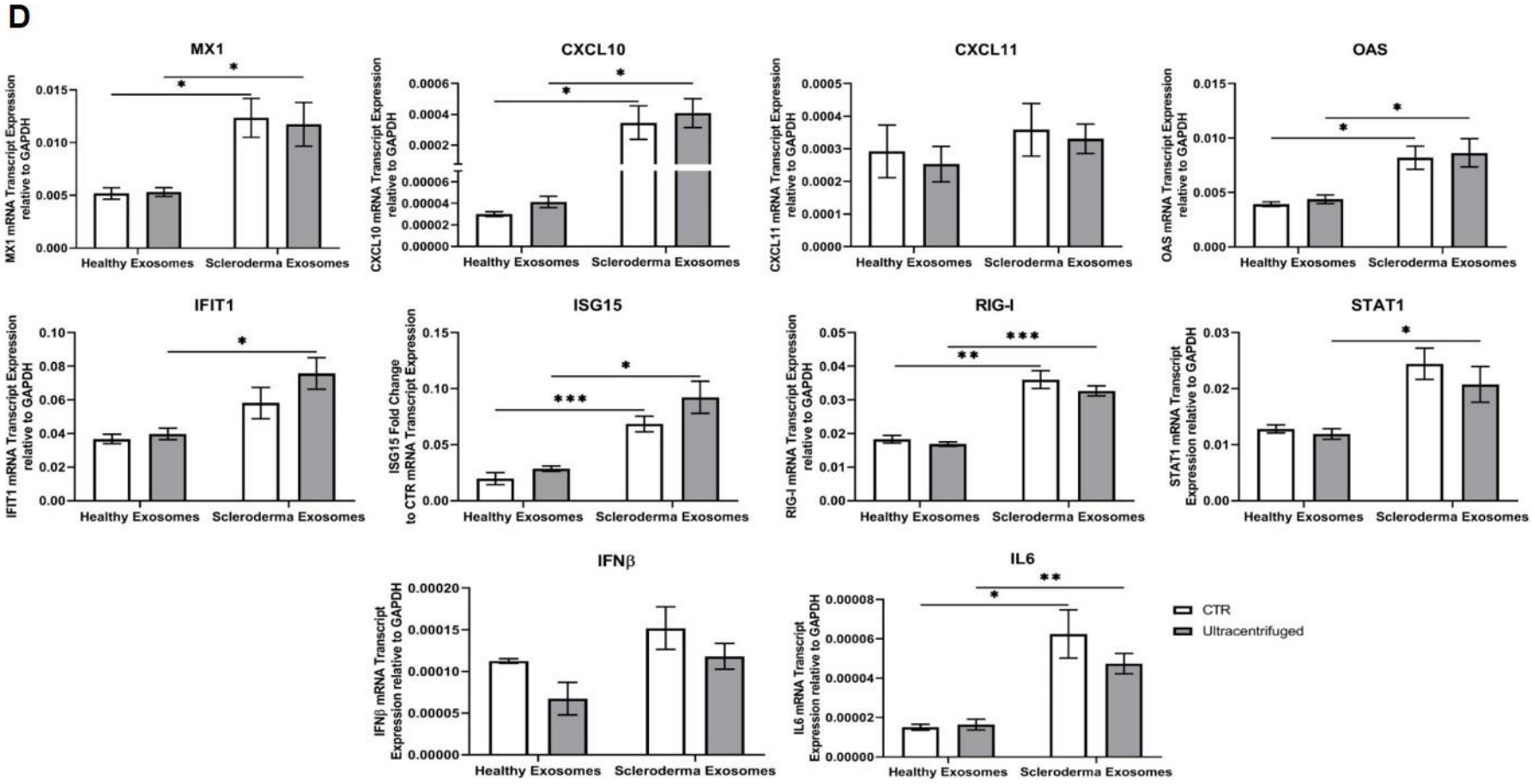
D
MX1
MX1 mRNA Transcript Expression relative to GAPDH
0.015
0.010
0.005
0.000
Healthy Exosomes
Scleroderma Exosomes
CXCL10
CXCL10 mRNA Transcript Expression relative to GAPDH
0.0006
0.0004
0.0002
0.00006
0.00004
0.00002
0.00000
CXCL11
CXCL11 mRNA Transcript Expression relative to GAPDH
0.0005
0.0004
0.0003
0.0002
0.0001
0.0000
OAS
OAS mRNA Transcript Expression relative to GAPDH
0.015
0.010
0.005
0.000
IFIT1
IFIT1 mRNA Transcript Expression relative to GAPDH
0.10
0.08
0.06
0.04
0.02
0.00
ISG15
ISG15 Fold Change to CTR mRNA Transcript Expression
0.15
0.10
0.05
0.00
RIG-I
RIG-I mRNA Transcript Expression relative to GAPDH
0.05
0.04
0.03
0.02
0.01
0.00
STAT1
STAT1 mRNA Transcript Expression relative to GAPDH
0.03
0.02
0.01
0.00
IFNβ
IFNβ mRNA Transcript Expression relative to GAPDH
0.00020
0.00015
0.00010
0.00005
0.00000
IL6
IL6 mRNA Transcript Expression relative to GAPDH
0.00008
0.00006
0.00004
0.00002
0.00000
CTR
Ultracentrifuged

Figure 4.9. Removal of exosomes from scleroderma fibroblast cultured serum-depleted DMEM, via ultracentrifugation, does not reduce pSTAT1 and ISG induction.

A) A flow chart schematic to illustrate the experimental design of removing exosomes from cultured supernatant and adding to HaCats for 48 hours, to understand the importance of exosomes in the induction of the type 1 interferon response. B) Immunoblots for RIG-I, pSTAT1, STAT1, pIRF3 and IRF3, as well as β-actin which was used as a loading control. C) Bar charts illustrating densitometry analysis of western blots shown in B, calculated using Image Lab. D) mRNA transcript expression of interferon-related genes, normalised housing keeping genes; GAPDH and ribosomal protein. Data represents means ± SE from three biological repeats. Statistical analysis by a multiple comparison two-way ANOVA, normalised to Tukey. *p<0.05, **p<0.01, ***p<0.001.

4.3. Discussion

Fibroblasts are the key cellular elements of fibrosis in scleroderma pathogenesis. Dysregulated immune activation is also associated with SSc pathogenesis, however the link between immune abnormalities and fibrosis in SSc is poorly understood, where no mechanisms have been identified to explain the interplay between fibrosis and autoimmunity. Further, aberrant immune activation in scleroderma is commonly characterised by the production of autoantibodies, cytokines, and the activation and recruitment of immune cells (Fett, N., 2013). Many studies have associated immune activation as a cause and/or contributor of fibrosis in SSc, while others have suggested that fibrosis contributes to immune cell activation (Ah Kioon et al., 2018, Brkic et al., 2016, Farina et al., 2010).

Primarily, fibrosis in early disease SSc patients mainly occurs in the skin layer, which is an early clinical feature of the disease (Fett, N., 2013). Likewise, fibrosis occurs due to excessive release of ECM proteins by aberrant activation of fibroblasts (Gilbane et al., 2013). Further, it is commonly hypothesised that fibroblasts are the target of immunopathogenesis, where immune cells activate

fibroblasts to induce a pro-fibrotic response (Ah Kioon et al., 2018, Brkic et al., 2016, Farina et al., 2010). In addition, studies have observed IFN signatures in early disease SSc patient skin biopsies before fibrosis onset (Assassi et al., 2010), which supports the hypothesis that excessive IFN precedes fibrosis and thus could contribute to the development of a pro-fibrotic response in fibroblasts.

This study illustrates that scleroderma fibroblasts can act as an immune driver, by releasing exosomes which contain biological materials capable of inducing IFN signalling in recipient keratinocytes. Recently, Bhandari et al., (2022) studied the cross talk between scleroderma dermal fibroblasts and macrophages to investigate the link between inflammation and fibrosis in SSc pathogenesis. Bhandari et al., (2022) illustrated that SSc fibroblast exosomes can induce pro-inflammatory cytokines in macrophages, after 48 hours, which when co-cultured with SSc fibroblasts can prolong activated fibroblasts and thus promote a pro-fibrotic phenotype. Further, Wermuth et al., (2017) showed that SSc serum exosomes can induce a profibrotic phenotype in healthy dermal fibroblasts. Overall, the literature has heavily focused on the link between exosomes and fibrosis in scleroderma, were both Bhandari et al., (2022) and Wermuth et al., (2017) investigated a small number of genes associated with the fibrotic response. Here we aimed to thoroughly explore the crosstalk between scleroderma fibroblasts and healthy keratinocytes by performing genome wide RNA sequencing, which illustrated that exosomes from scleroderma fibroblasts induce the upregulation of genes associated with interferon signalling and responses to cytokines in recipient keratinocytes, illustrating for the first time the potential importance of mesenchymal-epithelial cross talk and implications to the IFN signature seen in SSc.

Interestingly, KEGG analysis of SSc exosome treated HaCats showed an upregulation in pathways associated with fatty acid metabolism. Arachidonic and Linoleic acid are pre-cursors of eicosanoids, which are important signalling molecules that regulate the inflammatory response (Gogulska et al., 2021). Further, Ottria et al., (2020) illustrated that SSc patients have altered levels of fatty acids and L-carnitine in their blood and immune cells. They further discussed that dysregulated fatty acids led to an increase in fatty acid oxidation and release of pro-inflammatory cytokines, which resulted in a pro-fibrotic response. Collectively, this data indicates that SSc fibroblast exosomes induce ISGs in keratinocytes. However, KEGG analysis suggests SSc exosomes could also hold a secondary role in altering fatty acid metabolism in recipient cells, which as a result could promote a pro-fibrotic phenotype.

Moreover, CAF-derived exosomes have been shown to initiate interferon signalling through RIG-I (Nabet et al., 2017, Cui et al., 2022). Thus, we investigated ISG induction by exosomes, alongside a RIG-I agonist, over a 48 hour time course. This study illustrates that a 5’triphosphate RNA, mixed with lipofectamine2000, can induce ISGs and pSTAT1 expression, as early as 6 hours. However, exosomes induced interferon stimulated gene and phosphorylation of STAT1 after 48 hours. Likewise, exosome internalisation experiments illustrated that exosomes accumulated in HaCats over a time-period, which peaked at 48 hours, and thus, exosome uptake and processing may take significantly longer than lipofectamine transfection, which could offer an explanation behind the variation in timescales. Alternatively, SSc fibroblast exosomes may not stimulate RIG-I and therefore induce type I IFN signalling through a different signalling cascade.

HaCats are a common immortalised keratinocyte cell line, widely used in scientific research, which was also used in this study to represent healthy keratinocytes found in the skin. However, to develop a more accurate in-vitro skin environment, healthy primary and immortalised keratinocytes were intended to replace HaCats in further co-culture and exosome stimulation experiments. However, starvation and immortalisation of healthy keratinocytes led to reduced cell viability, and thus SSc immortalised keratinocytes were incorporated into the model. This study illustrated that scleroderma immortalised keratinocytes responded differently to scleroderma-fibroblast exosomes, compared to scleroderma exosome treated HaCats. Signalling between scleroderma cell types via exosomes is likely to differ as scleroderma keratinocytes will already display perturbed pro-inflammatory and/or pro-fibrotic signalling. A pitfall to this work is that only one SSc keratinocyte cell line was used for exosome stimulation experiments and the basal level of ISGs and IFN-related proteins weren't assessed between healthy and SSc keratinocytes. Therefore, due to the unavailability and viability of using primary or immortalised healthy keratinocytes, HaCats were continued to be used as a healthy keratinocyte cell model.

To further investigate the crosstalk between SSc fibroblasts and keratinocytes a co-culture experiment was performed, which illustrated an upregulation of ISGs and protein expression of pSTAT1 and pIRF3. Interestingly, co-culture experiments showed greater induction of pSTAT1, as well as a novel induction of IFNβ gene expression, which is undetectable in HaCats stimulated with exosomes (data not shown), as well as a significant increase in the phosphorylation of IRF3, when compared to exosome stimulated HaCats.

Likewise, IRF3 and IRF7 are transcription factors which induce the expression of type I IFN. Co-culture of SSc fibroblasts with HaCats show significantly more phosphorylated IRF3 and upregulated gene expression of IFNβ, which suggests activation of an upstream PRR, such as RIG-I, STING or TLRs.

As phosphorylated IRF3 is strongly basally expressed in serum-starved HaCats, a weak induction by SSc exosomes may not be observed by immunoblotting and densitometry analysis, as immunoblotting is a non-sensitive semi-quantitative measure. Thus, expression of IRF7, which is solely expressed by IFN-induction, was investigated to determine if exosomes can induce IRFs. IRF7 protein expression was not observed in exosome treated HaCats or co-cultured HaCats (data not shown). Further, as HaCats stimulated with RIG-I agonist requires IRF3 and IRF7 phosphorylation and dimerization to induce gene expression, and RIG-I agonist induces CXCL10/11 by ~1000-fold greater than SSc exosomes; IRF7 protein expression was measured in RIG-I agonist treated HaCats. No protein expression of IRF7 was observed in RIG-I agonist stimulated HaCats (data not shown), and thus, subsequently, immunoblotting for IRF7 was not sufficient to determine if exosomes can induce the phosphorylation of IRFs.

Co-culture experiments are predominantly used in the literature, when investigating exosomes. However, the discrepancies between co-culture experiments and sole exosome experiments aren't commonly addressed. Furthermore, co-culture experiments are better in-vitro models, when compared to adding exosomes separately to cell, as exosome isolation requires multiple steps which can disrupt vesicles. For instance, isolation of exosomes requires ultracentrifugation and precipitation, where the force of centrifugation could

potentially alter vesicle composition and induce aggregation, as well as precipitation methods causing buffer contamination (Patel et al., 2019). Further, freeze-thaw of samples can change exosome concentration and sample purity (Gelibter et al., 2022). In addition, co-culture experiments allow a constant crosstalk between cells, where in this experiment, HaCats could also release exosomes, upon recipient of SSc fibroblast exosomes, which could further influence the fibroblasts, however this wasn't further investigated in this project.

Since co-culture of HaCats with SSc fibroblasts displayed enhanced type I IFN-related signalling, compared to SSc exosome stimulated HaCats, development of a small molecule exosome inhibitor (GW4869) was used to investigate the involvement of exosome in upregulated IFN-signalling. Surprisingly, it was observed that GW4869 induced exosome release in HaCats and fibroblasts after 48 hours. A limitation of this work is that the concentration of exosomes was solely characterised by TSG101 protein expression. Menck et al., (2017) treated breast cancer cells with 5µM GW4869 and observed an increase in the release of large vesicles (100-200nm), and a reduction in the release of small vesicles. Since, TSG101 is involved in all vesicle formation, and thus present on all extracellular vesicles, it is ineffective in calculating exosome concentration post inhibition.

Although, GW4869 has been intensively studied as a common inhibitor of exosome release; most studies don't characterise exosomes post GW4869-treatment and thus are unable to determine true exosome inhibition. For instance, Hu et al., (2015) showed that cultured media and exosomes from CAFs could induce tumour growth in cancer stem cells, which was alleviated by treatment with 10µM of GW4869. However, inhibited exosome release by

GW4869 wasn't experimentally shown, and only the effect on tumour growth with/without treatment was investigated. In addition, Hekmatirad et al., (2021) inhibited exosome release of myeloid leukaemia cells using GW4869 and evaluated exosome inhibition via measuring protein concentration between samples. Hekmatirad et al., (2021) further illustrated that GW4869 treatment significantly increased cytotoxic cell death, which was hypothesised as an exosome-dependent mechanism, however they never investigated or hypothesised that cytotoxicity could be related to the inhibitor. Likewise, we illustrated that GW4869 was toxic to cells in culture, and cell toxicity could additionally affect extracellular vesicle release and their contents.

Therefore, to further characterise exosome involvement; exosomes were removed from cultured-supernatant by ultracentrifugation and centrifuged/non-centrifuged cultured supernatant was added to HaCats to determine the level in which SSc fibroblast exosomes contribute to IFN-signalling induction in keratinocytes. Interestingly, this study observed that ultracentrifuged supernatant (exosomes removed) induced ISGs and the phosphorylation of pSTAT1, similarly, to cultured-supernatant which contained exosomes. Although no observable differences are determined between centrifuged and non-centrifuged supernatant, isolated exosomes induced ISGs and pSTAT1 in HaCats, and thus are a contributor to enhance IFN-signalling.

A limitation to this experimental design is that exosomes are commonly isolated from fibroblasts grown in 10% exosome-depleted FBS supplemented media for 48-72 hours and then added to serum-starved HaCats. Since exosome stimulation experiments were performed in starved conditions; serum-free DMEM was added to fibroblasts and then ultracentrifuged to remove exosomes.

Subsequently, starved, and non-starved fibroblasts may release exosomes with different contents, and as observed starved fibroblasts release less exosomes, when compared to non-starved fibroblasts (data not shown). Further, it is well documented that SSc fibroblasts secrete various autocrine and paracrine mediators, such as VEGF, CTGF, TGFβ, as well pro-inflammatory cytokines and chemokines, which can affect numerous signalling cascades (Gilbane et al., 2013). We illustrated that fibroblasts are secreting factors, which are capable of inducing a local IFN response, even after the removal of exosomes. However, this work has illustrated that exosomes alone are capable of inducing IFN in healthy keratinocytes. Indeed, secretion factors are capable of inducing a local response, however exosomes are capable of traveling longer distances, through multiple organs and bodily fluids, and thus are capable of inducing an IFN response at a distance to the site of release. However, this hypothesis wasn't further explored in this project. Likewise, early and late disease progression is an additional factor which could affect exosome contents and chemokine/cytokine secretion from fibroblasts, were genome wide studies of SSc fibroblasts illustrated sub-classes of fibroblasts linked with disease duration and progression (Johnson et al., 2015). Further, starvation of fibroblasts could result in induced cell stress and thus promote the release of excessive cytokines/chemokines, as well as stress-induced cell-free DNA, which is capable of activating cGAS-STING and inducing IFN (Decout et al., 2021).

Overall, this data indicates that scleroderma fibroblasts secrete exosomes, as well as other autocrine/paracrine mediators, which can induce the expression of interferon stimulated genes in keratinocytes, through the phosphorylation of STAT1. Indeed, to investigate the extent in which SSc exosomes induce ISGs

in keratinocytes in co-culture; exosome release in fibroblasts should be inhibited. Since, small molecule inhibitors cause cell toxicity; a siRNA knockdown of proteins directly associated with exosome biogenesis and release are viable options. However, this study has demonstrated by genome wide sequencing that SSc fibroblast-derived exosomes alone can induce interferon signalling in keratinocytes, which was further observed by induced ISG expression and pSTAT levels.

Fibroblasts are predominantly known for their pivotal role in fibrosis in scleroderma; this study changes the narrative of fibroblasts in the pathogenic processes of SSc by demonstrating that crosstalk between fibroblasts and keratinocytes can induce a pro-inflammatory response. Thus, this data suggests for the first time that fibroblasts are no longer the target of the dysregulated immune signalling commonly observed in early disease scleroderma patients, but instead a central source and driver of IFN signalling, which further highlights the interplay between hyper activated IFN signalling and fibrosis in SSc pathogenesis.

5. Investigating the Mechanism in which Scleroderma Fibroblast Exosomes induce the Interferon Response in Human Keratinocytes (HaCats).

5.1. Introduction

Fibroblasts are known to be key mediators of fibrosis and are commonly associated to be the targets of immune activated cells (Fett et al., 2013, Gilbane et al., 2013), which further drive the fibrotic phenotype associated with SSc pathogenesis (Ah Kioon et al., 2018, Brkic et al., 2016, Farina et al., 2010). As previously described, SSc patients have an upregulation of IFN-related genes in their blood and skin, which is observed before skin fibrosis (Brkic et al., 2016, Assassi et al., 2010). Likewise, detection of an IFN signature, autoantibodies and skin fibrosis are early clinical features of the disease (Skaug et al., 2020). Further, chemokine levels are positively correlated with the severity of skin involvement in SSc patients (Liu et al., 2013). Likewise, early diffuse scleroderma patients display an increase in skin thickening, which is positively associated with internal organ involvement and increased mortality (Khanna 2017). However, the role of dysregulated immune-activation and its contribution to the pro-fibrotic phenotype is poorly understood in scleroderma. Since, we observed that SSc fibroblasts release exosomes, which drive immune activation in keratinocytes; fibroblasts could hold a pivotal role acting as an immune driver in the skin and thus, fibroblasts are central to the pro-fibrotic and dysregulated immunopathogenesis associated with early disease progression in SSc patients.

There are no current cures for scleroderma, only therapeutics which can alleviate and manage symptoms, thus the disease is associated in high mortality

(Bairkdar et al., 2021). However, recent trials in early ILD SSc patients with a tyrosine protein kinase inhibitor (Nintedanib) and Tocilizumab (IL-6 receptor inhibitor) have shown a decline in lung deterioration, compared to the placebo groups (Distler et al., 2019, Denton et al., 2022, Khanna et al., 2018, Khanna et al., 2022). Likewise, a recent anti-IFNAR monoclonal antibody (Anifrolumab) trial illustrated that Anifrolumab significantly reduced the IFN signature of whole blood and skin of SSc patients, as well as a reduction in TGFβ signalling (Goldberg et al., 2014), which is commonly associated with fibrosis in SSc pathogenesis (Chakraborty et al., 2017, Pedroza et al., 2016, Pedroza et al., 2018). It is essential to develop a theraputic, which targets early disease in SSc patients to reduce the IFN signature and skin fibrosis and thus, prevent disease progression and mortality.

We observed that SSc fibroblast-derived exosomes induce IFN signalling in keratinocytes. Wermuth et al., (2017) showed that SSc serum exosomes induced a profibrotic phenotype in healthy dermal fibroblasts. Further, Bhandari et al., (2022) illustrated that SSc fibroblast exosomes can induce pro-inflammatory cytokines in macrophages, which can further prolong the profibrotic phenotype in SSc fibroblasts. Subsequently, this data illustrates that SSc fibroblast-derived exosomes have a role in driving fibrosis and immune activation in recipient cells, thus offers the rare opportunity of a single therapeutic target which may act on multiple levels to reduce disease progression. The mechanism in which SSc fibroblast exosomes induce pro-fibrotic and immune activation is unknown. Thus, determination of the mechanism in which SSc fibroblast-derived exosomes induce IFN signalling in keratinocytes was investigated.

Pattern recognition receptor TLR3 has been implicated in SSc pathogenesis, where Agarwal et al., (2011) found upregulated TLR3 expression in the dermis of SSc patients skin. Likewise, chronic stimulation with a TLR3 ligand led to inflammation and dermal fibrosis in a bleomycin mouse model. Further, serum exosomes from SLE patients induced IFNα and pro-inflammatory cytokines in PBMCs, which was prevented after TLR inhibition (Lee et al., 2016). In addition, the RIG-I/MDA5-MAVS signalling cascade has also been implicated in SLE, where Shao et al., (2016) observed that one third of SLE patients had MAVs aggregation and the presence of MAVs aggregates positively correlated with IFN signature. Moreover, CAF-derived exosomes have been shown to induce antiviral signalling, through RIG-I (Nabet et al., 2017, Cui et al., 2022). Overall, dysregulated activation of PRRs have been associated with cancer, SLE and SSc, where exosomes have acted to induce innate immune signalling. Thus, PRRs and the antiviral cascade is an appealing target to investigate as the potential mechanism of dysregulated interferon signalling induced by SSc dermal fibroblast secreted exosomes on keratinocytes.

5.2. Results

5.2.1. Short-hairpin lentivirus knockdown of RIG-I does not prevent induction of ISGs and pSTAT1 by scleroderma fibroblast exosomes

CAF-derived exosomes have been shown to induce innate immune signalling through the PRR RIG-I I (Nabet et al., 2017, Cui et al., 2022). To investigate if SSc exosomes use a similar mechanism, RIG-I was knocked down using a short hairpin lentivirus, which targeted RIG-I (shRIG-I). In addition, a short hairpin

lentivirus containing a scramble RNA was created as a positive control (shScramble). Post selection, shRIG-I HaCats had a 76% reduction of RIG-I gene expression, as well as a 99% knockdown in RIG-I protein expression, when compared to shScramble HaCats (Figure 5.1.A). To investigate the effects of a RIG-I knockdown through the innate immune cascade, 10ng/mL of RIG-I agonist was added to both shRIG-I and shScramble HaCats for 48 hours. The RIG-I agonist induced RIG-I, pSTAT1 and STAT1 protein expression in both shRIG-I and shScramble HaCats, where interestingly pSTAT1 expression was greater in shRIG-I stimulated cells, after 48 hours. As expected, RIG-I agonist induced pIRF3 in shScramble HaCats, compared to shRIG-I, and both IRF3 and β-actin levels remained consistent (Figure 5.1.B).

Likewise, mRNA transcript expression of type I IFN-related genes in RIG-I agonist treated shRIG-I and shScramble HaCats illustrated that chemokines (CXCL10 and CXCL11), which are genes directly downstream of RIG-I, were partially increased in shScramble HaCats, compared to shRIG-I. Likewise, treatment with RIG-I agonist induced RIG-I gene expression in shRIG-I and shScramble HaCats, however RIG-I expression was significantly downregulated in shRIG-I (0.42-fold, $p<0.05$), compared to shScramble.

MX1, OAS, IFIT1 and STAT1, which are ISGs associated with type I IFN signalling, were upregulated in shRIG-I HaCats treated with RIG-I agonist, compared to shScramble, by 1.77-fold, 2-fold, 1.89-fold and 1.74-fold, respectively (Figure 5.1.C). Although these results aren't significant; there is a clear trend that induction of RIG-I, post knockdown, leads to an increase in the

expression of type I IFN related ISGs, which is further supported by a stronger induction in pSTAT1, observed in Figure 5.1.B.

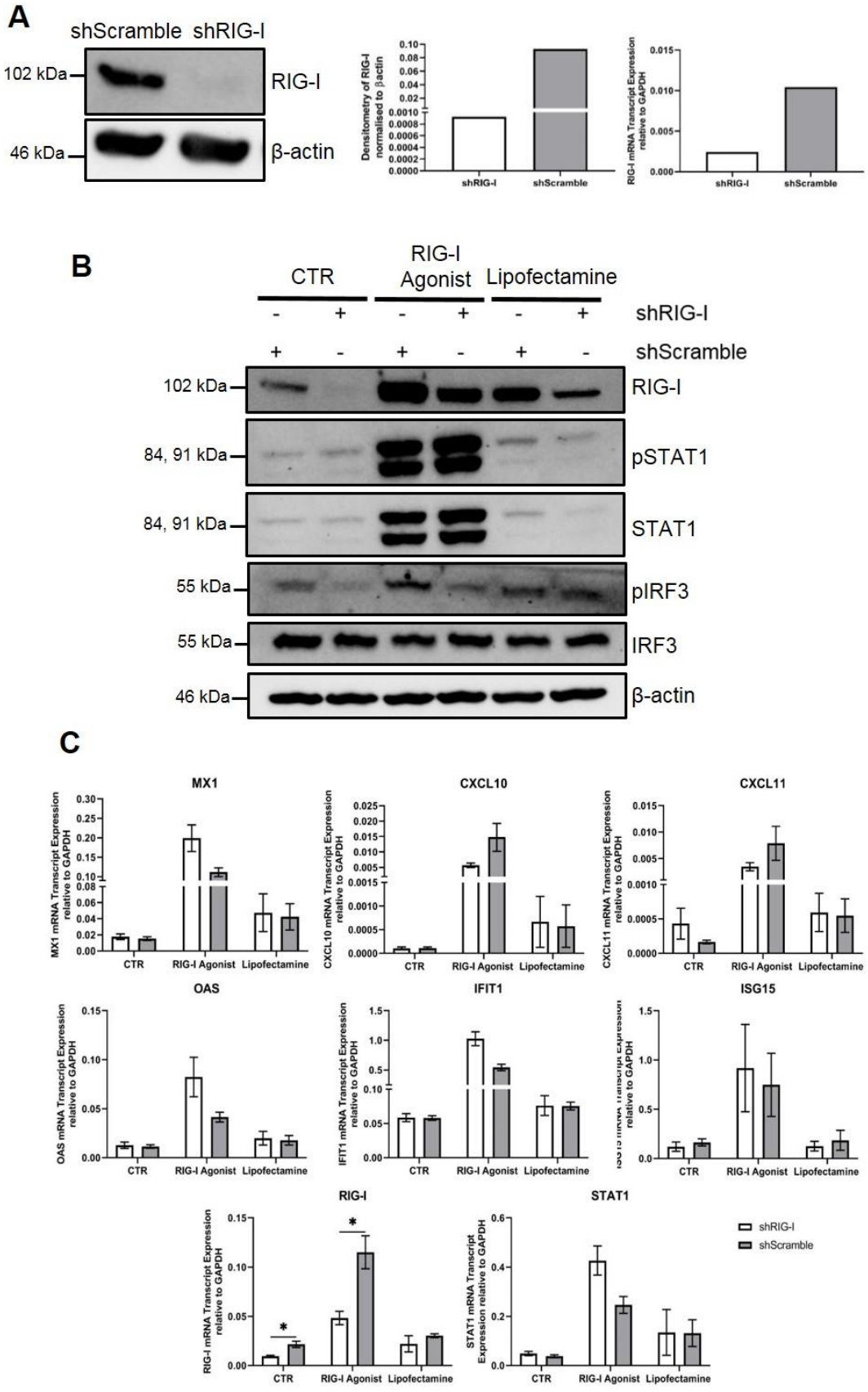

Figure 5.1. Activation of shRIG-I, by RIG-I agonist, shows positive feedback signalling through RIG-I.

HaCats were transduced with a lentivirus against RIG-I, as well as a scramble control, and then selected using puromycin. RNA and Protein was then collected from the selected cells. A) Immunoblotting and mRNA expression of RIG-I, normalised to β-actin and GAPDH respectively, post selection but prior to experimental set up to show successful RIG-I knockdown (n=1). shRIG-I and shScramble HaCats were stimulated with 10ng/mL of RIG-I agonist and Lipofectamine2000 in serum-starved DMEM, for 48 hours. B) Representative immunoblots (n=3) for RIG-I, pSTAT1, STAT1, pIRF3 and IRF3, as well as β-actin which was used as a loading control. C) mRNA transcript expression of interferon-related genes, normalised to housing keeping genes; GAPDH. Data represents means ± SE from three biological repeats. Data was checked for normality and then statistically analysed using a two-tailed unpaired Mann Whitney T-test assuming equal variance. *p<0.05.

Treatment of shRIG-I and shScramble HaCats with healthy and SSc exosomes displayed no statistically significant changes in protein expression (Figure 5.2.A-B). SSc exosomes induced pSTAT1 in shScramble HaCats by 1.17-fold (NS), when compared to healthy. Further, RIG-I protein expression was significantly greater in shScramble HaCats (5.6-fold, p<0.0001), compared to shRIG-I, irrespective of exosome treatment (Figure 5.2.B). Likewise, exosome treatment reduced pIRF3 in both shRIG-I and shScramble HaCats, when compared to the control (Figure 5.2.A).

Interestingly, SSc exosomes induced gene expression in shRIG-I HaCats of MX1, (1.33-fold), CXCL10 (1.41-fold), CXCL11 (1.31-fold) and OAS (1.53-fold), when compared to healthy exosomes (NS). Further, SSc exosomes reduced gene expression of ISGs; IFIT (0.889-fold, p<0.05), CXCL10 (0.61-fold, NS), ISG15 (0.547-fold, NS) and CXCL11 (0.625-fold, NS) in shScramble HaCats, compared to healthy exosomes. Healthy and SSc exosome treatments did not affect the gene expression of RIG-I, which was significantly reduced by 0.48-fold (P<0.01) in shRIG-I HaCats, compared to shScramble (Figure 5.2.C).

Although most results are deemed statistically insignificant, there is a general trend that SSc exosomes are inducing ISGs, in a similar fashion to the RIG-I agonist at 48 hours, where knockdown of RIG-I leads to the induction of type 1 IFN related genes. However, it is plausible that treatment with a lentivirus alone could cause upregulation of antiviral signalling (Kenworthy et al., 2009).

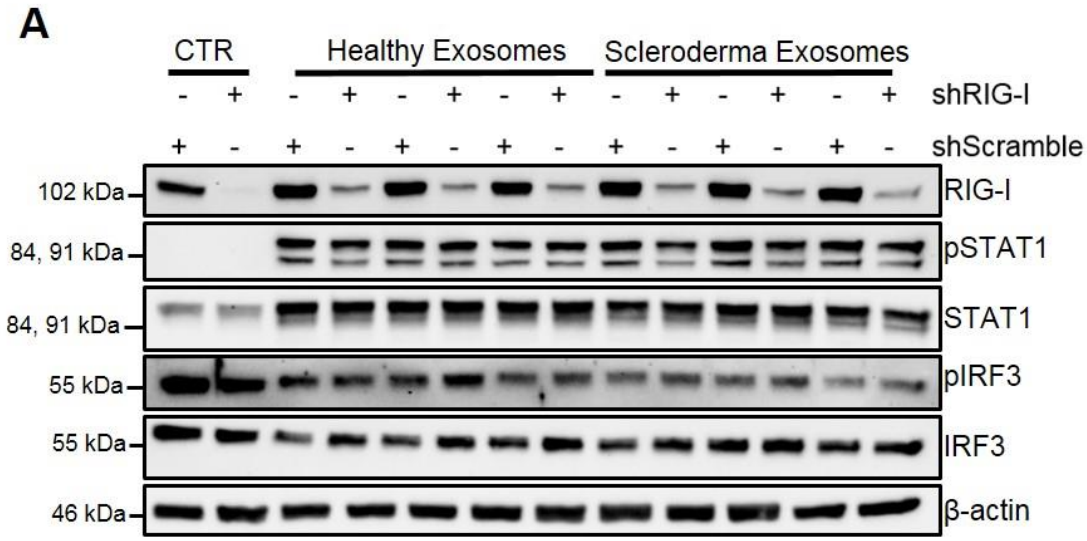

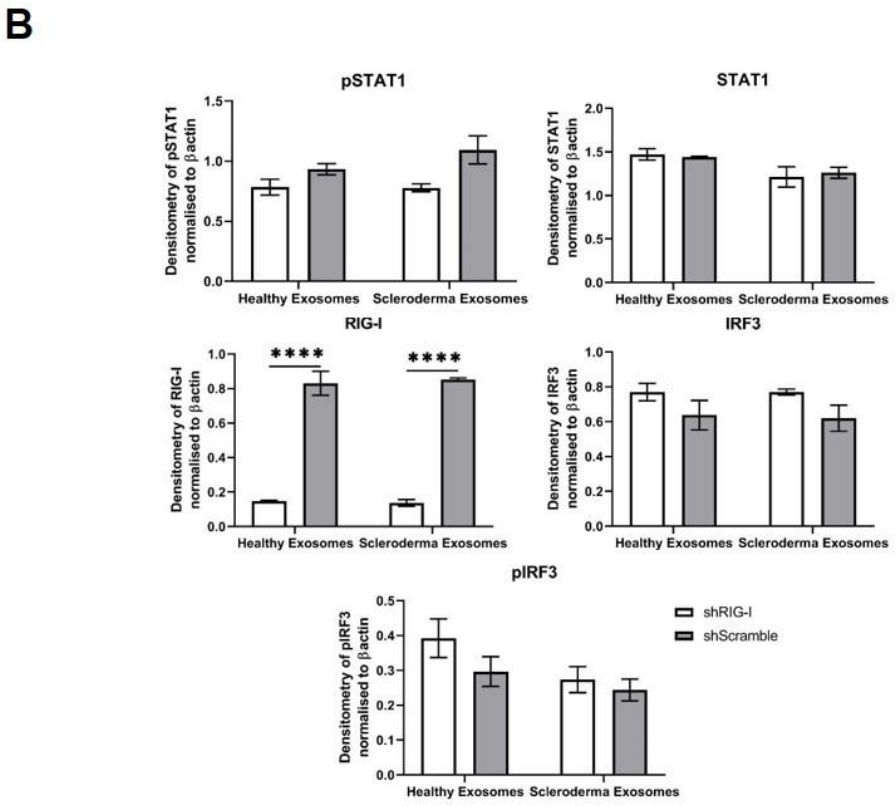

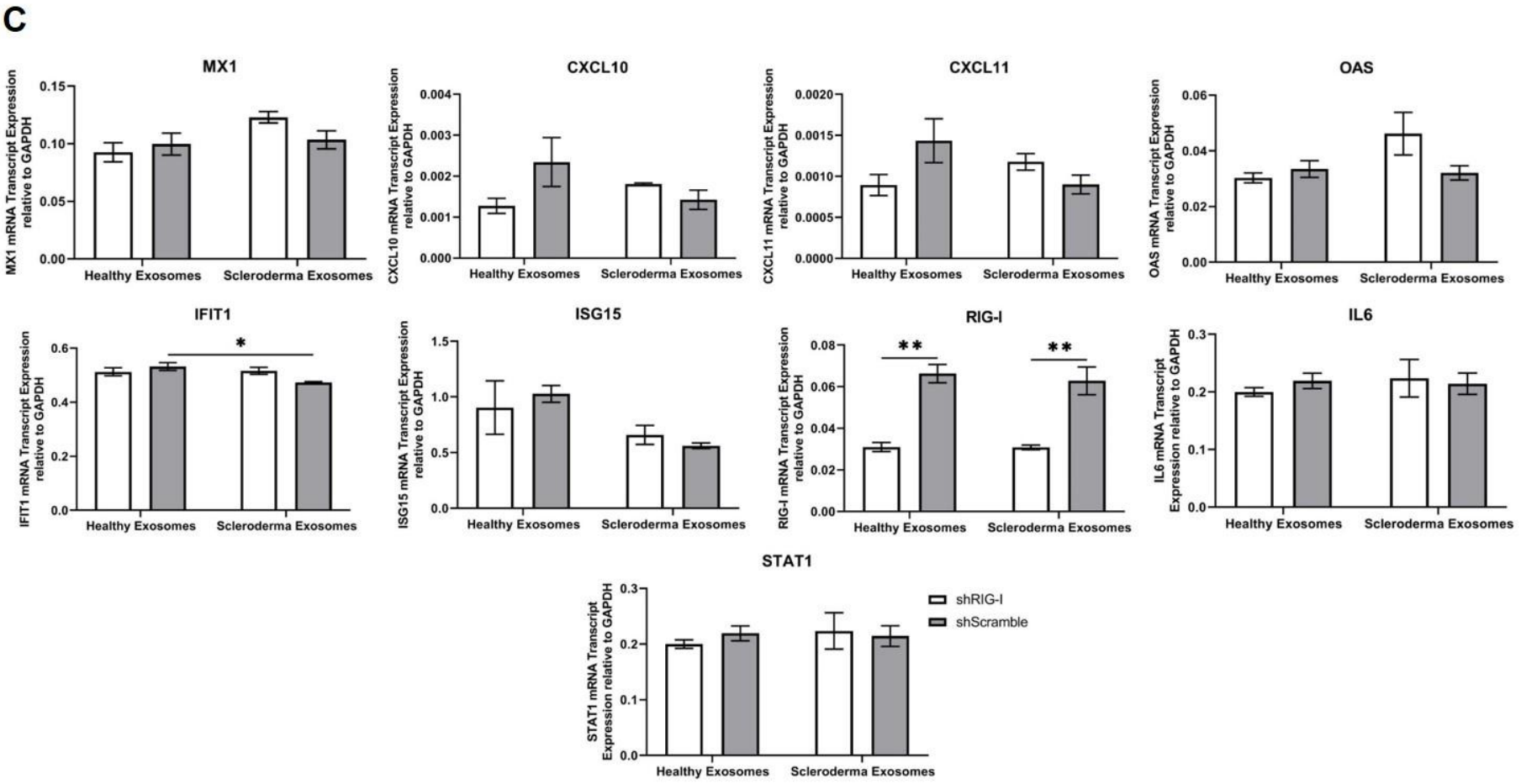
C
MX1
MX1 mRNA Transcript Expression relative to GAPDH
0.15
0.10
0.05
0.00
Healthy Exosomes
Scleroderma Exosomes
CXCL10
CXCL10 mRNA Transcript Expression relative to GAPDH
0.004
0.003
0.002
0.001
0.000
Healthy Exosomes
Scleroderma Exosomes
CXCL11
CXCL11 mRNA Transcript Expression relative to GAPDH
0.0020
0.0015
0.0010
0.0005
0.0000
Healthy Exosomes
Scleroderma Exosomes
OAS
OAS mRNA Transcript Expression relative to GAPDH
0.06
0.04
0.02
0.00
Healthy Exosomes
Scleroderma Exosomes
IFIT1
IFIT1 mRNA Transcript Expression relative to GAPDH
*
0.6
0.4
0.2
0.0
Healthy Exosomes
Scleroderma Exosomes
ISG15
ISG15 mRNA Transcript Expression relative to GAPDH
1.5
1.0
0.5
0.0
Healthy Exosomes
Scleroderma Exosomes
RIG-I
RIG-I mRNA Transcript Expression relative to GAPDH
**
**
0.08
0.06
0.04
0.02
0.00
Healthy Exosomes
Scleroderma Exosomes
IL6
IL6 mRNA Transcript Expression relative to GAPDH
0.3
0.2
0.1
0.0
Healthy Exosomes
Scleroderma Exosomes
STAT1
STAT1 mRNA Transcript Expression relative to GAPDH
0.3
0.2
0.1
0.0
Healthy Exosomes
Scleroderma Exosomes
shRIG-I
shScramble

Figure 5.2. Induction of ISGs and pSTAT1 by scleroderma exosomes is independent of RIG-I.

Healthy and scleroderma fibroblast exosomes were added to shRIG-I and shScramble HaCats for 48 hours to investigate the role of RIG-I, in exosome-induced interferon. A) Immunoblots for RIG-I, pSTAT1, STAT1, pIRF3 and IRF3, as well as β-actin which was used as a loading control. Healthy exosome (n=3), Scleroderma exosome (n=3) B) Bar charts illustrating densitometry analysis of western blots shown in B, calculated using Image Lab. C) mRNA transcript expression of interferon-related genes, normalised to housing keeping genes; GAPDH. Data represents means ± SE from three biological repeats (Healthy Exosomes), and five biological repeats (Scleroderma Exosomes). Data was checked for normality and then statistically analysed by a multiple comparison two-way ANOVA, normalised to Tukey. *p<0.05. **p<0.01.

5.2.2. GSK8612 is a more potent inhibitor of Tank-binding Kinase 1 (TBK1), when compared to Amlexanox

TBK1 is an enzyme with kinase activity that holds a pivotal role in innate immune antiviral signalling. TBK1 is directly downstream of most PRR, such as cGASSTING, RIG-I and Toll-like Receptors, and activates transcription factors through phosphorylation, which promote the expression of type I IFN and chemokines (Gui et al., 2019, Li et al., 2014, Behzadi et al., 2021). Thus, we aimed to inhibit TBK1 using small molecule inhibitors, Amlexanox and GSK8612, to block the activation of innate immune signalling, post recognition receptor activation and before ISG expression. Amlexanox is a clinical drug, known to inhibit TBK1, commonly used to treat canker sores. However, in the US this has been discontinued due to its non-specificity (Dosanjh et al., 2020). Further, GSK8612 is a new highly selective potent inhibitor of TBK1, which has been developed for clinical research (Thomson et al., 2019).

Firstly, we compared the effectiveness of Amlexanox and GSK8612, by creating a dose-range response of each inhibitor on HaCats stimulated with 10ng/mL of RIG-I agonist for 6 and 48 hours and investigated the mRNA expression of type

I IFN related genes. Dose response analysis illustrated that GSK8612 and Amlexanox both reduced gene expression of ISGs; MX1, OAS, IFIT, ISG15 and STAT1 by similar degrees, at both 6 and 48 hours (Figure 5.3.A). Further, GSK8612 decreased CXCL10 and CXCL11 induced gene expression quicker and at reduced doses, compared to Amlexanox. Surprisingly, 50μM of Amlexanox induced gene expression of CXCL10 and CXCL11 after 6 hours of RIG-I agonist treatment (Figure 5.3.A). In addition, 200μM of Amlexanox was cytotoxic to cells and led to a reduction in cell viability (data not shown), and thus 150μM of Amlexanox was used in further experiments.

HaCats were treated with 10μM GSK8612 and 150μM Amlexanox and then stimulated with 10 ng/mL of RIG-I agonist for 6 and 48 hours to investigate changes in protein expression. After 6 hours, GSK8612 treatment reduced the phosphorylation of STAT1 and pIRF3 when compared to Amlexanox, which displayed similar expression levels to RIG-I agonist stimulated HaCats. Similarly at 48 hours, GSK8612 treatment reduced RIG-I, STAT1 and pIRF3 in RIG-I agonist HaCats, when compared to Amlexanox. Likewise, GSK8612 treatment in basal conditions, completely reduced pIRF3. IRF3 and β-actin levels were consistent across all treatments (Figure 5.3.B). Since, TBK1 is directly upstream of IRF3, and can somewhat influence NF-κB signalling, we investigated the phosphorylation and degradation of IKKαβ. After 6 hours of treatment with RIG-I agonist, all conditions displayed pIKKα/β and consistent IKKα/β expression. Interestingly, after 48 hours GSK8612 reduced IKKα/β expression in basal conditions, and after stimulation. This suggests blocking of TBK1, may induce IKK signalling complex through NF-Kb, indicated by degradation of IKKα/β at basal levels (Figure 5.3.B).

Since, GSK8612 reduced pSTAT1 and pIRF3 more sufficiently than Amlexanox at both time periods, we decided to investigate a GSK8612 dose response of type I IFN-related protein expression in RIG-I agonist stimulated HaCats. After 6 hours, 7.5-10μM of GSK8612 successfully reduced protein expression of pIRF3 and pSTAT1, compared to RIG-I agonist stimulated HaCats (Figure 5.3.C). Considering, 10μM GSK8612 reduced pSTAT1 protein expression considerably more than 7.5μM and 10μM GSK8612 is recommended in the literature (Thomson et al., 2019), HaCats were serum-starved and inhibited with 10μM GSK8612 prior to exosome addition.

A

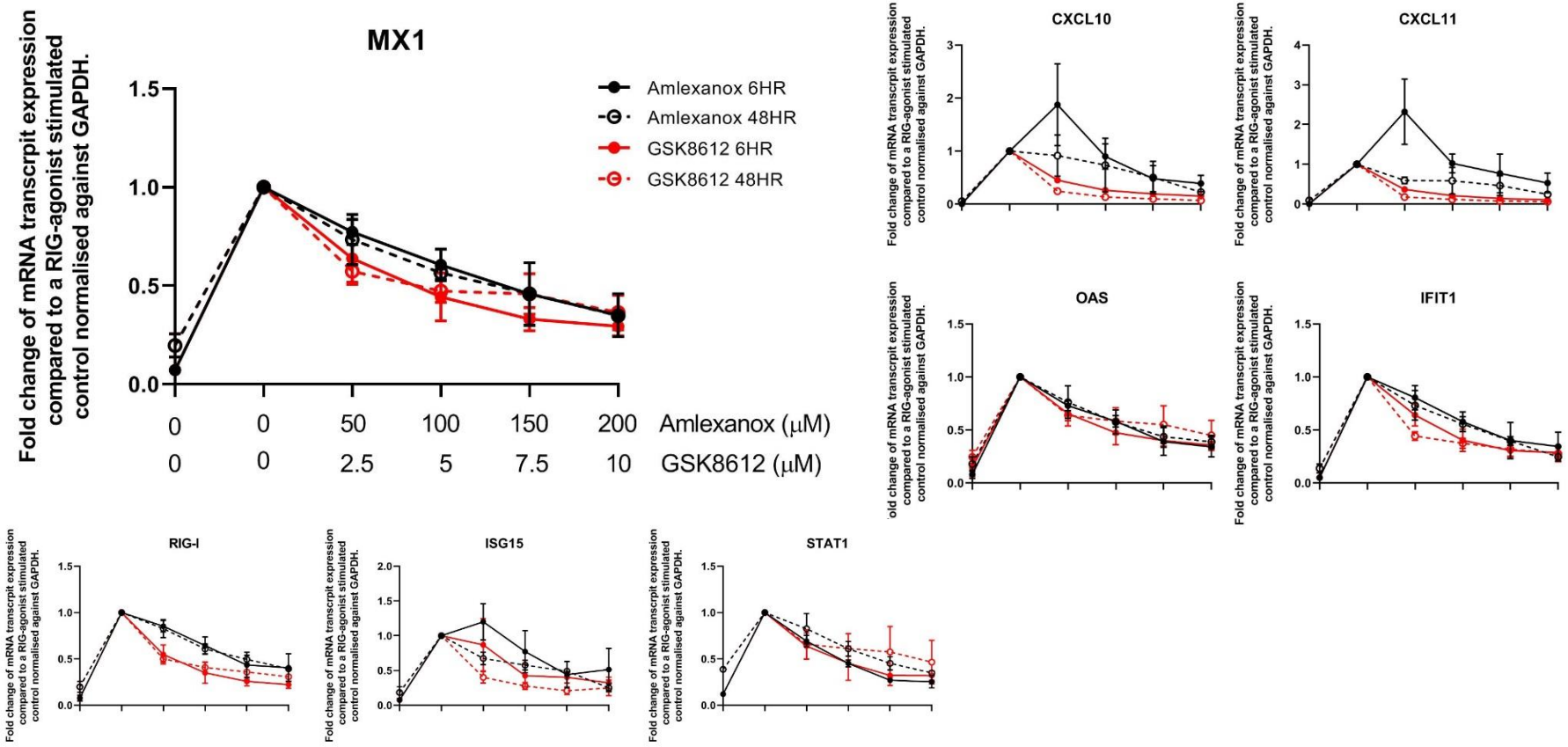
MX1
Fold change of mRNA transcrpit expression compared to a RIG-agonist stimulated control normalised against GAPDH.
Amlexanox 6HR
Amlexanox 48HR
GSK8612 6HR
GSK8612 48HR
0 0 50 100 150 200 Amlexanox (μM)
0 0 2.5 5 7.5 10 GSK8612 (μM)
CXCL10
CXCL11
OAS
IFIT1
RIG-I
ISG15
STAT1

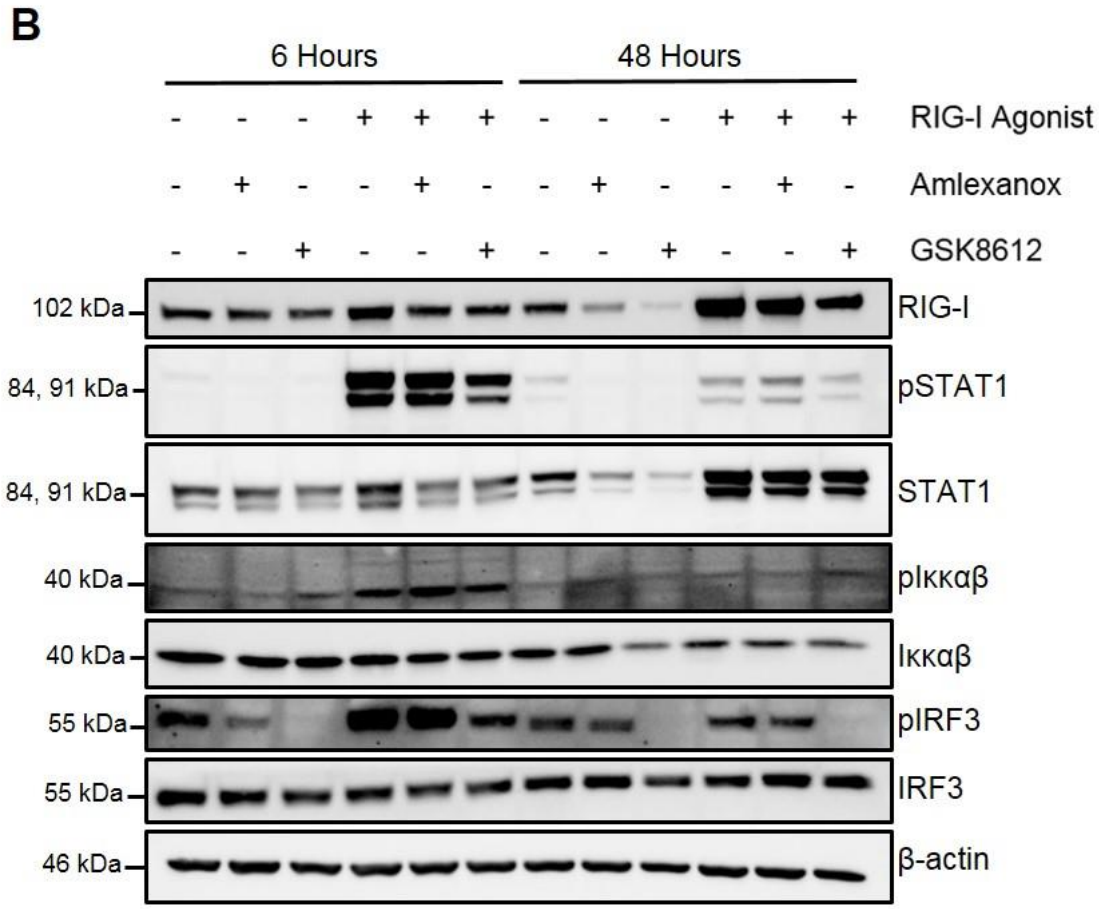
B
6 Hours
48 Hours
RIG-I Agonist
Amlexanox
GSK8612
102 kDa
RIG-I
84, 91 kDa
pSTAT1
84, 91 kDa
STAT1
40 kDa
pIκκαβ
40 kDa
Iκκαβ
55 kDa
pIRF3
55 kDa
IRF3
46 kDa
β-actin

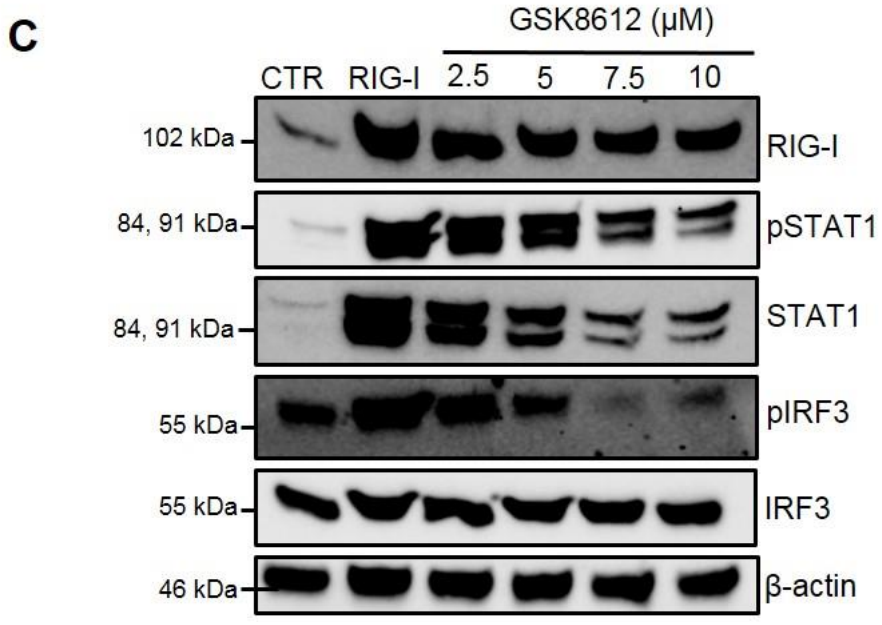
C
GSK8612 (μM)
CTR
RIG-I
2.5
5
7.5
10
102 kDa
RIG-I
84, 91 kDa
pSTAT1
84, 91 kDa
STAT1
55 kDa
pIRF3
55 kDa
IRF3
46 kDa
β-actin

Figure 5.3. Dose-response analysis of HaCats stimulated with RIG-I agonist and then inhibited by Tank-binding Kinase 1 inhibitor; GSK8612 and Amlexanox.

HaCats were treated with inhibitors GSK8612 and Amlexanox, solubilised in DMSO, 1 hour before stimulation with 10ng/mL RIG-I agonist and Lipofectamine2000. A) Dose-response curve, which shows the fold change reduction of mRNA transcript expression of interferon-related genes when stimulated with different concentrations of GSK8612 (0 – 10 μM) and Amlexanox (0 – 200 μM) at 6 and 48 hours. Figure legend of axis of enlarged graph (MX1) is representative to all graphs. Data represents means ± SE from three biological repeats. B) Immunoblotting for HaCats treated with 10 μM GSK8612 and 150 μM Amlexanox and then stimulated with 10 ng/mL RIG-I agonist at 6 and 48 hours. Blot is representative of three biological repeats. C) Immunoblotting against interferon-related proteins for HaCats stimulated with 10 ng/mL RIG-I agonist, which illustrates a dose-response to different concentrations of GSK8612 (0 – 10 μM) after 6 hours, where immunoblots demonstrate representative images from three biological repeats.

5.2.3. Inhibition of Tank-binding Kinase 1 (TBK1), using GSK8612, reduces scleroderma fibroblast-derived exosome induction of pSTAT1 and ISG's in HaCats

To evaluate the role of TBK in SSc exosome induced IFN signalling in HaCats, 10μM of GSK8612 was added to serum-starved HaCats for 1 hour before healthy and scleroderma exosome-incubation. GSK8612 reduced the basal expression of all proteins, apart from IRF3 and β-actin, where pIRF3 ($p<0.001$) and pSTAT1 expression was below detection (Figure 5.4.A). Further, SSc exosomes induced the protein expression of pSTAT1 by 2.02-fold ($p<0.05$) and RIG-I by 1.32-fold ($p<0.001$) in control conditions, when compared to healthy exosomes. The inhibition of TBK, by GSK8612, removed the induction of pSTAT1 by SSc exosomes. However, SSc exosomes induced protein expression of RIG-I (2.65-fold, NS) and STAT1 (2.31-fold, $p<0.001$) in HaCats treated with GSK8612, when compared to healthy exosomes (Figure 5.4.B). Likewise, SSc exosomes induced ISG15 protein expression by 1.30-fold, were immunoblotting investigating ISG15 protein-conjugates highlights an increase in SSc exosome treated HaCats in control conditions (Figure 5.4.C).

Moreover, GSK8612 significantly downregulated the gene expression of all ISGs illustrated in Figure 5.4.D, irrespective of exosome treatment. SSc exosomes significantly induced gene expression of CXCL10 (1.83-fold, $p<0.01$), CXCL11 (1.84-fold, $p<0.01$), ISG15 (2.46-fold, $p<0.0001$) and RIG-I (1.32-fold, $p<0.01$) in CTR HaCats, when compared to healthy exosomes. SSc exosomes did not significantly induce any ISGs in GSK8612 treated HaCats, when comparing to healthy exosomes. However, SSc exosomes did induce CXCL11 (1.42-fold, NS) and ISG15 (3.20-fold, NS) in GSK8612 treated HaCats, compared to healthy exosomes. Collectively, the inhibition of TBK prevented the induction of gene expression of ISGs and protein expression of pSTAT1 by SSc fibroblast-derived exosomes, and thus, SSc exosomes require TBK to be fully functional to induce IFN signalling in HaCats. Likewise, SSc exosomes significantly alleviated the downregulation of protein expression of STAT1 and RIG-I by TBK inhibition.

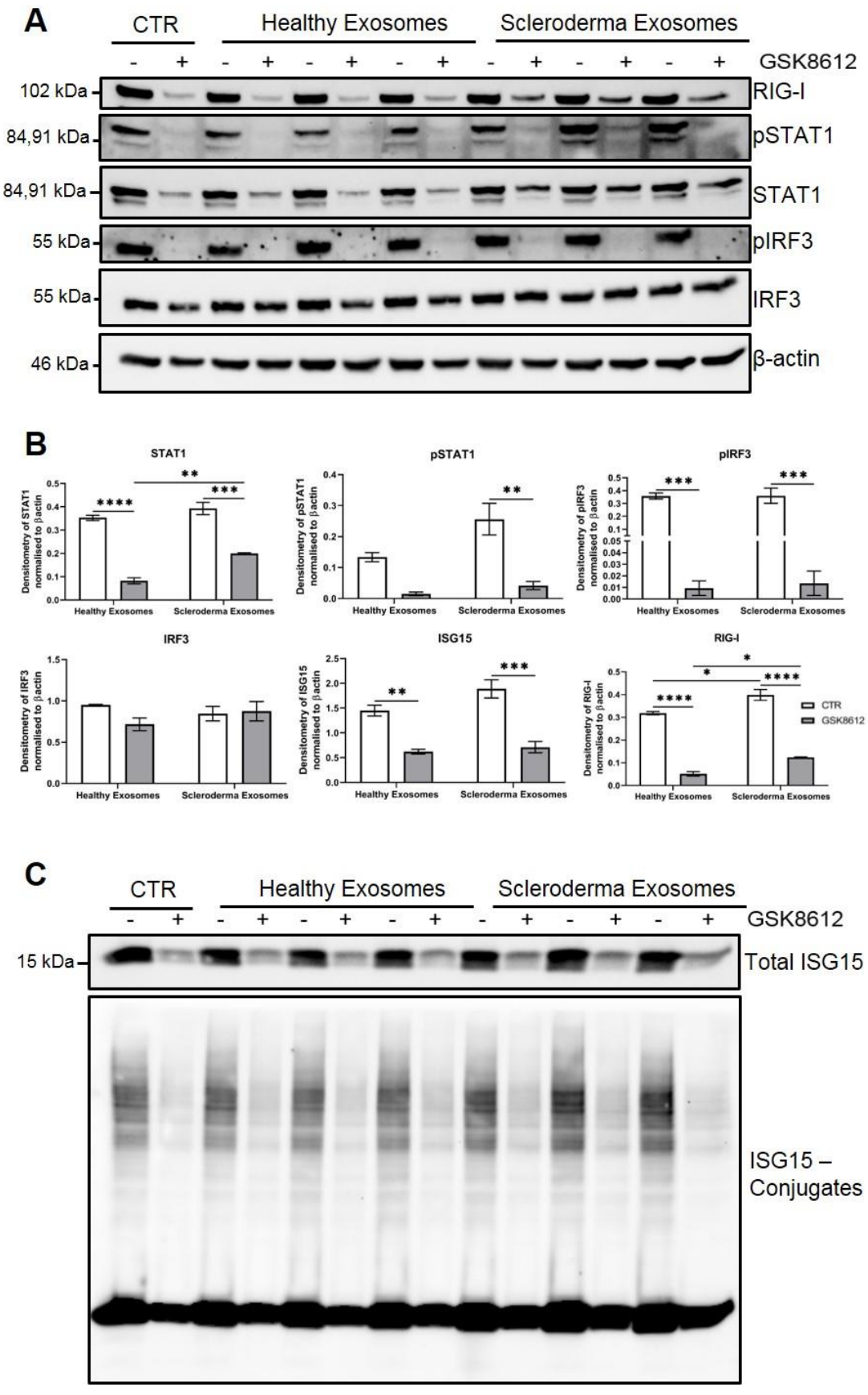
A
CTR
Healthy Exosomes
Scleroderma Exosomes
GSK8612
102 kDa
RIG-I
84,91 kDa
pSTAT1
84,91 kDa
STAT1
55 kDa
pIRF3
55 kDa
IRF3
46 kDa
β-actin
B
STAT1
pSTAT1
pIRF3
IRF3
ISG15
RIG-I
Densitometry of STAT1 normalised to βactin
Densitometry of pSTAT1 normalised to βactin
Densitometry of pIRF3 normalised to βactin
Densitometry of IRF3 normalised to βactin
Densitometry of ISG15 normalised to βactin
Densitometry of RIG-I normalised to βactin
Healthy Exosomes
Scleroderma Exosomes
CTR
GSK8612
C
CTR
Healthy Exosomes
Scleroderma Exosomes
GSK8612
15 kDa
Total ISG15
ISG15 – Conjugates

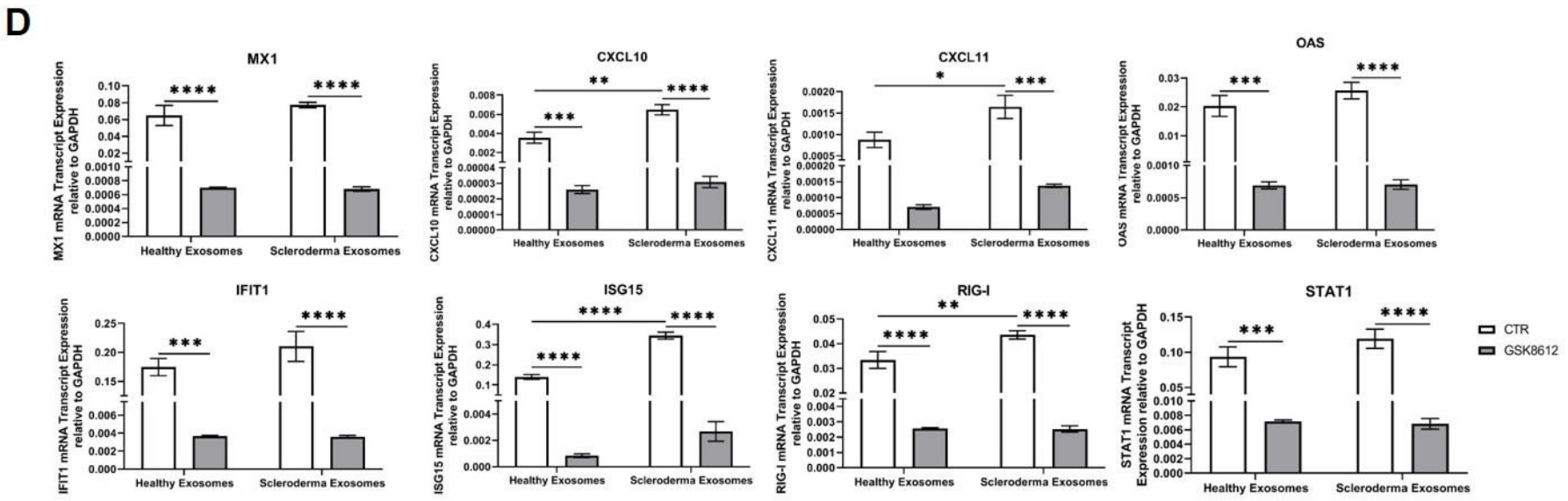

Figure 5.4. Effect of Tank-binding Kinase 1 (TBK1) inhibitor GSK8612, on fibroblast-derived exosome induction of pSTAT1 and ISG's in HaCats.

HaCats were serum-starved and treated with 10 µM GSK8612, solubilised in DMSO, 1 hour before stimulation with Healthy and Scleroderma Exosomes. Control (CTR) was treated with 0.1% DMSO, equivalent to GSK8612. A) Immunoblots for RIG-I, pSTAT1, STAT1, pIRF3 and IRF3, as well as β-actin, which was used as a loading control. Immunoblotting of ISG15 illustrates Total ISG15 (30 second exposure) and ISG15 linked conjugates (2 minute exposure). B) Bar charts illustrating densitometry analysis of western blots shown in A, calculated using Image Lab. Data represents means ± SE from three biological repeats. C) mRNA transcript expression of interferon-related genes, normalised by housing keeping gene GAPDH. Data represents means ± SE from three biological repeats (Healthy Exosomes), and four biological repeats (Scleroderma Exosomes). Statistical analysis by a multiple comparison two-way ANOVA, normalised to Tukey. *p<0.05. **p<0.01. ***p<0.001. ****p<0.0001.

5.2.4. Inhibition of JAK1/3 using Tofacitinib, reduces scleroderma fibroblast-derived exosome induction of pSTAT1 and ISG's in HaCats

Since scleroderma fibroblast exosomes induce pSTAT1 and interferon-related genes in HaCats, we hypothesised that this activation could be through the IFNAR. Thus, to target the phosphorylation of STAT1 we inhibited JAK, using the small molecule drug inhibitor, Tofacitinib (TOF). Tofacitinib is a drug used in the clinic to treat rheumatology based autoimmune diseases, such as RA, which inhibits the kinase activity of JAK1/3 (Dhillon., S, 2017). Indeed, JAK1 is directly downstream of the IFN receptor and is therefore an ideal target to investigate IFNAR signalling (Quelle et al., 1995). However, JAKs are also essential for other receptor cytokine signalling cascades, such as IL-6. Since, IL-6 is also a contributor to SSc pathogenesis, we investigated the effect of Tofacitinib on the IL6-receptor downstream transcription factor STAT3 (Cardoneanu et al., 2022).

HaCats were serum-starved, treated with 20μM Tofacitinib and then stimulated with 10ng/mL RIG-I agonist for 48 hours, as well as 20ng/mL of IFNα for 1 hour, to investigate the effectiveness of Tofacitinib as a JAK inhibitor. Tofacitinib reduced basal protein expression of RIG-I, pSTAT1, STAT1, pSTAT3 (Tyr705) and STAT3. After stimulation with RIG-I agonist and IFNα, TOF reduced pSTAT1 and pSTAT3 protein expression below detectable expression levels (Figure 5.5.A). Further, TOF significantly reduced basal ISG expression levels of MX1 (0.087-fold, $p<0.01$), CXCL10 (0.12-fold, $p<0.001$), OAS (0.234-fold, $p<0.01$) and IFIT1 (0.358-fold, $p<0.05$). TOF treatment reduced ISG expression in HaCats stimulated with RIG-I agonist of: RIG-I, ISG15, IFIT1, CXCL10 and CXCL11

(n=2). Whereas TOF treatment did not affect the gene expression of MX1, STAT1 and OAS in RIG-I agonist stimulated HaCats, compared to CTR (n=2). Likewise, IFN treatment induced ISG expression, which was significantly reduced by TOF for ISGs; MX1 (0.038-fold, $p<0.001$), CXCL10 (0.0104-fold, $p<0.001$), OAS (0.16-fold, $p<0.0001$), IFIT1 (0.12-fold, $p<0.01$), ISG15 (0.266-fold, $p<0.001$), RIG-I (0.363-fold, $p<0.001$) and STAT1 (0.085-fold, $p<0.0001$). However, CXCL11 expression did not change in IFN-treated or CTR-starved HaCats, when TOF-treated, compared to CTR. (Figure 5.5B).

Collectively, TOF can inhibit gene expression of ISGs and phosphorylation of STATs, more specifically for IFN-induced ISGs compared to RIGI-agonist induced ISGs. Thus, to determine if JAK-STAT signalling is required for SSc exosome-induced IFN signalling in HaCats; healthy and SSc exosomes were added to serum-starved HaCats, pre-treated with 20μM Tofacitinib. TOF significantly reduced protein expression of RIG-I and STAT1 ($p<0.01$), irrespective of exosome treatment. Likewise, TOF reduced protein expression of pSTAT1 and pSTAT3 (Tyr705) below detection levels (Figure 5.5.C). SSc exosomes significantly induced pSTAT1 (1.66-fold, $p<0.05$), STAT3 (2.22-fold, $p<0.05$) and pSTAT3 (Tyr705) (4.41-fold, $p<0.0001$), in control conditions, compared to healthy exosomes. Further, SSc exosomes induced pSTAT3 (Ser727) by 2.22-fold (NS) in CTR conditions and 1.60-fold (NS) in TOF-treated HaCats (Figure 5.5.D).

Additionally, TOF significantly reduced the gene expression of ISGs; MX1, OAS, IFIT1, RIG-I and STAT1 ($p<0.05$). SSc exosomes significantly induced gene expression of MX1 (1.6-fold, $p<0.05$), OAS (1.66-fold, $p<0.05$) and IFIT1 (1.46-

fold, $p<0.01$), in CTR HaCats when compared to healthy exosomes, which was alleviated by TOF-treatment. SSc exosomes induced CXCL11 (1.59-fold, NS) and ISG15 (1.15-fold, NS) in CTR HaCats, when compared to healthy exosomes. Interestingly, TOF-treatment only significantly reduced gene expression of CXCL11 ($p<0.01$) and ISG15 ($p<0.0001$) in HaCats, treated with SSc exosomes. Overall, TOF alleviated the induction of ISGs and pSTAT1 by SSc exosomes in HaCats, and thus signalling through JAK-STAT is important for the mechanism in which exosomes exert their effects.

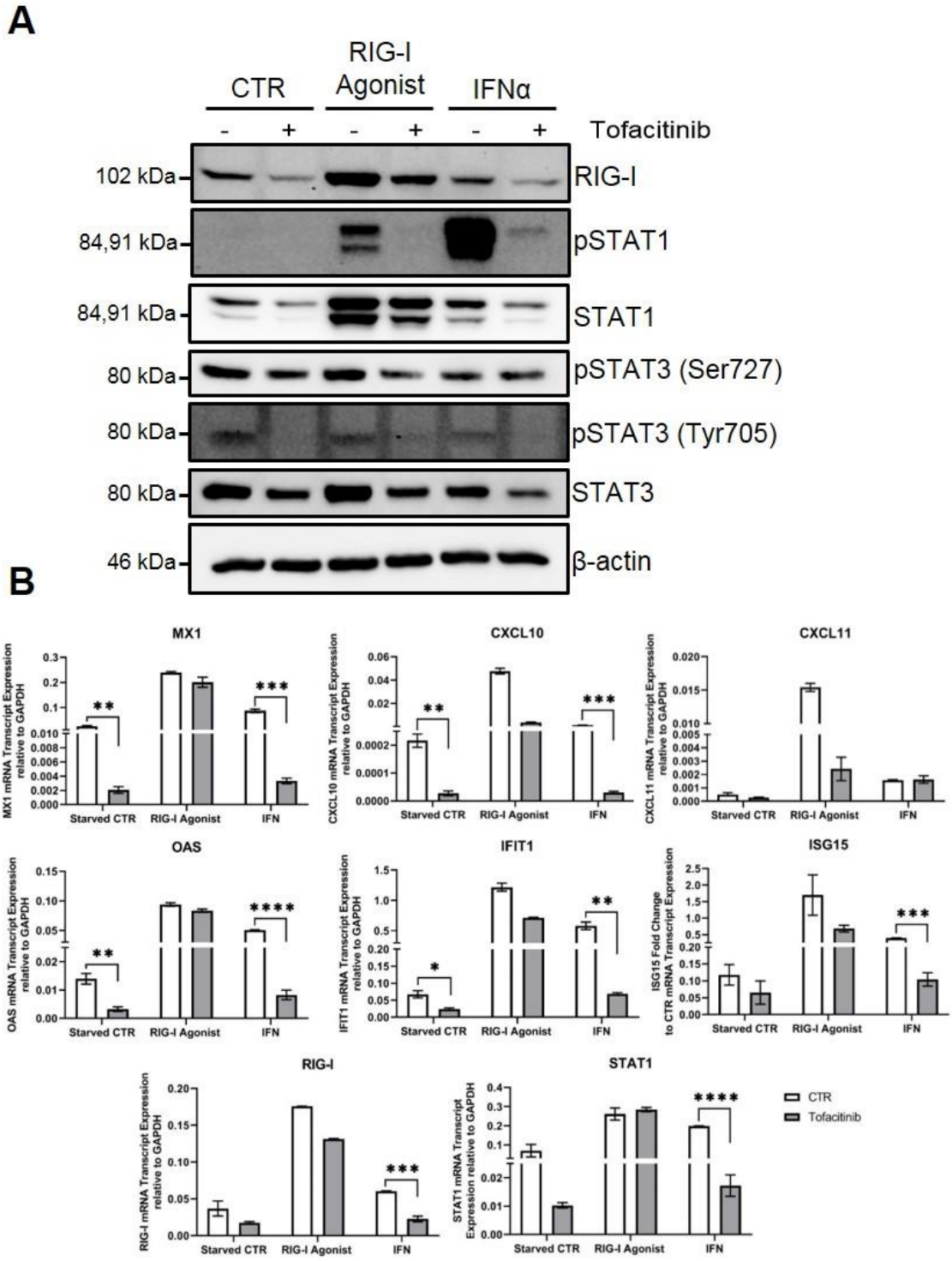
A
CTR
RIG-I Agonist
IFNα
- + - + - +
Tofacitinib
102 kDa
RIG-I
84,91 kDa
pSTAT1
84,91 kDa
STAT1
80 kDa
pSTAT3 (Ser727)
80 kDa
pSTAT3 (Tyr705)
80 kDa
STAT3
46 kDa
β-actin
B
MX1
MX1 mRNA Transcript Expression relative to GAPDH
CXCL10
CXCL10 mRNA Transcript Expression relative to GAPDH
CXCL11
CXCL11 mRNA Transcript Expression relative to GAPDH
OAS
OAS mRNA Transcript Expression relative to GAPDH
IFIT1
IFIT1 mRNA Transcript Expression relative to GAPDH
ISG15
ISG15 Fold Change to CTR mRNA Transcript Expression
RIG-I
RIG-I mRNA Transcript Expression relative to GAPDH
STAT1
STAT1 mRNA Transcript Expression relative to GAPDH
Starved CTR
RIG-I Agonist
IFN
CTR
Tofacitinib

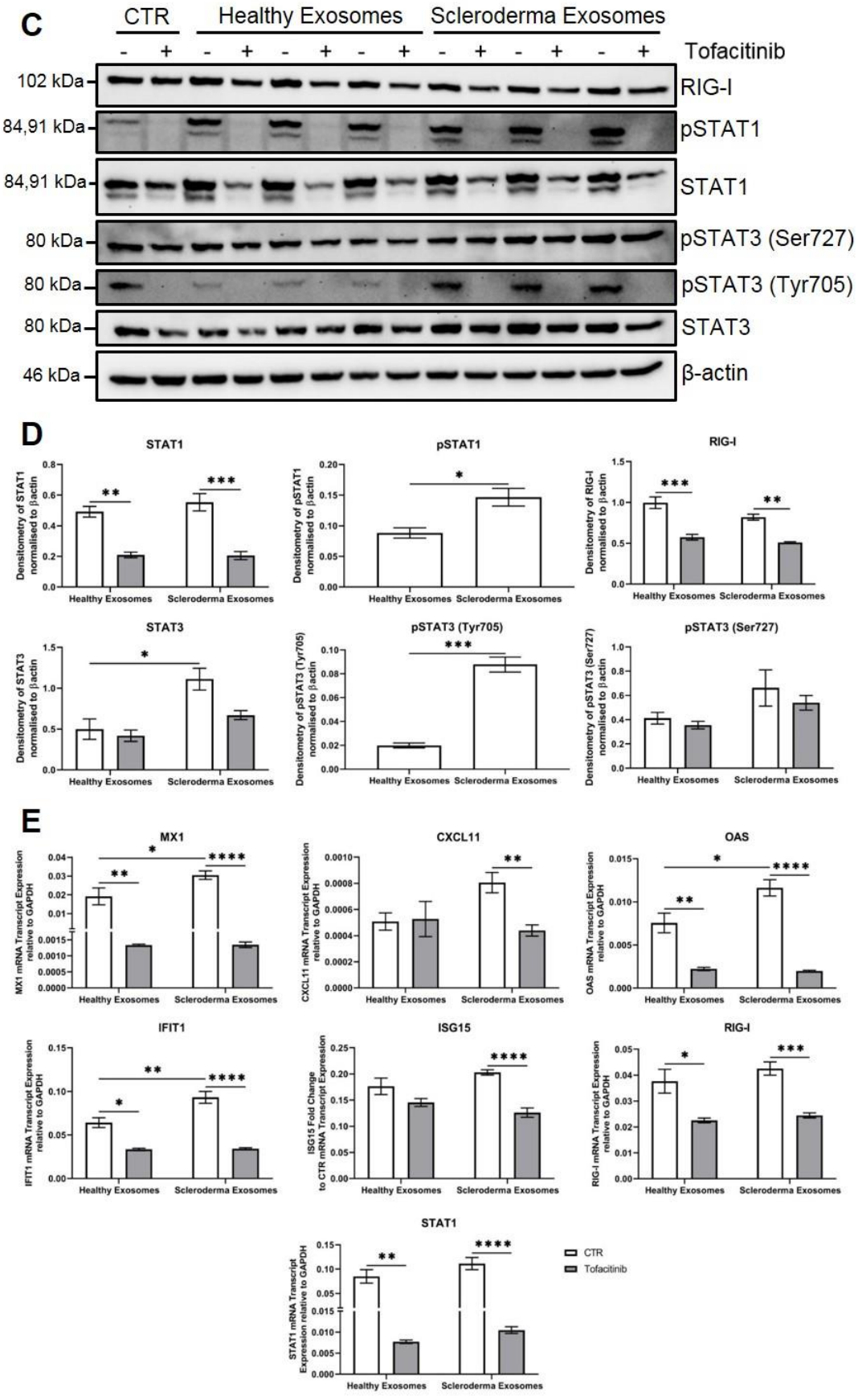
C
CTR
Healthy Exosomes
Scleroderma Exosomes
Tofacitinib
102 kDa
RIG-I
84,91 kDa
pSTAT1
84,91 kDa
STAT1
80 kDa
pSTAT3 (Ser727)
80 kDa
pSTAT3 (Tyr705)
80 kDa
STAT3
46 kDa
β-actin
D
STAT1
pSTAT1
RIG-I
STAT3
pSTAT3 (Tyr705)
pSTAT3 (Ser727)
Densitometry of STAT1 normalised to βactin
Densitometry of pSTAT1 normalised to βactin
Densitometry of RIG-I normalised to βactin
Densitometry of STAT3 normalised to βactin
Densitometry of pSTAT3 (Tyr705) normalised to βactin
Densitometry of pSTAT3 (Ser727) normalised to βactin
Healthy Exosomes
Scleroderma Exosomes
E
MX1
CXCL11
OAS
IFIT1
ISG15
RIG-I
STAT1
MX1 mRNA Transcript Expression relative to GAPDH
CXCL11 mRNA Transcript Expression relative to GAPDH
OAS mRNA Transcript Expression relative to GAPDH
IFIT1 mRNA Transcript Expression relative to GAPDH
ISG15 Fold Change to CTR mRNA Transcript Expression
RIG-I mRNA Transcript Expression relative to GAPDH
STAT1 mRNA Transcript Expression relative to GAPDH
Healthy Exosomes
Scleroderma Exosomes
CTR
Tofacitinib

Figure 5.5. Inhibition of JAK1/3 using Tofacitinib, reduces scleroderma fibroblast-derived exosome induction of pSTAT1 and ISG's in HaCats.

A) HaCats treated with Tofacitinib were stimulated with 10 ng/mL of RIG-I agonist for 48 hours and 20 ng/mL IFNα 1 hour prior to harvest. Immunoblots illustrate Interferon-related protein expression and are representative of three biological repeats. B) mRNA transcript expression of interferon-related genes, normalised by housing keeping gene GAPDH. Data represents means ± SE from two biological repeats (RIG-I agonist) and three biological repeats (CTR and IFN). C) HaCats were serum-starved and treated with 20 μM Tofacitinib, solubilised in DMSO, 1 hour before stimulation with Healthy and Scleroderma Exosomes. Control (CTR) was treated with 0.1% DMSO, equivalent to Tofacitinib. Immunoblots for RIG-I, pSTAT1, STAT1, pIRF3, pSTAT3 (Tyr705), pSTAT3 (Ser727), STAT3 and IRF3, as well as β-actin, which was used as a loading control. E) Bar charts illustrating densitometry analysis of western blots shown in A, calculated using Image Lab. Data represents means ± SE from three biological repeats. E) mRNA transcript expression of interferon-related genes, normalised by housing keeping gene GAPDH. Data represents means ± SE from three biological repeats (Healthy Exosomes), and six biological repeats (Scleroderma Exosomes). Statistical analysis was performed using a two-tailed student T-Test, assuming equal variances, as well as multiple comparison two-way ANOVA, normalised to Tukey. *p<0.05. **p<0.01. ***p<0.001. ****p<0.0001.

5.2.5. Scleroderma Fibroblasts induce STAT3 and pSTAT3 in HaCats, when co-cultured for 48 hours

Since, we observed that SSc exosomes can induce total STAT3 and pSTAT3 (Tyr705) in HaCats, when compared to healthy exosomes, we investigated if co-culturing SSc fibroblasts with HaCats, induced STAT3 and pSTAT3 (Tyr705) expression. SSc fibroblasts significantly induced pSTAT3 (Tyr705) expression by 4.21-fold ($p<0.05$) in HaCats, compared to healthy fibroblasts (Figure 5.6.A-B). Indeed, SSc fibroblasts induced expression of STAT3 (2.86-fold) (Figure 5.6.B), however this was unsignificant, unlike SSc exosome stimulated HaCats (Figure 5.5.E). Likewise, HaCats co-cultured with healthy and SSc fibroblasts displayed similar levels of pSTAT3 (Ser727) (Figure 5.6.B).

As STAT3 signalling can influence epithelial mesenchymal transition (EMT) (Lamouille et al., 2014, Pedroza et al., 2017), we investigated protein and gene expression involved in EMT. HaCats co-cultured with healthy and SSc fibroblasts

displayed similar protein expression of E-Cadherin and N-Cadherin. However, HaCats co-cultured with SSc fibroblasts displayed significantly downregulated E-cadherin gene expression (0.81-fold, $p<0.05$), when compared to healthy. Whereas, no difference in the gene expression of N-Cadherin, COL1A1 and vimentin was observed in SSc fibroblast co-cultured HaCats, compared to healthy (Figure 5.6.C).

To further validate the induction in STAT3 and pSTAT3 (Tyr705) by SSc fibroblast-derived exosomes, we treated serum-starved HaCats with 1% healthy and scleroderma exosomes (n=3) and then investigated STAT3 localisation by immunofluorescence. SSc exosomes significantly induced nuclear translocation and expression of STAT3 ($p<0.0001$), compared to healthy exosomes (Figure 5.6.E), where Figure 5.6.F illustrates the mean STAT3 nuclei intensity for each biological repeat. Likewise, HaCats treated with healthy exosomes display a uniformed distribution of STAT3, within the cytosol and nucleus. Whereas, SSc exosome treated HaCats contain some cytosolic STAT3, but a predominant accumulation of STAT3 in the nucleus (Figure 5.6.D).

Collectively, scleroderma fibroblast-derived exosomes induce the phosphorylation of STAT3 at Tyrosine 705, however do not influence the phosphorylation of the Serine727 site. Further, SSc fibroblast-derived exosomes induce total protein level of STAT3. Collectively, immunofluorescent labelling of STAT3 indicates that SSc exosomes can induce nuclear translocation of STAT3, and thus enhance its transcription factor activity.

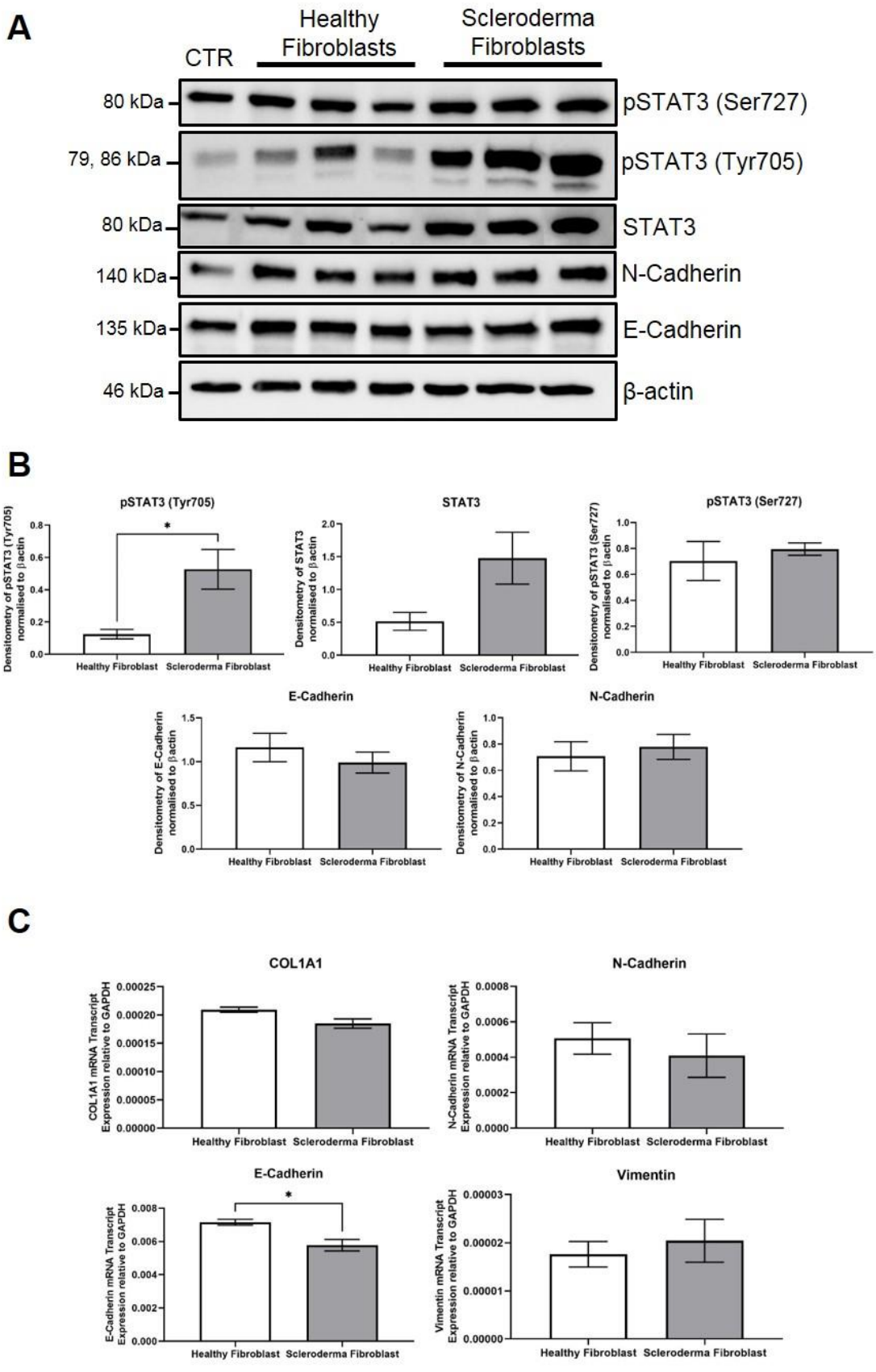
A
CTR
Healthy Fibroblasts
Scleroderma Fibroblasts
80 kDa
pSTAT3 (Ser727)
79, 86 kDa
pSTAT3 (Tyr705)
80 kDa
STAT3
140 kDa
N-Cadherin
135 kDa
E-Cadherin
46 kDa
β-actin
B
pSTAT3 (Tyr705)
Densitometry of pSTAT3 (Tyr705) normalised to βactin
Healthy Fibroblast
Scleroderma Fibroblast
STAT3
Densitometry of STAT3 normalised to βactin
pSTAT3 (Ser727)
Densitometry of pSTAT3 (Ser727) normalised to βactin
E-Cadherin
Densitometry of E-Cadherin normalised to βactin
N-Cadherin
Densitometry of N-Cadherin normalised to βactin
C
COL1A1
COL1A1 mRNA Transcript Expression relative to GAPDH
N-Cadherin
N-Cadherin mRNA Transcript Expression relative to GAPDH
E-Cadherin
E-Cadherin mRNA Transcript Expression relative to GAPDH
Vimentin
Vimentin mRNA Transcript Expression relative to GAPDH

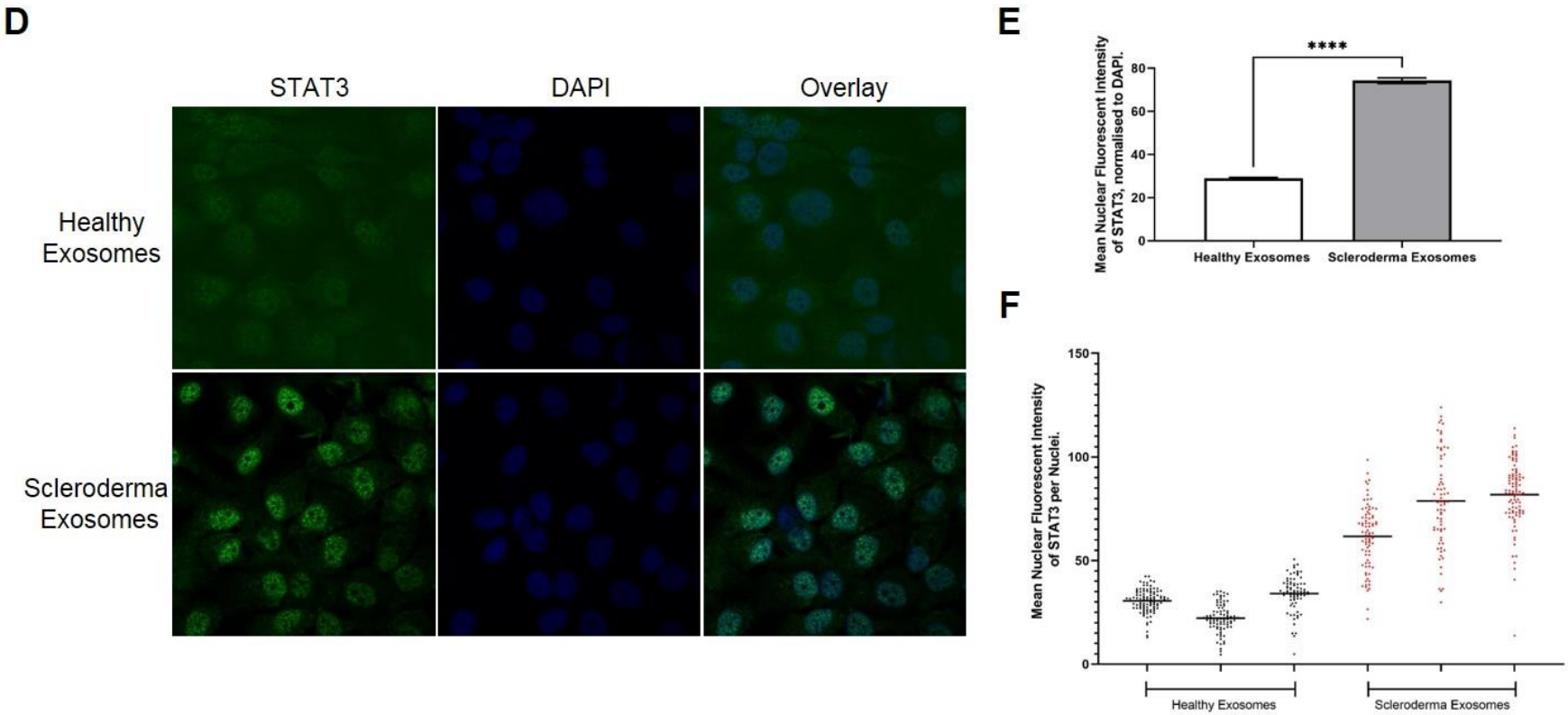
D
STAT3
DAPI
Overlay
Healthy Exosomes
Scleroderma Exosomes
E
****
Mean Nuclear Fluorescent Intensity of STAT3, normalised to DAPI.
0
20
40
60
80
Healthy Exosomes
Scleroderma Exosomes
F
Mean Nuclear Fluorescent Intensity of STAT3 per Nuclei.
0
50
100
150
Healthy Exosomes
Scleroderma Exosomes

Figure 5.6. Scleroderma Fibroblasts induce STAT3 and pSTAT3 in HaCats, when co-cultured after 48 hours.

Healthy (n=3) and Scleroderma (n=3) fibroblasts were co-cultured in a 0.4 μM low protein binding PET membrane cell culture inserts with HaCats for 48 hours in serum-free conditions. A) Immunoblots for pSTAT3 (Tyr705), pSTAT3 (Ser727), STAT3, E-Cadherin, N-Cadherin and β-actin, which was used as a loading control. B) Densitometry analysis of Immunoblots illustrated in A, calculated using Image Lab software. C) mRNA transcript expression for common EMT markers, COL1A1, N-Cadherin, E-Cadherin and Vimentin, which are normalised to housekeeping genes GAPDH and RIBO. Data represents means ± SE from three biological repeats. Statistical analysis was performed using a two-tailed student T-Test, assuming equal variances *$p<0.05$. D) HaCats were grown in 6-well plates onto glass slides and stimulated with 1% healthy and scleroderma exosomes for 48 hours. HaCats were fixed, permeabilised and then stained for STAT3. D) Representative confocal images of HaCats stained with STAT3 and DAPI nuclei stain. 5 Images were taken of three biological repeats, where images were taken from each corner and a central images per sample. Images were taken at 40x magnification on an oil-immersed inverted lens, using ZEN Black software. E) Bar chart to illustrated mean nuclei fluorescent intensity of STAT3, normalised to number of nuclei. Fluorescent intensity was calculated using binary on Image J. Data represents means ± SE from three biological repeats. Data was statistically analysed using a two-tailed Mann Whitney test. ****$p<0.0001$. F) Dot plot which illustrates mean STAT3 intensity, normalised to nuclei, in each biological sample. Black line indicates mean. Data represents all raw data.

5.2.6. RNASeq of scleroderma-fibroblast derived exosome RNA illustrates 214 differentially expressed genes

We observed that scleroderma fibroblast exosomes induce interferon signalling in keratinocytes, which requires TBK and JAK to be fully functional to evoke the response. However, the biological component of the SSc exosome, which induces this signalling cascade is unknown. Previously, Wermuth et al., (2017) extracted RNA from SSc serum exosomes and showed that SSc exosomes contained pro-fibrotic and anti-fibrotic micro-RNAs. Further, Nabet et al., (2017) illustrated that CAF derived exosomes contain unshielded RNA, which can promote innate immune signalling, by activating RIG-I. Thus, to evaluate the biological component responsible for triggering IFN signalling, healthy and

scleroderma exosomes were isolated and RNA was extracted for exosome mRNA and lncRNA Sequencing.

RNA sequencing of scleroderma fibroblast-derived exosomes (n=3) highlights 214 differentially expressed genes (DEGs), compared to healthy fibroblast exosomal RNA (n=3), where 137 were upregulated and 77 downregulated. All DEGs were then plotted as a volcano plot were log2(fold change) is on the x-axis, -log10(p-value) is the y axis and the highly abundance significantly expressed genes are labelled in red (Figure 5.7.C). As exosomal RNA contains an abundance of DEGs, the top 20 most abundant significantly expressed genes were summarised as a bar chart in Figure 5.7.B. The key function of each gene is listed in Appendix Table 17. Further, GO, KEGG, and Reactome pathway analysis indicated no significantly upregulated biological pathways associated with DEGs from SSc exosome RNA, compared to healthy exosome RNA (data not shown). Moreover, H19 was the most abundant significantly expressed DEG in SSc exosome RNA, compared to healthy exosome RNA. Interestingly, H19 has been shown to be a key mediator in TGF-β driven fibrosis (Pachera et al., 2020).

Overall, no known RNA molecules were observed in the RNA sequencing of SSc exosome RNA, which could be possess the ability to stimulate IFN signalling in HaCats. Further work is required to investigate if the significantly abundant genes present in SSc exosomes, compared to healthy exosomes, are contributors to SSc pathogenesis, however, this further investigation is beyond the scope of this project.

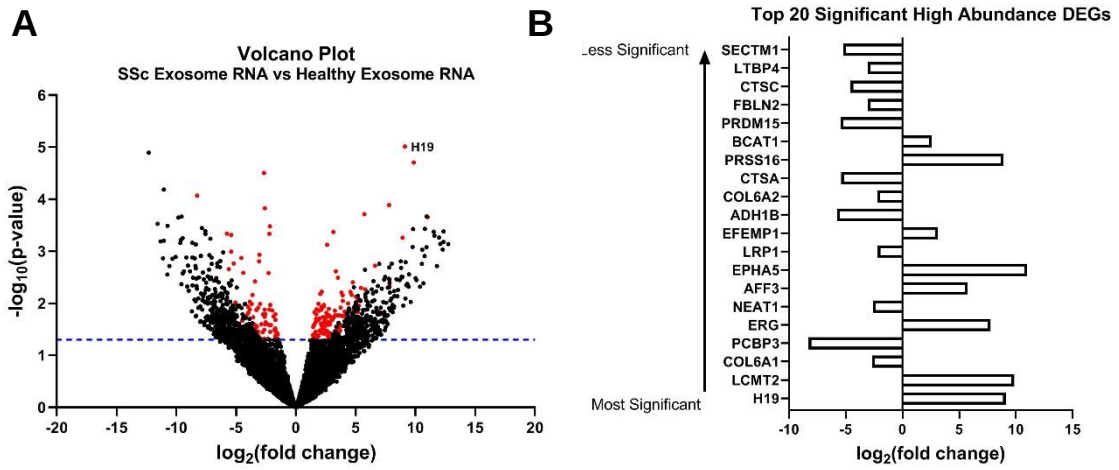

Figure 5.7. RNA sequencing of scleroderma fibroblast-derived exosome RNA, highlights 214 differentially expressed genes, compared to healthy fibroblast exosome RNA.

A) Volcano plot which illustrates log2(fold change) against -log10(p-value) for each DEG of scleroderma exosome RNA, when compared against healthy exosome RNA. Blue line = p-value<0.05. Red = significant high abundance DEGs. B) A bar chart which shows the top 20 most significantly abundant differentially expressed genes, which are the most abundance in SSc exosomes, as log2(fold change) of DEGs from scleroderma exosome RNA, which are significantly (p-value<0.05) upregulated and downregulated, compared to healthy exosome RNA.

5.3. Discussion

Consistently we have shown that scleroderma fibroblast-derived exosomes induce pSTAT1 and ISG expression in recipient keratinocytes after 48 hours. However, the mechanism of action is unknown and thus must be investigated further. Knockdown of RIG-I using a lentivirus prevented the induction of phosphorylation of STAT1 by SSc exosomes. However, SSc exosomes did not induce pSTAT1 in shScramble HaCats. Whereas, SSc exosomes induced ISGs in shRIG-I HaCats, compared to healthy exosomes, which insinuates that phosphorylation of STAT1 isn't required to induce ISGs in shRIG-I HaCats, stimulated with SSc exosomes. Indeed, it is possible that lentivirus transduction can induce antiviral signalling, through RIG-I (Kenworthy et al., 2009), and thus both cell lines could contain perturbed signalling.

Subsequently, RIG-I has been previously knocked down using siRNA in the literature (Boelens et al., 2014, Nabet et al., 2017), thus we treated cells with siRNA against RIG-I and investigated RIG-I expression levels after 72 hours, which illustrated no reduction in RNA/Protein expression (Appendix Figure 1). Further, stimulation of shRIG-I HaCats with RIG-I agonist illustrated that knockdown of RIG-I slowed negative feedback regulation of the antiviral cascade and thus led to an increase in pSTAT1 and ISGs at 48 hours, compared to shScramble. Indeed, we have observed that the timescale in which exosomes and RIG-I agonist induce the innate immune response is different, however both RIG-I agonist and SSc exosomes induce ISGs in shRIG-I HaCats after 48 hours. Moreover, the RIG-I agonist induces pSTAT1 levels to be greater at 48 hours in shRIG-I HaCats compared to shScramble, and thus induced ISGs further. In

contrast, SSc exosome stimulation did not induce pSTAT1 in shRIG-I compared to shScramble, and thus must induce ISGs using an alternative mechanism. Overall, knockdown of RIG-I does not prevent exosome-induction of ISGs, and therefore isn't the primary activator of interferon signalling induced by SSc exosomes. Although we observed that RIG-I isn't fully required for SSc exosome induction of ISGs; the RIG-I agonist was continually used as a positive control as stimulation of RIG-I signalling led to the activation of key downstream components essential for antiviral signalling, such as phosphorylation of IRF3 and STAT1, which were used as read-outs for IFN signalling in this study. Thus, to investigate the antiviral response through other pattern recognition receptors, the RIG-I agonist was still a viable positive control.

To further investigate the mechanism in which SSc exosomes induce pSTAT1 and ISGs, TBK1 was inhibited. TBK1 has a pivotal role in the innate immune antiviral response, as it acts downstream of all pattern recognition receptors (RIG-I, TLRs and cGAS-STING) (Louis et al., 2018). Therefore, targeting TBK1 acts as a bottleneck, to investigate if SSc exosomes require PRRs to induce pSTAT1 and ISGs in recipient keratinocytes, where it has been documented that TLRs have implications in various autoimmune and auto-inflammatory conditions, including SLE and SSc (Agarwal et al., 2011, Ah Kioon et al., 2018, Lee et al., 2016).

Firstly, the pharmacologically inhibition of TBK was investigated using approved clinical drug Amlexanox and small molecule inhibitor GSK8612. Amlexanox is an anti-inflammatory drug used in Japan to treat asthma and pulmonary inflammation diseases, which targets TBK and IKKε. Amlexanox was discontinued in the USA in 2017, as better options became available. Amlexanox

has been characterised as an anti-inflammatory mediator, however, has demonstrated many other potential effects including diabetes, obesity, liver disease and metabolic dysfunction (Dosanjh et al., 2020). Whereas GSK8612 is a recently discovered highly selective inhibitor for TBK1 (Thomson et al., 2019). Dose-response illustrated that Amlexanox and GSK8612 inhibited ISGs to a similar degree, apart from CXCL10 and CXCL11, where GSK8612 inhibited expression at a lower dose. Interestingly, a low dose of Amlexanox induced CXCL11 and CXCL10 expression after 6 hours. Further, protein expression indicated that GSK8612 inhibited phosphorylation of IRF3, directly downstream of TBK1, in both basal and stimulated HaCats at 6 and 48 hours, considerably more than Amlexanox and thus was used in exosome experiments. Likewise, TBK1 and pTBK1 levels were investigated with inhibitors, however data was not shown due to non-specific bands, and thus downstream phosphorylation of IRF3 was used to determined effectiveness of inhibition.

Inhibition of TBK1 by GSK8612, prevented the induction of ISGs and pSTAT1 by SSc exosomes. A limitation to the effectiveness of GSK8612, is that basal level expression of pSTAT1 and pIRF3 was removed to below detection and thus phosphorylation cannot be detected. Therefore, a reduced concentration of GSK8612 is required to only partially reduce basal expression levels of pSTAT1. Likewise, GSK8612 reduced the total protein levels of RIG-I and STAT1 in all HaCats, however this was somewhat alleviated in SSc exosome treated HaCats. Further, SSc exosomes induced ISG15 and CXCL11 gene expression in GSK8612-treated HaCats, which suggests induction of ISG15 and CXCL11 gene expression by SSc exosomes could be independent of TBK1. Although, SSc

exosomes induced ISG15 in HaCats treated with GSK8612, protein expression remained unchanged.

As discussed, scleroderma patients have dysregulated type I IFN signalling in their blood and skin (Skaug and Assassi., 2020, Brkic et al., 2016). Since, type I IFN signalling requires activation of the IFNAR, an anti-IFNAR monoclonal antibody (Anifrolumab) has been created clinically to treat SSc. Phase I trials have indicated a significant reduction in the IFN signature in the whole blood and skin of SSc patients within days of taking the drug (Goldberg et al., 2014). Further, Guo et al., (2015) observed multiple suppressed transcripts of TGF-β related genes in the skin biopsies of SSc patients taking Anifrolumab. Likewise, Tofacitinib is a small molecule drug inhibitor, which targets JAK-STAT that is downstream of many cytokine receptors, such as IFNAR and IL6 (Palmroth et al., 2021). You et al., (2021) showed that SSc patients treated with Tofacitinib had reduced mRSS scores, which improved more so than patients treated with conventional immunosuppressant (CYC and MMF).

Tofacitinib treatment prevented the induced phosphorylation of STAT1 and interferon gene expression by SSc exosomes, which suggests that SSc exosomes require JAK expression to evoke interferon signalling in keratinocytes. A limitation to this work is that JAKs are downstream tyrosine kinases, which induce many cellular pathways associated with immune response, inflammation, apoptosis, and cell proliferation (Harrison., A, D., 2012). Thus, to investigate if the IFNAR is required for SSc exosome induction of ISGs, a direct inhibitor, such as Anifrolumab is required. An additional limitation to this study is that levels of type I IFNs weren’t quantified. Quantification BY ELISA, qPCR and immunoblotting for

IFNα/β was below detection in exosome stimulated HaCats (data not shown). Likewise, RNASeq of exosome stimulated HaCats illustrated no changes in gene expression of IFNα and IFNβ. Further, an IFNβ luciferase assay was produced in HaCats to determine type I IFN expression, however due to the cell-cell and cell-plastic robustness of HaCats, problems with lysis and excessive manipulation to successfully lyse cells prevented reliable quantification of results (data not shown).

Since, JAK is directly downstream of IL-6 and phosphorylates STAT3, where dysregulated IL-6 signalling is implicated in SSc pathogenesis (Chakraborty et al., 2017), we investigated the effect of Tofacitinib inhibition of JAK on levels of pSTAT3 and STAT3 in HaCats stimulated with exosomes. Interestingly, we observed that SSc fibroblast exosomes induced protein expression of STAT3 and pSTAT3 (Tyr705) by immunoblotting, where pSTAT3 (Tyr705) was inhibited by Tofacitinib treatment. STAT3 activation as a transcription factor was further evaluated by immunofluorescent labelling of STAT3, which showed nuclear localisation of STAT3 in SSc exosome stimulated HaCats. Further, we observed no induction of pSTAT3 (Ser727) by SSc fibroblast exosomes. The phosphorylation of STAT3 at Tyrosine 705 is widely known to induce dimerization and nuclear translocation of STAT3. Whereas the role of Ser727 phosphorylation has been implicated to modulate the transcriptional activity of STAT3 by enhancing Tyr705 dephosphorylation (Wakahara et al., 2012, Yang et al., 2020).

STAT3 is a transcription factor, which is activated by many cytokine receptors such as IL-6, which regulates many cellular responses including the inflammatory response (Tsai et al., 2019). STAT3 has been described as a key regulator of the

immune response, as it negatively regulates interferon signalling by sequestering STAT1 into heterodimers (Ho et al., 2006), as well as inducing the gene expression of the IFNAR negative regulator: suppressor of cytokine signalling 3 (SOCS3) (Hong et al., 2002). A limitation to this work is that mRNA expression of STAT3 was not measured in HaCats treated with healthy and SSc exosomes. However, RNA sequencing of HaCats treated with exosomes illustrated no significant changes in gene expression of STAT3 or SOCS3 in SSc, compared to healthy.

Although STAT3 acts as a negative regulator in IFN signalling, it has been implicated in the pathogenesis of SSc. Pedroza et al., (2017) observed increased mRNA expression of STAT3 in SSc skin biopsies, as well as nuclear location of pSTAT3 (Tyr705) in SSc fibroblasts. Further, knockdown of STAT3 in bleomycin mice reduced the expression of pro-fibrotic genes and immunohistochemistry illustrated a reduction in dermal thickness. In addition, Pedroza et al., (2017) observed that TGF-β signalling can induce pSTAT3 (Tyr705) in a SMAD3 dependent mechanism. Additionally, Chakraborty et al., (2017) inhibited STAT3 in pro-fibrotic mouse models, which ameliorated skin fibrosis. Overall, STAT3 has been shown to promote a pro-fibrotic environment in fibroblasts.

Primarily, STAT3 is described as a down regulator of IFN signalling, however, Yang et al., (2007) illustrated that STAT3 can drive IFN expression by binding to the CXCL11 promoter and inducing CXCL11 gene transcription, independent of the phosphorylation of its tyrosine 705 domain. Likewise, STAT3 ability to drive CXCL11 expression could explain why SSc exosomes induce CXCL11 gene expression under TBK1 inhibition, as SSc exosomes were shown to induce

STAT3 levels. However, this cannot be determined as STAT3 expression wasn't investigated in GSK8612-treated HaCats.

A limitation to this study is that the pro-fibrotic nature of STAT3 wasn't explored in keratinocytes stimulated with SSc exosomes. However, as STAT3 is an upstream mediator of EMT, we investigated the protein and gene expression of key EMT proteins in HaCats after co-culture with healthy and SSc fibroblasts. SSc fibroblasts significantly reduced gene expression of E-Cadherin, however protein expression was unchanged. As downregulation of E-Cadherin is a key hallmark of EMT it is possible that SSc fibroblasts exosomes could be driving EMT in keratinocytes, through the upregulation of STAT3 (Lamouille et al., 2014). However, an increase in gene expression of N-Cadherin, which occurs subsequently from down-regulation of E-Cadherin, wasn't observed in HaCats co-cultured with SSc fibroblasts. Thus, further work is required to investigate if SSc fibroblasts exosomes can induce EMT in keratinocytes overtime, as EMT is normally observed after 72 hours of stimulus (Sabbineni et al., 2018).

To evaluate the biological component responsible for induced IFN signalling in SSc exosomes, exosomal RNA was sequenced and compared to healthy fibroblast exosomes. GO and KEGG pathway analysis illustrated no links between SSc exosome RNA and type I IFN signalling. However, GO and KEGG pathway analysis normally indicates cellular effects. Since RNA is isolated from exosomes it is unlikely that GO and KEGG pathway analysis are useful when investigating exosome contents. Interestingly, SSc exosomes contained significantly more H19, compared to healthy exosomes. H19 is a long noncoding RNA, which has been shown to act as a key mediator in TGF-β induced ECM

remodelling and pro-fibrotic effects in fibroblasts (Pachera et al., 2020). Likewise, Wang et al., (2019) illustrated that H19 acted as a sponge for miR-140, which prevented miR-140 from inhibiting TGF-β/SMAD3 cascade in pulmonary fibrosis. Further, Liu et al., (2019) observed that H19 could induce STAT3 induced EMT, by binding to miR-29b-3p, which regulates STAT3 expression, in lung fibrosis. Since, dysregulated TGF-β signalling is predominantly known as the cause of the pro-fibrotic environment in scleroderma pathogenesis, it is feasible that SSc fibroblast exosomes could be potentiating the pro-fibrotic drive, as well as an immune-drive, onto surrounding cells by the delivery of H19.

Moreover, Wermuth et al., (2017) illustrated that SSc sera exosomes contained pro-fibrotic and anti-fibrotic micro-RNAs, which could induce collagen in fibroblasts, and thus it was hypothesised that SSc serum exosomes could drive fibrosis. A limitation to this work is that RNA sequencing was performed on three different biological samples and a large proportion of results were from low abundance differentially expressed genes, which makes data interpretation unreliable. In addition, exosomes predominantly contain sRNAs, whereas this study investigated sequencing of mRNA and lncRNA in healthy and SSc exosomes. Thus, parallel investigation of miRNAs by small RNA-Seq would allow a full investigation into the functional relevance of altered miRNA and other sRNA content in SSc exosomes, which can predict the effects on recipient cells. Further, a limitation to RNA sequencing is that it only gives information on the sequence of the RNA and not the structure, where double-stranded RNA can act as danger-associated molecular patterns and induce PRRs to induce the innate immune response (Preissner et al., 2020).

Overall, inhibition of key proteins important in IFN signalling prevented the induction of pSTAT1 and ISGs caused by SSc exosomes, and thus basal IFN signalling is required for SSc exosomes to evoke an IFN response in HaCats. Further, RNA Sequencing of exosome RNA illustrated no potential molecules, which could induce IFN signalling in HaCats. However, RNASeq highlighted that SSc exosomes contained H19, which has been implicated to drive fibrosis and ECM remodelling through TGF-β and STAT3 signalling. Although more work is required to investigate how SSc exosomes induce IFN signalling, and the exosome components which are responsible for the IFN response, this study illustrates that SSc fibroblast derived exosomes can induce IFN signalling in keratinocytes and contain RNA contents capable of promoting a fibrotic phenotype in recipient cells, which needs to be further evaluated.

6. Conclusion

In scleroderma, there are many molecular and immunological mechanisms which contribute to the disease pathogenesis and progression. It is clear that dysregulated immune activation is a major contributor to disease severity and fibrosis in SSc, however the exact role of type I IFN and its origination and amplification in early disease pathogenesis is unclear. For the first time, we have illustrated that scleroderma dermal fibroblast exosomes can drive interferon signalling in recipient healthy keratinocytes.

Scleroderma fibroblasts are commonly seen as “effector cells”, as they act as key mediators of fibrosis in SSc, and thus research primarily focuses on how surrounding cells target and influence SSc fibroblasts to drive a pro-fibrotic response. The current literature consensus is that SSc fibroblasts are targeted by activated immune cells, which promotes fibroblast activation and a pro-fibrotic drive. The work carried out in this thesis changes the narrative of the SSc fibroblast as an ‘effector cell’ and instead illustrates that SSc dermal fibroblasts can act as immune-drivers to recipient cells, through paracrine signalling by the release of exosomes.

Screening of exosome cargo by RNA sequencing investigating mRNA and lncRNA illustrated no potential candidates, which could be driving an innate immune response. A limitation to this work is that exosome RNA was only profiled from three healthy and three dcSSc fibroblast-derived exosomes. In addition to this, exosome RNA contains a wealth of low abundant genes, which are unreliable to quantify, and thus a larger cohort would give more definitive and

informative data. Further work would include screening exosome RNA cargo for small-RNAs (miRNA), which would inform the functional relevance of SSc exosome RNA and predict its effects on target cells, which could further validate our findings and potentially isolate an RNA responsible for the innate immune activation.

Nevertheless, exosome RNA sequencing indicated that H19 was the most significantly abundant gene, which was upregulated in SSc fibroblast exosomes. H19 is a long non-coding RNA, which has been implicated in mediating TGFβ induced fibroblast activation and ECM remodelling. Likewise, H19 can also influence STAT3 expression in lung fibrosis, which led to a drive in EMT. Our data illustrated that SSc exosomes induced protein expression of STAT3 and pSTAT3 (Tyr705), as well as nuclear localisation of STAT3 in keratinocytes. Although, we observed that SSc exosomes did not affect protein and gene expression of key EMT-related proteins, apart from a significant downregulation of E-Cadherin gene expression; experiments were harvested after 48 hours, whereas EMT normally occurs after 72 hours of stimulus. A limitation to this work is that we didn't investigate the effect SSc exosomes had on STAT3 gene expression. Further work is required to investigate how SSc exosomes induce STAT3 and pSTAT3 (Tyr705) and if this is in a H19-dependent manner. In addition, the result of increased STAT3 expression needs to be further explored to investigate if SSc exosomes can drive EMT and/or fibrosis in keratinocytes, in a STAT3 dependent manner.

Little is known about the interplay between excessive type I IFN and fibrosis in SSc pathogenesis and a better understanding will aid clinical outcome to slow the

fibrotic process, observed in early disease. Recent research has highlighted that SSc fibroblasts can induce healthy fibroblasts to become pro-fibrotic. Collectively, this work highlights that dermal fibroblast exosomes could be key mediators in dysregulated IFN and profibrotic signalling and thus be the missing link between immunopathogenesis and fibrosis in early SSc. However, more work is required to investigate if SSc fibroblast exosomes can induce fibrosis in keratinocytes in a STAT3 dependent manner.

Moreover, CAF-derived exosomes have been shown to induce an innate immune response through RIG-I in breast cancer. A short-hairpin knockdown of RIG-I illustrated that SSc exosomes do not require RIG-I to induce an innate immune response. However, inhibition of TBK1 prevented SSc exosome induced type I IFN signalling. TBK1 is a central kinase downstream of all PRR and thus SSc exosomes could be inducing type I IFN through a different PRR, opposed to RIG-I, such as MDA5 and TLR3, which are also viral RNA sensors. Likewise, inhibition of JAK-STAT by Tofacitinib prevented induced phosphorylation of STAT1 and STAT3 by SSc exosomes, and thus alleviated upregulated ISG expression. Tofacitinib was used to investigate the role of the IFNAR in SSc exosome induced type I IFN signalling, however Tofacitinib inhibits all JAK-STAT pathways, and as we observed SSc exosomes also induced STAT3 expression and phosphorylation (Tyr705). Thus, investigations into the role of the IFNAR would require a direct inhibition of the IFNAR.

A major limitation to this study is that all experiments were carried out using immortalized healthy and scleroderma fibroblasts, as well as HaCats, as a keratinocyte model. Although, exosomes were collected from immortalised

fibroblasts before passage 8, it is unknown if immortalized cells shed exosomes containing different cargo, compared to their primary equivalent. Healthy primary keratinocytes were starved and stimulated with healthy and SSc fibroblast-derived exosomes, however after 48 hours the primary keratinocytes had reduced viability, due to starvation. Further, healthy keratinocytes were stimulated with healthy and SSc fibroblast-cultured supernatant, however this drove keratinocyte cell differentiation. Thus, due to lack of accessibility of a healthy keratinocyte cell line; HaCats were used to model keratinocytes. Future work is required to investigate the effect of primary SSc fibroblast exosomes on primary healthy keratinocytes.

Similarly, scleroderma is a highly heterogeneous disease and the patient fibroblasts used in this study come from a range of subsets within the disease, where patients have different disease durations and mR skin scores. Most experiments during this project were carried out using exosomes isolated from three to six SSc dermal fibroblasts and compared against three healthy fibroblast donors. To further explore and validate the role of SSc dermal fibroblast exosomes in the induction of type I IFN signalling additional biological repeats are required, which will also aid significant consistent results, when investing gene and protein expression. In addition, experiments on early SSc patients will explore the ability of SSc exosomes to drive IFN signalling in early disease.

Overall, this study provides evidence that SSc dermal fibroblasts release exosomes, which can induce type I IFN signalling in keratinocytes, in a TBK and JAK-STAT dependent manner. This work illustrates that fibroblasts act as immune drivers in SSc pathogenesis. Further evaluation into the mechanism and

biological molecule, inside SSc fibroblast exosomes, responsible for induced type I IFN signalling in keratinocytes will aid the understanding behind immunopathogenesis in SSc, as well as provide a potential therapeutic target to alleviate the IFN signature observed in early disease. Likewise, RNA and protein screening of sera and fibroblast exosomes from scleroderma patients could result in the identification of a biomarker associated with early disease prognosis and severity. Further exploration into the role of H19, observed in SSc fibroblast-derived exosomes, and STAT3 induced expression and phosphorylation could aid a better understanding behind the relationship between fibrosis and type I IFN in scleroderma pathogenesis and thus bring us closer to reversing the irrepressible fibrotic process observed in patients suffering with scleroderma.

7. Appendix

Table 16. A table which describes the key function of each of the top 25 most significant DEGs in SSc exosome treated HaCats.

Gene	Fold-Change	P-value	Description
GBP1	0.77	8.68E-05	Guanylate-binding protein 1 is an interferon-induced GTPase which can act as a PRR for bacterial lipopolysaccharise (LPS) and promote noncanonical inflammasome activation (Kutsch and Coers, 2021).
DDX58	0.51	1.64E-04	Gene which encodes RIG-I, which acts as a PRR for double-stranded RNA and regulates the antiviral innate immune response (O'Neill and Bowie, 2011)
RTP4	0.90	2.23E-04	Receptor Transport Protein 4 induced by type I IFN and binds to TBK to negatively regulate TBK signalling (He et al., 2020).
PLA2G2A	0.80	5.32E-04	Phospholipase A2 is an antimicrobial enzyme, which is part of a family that regulates phospholipid metabolism (Okita et al., 2016).
RSAD2	0.53	6.75E-04	Radical S-adenosyl methionine domain-containing protein 2 is an interferon stimulated gene, which disrupts DNA and RNA viral infection (Kurokawa et al., 2019).
ZG16B	1.46	9.97E-04	Zymogen Granule Protein 16B is a secretory lectin protein, which is located in extracellular vesicles (Costa-da-Silva et al., 2022).
IFIH1	0.44	1.08E-03	Encodes melanoma differentiation-associated protein 5, which is a RIG-I-like receptor, that senses viral RNA and triggers an innate immune response (Dias Junior et al., 2019).

IFIT1	0.50	1.27E-03	interferon-induced protein with tetratricopeptide repeats 1 is an antiviral protein, which can act as a PRR for 5-triphosphate RNA (Vladimer et al., 2014)
BST2	0.54	1.84E-03	Encodes Tetherin, which is an IFN-dependent protein, which inhibits viral infection by preventing diffusion of viral particles from infected cells (Perez-Caballero et al., 2009).
CACNG6	1.18	2.06E-03	Calcium voltage-gated channel auxiliary subunit gamma 6 is a subunit of calcium channel γ, which is important for regulating calcium influx (Chen et al., 2007).
TMPRSS11E	0.89	2.16E-03	Transmembrane protease, serine 2 11E is part of a serine protease, shown to be essential in SARS-CoV-2 cell entry (Hoffmann et al., 2020).
TMEM151A	-1.52	2.67E-03	Transmembrane Protein 151A is an uncharacterised gene, which has been shown to act as a causative gene for Paroxysmal Kinesigneic Dyskinesian (Tian et al., 2022).
HRNR	-1.19	3.01E-03	Hornerin is a member of S-100 fused protein family, which have been implicated to regulate protein phosphorylation, calcium homeostasis, cell proliferation, differentiation, and death, as well as inflammatory and immune reactions (Fu et al., 2018).
CLEC2B	0.41	3.32E-03	C-type lectin domain family 2 member B gene is associated with immune cell infiltration, immune checkpoints and is differentially expressed in a variety of cancers (Li et al., 2022).
ANXA2R-AS1	1.03	3.38E-03	Annexin A2 receptor-Antisense RNA 1.
DDX60	0.40	3.45E-03	DEAD box protein 60 is an IFN-inducible RNA helicase which acts as an antiviral factor that promotes RIG-I-like receptor signalling (Miyashita et al., 2011).

PPP1R36	1.52	3.63E-03	Interactive protein of protein phosphatase 1 (PP1), which promotes starvation-induced autophagy (Zhang et al., 2016).
VSIG1	-1.12	3.65E-03	v-set and immunoglobulin domain containing 1.
IFI44	0.42	3.69E-03	Interferon-induced protein 44 acts by negatively regulating the antiviral response (DeDiego et al., 2019).
RDM1P5	1.91	3.70E-03	Pseudogene.
HPGD	0.73	3.75E-03	15-hydroxyprostaglandin dehydrogenase responsible for inactivation of prostaglandin E2 catabolism (Kim et al., 2015).
HSH2D	0.93	4.13E-03	Hematopoietic SH2 Domain Containing protein important in T-cell activity and inhibition on transcriptional activation of IL-2 promoter (Wang and Xiong, 2020).
AFTPH-DT	1.48	4.20E-03	Aftiphilin divergent transcript
IRF7	0.43	4.21E-03	Interferon regulatory factor 7 inducible by IFN signalling and promotes transcriptional activation of type I IFN genes and viral-inducible genes (Wu et al., 2019)
HCN2	-1.27	4.31E-03	Potassium/sodium hyperpolarization-activated cyclic nucleotide-gated ion channel. Function Unknown.

Table 17. A table which describes the key function of each of the top 20 most significantly abundant DEGs in SSc exosomes, compared to Healthy.

Gene	Fold Change	P-value	Description
H19	9.12	9.65E-06	H19 imprinted maternally expressed transcript is a long non-coding RNA, which functions as a tumour suppressor (Raveh et al., 2015).
LCMT2	9.86	1.96E-05	Leucine Carboxyl Methyltransferase 2.
COL6A1	-2.67	3.13E-05	Collagen Type VI Alpha 1 Chain is related to collagen chain trimerization and the integrin pathway (Cescon et al., 2015).
PCBP3	-8.26	8.53E-05	Poly(RC) Binding Protein 3 is important in nucleic acid and single/double stranded DNA binding (Kang et al., 2012).
ERG	7.79	1.29E-04	ETS Transcription Factor is a protein coding gene, important in platelet adhesion, vascular cell remodelling and chromatic regulation (Mullen et al., 2022).
NEAT1	-2.60	1.49E-04	Nuclear Paraspeckle Assembly Transcript 1 is a long non-coding RNA important in the formation and maintenance of paraspeckles (Yamazaki et al., 2018).
AFF3	5.73	1.93E-04	ALF Transcription Elongation Factor 3 may function in lymphoid development and oncogenesis (Ma and Staudt, 1996).
EPHA5	11.01	2.21E-04	EPH Receptor A5 is a protein-tyrosine kinase family membrane, which is abnormally expressed in tumours and can play an important role in tumorigenesis (Li et al., 2019).
LRP1	-2.18	3.33E-04	LDL Receptor Related Protein 1 important in intracellular signalling, lipid homeostasis and clearing of apoptotic cells (Storck et al., 2016).

EFEMP1	3.13	4.26E-04	EGF Containing Fibulin Extracellular Matrix Protein 1 associated with Integrin Pathway and ERK Signalling (Zhang and Marmorstein, 2010).
ADH1B	-5.77	4.59E-04	Alcohol Dehydrogenase 1B important in oxidation by cytochrome P450 and ethanol degradation (Polimanti and Gelernter, 2018).
COL6A2	-2.22	4.62E-04	Collagen Type VI Alpha 1 Chain is related to collagen chain trimerization and the integrin pathway (Cescon et al., 2015).
CTSA	-5.42	4.87E-04	Cathepsin A is an enzyme which acts as a scaffold in the lysosomal multi-enzyme complex (Timur et al., 2016).
PRSS16	8.92	5.48E-04	Serine Protease 16 plays a role in alternative antigen presenting pathway during positive selection of T cells (Brisson and Carrier, 2015).
BCAT1	2.61	7.53E-04	Branched Chain Amino Acid Transaminase 1 catalyses the first reaction in the catabolism of branched chain amino acids isoleucine, leucine and valine. Metabolic reprograming of activated macrophages (Papathanassiu et al., 2017).
PRDM15	-5.42	1.02E-03	PR/SET Domain 15 is a sequence-specific DNA-binding transcriptional regulator, which is associated with positive regulation of transcription by RNA Polymerase II, regulation of signal transduction, stem cell division and B-cell lymphomagenesis (Mzoughi et al., 2020).
FBLN2	-3.05	1.16E-03	Fibulin 2 is a calcium-dependent extracellular protein, which has an important role during organ development, tissue development and remodelling (Ibrahim et al., 2018).
CTSC	-4.56	1.35E-03	Cathepsin C is a lysosomal cysteine protease, which coordinates activation of serine proteases in immune cells (Korkmaz et al., 2018).
LTBP4	-3.07	1.57E-03	Latent Transforming Growth Factor Beta Binding Protein 4 which controls TGF-beta activation by maintaining it into a latent state (Robertson et al., 2015).
SECTM1	-5.20	1.72E-03	Secreted and Transmembrane 1 is protein which is associated with hematopoietic and/or immune system processes. Acts as a natural ligand for the CD7 receptor (Huyton et al., 2011).

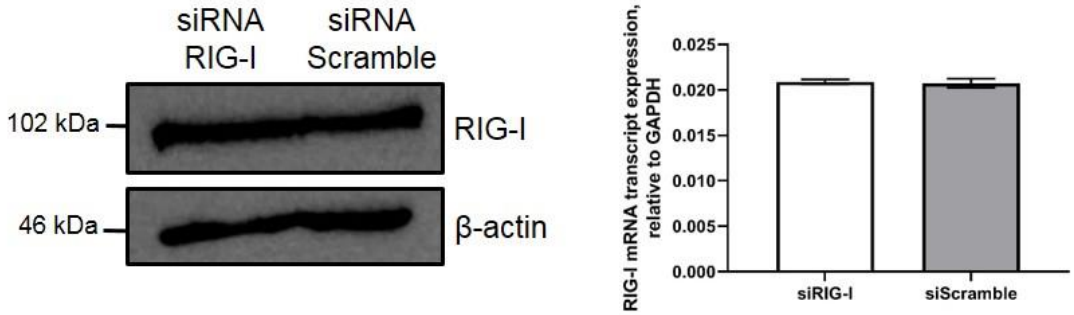

Figure 7.1. siRNA knockdown targeting RIG-I did not significantly reduce protein or mRNA transcription expression of RIG-I.

HaCats were transfected with 5 different siRNA's against RIG-I, as well as a scramble control using Lipofectamine 2000. RNA and Protein was then collected from the selected cells. A) Immunoblotting of RIG-I protein expression, normalised to β-actin (n=1). B) mRNA transcript expression of RIG-I, normalised to housing keeping genes; GAPDH (n=1).

8. Bibliography

Aarreberg, L. D., K. Esser-Nobis, C. Driscoll, A. Shuvarikov, J. A. Roby and M. Gale, Jr. (2019). "Interleukin-1β Induces mtDNA Release to Activate Innate Immune Signaling via cGAS-STING." Mol Cell **74**(4): 801-815.e806.

Agarwal, S. K., M. Wu, C. K. Livingston, D. H. Parks, M. D. Mayes, F. C. Arnett and F. K. Tan (2011). "Toll-like receptor 3 upregulation by type I interferon in healthy and scleroderma dermal fibroblasts." Arthritis Res Ther **13**(1): R3.

Ah Kioon, M. D., C. Tripodo, D. Fernandez, K. A. Kirou, R. F. Spiera, M. K. Crow, J. K. Gordon and F. J. Barrat (2018). "Plasmacytoid dendritic cells promote systemic sclerosis with a key role for TLR8." Sci Transl Med **10**(423).

Assassi, S., M. D. Mayes, F. C. Arnett, P. Gourh, S. K. Agarwal, T. A. McNearney, D. Chaussabel, N. Oommen, M. Fischbach, K. R. Shah, J. Charles, V. Pascual, J. D. Reveille and F. K. Tan (2010). "Systemic sclerosis and lupus: points in an interferon-mediated continuum." Arthritis Rheum **62**(2): 589-598.

Assassi, S., W. R. Swindell, M. Wu, F. D. Tan, D. Khanna, D. E. Furst, D. P. Tashkin, R. R. Jahan-Tigh, M. D. Mayes, J. E. Gudjonsson and J. T. Chang (2015). "Dissecting the heterogeneity of skin gene expression patterns in systemic sclerosis." Arthritis Rheumatol **67**(11): 3016-3026.

Azuma, A., Y. J. Li, S. Abe, J. Usuki, K. Matsuda, S. Henmi, Y. Miyauchi, K. Ueda, A. Izawa, S. Sone, S. Hashimoto and S. Kudoh (2005). "Interferon-{beta} inhibits bleomycin-induced lung fibrosis by decreasing transforming growth factor-{beta} and thrombospondin." Am J Respir Cell Mol Biol **32**(2): 93-98.

Bairkdar, M., M. Rossides, H. Westerlind, R. Hesselstrand, E. V. Arkema and M. Holmqvist (2021). "Incidence and prevalence of systemic sclerosis globally: a comprehensive systematic review and meta-analysis." Rheumatology (Oxford) **60**(7): 3121-3133.

Balka, K. R., C. Louis, T. L. Saunders, A. M. Smith, D. J. Calleja, D. B. D'Silva, F. Moghaddas, M. Tailler, K. E. Lawlor, Y. Zhan, C. J. Burns, I. P. Wicks, J. J. Miner, B. T. Kile, S. L. Masters and D. De Nardo (2020). "TBK1 and IKKε Act Redundantly to Mediate STING-Induced NF-κB Responses in Myeloid Cells." Cell Rep **31**(1): 107492.

Baqir, M., A. Makol, T. G. Osborn, B. J. Bartholmai and J. H. Ryu (2017). "Mycophenolate mofetil for scleroderma-related interstitial lung disease: A real world experience." PLoS One **12**(5): e0177107.

Barrat, F. J., K. B. Elkon and K. A. Fitzgerald (2016). "Importance of Nucleic Acid Recognition in Inflammation and Autoimmunity." Annu Rev Med **67**: 323-336.

Behzadi, P., H. A. García-Perdomo and T. M. Karpiński (2021). "Toll-Like Receptors: General Molecular and Structural Biology." J Immunol Res **2021**: 9914854.

Belgnaoui, S. M., S. Paz and J. Hiscott (2011). "Orchestrating the interferon antiviral response through the mitochondrial antiviral signaling (MAVS) adapter." Curr Opin Immunol **23**(5): 564-572.

Bhandari, R., H. Yang, N. N. Kosarek, A. E. Smith, J. A. Garlick, M. Hinchcliff, M. L. Whitfield and P. A. Pioli (2022). "Human Dermal Fibroblast-derived Exosomes Induce Macrophage Activation in Systemic Sclerosis." Rheumatology (Oxford).

Black, C. M., A. J. Silman, A. I. Herrick, C. P. Denton, H. Wilson, J. Newman, L. Pompon and X. Shi-Wen (1999). "Interferon-alpha does not improve outcome at one year in patients with diffuse cutaneous scleroderma: results of a randomized, double-blind, placebo-controlled trial." Arthritis Rheum **42**(2): 299-305.

Blaszczyk, K., A. Olejnik, H. Nowicka, L. Ozgyin, Y. L. Chen, S. Chmielewski, K. Kostyrko, J. Wesoly, B. L. Balint, C. K. Lee and H. A. Bluyssen (2015). "STAT2/IRF9 directs a prolonged ISGF3-like transcriptional response and antiviral activity in the absence of STAT1." Biochem J **466**(3): 511-524.

Boelens, M. C., T. J. Wu, B. Y. Nabet, B. Xu, Y. Qiu, T. Yoon, D. J. Azzam, C. Twyman-Saint Victor, B. Z. Wiemann, H. Ishwaran, P. J. Ter Brugge, J. Jonkers, J. Slingerland and A. J. Minn (2014). "Exosome transfer from stromal to breast cancer cells regulates therapy resistance pathways." Cell **159**(3): 499-513.

Brisson, L. and A. Carrier (2015). "A novel actor in antitumoral immunity: The thymus-specific serine protease TSSP/PRSS16 involved in CD4(+) T-cell maturation." Oncoimmunology **4**(9): e1026536.

Brkic, Z., L. van Bon, M. Cossu, C. G. van Helden-Meeuwsen, M. C. Vonk, H. Knaapen, W. van den Berg, V. A. Dalm, P. L. Van Daele, A. Severino, N. I. Maria, S. Guillen, W. A. Dik, L. Beretta, M. A. Versnel and T. Radstake (2016). "The interferon type I signature is present in systemic sclerosis before overt fibrosis and might contribute to its pathogenesis through high BAFF gene expression and high collagen synthesis." Ann Rheum Dis **75**(8): 1567-1573.

Cardoneanu, A., A. M. Burlui, L. A. Macovei, I. Bratoiu, P. Richter and E. Rezus (2022). "Targeting Systemic Sclerosis from Pathogenic Mechanisms to Clinical Manifestations: Why IL-6?" Biomedicines **10**(2).

Cescon, M., F. Gattazzo, P. Chen and P. Bonaldo (2015). "Collagen VI at a glance." J Cell Sci **128**(19): 3525-3531.

Chakrabarti, A., B. K. Jha and R. H. Silverman (2011). "New insights into the role of RNase L in innate immunity." J Interferon Cytokine Res **31**(1): 49-57.

Chakraborty, D., B. Sumova, T. Mallano, C. W. Chen, A. Distler, C. Bergmann, I. Ludolph, R. E. Horch, K. Gelse, A. Ramming, O. Distler, G. Schett, L. Senolt and J. H. W. Distler (2017). "Activation of STAT3 integrates common profibrotic pathways to promote fibroblast activation and tissue fibrosis." Nat Commun **8**(1): 1130.

Chakraborty, D., B. Šumová, T. Mallano, C.-W. Chen, A. Distler, C. Bergmann, I. Ludolph, R. E. Horch, K. Gelse, A. Ramming, O. Distler, G. Schett, L. Šenolt and J. H. W. Distler (2017). "Activation of STAT3 integrates common profibrotic pathways to promote fibroblast activation and tissue fibrosis." Nature Communications **8**(1): 1130.

Champoux, J. J. (2001). "DNA topoisomerases: structure, function, and mechanism." Annu Rev Biochem **70**: 369-413.

Chang, Z. L. (2010). "Important aspects of Toll-like receptors, ligands and their signaling pathways." Inflamm Res **59**(10): 791-808.

Wu, J. and Z. J. Chen (2014). "Innate Immune Sensing and Signaling of Cytosolic Nucleic Acids." Annual Review of Immunology **32**(1): 461-488.

Chen, R. S., T. C. Deng, T. Garcia, Z. M. Sellers and P. M. Best (2007). "Calcium channel gamma subunits: a functionally diverse protein family." Cell Biochem Biophys **47**(2): 178-186.

Clements, P. J., P. A. Lachenbruch, J. R. Seibold, B. Zee, V. D. Steen, P. Brennan, A. J. Silman, N. Allegar, J. Varga, M. Massa and et al. (1993). "Skin thickness score in systemic sclerosis: an assessment of interobserver variability in 3 independent studies." J Rheumatol **20**(11): 1892-1896.

Colletti, M., A. Galardi, M. De Santis, G. M. Guidelli, A. Di Giannatale, L. Di Luigi and C. Antinozzi (2019). "Exosomes in Systemic Sclerosis: Messengers Between Immune, Vascular and Fibrotic Components?" Int J Mol Sci **20**(18).
Conde-Vancells, J., E. Rodriguez-Suarez, N. Embade, D. Gil, R. Matthiesen, M. Valle, F. Elortza, S. C. Lu, J. M. Mato and J. M. Falcon-Perez (2008). "Characterization and comprehensive proteome profiling of exosomes secreted by hepatocytes." J Proteome Res **7**(12): 5157-5166.

Costa-da-Silva, A. C., M. H. Aure, J. Dodge, D. Martin, S. Dhamala, M. Cho, J. J. Rose, C. W. Bassim, K. Ambatipudi, F. T. Hakim, S. Z. Pavletic and J. W. Mays (2022). "Salivary ZG16B expression loss follows exocrine gland dysfunction related to oral chronic graft-versus-host disease." iScience **25**(1): 103592.

Cui, S., K. Eisenächer, A. Kirchhofer, K. Brzózka, A. Lammens, K. Lammens, T. Fujita, K. K. Conzelmann, A. Krug and K. P. Hopfner (2008). "The C-terminal regulatory domain is the RNA 5'-triphosphate sensor of RIG-I." Mol Cell **29**(2): 169-179.

Cui, Y., S. Zhang, X. Hu and F. Gao (2022). "Tumor-associated fibroblasts derived exosomes induce the proliferation and cisplatin resistance in esophageal squamous cell carcinoma cells through RIG-I/IFN-β signaling." Bioengineered **13**(5): 12462-12474.

Darnell, J. E., Jr., I. M. Kerr and G. R. Stark (1994). "Jak-STAT pathways and transcriptional activation in response to IFNs and other extracellular signaling proteins." Science **264**(5164): 1415-1421.

de Weerd, N. A. and T. Nguyen (2012). "The interferons and their receptors--distribution and regulation." Immunol Cell Biol **90**(5): 483-491.

Decout, A., J. D. Katz, S. Venkatraman and A. Ablasser (2021). "The cGAS–STING pathway as a therapeutic target in inflammatory diseases." Nature Reviews Immunology **21**(9): 548-569.

DeDiego, M. L., A. Nogales, L. Martinez-Sobrido and D. J. Topham (2019). "Interferon-Induced Protein 44 Interacts with Cellular FK506-Binding Protein 5, Negatively Regulates Host Antiviral Responses, and Supports Virus Replication." mBio **10**(4).

Del Galdo, F., C. Hartley and Y. Allanore (2020). "Randomised controlled trials in systemic sclerosis: patient selection and endpoints for next generation trials." The Lancet Rheumatology **2**(3): e173-e184.

Deng, L., H. Liang, M. Xu, X. Yang, B. Burnette, A. Arina, X. D. Li, H. Mauceri, M. Beckett, T. Darga, X. Huang, T. F. Gajewski, Z. J. Chen, Y. X. Fu and R. R. Weichselbaum (2014). "STING-Dependent Cytosolic DNA Sensing Promotes Radiation-Induced Type I Interferon-Dependent Antitumor Immunity in Immunogenic Tumors." Immunity **41**(5): 843-852.

Dhillon, S. (2017). "Tofacitinib: A Review in Rheumatoid Arthritis." Drugs **77**(18): 1987-2001.

Dias Junior, A. G., N. G. Sampaio and J. Rehwinkel (2019). "A Balancing Act: MDA5 in Antiviral Immunity and Autoinflammation." Trends Microbiol **27**(1): 75-85.

Distler, O., K. B. Highland, M. Gahlemann, A. Azuma, A. Fischer, M. D. Mayes, G. Raghu, W. Sauter, M. Girard, M. Alves, E. Clerisme-Beaty, S. Stowasser, K. Tetzlaff, M. Kuwana and T. M. Maher (2019). "Nintedanib for Systemic Sclerosis-Associated Interstitial Lung Disease." N Engl J Med **380**(26): 2518-2528.

Dobbs, N., N. Burnaevskiy, D. Chen, V. K. Gonugunta, N. M. Alto and N. Yan (2015). "STING Activation by Translocation from the ER Is Associated with Infection and Autoinflammatory Disease." Cell Host Microbe **18**(2): 157-168.

Dobrota, R., B. Maurer, N. Graf, S. Jordan, C. Mihai, O. Kowal-Bielecka, Y. Allanore and O. Distler (2016). "Prediction of improvement in skin fibrosis in diffuse cutaneous systemic sclerosis: a EUSTAR analysis." Ann Rheum Dis **75**(10): 1743-1748.

Dosanjh, A. and C. Y. Won (2020). "Amlexanox: A Novel Therapeutic for Atopic, Metabolic, and Inflammatory Disease." Yale J Biol Med **93**(5): 759-763.

Duan, H., J. Fleming, D. K. Pritchard, L. M. Amon, J. Xue, H. A. Arnett, G. Chen, P. Breen, J. H. Buckner, J. A. Molitor, K. B. Elkon and S. M. Schwartz (2008). "Combined analysis of monocyte and lymphocyte messenger RNA expression with serum protein profiles in patients with scleroderma." Arthritis Rheum **58**(5): 1465-1474.

Duan, T., Y. Du, C. Xing, H. Y. Wang and R. F. Wang (2022). "Toll-Like Receptor Signaling and Its Role in Cell-Mediated Immunity." Front Immunol **13**: 812774.

Farina, G. A., M. R. York, M. Di Marzio, C. A. Collins, S. Meller, B. Homey, I. R. Rifkin, A. Marshak-Rothstein, T. R. Radstake and R. Lafyatis (2010). "Poly(I:C) drives type I IFN- and TGFβ-mediated inflammation and dermal fibrosis simulating altered gene expression in systemic sclerosis." J Invest Dermatol **130**(11): 2583-2593.

Fett, N. (2013). "Scleroderma: nomenclature, etiology, pathogenesis, prognosis, and treatments: facts and controversies." Clin Dermatol **31**(4): 432-437.

Fu, S. J., S. L. Shen, S. Q. Li, Y. P. Hua, W. J. Hu, B. Guo and B. G. Peng (2018). "Hornerin promotes tumor progression and is associated with poor prognosis in hepatocellular carcinoma." BMC Cancer **18**(1): 815.

Ganesan, M., L. Y. Poluektova, D. J. Tuma, K. K. Kharbanda and N. A. Osna (2016). "Acetaldehyde Disrupts Interferon Alpha Signaling in Hepatitis C Virus-Infected Liver Cells by Up-Regulating USP18." Alcohol Clin Exp Res **40**(11): 2329-2338.

Gao, S., A. von der Malsburg, S. Paeschke, J. Behlke, O. Haller, G. Kochs and O. Daumke (2010). "Structural basis of oligomerization in the stalk region of dynamin-like MxA." Nature **465**(7297): 502-506.

Gay, N. J., M. F. Symmons, M. Gangloff and C. E. Bryant (2014). "Assembly and localization of Toll-like receptor signalling complexes." Nat Rev Immunol **14**(8): 546-558.

Gelibter, S., G. Marostica, A. Mandelli, S. Siciliani, P. Podini, A. Finardi and R. Furlan (2022). "The impact of storage on extracellular vesicles: A systematic study." J Extracell Vesicles **11**(2): e12162.

Gilbane, A. J., C. P. Denton and A. M. Holmes (2013). "Scleroderma pathogenesis: a pivotal role for fibroblasts as effector cells." Arthritis Res Ther **15**(3): 215.

Gillespie, J., R. L. Ross, C. Corinaldesi, F. Esteves, E. Derrett-Smith, M. F. McDermott, G. M. Doody, C. P. Denton, P. Emery and F. Del Galdo (2018). "Transforming Growth Factor β Activation Primes Canonical Wnt Signaling Through Down-Regulation of Axin-2." Arthritis Rheumatol **70**(6): 932-942.

Gogulska, Z., Z. Smolenska, J. Turyn, A. Mika and Z. Zdrojewski (2021). "Lipid Alterations in Systemic Sclerosis." Front Mol Biosci **8**: 761721.

Goldberg, A., T. Geppert, E. Schiopu, T. Frech, V. Hsu, R. W. Simms, S. L. Peng, Y. Yao, N. Elgeioushi, L. Chang, B. Wang and S. Yoo (2014). "Dose-escalation of human anti-interferon-α receptor monoclonal antibody MEDI-546 in subjects with systemic sclerosis: a phase 1, multicenter, open label study." Arthritis Res Ther **16**(1): R57.

Gui, X., H. Yang, T. Li, X. Tan, P. Shi, M. Li, F. Du and Z. J. Chen (2019). "Autophagy induction via STING trafficking is a primordial function of the cGAS pathway." Nature **567**(7747): 262-266.

Guiducci, S., J. H. Distler, A. Jüngel, D. Huscher, L. C. Huber, B. A. Michel, R. E. Gay, D. S. Pisetsky, S. Gay, M. Matucci-Cerinic and O. Distler (2008). "The relationship between plasma microparticles and disease manifestations in patients with systemic sclerosis." Arthritis Rheum **58**(9): 2845-2853.

Guo, X., B. W. Higgs, A. C. Bay-Jensen, M. A. Karsdal, Y. Yao, L. K. Roskos and W. I. White (2015). "Suppression of T Cell Activation and Collagen Accumulation by an Anti-IFNAR1 mAb, Anifrolumab, in Adult Patients with Systemic Sclerosis." J Invest Dermatol **135**(10): 2402-2409.

Gurunathan, S., M. H. Kang, M. Jeyaraj, M. Qasim and J. H. Kim (2019). "Review of the Isolation, Characterization, Biological Function, and Multifarious Therapeutic Approaches of Exosomes." Cells **8**(4).

Gurunathan, S., M. H. Kang and J. H. Kim (2021). "A Comprehensive Review on Factors Influences Biogenesis, Functions, Therapeutic and Clinical Implications of Exosomes." Int J Nanomedicine **16**: 1281-1312.

Hardy, M.-P., É. Audemard, F. Migneault, A. Feghaly, S. Brochu, P. Gendron, É. Boilard, F. Major, M. Dieudé, M.-J. Hébert and C. Perreault (2019). "Apoptotic endothelial cells release small extracellular vesicles loaded with immunostimulatory viral-like RNAs." Scientific Reports **9**(1): 7203.

Harrison, D. A. (2012). "The Jak/STAT pathway." Cold Spring Harb Perspect Biol **4**(3).

He, X., A. W. Ashbrook, Y. Du, J. Wu, H. H. Hoffmann, C. Zhang, L. Xia, Y. C. Peng, K. C. Tumas, B. K. Singh, C. F. Qi, T. G. Myers, C. A. Long, C. Liu, R. Wang, C. M. Rice and X. Z. Su (2020). "RTP4 inhibits IFN-I response and enhances experimental cerebral malaria and neuropathology." Proc Natl Acad Sci U S A **117**(32): 19465-19474.

Hekmatirad, S., M. Moloudizargari, A. A. Moghadamnia, S. Kazemi, M. Mohammadnia-Afrouzi, M. Baeeri, F. Moradkhani and M. H. Asghari (2021). "Inhibition of Exosome Release Sensitizes U937 Cells to PEGylated Liposomal Doxorubicin." Front Immunol **12**: 692654.

Ho, H. H. and L. B. Ivashkiv (2006). "Role of STAT3 in type I interferon responses. Negative regulation of STAT1-dependent inflammatory gene activation." J Biol Chem **281**(20): 14111-14118.

Ho, K. T. and J. D. Reveille (2003). "The clinical relevance of autoantibodies in scleroderma." Arthritis Res Ther **5**(2): 80-93.

Hoffmann, M., H. Kleine-Weber, S. Schroeder, N. Krüger, T. Herrler, S. Erichsen, T. S. Schiergens, G. Herrler, N. H. Wu, A. Nitsche, M. A. Müller, C. Drosten and S. Pöhlmann (2020). "SARS-CoV-2 Cell Entry Depends on ACE2 and TMPRSS2 and Is Blocked by a Clinically Proven Protease Inhibitor." Cell **181**(2): 271-280.e278.

Honda, K., A. Takaoka and T. Taniguchi (2006). "Type I interferon [corrected] gene induction by the interferon regulatory factor family of transcription factors." Immunity **25**(3): 349-360.

Honda, K., H. Yanai, H. Negishi, M. Asagiri, M. Sato, T. Mizutani, N. Shimada, Y. Ohba, A. Takaoka, N. Yoshida and T. Taniguchi (2005). "IRF-7 is the master regulator of type-I interferon-dependent immune responses." Nature **434**(7034): 772-777.

Hong, F., B. Jaruga, W. H. Kim, S. Radaeva, O. N. El-Assal, Z. Tian, V. A. Nguyen and B. Gao (2002). "Opposing roles of STAT1 and STAT3 in T cell-mediated hepatitis: regulation by SOCS." J Clin Invest **110**(10): 1503-1513.

Horisberger, M. A., P. Staeheli and O. Haller (1983). "Interferon induces a unique protein in mouse cells bearing a gene for resistance to influenza virus." Proc Natl Acad Sci U S A **80**(7): 1910-1914.

Hou, Y., H. Liang, E. Rao, W. Zheng, X. Huang, L. Deng, Y. Zhang, X. Yu, M. Xu, H. Mauceri, A. Arina, R. R. Weichselbaum and Y. X. Fu (2018). "Non-canonical NF-κB Antagonizes STING Sensor-Mediated DNA Sensing in Radiotherapy." Immunity **49**(3): 490-503.e494.

Hu, Y., C. Yan, L. Mu, K. Huang, X. Li, D. Tao, Y. Wu and J. Qin (2015). "Fibroblast-Derived Exosomes Contribute to Chemoresistance through Priming Cancer Stem Cells in Colorectal Cancer." PLoS One **10**(5): e0125625.

Huyton, T., W. Göttmann, C. Bade-Döding, A. Paine and R. Blasczyk (2011). "The T/NK cell co-stimulatory molecule SECTM1 is an IFN "early response gene" that is negatively regulated by LPS in human monocytic cells." Biochim Biophys Acta **1810**(12): 1294-1301.

Ibrahim, A. and E. Marbán (2016). "Exosomes: Fundamental Biology and Roles in Cardiovascular Physiology." Annu Rev Physiol **78**: 67-83.

Ibrahim, A. M., S. Sabet, A. A. El-Ghor, N. Kamel, S. E. Anis, J. S. Morris and T. Stein (2018). "Fibulin-2 is required for basement membrane integrity of mammary epithelium." Sci Rep **8**(1): 14139.

Ivashkiv, L. B. and L. T. Donlin (2014). "Regulation of type I interferon responses." Nature Reviews Immunology **14**(1): 36-49.

Jefferies, C. A. (2019). "Regulating IRFs in IFN Driven Disease." Front Immunol **10**: 325.

Johnson, M. E., J. M. Mahoney, J. Taroni, J. L. Sargent, E. Marmarelis, M. R. Wu, J. Varga, M. E. Hinchcliff and M. L. Whitfield (2015). "Experimentally-derived fibroblast gene signatures identify molecular pathways associated with distinct subsets of systemic sclerosis patients in three independent cohorts." PLoS One **10**(1): e0114017.

Johnstone, R. M., M. Adam, J. R. Hammond, L. Orr and C. Turbide (1987). "Vesicle formation during reticulocyte maturation. Association of plasma membrane activities with released vesicles (exosomes)." J Biol Chem **262**(19): 9412-9420.

Kang, D. H., K. Y. Song, H. S. Choi, P. Y. Law, L. N. Wei and H. H. Loh (2012). "Novel dual-binding function of a poly (C)-binding protein 3, transcriptional factor which binds the double-strand and single-stranded DNA sequence." Gene **501**(1): 33-38.

Kato, Y., J. Park, H. Takamatsu, H. Konaka, W. Aoki, S. Aburaya, M. Ueda, M. Nishide, S. Koyama, Y. Hayama, Y. Kinehara, T. Hirano, Y. Shima, M. Narazaki and A. Kumanogoh (2018). "Apoptosis-derived membrane vesicles drive the cGAS-STING pathway and enhance type I IFN production in systemic lupus erythematosus." Ann Rheum Dis **77**(10): 1507-1515.

Kenworthy, R., D. Lambert, F. Yang, N. Wang, Z. Chen, H. Zhu, F. Zhu, C. Liu, K. Li and H. Tang (2009). "Short-hairpin RNAs delivered by lentiviral vector transduction trigger RIG-I-mediated IFN activation." Nucleic Acids Res **37**(19): 6587-6599.

Khanna, D., C. P. Denton, A. Jahreis, J. M. van Laar, T. M. Frech, M. E. Anderson, M. Baron, L. Chung, G. Fierlbeck, S. Lakshminarayanan, Y. Allanore, J. E. Pope, G. Riemekasten, V. Steen, U. Müller-Ladner, R. Lafyatis, G. Stifano, H. Spotswood, H. Chen-Harris, S. Dziadek, A. Morimoto, T. Sornasse, J. Siegel and D. E. Furst (2016). "Safety and efficacy of subcutaneous tocilizumab in adults with systemic sclerosis (faSScinate): a phase 2, randomised, controlled trial." Lancet **387**(10038): 2630-2640.

Khanna, D., D. E. Furst, P. J. Clements, Y. Allanore, M. Baron, L. Czirjak, O. Distler, I. Foeldvari, M. Kuwana, M. Matucci-Cerinic, M. Mayes, T. Medsger, Jr., P. A. Merkel, J. E. Pope, J. R. Seibold, V. Steen, W. Stevens and C. P. Denton (2017). "Standardization of the modified Rodnan skin score for use in clinical trials of systemic sclerosis." J Scleroderma Relat Disord **2**(1): 11-18.
Khanna, D., C. J. F. Lin, D. E. Furst, J. Goldin, G. Kim, M. Kuwana, Y. Allanore, M. Matucci-Cerinic, O. Distler, Y. Shima, J. M. van Laar, H. Spotswood, B. Wagner, J. Siegel, A. Jahreis and C. P. Denton (2020). "Tocilizumab in systemic sclerosis: a randomised, double-blind, placebo-controlled, phase 3 trial." Lancet Respir Med **8**(10): 963-974.

Kim, D., A. Peck, D. Santer, P. Patole, S. M. Schwartz, J. A. Molitor, F. C. Arnett and K. B. Elkon (2008). "Induction of interferon-α by scleroderma sera containing autoantibodies to topoisomerase I: Association of higher interferon-α activity with lung fibrosis." Arthritis & Rheumatism **58**(7): 2163-2173.

Kim, H. J., S. Lee, H. Y. Lee, H. Won, S. H. Chang and S. S. Nah (2015). "15-hydroxyprostaglandin dehydrogenase is upregulated by hydroxychloroquine in rheumatoid arthritis fibroblast-like synoviocytes." Mol Med Rep **12**(3): 4141-4148.

Kim, M. J., S. Y. Hwang, T. Imaizumi and J. Y. Yoo (2008). "Negative feedback regulation of RIG-I-mediated antiviral signaling by interferon-induced ISG15 conjugation." J Virol **82**(3): 1474-1483.

Korkmaz, B., G. H. Caughey, I. Chapple, F. Gauthier, J. Hirschfeld, D. E. Jenne, R. Kettritz, G. Lalmanach, A. S. Lamort, C. Lauritzen, M. Łęgowska, A. Lesner, S. Marchand-Adam, S. J. McKaig, C. Moss, J. Pedersen, H. Roberts, A. Schreiber, S. Seren and N. S. Thakker (2018). "Therapeutic targeting of cathepsin C: from pathophysiology to treatment." Pharmacol Ther **190**: 202-236.

Kowal, J., G. Arras, M. Colombo, M. Jouve, J. P. Morath, B. Primdal-Bengtson, F. Dingli, D. Loew, M. Tkach and C. Théry (2016). "Proteomic comparison defines novel markers to characterize heterogeneous populations of extracellular vesicle subtypes." Proc Natl Acad Sci U S A **113**(8): E968-977.

Kubo, M., H. Ihn, K. Yamane and K. Tamaki (2002). "Upregulated expression of transforming growth factor-beta receptors in dermal fibroblasts of skin sections from patients with systemic sclerosis." J Rheumatol **29**(12): 2558-2564.

Kurokawa, C., I. D. Iankov and E. Galanis (2019). "A key anti-viral protein, RSAD2/VIPERIN, restricts the release of measles virus from infected cells." Virus Res **263**: 145-150.

Kutsch, M. and J. Coers (2021). "Human guanylate binding proteins: nanomachines orchestrating host defense." Febs j **288**(20): 5826-5849.

Lamouille, S., J. Xu and R. Derynck (2014). "Molecular mechanisms of epithelial-mesenchymal transition." Nat Rev Mol Cell Biol **15**(3): 178-196.

Leask, A. (2011). "The role of endothelin-1 signaling in the fibrosis observed in systemic sclerosis." Pharmacol Res **63**(6): 502-503.

Lee, J. Y., J. K. Park, E. Y. Lee, E. B. Lee and Y. W. Song (2016). "Circulating exosomes from patients with systemic lupus erythematosus induce an proinflammatory immune response." Arthritis Res Ther **18**(1): 264.

LeRoy, E. C. and T. A. Medsger, Jr. (2001). "Criteria for the classification of early systemic sclerosis." J Rheumatol **28**(7): 1573-1576.

Li, C., A. F. Teixeira, H. J. Zhu and P. Ten Dijke (2021). "Cancer associated-fibroblast-derived exosomes in cancer progression." Mol Cancer **20**(1): 154.

Li, L., X. Zuo, D. Liu, H. Luo and H. Zhu (2020). "The profiles of miRNAs and lncRNAs in peripheral blood neutrophils exosomes of diffuse cutaneous systemic sclerosis." J Dermatol Sci **98**(2): 88-97.

Li, S., J. Wu, S. Zhu, Y. J. Liu and J. Chen (2017). "Disease-Associated Plasmacytoid Dendritic Cells." Front Immunol **8**: 1268.
Li, X., X. Tao and X. Ding (2022). "An integrative analysis to reveal that CLEC2B and ferroptosis may bridge the gap between psoriatic arthritis and cancer development." Scientific Reports **12**(1): 14653.

Li, Y., J. Chu, W. Feng, M. Yang, Y. Zhang, Y. Zhang, Y. Qin, J. Xu, J. Li, S. N. Vasilatos, Z. Fu, Y. Huang and Y. Yin (2019). "EPHA5 mediates trastuzumab resistance in HER2-positive breast cancers through regulating cancer stem cell-like properties." Faseb j **33**(4): 4851-4865.

Lin, J., J. Li, B. Huang, J. Liu, X. Chen, X. M. Chen, Y. M. Xu, L. F. Huang and X. Z. Wang (2015). "Exosomes: novel biomarkers for clinical diagnosis." ScientificWorldJournal **2015**: 657086.

Liu, L., L. Liu and S. Lu (2019). "lncRNA H19 promotes viability and epithelial-mesenchymal transition of lung adenocarcinoma cells by targeting miR-29b-3p and modifying STAT3." Int J Oncol **54**(3): 929-941.

Liu, S., X. Cai, J. Wu, Q. Cong, X. Chen, T. Li, F. Du, J. Ren, Y. T. Wu, N. V. Grishin and Z. J. Chen (2015). "Phosphorylation of innate immune adaptor proteins MAVS, STING, and TRIF induces IRF3 activation." Science **347**(6227): aaa2630.

Liu, X., M. D. Mayes, F. K. Tan, M. Wu, J. D. Reveille, B. E. Harper, H. T. Draeger, E. B. Gonzalez and S. Assassi (2013). "Correlation of interferon-inducible chemokine plasma levels with disease severity in systemic sclerosis." Arthritis Rheum **65**(1): 226-235.

Louis, C., C. Burns and I. Wicks (2018). "TANK-Binding Kinase 1-Dependent Responses in Health and Autoimmunity." Front Immunol **9**: 434.

Ma, C. and L. M. Staudt (1996). "LAF-4 encodes a lymphoid nuclear protein with transactivation potential that is homologous to AF-4, the gene fused to MLL in t(4;11) leukemias." Blood **87**(2): 734-745.

Maehara, T., N. Kaneko, C. A. Perugino, H. Mattoo, J. Kers, H. Allard-Chamard, V. S. Mahajan, H. Liu, S. J. Murphy, M. Ghebremichael, D. Fox, A. S. Payne, R. Lafyatis, J. H. Stone, D. Khanna and S. Pillai (2020). "Cytotoxic CD4+ T lymphocytes may induce endothelial cell apoptosis in systemic sclerosis." J Clin Invest **130**(5): 2451-2464.

Majoros, A., E. Platanitis, D. Szappanos, H. Cheon, C. Vogl, P. Shukla, G. R. Stark, V. Sexl, R. Schreiber, C. Schindler, M. Müller and T. Decker (2016). "Response to interferons and antibacterial innate immunity in the absence of tyrosine-phosphorylated STAT1." EMBO Rep **17**(3): 367-382.

Marié, I., J. E. Durbin and D. E. Levy (1998). "Differential viral induction of distinct interferon-alpha genes by positive feedback through interferon regulatory factor-7." Embo j **17**(22): 6660-6669.

Medzhitov, R., P. Preston-Hurlburt and C. A. Janeway (1997). "A human homologue of the Drosophila Toll protein signals activation of adaptive immunity." Nature **388**(6640): 394-397.

Menck, K., C. Sönmezer, T. S. Worst, M. Schulz, G. H. Dihazi, F. Streit, G. Erdmann, S. Kling, M. Boutros, C. Binder and J. C. Gross (2017). "Neutral sphingomyelinases control extracellular vesicles budding from the plasma membrane." J Extracell Vesicles **6**(1): 1378056.

Miao, C., X. Wang, W. Zhou and J. Huang (2021). "The emerging roles of exosomes in autoimmune diseases, with special emphasis on microRNAs in exosomes." Pharmacol Res **169**: 105680.

Miyashita, M., H. Oshiumi, M. Matsumoto and T. Seya (2011). "DDX60, a DEXD/H box helicase, is a novel antiviral factor promoting RIG-I-like receptor-mediated signaling." Mol Cell Biol **31**(18): 3802-3819.

Mostafavi, S., H. Yoshida, D. Moodley, H. LeBoité, K. Rothamel, T. Raj, C. J. Ye, N. Chevrier, S. Y. Zhang, T. Feng, M. Lee, J. L. Casanova, J. D. Clark, M. Hegen, J. B. Telliez, N. Hacohen, P. L. De Jager, A. Regev, D. Mathis and C. Benoist (2016). "Parsing the Interferon Transcriptional Network and Its Disease Associations." Cell **164**(3): 564-578.
Mullen, D., K. Nowak and R. Chetty (2022). "Gene of the month: ERG." J Clin Pathol **75**(9): 577-580.

Murad, S. (2014). "Toll-like receptor 4 in inflammation and angiogenesis: a double-edged sword." Front Immunol **5**: 313.

Muskardin, T. L. W. and T. B. Niewold (2018). "Type I interferon in rheumatic diseases." Nat Rev Rheumatol **14**(4): 214-228.

Mzoughi, S., J. Y. Fong, D. Papadopoli, C. M. Koh, L. Hulea, P. Pigini, F. Di Tullio, G. Andreacchio, M. M. Hoppe, H. Wollmann, D. Low, M. J. Caldez, Y. Peng, D. Torre, J. N. Zhao, O. Uchenunu, G. Varano, C.-M. Motofeanu, M. Lakshmanan, S. X. Teo, C. M. Wun, G. Perini, S. Y. Tan, C. B. Ong, M. Al-Haddawi, R. Rajarethinam, S. S.-S. Hue, S. T. Lim, C. K. Ong, D. Huang, S.-B. Ng, E. Bernstein, D. Hasson, K. B. Wee, P. Kaldis, A. Jeyasekharan, D. Dominguez-sola, I. Topisirovic and E. Guccione (2020). "PRDM15 is a key regulator of metabolism critical to sustain B-cell lymphomagenesis." Nature Communications **11**(1): 3520.

Nabet, B. Y., Y. Qiu, J. E. Shabason, T. J. Wu, T. Yoon, B. C. Kim, J. L. Benci, A. M. DeMichele, J. Tchou, J. Marcotrigiano and A. J. Minn (2017). "Exosome RNA Unshielding Couples Stromal Activation to Pattern Recognition Receptor Signaling in Cancer." Cell **170**(2): 352-366.e313.

Nakamura, K., M. Jinnin, M. Harada, H. Kudo, W. Nakayama, K. Inoue, A. Ogata, I. Kajihara, S. Fukushima and H. Ihn (2016). "Altered expression of CD63 and exosomes in scleroderma dermal fibroblasts." J Dermatol Sci **84**(1): 30-39.

Nannini, C., C. P. West, P. J. Erwin and E. L. Matteson (2008). "Effects of cyclophosphamide on pulmonary function in patients with scleroderma and interstitial lung disease: a systematic review and meta-analysis of randomized controlled trials and observational prospective cohort studies." Arthritis Res Ther **10**(5): R124.

Newman, L. A., A. Fahmy, M. J. Sorich, O. G. Best, A. Rowland and Z. Useckaite (2021). "Importance of between and within Subject Variability in Extracellular Vesicle Abundance and Cargo when Performing Biomarker Analyses." Cells **10**(3).

O'Neill, L. A. and A. G. Bowie (2011). "The powerstroke and camshaft of the RIG-I antiviral RNA detection machine." Cell **147**(2): 259-261.

Okita, Y., T. Shiono, A. Yahagi, S. Hamada, M. Umemura and G. Matsuzaki (2016). "Interleukin-22-induced antimicrobial phospholipase A2 group IIA mediates protective innate immunity of nonhematopoietic cells against Listeria monocytogenes." Infection and immunity **84**(2): 573-579.

Ottria, A., A. T. Hoekstra, M. Zimmermann, M. van der Kroef, N. Vazirpanah, M. Cossu, E. Chouri, M. Rossato, L. Beretta, R. G. Tieland, C. G. K. Wichers, E. Stigter, C. Gulersonmez, F. Bonte-Mineur, C. R. Berkers, T. Radstake and W. Marut (2020). "Fatty Acid and Carnitine Metabolism Are Dysregulated in Systemic Sclerosis Patients." Front Immunol **11**: 822.

Pachera, E., S. Assassi, G. A. Salazar, M. Stellato, F. Renoux, A. Wunderlin, P. Blyszczuk, R. Lafyatis, F. Kurreeman, J. de Vries-Bouwstra, T. Messemaker, C. A. Feghali-Bostwick, G. Rogler, W. T. van Haaften, G. Dijkstra, F. Oakley, M. Calcagni, J. Schniering, B. Maurer, J. H. Distler, G. Kania, M. Frank-Bertoncelj and O. Distler (2020). "Long noncoding RNA H19X is a key mediator of TGF-β-driven fibrosis." J Clin Invest **130**(9): 4888-4905.

Palmroth, M., K. Kuuliala, R. Peltomaa, A. Virtanen, A. Kuuliala, A. Kurttila, A. Kinnunen, M. Leirisalo-Repo, O. Silvennoinen and P. Isomäki (2021). "Tofacitinib Suppresses Several JAK-STAT Pathways in Rheumatoid Arthritis In Vivo and Baseline Signaling Profile Associates With Treatment Response." Front Immunol **12**: 738481.
Panne, D., S. M. McWhirter, T. Maniatis and S. C. Harrison (2007). "Interferon regulatory factor 3 is regulated by a dual phosphorylation-dependent switch." J Biol Chem **282**(31): 22816-22822.

Papathanassiu, A. E., J.-H. Ko, M. Imprialou, M. Bagnati, P. K. Srivastava, H. A. Vu, D. Cucchi, S. P. McAdoo, E. A. Ananieva, C. Mauro and J. Behmoaras (2017). "BCAT1 controls metabolic reprogramming in activated human macrophages and is associated with inflammatory diseases." Nature Communications **8**(1): 16040.

Patel, G. K., M. A. Khan, H. Zubair, S. K. Srivastava, M. d. Khushman, S. Singh and A. P. Singh (2019). "Comparative analysis of exosome isolation methods using culture supernatant for optimum yield, purity and downstream applications." Scientific Reports **9**(1): 5335.

Paul, S., M. H. Kaplan, D. Khanna, P. M. McCourt, A. K. Saha, P. S. Tsou, M. Anand, A. Radecki, M. Mourad, A. H. Sawalha, D. M. Markovitz and R. Contreras-Galindo (2022). "Centromere defects, chromosome instability, and cGAS-STING activation in systemic sclerosis." Nat Commun **13**(1): 7074.

Pedroza, M., T. T. Le, K. Lewis, H. Karmouty-Quintana, S. To, A. T. George, M. R. Blackburn, D. J. Tweardy and S. K. Agarwal (2016). "STAT-3 contributes to pulmonary fibrosis through epithelial injury and fibroblast-myofibroblast differentiation." FASEB J **30**(1): 129-140.

Pedroza, M., S. To, S. Assassi, M. Wu, D. Tweardy and S. K. Agarwal (2018). "Role of STAT3 in skin fibrosis and transforming growth factor beta signalling." Rheumatology (Oxford) **57**(10): 1838-1850.
Pedroza, M., S. To, S. Assassi, M. Wu, D. Tweardy and S. K. Agarwal (2018). "Role of STAT3 in skin fibrosis and transforming growth factor beta signalling." Rheumatology (Oxford) **57**(10): 1838-1850.

Pellar, R. E. and J. E. Pope (2017). "Evidence-based management of systemic sclerosis: Navigating recommendations and guidelines." Semin Arthritis Rheum **46**(6): 767-774.

Perez-Caballero, D., T. Zang, A. Ebrahimi, M. W. McNatt, D. A. Gregory, M. C. Johnson and P. D. Bieniasz (2009). "Tetherin inhibits HIV-1 release by directly tethering virions to cells." Cell **139**(3): 499-511.

Platanias, L. C. (2005). "Mechanisms of type-I- and type-II-interferon-mediated signalling." Nature Reviews Immunology **5**(5): 375-386.

Polimanti, R. and J. Gelernter (2018). "ADH1B: From alcoholism, natural selection, and cancer to the human phenome." Am J Med Genet B Neuropsychiatr Genet **177**(2): 113-125.

Preissner, K. T., S. Fischer and E. Deindl (2020). "Extracellular RNA as a Versatile DAMP and Alarm Signal That Influences Leukocyte Recruitment in Inflammation and Infection." Front Cell Dev Biol **8**: 619221.

Ragimbeau, J., E. Dondi, A. Alcover, P. Eid, G. Uzé and S. Pellegrini (2003). "The tyrosine kinase Tyk2 controls IFNAR1 cell surface expression." Embo j **22**(3): 537-547.

Rajagopalan, S., E. C. Somers, R. D. Brook, C. Kehrer, D. Pfenninger, E. Lewis, A. Chakrabarti, B. C. Richardson, E. Shelden, W. J. McCune and M. J. Kaplan (2004). "Endothelial cell apoptosis in systemic lupus erythematosus: a common pathway for abnormal vascular function and thrombosis propensity." Blood **103**(10): 3677-3683.

Raveh, E., I. J. Matouk, M. Gilon and A. Hochberg (2015). "The H19 Long non-coding RNA in cancer initiation, progression and metastasis - a proposed unifying theory." Mol Cancer **14**: 184.

Ritchie, K. J., C. S. Hahn, K. I. Kim, M. Yan, D. Rosario, L. Li, J. C. de la Torre and D. E. Zhang (2004). "Role of ISG15 protease UBP43 (USP18) in innate immunity to viral infection." Nat Med **10**(12): 1374-1378.

Robertson, I. B., M. Horiguchi, L. Zilberberg, B. Dabovic, K. Hadjiolova and D. B. Rifkin (2015). "Latent TGF-β-binding proteins." Matrix Biol **47**: 44-53.

Rock, F. L., G. Hardiman, J. C. Timans, R. A. Kastelein and J. F. Bazan (1998). "A family of human receptors structurally related to Drosophila Toll." Proc Natl Acad Sci U S A **95**(2): 588-593.

Rodnan, G. P., E. Lipinski and J. Luksick (1979). "Skin thickness and collagen content in progressive systemic sclerosis and localized scleroderma." Arthritis Rheum **22**(2): 130-140.

Roers, A., B. Hiller and V. Hornung (2016). "Recognition of Endogenous Nucleic Acids by the Innate Immune System." Immunity **44**(4): 739-754.

Ross, R. L., C. Corinaldesi, G. Migneco, I. M. Carr, A. Antanaviciute, C. W. Wasson, A. Carriero, J. H. W. Distler, S. Holmes, Y. M. El-Sherbiny, C. S. McKimmie and F. Del Galdo (2021). "Targeting human plasmacytoid dendritic cells through BDCA2 prevents skin inflammation and fibrosis in a novel xenotransplant mouse model of scleroderma." Ann Rheum Dis **80**(7): 920-929.

Sabbineni, H., A. Verma and P. R. Somanath (2018). "Isoform-specific effects of transforming growth factor β on endothelial-to-mesenchymal transition." J Cell Physiol **233**(11): 8418-8428.

Salvi, V., V. Gianello, S. Busatto, P. Bergese, L. Andreoli, U. D'Oro, A. Zingoni, A. Tincani, S. Sozzani and D. Bosisio (2018). "Exosome-delivered microRNAs promote IFN-α secretion by human plasmacytoid DCs via TLR7." JCI Insight **3**(10).

Sargent, J. L., A. Milano, S. Bhattacharyya, J. Varga, M. K. Connolly, H. Y. Chang and M. L. Whitfield (2010). "A TGFbeta-responsive gene signature is associated with a subset of diffuse scleroderma with increased disease severity." J Invest Dermatol **130**(3): 694-705.

Schneider, W. M., M. D. Chevillotte and C. M. Rice (2014). "Interferon-stimulated genes: a complex web of host defenses." Annu Rev Immunol **32**: 513-545.

Schoggins, J. W. (2019). "Interferon-Stimulated Genes: What Do They All Do?" Annu Rev Virol **6**(1): 567-584.

Scita, G. and P. P. Di Fiore (2010). "The endocytic matrix." Nature **463**(7280): 464-473.

Shao, W. H., D. H. Shu, Y. Zhen, B. Hilliard, S. O. Priest, M. Cesaroni, J. P. Ting and P. L. Cohen (2016). "Prion-like Aggregation of Mitochondrial Antiviral Signaling Protein in Lupus Patients Is Associated With Increased Levels of Type I Interferon." Arthritis Rheumatol **68**(11): 2697-2707.

Shi, H. X., K. Yang, X. Liu, X. Y. Liu, B. Wei, Y. F. Shan, L. H. Zhu and C. Wang (2010). "Positive regulation of interferon regulatory factor 3 activation by Herc5 via ISG15 modification." Mol Cell Biol **30**(10): 2424-2436.

Sircar, G., R. P. Goswami, D. Sircar, A. Ghosh and P. Ghosh (2018). "Intravenous cyclophosphamide vs rituximab for the treatment of early diffuse scleroderma lung disease: open label, randomized, controlled trial." Rheumatology (Oxford) **57**(12): 2106-2113.

Skaug, B. and S. Assassi (2020). "Type I interferon dysregulation in Systemic Sclerosis." Cytokine **132**: 154635.

Solans, R., J. A. Bosch, I. Esteban and M. Vilardell (2004). "Systemic sclerosis developing in association with the use of interferon alpha therapy for chronic viral hepatitis." Clin Exp Rheumatol **22**(5): 625-628.

Solé, C., T. Moliné, M. Vidal, J. Ordi-Ros and J. Cortés-Hernández (2019). "An Exosomal Urinary miRNA Signature for Early Diagnosis of Renal Fibrosis in Lupus Nephritis." Cells **8**(8): 773.
Steen, H. C. and A. M. Gamero (2013). "STAT2 phosphorylation and signaling." Jakstat **2**(4): e25790.

Steen, V. D. and T. A. Medsger, Jr. (2001). "Improvement in skin thickening in systemic sclerosis associated with improved survival." Arthritis Rheum **44**(12): 2828-2835.

Stetefeld, J., S. A. McKenna and T. R. Patel (2016). "Dynamic light scattering: a practical guide and applications in biomedical sciences." Biophys Rev **8**(4): 409-427.

Storck, S. E., S. Meister, J. Nahrath, J. N. Meißner, N. Schubert, A. Di Spiezio, S. Baches, R. E. Vandenbroucke, Y. Bouter, I. Prikulis, C. Korth, S. Weggen, A. Heimann, M. Schwaninger, T. A. Bayer and C. U. Pietrzik (2016). "Endothelial LRP1 transports amyloid-β(1-42) across the blood-brain barrier." J Clin Invest **126**(1): 123-136.

Takeda, K. and S. Akira (2015). "Toll-like receptors." Curr Protoc Immunol **109**: 14.12.11-14.12.10.

Takeuchi, O. and S. Akira (2010). "Pattern recognition receptors and inflammation." Cell **140**(6): 805-820.

Tanaka, Y., H. Tachiwana, K. Yoda, H. Masumoto, T. Okazaki, H. Kurumizaka and S. Yokoyama (2005). "Human centromere protein B induces translational positioning of nucleosomes on alpha-satellite sequences." J Biol Chem **280**(50): 41609-41618.

Taniguchi, T., K. Ogasawara, A. Takaoka and N. Tanaka (2001). "IRF family of transcription factors as regulators of host defense." Annu Rev Immunol **19**: 623-655.

Tashkin, D. P., M. D. Roth, P. J. Clements, D. E. Furst, D. Khanna, E. C. Kleerup, J. Goldin, E. Arriola, E. R. Volkmann, S. Kafaja, R. Silver, V. Steen, C. Strange, R. Wise, F. Wigley, M. Mayes, D. J. Riley, S. Hussain, S. Assassi, V. M. Hsu, B. Patel, K. Phillips, F. Martinez, J. Golden, M. K. Connolly, J. Varga, J. Dematte, M. E. Hinchcliff, A. Fischer, J. Swigris, R. Meehan, A. Theodore, R. Simms, S. Volkov, D. E. Schraufnagel, M. B. Scholand, T. Frech, J. A. Molitor, K. Highland, C. A. Read, M. J. Fritzler, G. H. J. Kim, C. H. Tseng and R. M. Elashoff (2016). "Mycophenolate mofetil versus oral cyclophosphamide in scleroderma-related interstitial lung disease (SLS II): a randomised controlled, double-blind, parallel group trial." Lancet Respir Med **4**(9): 708-719.

Taylor, D. D. and C. Gercel-Taylor (2008). "MicroRNA signatures of tumor-derived exosomes as diagnostic biomarkers of ovarian cancer." Gynecol Oncol **110**(1): 13-21.

Thomson, D. W., D. Poeckel, N. Zinn, C. Rau, K. Strohmer, A. J. Wagner, A. P. Graves, J. Perrin, M. Bantscheff, B. Duempelfeld, V. Kasparcova, J. M. Ramanjulu, G. S.

Pesiridis, M. Muelbaier and G. Bergamini (2019). "Discovery of GSK8612, a Highly Selective and Potent TBK1 Inhibitor." ACS Med Chem Lett **10**(5): 780-785.

Théry, C., L. Zitvogel and S. Amigorena (2002). "Exosomes: composition, biogenesis and function." Nature Reviews Immunology **2**(8): 569-579.

Tian, W. T., F. X. Zhan, Z. H. Liu, Z. Liu, Q. Liu, X. N. Guo, Z. W. Zhou, S. G. Wang, X. R. Liu, H. Jiang, X. H. Li, G. H. Zhao, H. Y. Li, J. G. Tang, G. H. Bi, P. Zhong, X. M. Yin, T. T. Liu, R. L. Ni, H. R. Zheng, X. L. Liu, X. H. Qian, J. Y. Wu, Y. W. Cao, C. Zhang, S. H. Liu, Y. Y. Wu, Q. F. Wang, T. Xu, W. Z. Hou, Z. Y. Li, H. Y. Ke, Z. Y. Zhu, L. Zheng, T. Wang, T. Y. Rong, L. Wu, Y. Zhang, K. Fang, Z. H. Wang, Y. K. Zhang, M. Zhang, Y. W. Zhao, B. S. Tang, X. H. Luan, X. J. Huang and L. Cao (2022). "TMEM151A Variants Cause Paroxysmal Kinesigenic Dyskinesia: A Large-Sample Study." Mov Disord **37**(3): 545-552.

Timur, Z. K., S. Akyildiz Demir and V. Seyrantepe (2016). "Lysosomal Cathepsin A Plays a Significant Role in the Processing of Endogenous Bioactive Peptides." Front Mol Biosci **3**: 68.

Tsai, M. H., L. M. Pai and C. K. Lee (2019). "Fine-Tuning of Type I Interferon Response by STAT3." Front Immunol **10**: 1448.
Valadi, H., K. Ekström, A. Bossios, M. Sjöstrand, J. J. Lee and J. O. Lötvall (2007). "Exosome-mediated transfer of mRNAs and microRNAs is a novel mechanism of genetic exchange between cells." Nat Cell Biol **9**(6): 654-659.

Valenzi, E., M. Bulik, T. Tabib, C. Morse, J. Sembrat, H. Trejo Bittar, M. Rojas and R. Lafyatis (2019). "Single-cell analysis reveals fibroblast heterogeneity and myofibroblasts in systemic sclerosis-associated interstitial lung disease." Ann Rheum Dis **78**(10): 1379-1387.

Valenzi, E., T. Tabib, A. Papazoglou, J. Sembrat, H. E. Trejo Bittar, M. Rojas and R. Lafyatis (2021). "Disparate Interferon Signaling and Shared Aberrant Basaloid Cells in Single-Cell Profiling of Idiopathic Pulmonary Fibrosis and Systemic Sclerosis-Associated Interstitial Lung Disease." Front Immunol **12**: 595811.

Vladimer, G. I., M. W. Górna and G. Superti-Furga (2014). "IFITs: Emerging Roles as Key Anti-Viral Proteins." Front Immunol **5**: 94.

Wakahara, R., H. Kunimoto, K. Tanino, H. Kojima, A. Inoue, H. Shintaku and K. Nakajima (2012). "Phospho-Ser727 of STAT3 regulates STAT3 activity by enhancing dephosphorylation of phospho-Tyr705 largely through TC45." Genes Cells **17**(2): 132-145.

Wang, J. and Y. Xiong (2020). "HSH2D contributes to methotrexate resistance in human T-cell acute lymphoblastic leukaemia." Oncol Rep **44**(5): 2121-2129.

Wang, X., Z. Cheng, L. Dai, T. Jiang, L. Jia, X. Jing, L. An, H. Wang and M. Liu (2019). "Knockdown of Long Noncoding RNA H19 Represses the Progress of Pulmonary Fibrosis through the Transforming Growth Factor β/Smad3 Pathway by Regulating MicroRNA 140." Mol Cell Biol **39**(12).

Wermuth, P. J., S. Piera-Velazquez and S. A. Jimenez (2017). "Exosomes isolated from serum of systemic sclerosis patients display alterations in their content of profibrotic and

antifibrotic microRNA and induce a profibrotic phenotype in cultured normal dermal fibroblasts." Clin Exp Rheumatol **35 Suppl 106**(4): 21-30.

West, A. P., W. Khoury-Hanold, M. Staron, M. C. Tal, C. M. Pineda, S. M. Lang, M. Bestwick, B. A. Duguay, N. Raimundo, D. A. MacDuff, S. M. Kaech, J. R. Smiley, R. E. Means, A. Iwasaki and G. S. Shadel (2015). "Mitochondrial DNA stress primes the antiviral innate immune response." Nature **520**(7548): 553-557.

Wu, J., N. Dobbs, K. Yang and N. Yan (2020). "Interferon-Independent Activities of Mammalian STING Mediate Antiviral Response and Tumor Immune Evasion." Immunity **53**(1): 115-126.e115.

Wu, M., B. Skaug, X. Bi, T. Mills, G. Salazar, X. Zhou, J. Reveille, S. K. Agarwal, M. R. Blackburn, M. D. Mayes and S. Assassi (2019). "Interferon regulatory factor 7 (IRF7) represents a link between inflammation and fibrosis in the pathogenesis of systemic sclerosis." Ann Rheum Dis **78**(11): 1583-1591.

Xu, P., S. Bailey-Bucktrout, Y. Xi, D. Xu, D. Du, Q. Zhang, W. Xiang, J. Liu, A. Melton, D. Sheppard, H. A. Chapman, J. A. Bluestone and R. Derynck (2014). "Innate antiviral host defense attenuates TGF-β function through IRF3-mediated suppression of Smad signaling." Mol Cell **56**(6): 723-737.

Yamazaki, T., S. Souquere, T. Chujo, S. Kobelke, Y. S. Chong, A. H. Fox, C. S. Bond, S. Nakagawa, G. Pierron and T. Hirose (2018). "Functional Domains of NEAT1 Architectural lncRNA Induce Paraspeckle Assembly through Phase Separation." Mol Cell **70**(6): 1038-1053.e1037.

Yang, C. H., L. Wei, S. R. Pfeffer, Z. Du, A. Murti, W. J. Valentine, Y. Zheng and L. M. Pfeffer (2007). "Identification of CXCL11 as a STAT3-dependent gene induced by IFN." J Immunol **178**(2): 986-992.

Yang, J., H. Kunimoto, B. Katayama, H. Zhao, T. Shiromizu, L. Wang, T. Ozawa, T. Tomonaga, D. Tsuruta and K. Nakajima (2019). "Phospho-Ser727 triggers a multistep inactivation of STAT3 by rapid dissociation of pY705–SH2 through C-terminal tail modulation." International Immunology **32**(2): 73-88.

Yang, X., Y. Li, L. Zou and Z. Zhu (2019). "Role of Exosomes in Crosstalk Between Cancer-Associated Fibroblasts and Cancer Cells." Front Oncol **9**: 356.

Yao, X., Q. Wang, P. Zeng, L. Hou, Y. Yang, D. Lu, Y. Huang, Q. Ning, H. Xu, Y. Cao, F. Tang, Y. An, J. Zhou, W. Huang and W. Ma (2021). "LncRNA HOTTIP from synovial fibroblast-derived exosomes: A novel molecular target for rheumatoid arthritis through the miR-1908-5p/STAT3 axis." Exp Cell Res **409**(2): 112943.

You, H., D. Xu, Y. Hou, J. Zhou, Q. Wang, M. Li and X. Zeng (2021). "Tofacitinib as a possible treatment for skin thickening in diffuse cutaneous systemic sclerosis." Rheumatology (Oxford) **60**(5): 2472-2477.

Zamora, A. C., P. J. Wolters, H. R. Collard, M. K. Connolly, B. M. Elicker, W. R. Webb, T. E. King, Jr. and J. A. Golden (2008). "Use of mycophenolate mofetil to treat scleroderma-associated interstitial lung disease." Respir Med **102**(1): 150-155.

Zhang, H. G., C. Liu, K. Su, S. Yu, L. Zhang, S. Zhang, J. Wang, X. Cao, W. Grizzle and R. P. Kimberly (2006). "A membrane form of TNF-alpha presented by exosomes delays T cell activation-induced cell death." J Immunol **176**(12): 7385-7393.

Zhang, Q., M. Gao, Y. Zhang, Y. Song, H. Cheng and R. Zhou (2016). "The germline-enriched Ppp1r36 promotes autophagy." Scientific Reports **6**(1): 24609.

Zhang, Y. and L. Y. Marmorstein (2010). "Focus on molecules: fibulin-3 (EFEMP1)." Exp Eye Res **90**(3): 374-375.

Zhao, C., M. N. Collins, T. Y. Hsiang and R. M. Krug (2013). "Interferon-induced ISG15 pathway: an ongoing virus-host battle." Trends Microbiol **21**(4): 181-186.